学校代码：10246
学　　号：19110190011

# 復旦大學

博 士 学 位 论 文

（学术学位）

# 关于 3d $\mathcal{N}=4$ 超对称理论中的幺正-正交辛对偶和纽结理论的研究

# Researches on the 3d $\mathcal{N}=4$ Unitary-Orthosymplectic Duality and Knot Theory

院　　系：　物理学系
专　　业：　理论物理
姓　　名：　王昊
指 导 教 师：绳田聪　青年研究员
完 成 日 期：　2022 年 8 月 6 日

# 指导小组成员

绳田聪　青年研究员

# Content

# List of Figures

# 摘　要

本论文的主题分为两个部分：第一部分是关于 3d $\mathcal{N}=4$ 超对称规范理论中的幺正-正交辛群箭图 (unitary-orthosymplectic quivers ) 之间的对偶；第二部分是有关纽结同调和 SO($N$) 量子 $6j$ 符号的研究。这两方面都与三维量子场论紧密相关。

首先本论文的主要内容及作者所得研究成果简述如下：

第一章是研究背景综述，主要介绍了 3d $\mathcal{N}=4$ 超对称场论的基本内容以及纽结同调和量子 $6j$ 符号的基本理论。第二章主要介绍了与本论文的研究对象紧密相关的三种精确配分函数：超对称共形指标、扭化指标以及三维球面配分函数。

第三章讨论了带有 $N_f$ 个基本表示下的物质场的 3d $\mathcal{N}=4$ Sp($k$) SQCD 的两种不同的镜像对偶理论，一种由幺正箭图给出，另一种由正交辛箭图给出。在这一章中，本论文作者有如下研究结果: 通过计算幺正/正交辛箭图对的超对称共形指标验证了它们在低能标时流向同一个红外段的超对称共形场论，并且所得的超对称共形指标在希格斯和库仑极限下可以分别得到人们已知的 3d $\mathcal{N}=4$ 理论的库仑和希格斯 Hilbert 级数；本文作者也通过计算了它们的 B-扭化指标发现了 Wilson 线算符在幺正和正交辛箭图中的匹配模式；此外，本文作者通过计算带有涡旋线算符的 3d Sp($k$) SQCD 以及带有 Wilson 线算符的镜像对偶理论的 $S^3$ 配分函数，同时也通过计算前者的 $A$-扭化指标和后者的 $B$-扭化指标，发现了在 3d Sp($k$) SQCD 中两种线算符之间的匹配模式。此外作者在本章利用 $S^3$ 配分函数也讨论了在 Sp($k$) 规范理论的两种不同的镜像理论中涡旋线算符之间的匹配模式。

第四章主要研究了 5d $\mathcal{N}=1$ Sp($k$) 超对称规范理论中，这一 5d $\mathcal{N}=1$ Sp($k$) SQCD 的 Higgs 分支可以由构造出的 3d $\mathcal{N}=4$ 磁箭图的 Coulomb 分支给出。在这一章中, 本文作者研究结果如下：首先计算了 $E_{4,5,6}$ 幺正和正交辛箭图的超对称共形指标与 $E_7$ 幺正和正交辛箭图的 $S^3$ 配分函数，并验证了这些精确配分函数对于每一对幺正/正交辛箭图而言都是相等的，这给出了它们在场论层面上流向同一个红外不动点的证据。第二，根据规范群的秩的不同，本文作者也分别讨论了幺正箭图和正交辛箭图中允许出现的 Wilson 线算符满足的条件。第三，本文作者通过计算带有 Wilson 线算符的不同情况的幺正和正交辛箭图 B-扭化指标，给出了 Wilson 线算符之间的对应模式。最后，本文作者通过计算精细化的库仑分支的 Hilbert 级数，讨论了全局对称性在幺正箭图和正交辛箭图之间是如何对应的。

本论文最后一章的主题是纽结理论，在这一章中本文作者得到了双行杨图着色的 HOMFLY-PT 同调的和单行杨图着色的 Kauffman 同调的庞加莱多项式之间的一个关系；此外本文作者也研究了 SO 类型的微分对超级 $A$ 多项式的作用；最后本文作者得到了在所有表示均为对称表示的情况下 SO($N$) 量子 $6j$ 符号以及 SO($N$) 融合矩阵的表达式，并利用这些结果计算出了单行着色 Kauffman 多项式，所得结果与利用上述 HOMFLY-PT 和 Kauffman 着色庞加莱多项式的关系所得结果一致。

最后在第六章总结与展望中对本文内容进行了总结，并提出了一些未来待解决的问题。在附录中我们列出了一些精确配分函数的结果。

下面对上述两个主题进行一些细致的说明。第一个主题与量子场论中的对偶性紧密相关。物理学中的对偶一般是指同一个物理系统的不同描述之间的等价性（这些描述常常互补）。对偶最简单的例子就是电磁对偶，此外还有更加复杂的对偶，比如弦论中的 T-对偶以及 S-对偶，以及场论中的 Seiberg-Witten 对偶 [2]等。对偶在处理量子场论中的强耦合问题的时候尤其重要，在这种情况下传统的微扰方法将会失效，但是对偶则是将强耦合问题转化为一个在物理上等价的弱耦合问题。通常，人们会基于两个理论中计算出来的某些可观测量相等猜测二者之间存在对偶，这些可观测量包括系统的对称性、量子反常、超对称配分函数等。此外值得注意的是，在某些情况下系统具有某种高阶形式对称性 (higher form symmetries)，这些高阶形式对称性是通常量子场论中全局对称性的推广，它们在描述量子场论的局域算符的层面以上的行为时发挥着非常重要的作用。而在这些高阶对称性下带荷的物体就是诸如缺陷 (defect) 一类的延展物体 (extended object)，比如对于 1-形式对称性而言，这一物体就是线缺陷。因此当考虑包含高阶形式对称性的情形时，对缺陷算符的理解是很重要的。

一个强耦合理论的例子是人们发现在不同维度由于出现一些新的动力学自由度，带 8 个超荷的理论的希格斯分支可以在某些特殊点发生引人注目的改变。如六维理论中会出现无张力的弦 (tensionless string), 这些弦会导致新的自由度的出现; 五维情形中则会出现无质量的规范瞬子，四维情形中则会出现所谓的 Argyres-Douglas 点。最近，人们提出了磁箭图 (magnetic quiver) [3–22]的理论以期可以统一处理四到六维中带 8 个超荷理论的希格斯分支。根据磁箭图理论，人们通过引入一个辅助性的箭图规范理论 (quiver gauge theory) $Q$ 使得其 3d $\mathcal{N}=4$ 库仑分支 $\mathcal{M}_C$ 给出理论 $T$ 在某一个相 $P$ 中的希格斯分支的一个几何描述，即

$$\mathcal{M}_H(T,P)=\mathcal{M}_C(Q(T,P))\ .$$

此前，人们已经利用三维理论的库仑分支研究四维 [23]、五维 [24, 25]及六维 [26–29]理论的希格斯分支。

3d $\mathcal{N}=4$ 超对称规范理论中存在着依赖于规范群 $G$ 的矢量多重态 (vector multiplet) 和依赖于规范群作用到 $\mathbb{H}^n$ 上的四元数表示 $Q$ 的超多重态 (hypermultiplet)，该类型的场论具有一些依赖于 $G$ 及其表示 $\rho: G\to \mathrm{Sp}(n)$ 的对称性，这其中包括 $R$ 对称性，味对称性 (flavor symmetry)。此外，为了给出 3d $\mathcal{N}=4$ 规范理论的拉格朗日量，通常人们需要引入质量参数和 Fayet–Iliopoulos 参数。3d $\mathcal{N}=4$ 理论可以用 IIB 型弦论中的膜系统实现 [30]，这种膜系统里存在三种膜：D5 膜，NS5 膜和 D3 膜。其中，D5 膜给出了箭图的味对称，NS5 膜把箭图中由双重基本超多重态 (bifundamental hypermultiplet) 相连接的相邻的规范群分开，D3 膜则表示规范群对应的圆形节点和方形的味节点之间的双重基本超多重态。这一膜系统将会破缺 IIB 型弦论的 10 维时空对称性来给出 3d $\mathcal{N}=4$ 理论中的转动对称性和 $R$ 对称性。

上面提到的库仑分支以及希格斯分支都是 3d $\mathcal{N}=4$ 超对称规范场论的真空，即模空间。超对称真空是一种场分量可以被所有超荷湮灭的场构型，在这种场构型下欧氏作用量取最小值。一般来说，不同场分量的真空期望值给出了模空间的不同分支。在 3d $\mathcal{N}=4$ 超对称场论的情况下，库仑分支 $\mathcal{M}_C$ 由矢量多重态中的标量场 $\sigma,\phi$ 及单极算符 (monopole operator) 的真空期望值给出，一般来说库仑分支需要考虑量子修正。希格斯分支则是由超多重态中的标量场 $X,Y$ 的真空期望值给出。对于一个特定的希格斯分支, 可能会对应数个磁箭图构造 $Q_i$ $(i=1,\cdots,n)$。这些磁箭图通常在如下方面存在差异：第一，箭图的节点包含了 3d $\mathcal{N}=4$ 超对称规范理论的动力学矢量多重态和背景矢量多重态的信息，尤其是规范群 $G$。第二，磁箭图节点之间的短线表示 3d $\mathcal{N}=4$ 场论的超多重态，这些短线表示按照相邻节点的规范

群直积的双重基本 (bifundamental) 表示变换的超多重态。除此之外还存在其他物质场，如携带较大荷的超多重态等。一个显著的问题是：这些不同的磁箭图 $Q_i$ 之间是什么关系？这些箭图可被视作 3d $\mathcal{N}=4$ 的规范理论，那它们之间仅是拥有同构的库仑分支还是存在更基本的关系？在目前所讨论的 3d $\mathcal{N}=4$ 规范理论的背景下，我们认为它们之间存在红外对偶 (IR-duality)，即两个在紫外端不同的 3d $\mathcal{N}=4$ 规范理论 $\mathcal{T}$ 和 $\mathcal{T}'$（在很多情况下这两个理论都具有拉格朗日描述）流向相同的红外端的共形不动点。不同的箭图规范理论的库仑分支其实是一样的，注意这里所说的都是指经过量子修正之后的红外端的超对称共形场论的库仑分支[31]。这种对偶不同于 3d $\mathcal{N}=4$ 的镜像对称 [30, 32]，后者会在两个理论之间交换模空间，全局对称性，质量参数与 FI 参数。按照镜像对称，存在量子修正的库仑分支的镜像希格斯分支也存在量子修正。

在第三章中，本论文考察了带 $N_f$ 个基本超多重态的 3d $\mathcal{N}=4$ Sp($k$) 规范理论的两种镜像理论，它们之间存在红外对偶。其中一种是全部由幺正节点 (即节点的规范群均为幺正群) 所组成的 D 型邓金箭图 [33], 而另一种则是正交辛箭图规范理论，这是一种由交替的正交群节点和辛群节点组成的线性链箭图 [34]。然而并非红外端的超对称共形场论的所有性质都会在紫外描述中呈现出来，如正交辛理论就由于缺少 FI 参数而导致其库仑分支的全局对称性不能显现。此外，也可在有线缺陷等延展算符的情况下考虑上述红外对偶。本论文中涉及延展算符主要是 Wilson 线算符和涡旋线 (vortex line) 算符。由于 Sp($k$) 理论和它的镜像理论都可以用膜系统实现，所以我们也可以从膜系统的角度考察线缺陷 [35, 36]，以及 1-形式对称性 [37].

在第五章中考察了无穷耦合情况下的五维的 Sp($k$) SQCD 也存在对应不同膜实现的两种磁箭图构造。同三维情形类似，这两种磁箭图其中一个是幺正磁箭图，另一个是正交辛磁箭图，一个自然的问题是考虑它们之间是否对偶。一些迹象表明这些磁箭图之间存在希格斯分支和库仑分支之间的对偶 [38]。本论文将会为 D 型邓金箭图和线性正交辛箭图之间的对偶提供进一步的证据。有以下办法可以测试两个 3d $\mathcal{N}=4$ 理论的对偶性：

(i) 计算希格斯分支和库仑分支的（四元数）维数。
(ii) 考察希格斯分支和库仑分支的全局对称性，以及质量和 FI 参数。
(iii) 计算希格斯分支和库仑分支的手征环 (chiral rings)，以及手征环的生成函数 [39–43]。
(iv) 考察希格斯分支和库仑分支的 Hasse 图 [5, 44, 45]。
(v) 计算超对称共形指标 [46]，A-扭化和 B-扭化指标 [47]，以及三维球面上的配分函数 [48].。
(vi) 考察诸如线算符等延展算符带来的影响 [35, 36, 49]。

其中 (i) 到 (iv) 关注于考察两个分支的几何结构，(v) 中提到的两种超对称指标主要是用来分析红外端超对称共形场论的结构，它们在特定的极限下会约化为希格斯分支和库仑分支的生成函数；而 (v) 中 $S^3$ 配分函数则主要是依赖于紫外端的形变参数，如质量和 FI 参数，但是 $S^3$ 配分函数相比起前两者而言容易计算得多。值得注意的是，(iii) 和 (v) 中所提到的这些精确配分函数，只有其中某些对于紫外描述下的规范群的整体结构较为敏感，这种敏感性发生在需要考虑精确选择磁晶格或者余特征标晶格的时候，比如单极公式，超对称共形指标，A-扭化指标等。其他诸如 $S^3$ 配分函数或者是希格斯分支的 Hilbert 级数等只对规范群对应的李代数有依赖。而延展算符——比如线缺陷——对于规范群的整体结构也非常敏感的，可以作为一个更加直接的探测手段。换句话说，线算符的谱依赖于 1-形式对称 [37]，而 1-形式对称对于规范群及其李代数结构都很敏感。因此，本论文了利用精确配分函数 (v)，包括考虑线算符的情况 (vi)，研究了关于幺正箭图和正交辛箭图之间的红外对偶。

下面简单介绍本论文第二部分的主题，即纽结同调与量子 $6j$ 符号。纽结是 $S^1$ 在三维欧氏空间 $\mathbb{R}^3$ 中的嵌入。纽结理论的发展起源于数学家尝试对纽结进行分类，而纽结理论和量子场论的美妙相遇是从爱德华 · 威腾著名的《量子场论与琼斯多项式》[50]一文开始的。在这篇论文中，威腾证明了陈-西蒙斯理论提供了一个诠释三维流形和纽结上的量子不变量的自然框架。三维流形 $M_3$ 上的 WRT 不变量由陈-西蒙斯泛函给出 [50, 51]。如果 $M_3$ 是三维球面 $S^3$，则沿纽结 $K$ 的 Wilson 圈关于 WRT 不变量的期望值给出了纽结的不变量，而具体是哪种纽结不变量则依赖于规范群的选取。这些量子纽结不变量有一个非常漂亮的性质，即它们都是整系数多项式。这一性质使得人们考虑这些纽结多项式实际上是一些纽结同调的庞加莱多项式。Khovanov [52]提出了量子纽结不变量的范畴化 (categorification)，他构建了一个双阶化 (bi-graded) 的同调，这个同调本身就是一个纽结不变量，而其 $q$-阶化的欧拉示性数即为某个纽结 $K$ 的琼斯多项式。之后，Khovanov 和 Rozansky 构造了一个三阶化 (triply-graded) 的纽结同调 [52]，其阶化 (graded) 的欧拉示性数给出 HOMFLY-PT 多项式。随后 Dunfield,Gukov 和 Rasmussen 猜想了 HOMFLY-PT 同调及其性质 [53]。类似地 Gukov 和 Walcher 猜想了 Kauffman 同调 [54]，其阶化的欧拉示性数给出 Kauffman 多项式。以上这些纽结同调理论也有其相应的着色同调的情形。其中，人们提出了四阶化 (quadruply-graded) 的着色 HOMFLY-PT 同调 [55, 56]并且研究了该同调的一系列结构以及对称性。之后，着色 Kauffman 同调也被提出 [57]。在论文中我们考察了关于同调细 (homologically-thin) 纽结的 $[r^2]$-着色的 HOMFLY-PT 同调和 $[r]$-着色的 Kauffman 同调二者及其庞加莱多项式之间的一个关系。

此外，在纽结理论中还有另外一个重要的猜想——体积猜想 [58, 59]，这个猜想是说，对于一个双曲纽结，其由单行杨图 $[r]$ (这表示一行长度为 $r$ 的杨图) 所着色的着色 Jones 多项式 $J_{[r]}(K;q)$ 在大色极限 (large color limit) 下的渐进行为给出了纽结补空间 $S^3\backslash K$ 的双曲体积。这一猜想后来被进一步推广 [60, 61]，给出了着色 Jones 多项式的大色极限和关于纽结补空间 $S^3\backslash K$ 的 $A$ 多项式之间的关系。$A$ 多项式最早是 Gukov 在考察三维 $\mathrm{SL}(2,\mathbb{C})$ 陈-西蒙斯场论、三维欧氏量子引力以及双曲三维流形的几何之间的关系时被提出的 [60]。Gukov 发现当在规范群的一个无限维表示中存在单个的成结的 Wilson 圈的时候，这个三维 $\mathrm{SL}(2,\mathbb{C})$ 陈-西蒙斯场论的经典和量子性质则是由纽结的 $A$ 多项式给出的，$A$ 多项式给出了一条代数曲线，并且纽结 $K$ 的 $A$ 多项式的零点给出了纽结群的 $\mathrm{SL}(2,\mathbb{C})$ 表示的特征簇。此外，人们也给出了对称表示着色的 HOMFLY-PT 和 Kauffman 多项式及其范畴化情形下的体积猜想 [57, 62–64]，这一猜想引出了超级-$A$ 多项式 (super-$A$-polynomial)。由于 Kauffman 同调可以通过一个微分和 HOMFLY-PT 同调联系起来，我们也考察了该微分对超级-$A$ 多项式的影响并且给出了一个 SU 和 SO 类型 $A$ 多项式之间的一个关系。

此外，还有另外一条路线可以得到量子纽结不变量，即量子 $6j$ 符号。人们可以分别是量子群（即 Hopf 代数）和共形场论中的 WZNW 模型两个视角考察量子 $6j$ 符号。量子群起源于对量子可积系统中量子逆散射方法的研究。需要注意的是，量子群虽然有“群”这个字眼，但是它不是群而是一个代数。量子群理论可以看成是对量子化方法的代数学阐述。从 Hopf 代数出发，人们可以研究量子包络代数 (quantum enveloping algebra) 的表示理论，在这一表示理论中，量子包络代数的两个不可约表示直积的直和分解给出了量子 CG 系数；而在考察三个不可约表示直积的直和分解的时候，则给出了量子 $6j$ 符号。而后来人们在共形场论的研究中发现，在带边三维流形上的陈-西蒙斯泛函积分是边界上 Hilbert 空间的一个元素，并且该 Hilbert 空间和 WZNW 共形块 (conformal block) 空间是同构的，因此量子纽结不变量也可以通过在 WNZW 共形块上通过编织 (braiding) 和融合 (fusion) 等操作构建出来 [65–69]。当 $q=\exp\left(\frac{\pi i}{k+h^\vee}\right)$ 时，WZNW 模型的融合矩阵和对应的量子群的量子 $6j$ 符号等价 (差了一个归一化因子)

[65, 70–74]。6$j$ 符号最初是由维格纳 [75, 76]和拉卡 [77]在研究角动量量子理论过程中提出来的，6$j$ 符号可以由超几何级数 ${}_4F_3$ 非常漂亮地表达出来。在 $\mathfrak{sl}_2$ 的情况下，可以写下量子 6$j$ 符号的显式表达式 [78]，该表达式是 $q$ 超几何级数 ${}_4\varphi_3$ 的一个自然的量子化。此外，对于只涉及对称表示的量子 6$j$ 符号，其信息可以从 $U_q(\mathfrak{sl}_N)$ 的量子纽结不变量中提取出来 [79]，并且可以用 $q$ 超几何级数 ${}_4\varphi_3$ 表示出来。接下来，本论文研究了所有表示均为对称表示的 SO($N$) 量子 6$j$ 符号。这一结果是由对 Alisauškas 的 SO($N$) 经典 6$j$ 符号进行自然的量子化得到 [80, 81]。在本论文中利用 SO($N$) 量子 6$j$ 符号表达式计算了当表示 $R = \square, \square\square$ 时的 WZNW 模型的 SO($N$) 融合矩阵，并且用这些融合矩阵得到了非环面纽结的 Kauffman 多项式，这说明了我们通过量子化 Alisauškas 的 SO($N$) 经典 6$j$ 符号得到的表达式是正确的。

**关键字**：幺正-正交辛对偶，线缺陷算符，纽结同调，超级-$A$ 多项式；量子 6$j$-符号

**中图分类号**：O413.4, O189.24

# Abstract

The thesis consists of two parts: the first part mainly focuses on the duality between 3d $\mathcal{N}=4$ unitary and orthosymplectic quivers, the second part mainly focuses on the knot homology and quantum $6j$-symbols.

In the introduction, some backgrounds of supersymmetric gauge theories and knot theory which are related to the main parts of the thesis were presented. In chapter 2, three types of exact partition functions were introduced, including superconformal indices, twisted indices, and sphere partition functions. They were utilized to check the 3d $\mathcal{N}=4$ unitary and orthosymplectic duality.

The duality between 3d $\mathcal{N}=4$ unitary and orthosymplectic quivers can be studied under a wider background of supersymmetric Sp($k$) SQCD with 8 supercharges in spacetime dimensions 3 to 6, which can be realized by two different type II brane configurations with orientifolds. Under this background, there are two different types of magnetic quivers that can describe the Higgs branch of the Sp($k$) SQCD theory which is a prominent case of a general phenomenon, that for a specified hyper-Kähler Higgs branch, it could correspond to a number of magnetic quiver constructions. Therefore, it is worth studying whether these different magnetic quivers described by 3d $\mathcal{N}=4$ theories are IR dual to each other. In chapter 3, the duality of unitary and orthosymplectic quivers with and without half-BPS line defects under 3d Sp($k$) SQCD were studied. In chapter 4, a similar duality was checked under the background of 5d Sp($k$) SQCD. Furthermore, the half-BPS line defects were also investigated from the perspective of exact results, brane configurations, and one-form symmetry.

Chapter 5 presents another topic of the thesis—knot theory. The knot homologies can be constructed from knot polynomials by the procedure so-called categorification. In this chapter, a rule of grading change from $[r^2]$-colored quadruply-graded HOMFLY-PT homology to $[r]$-colored quadruply-graded Kauffman homology for thin knots is presented, which originates from the isomorphism between representations $(\mathfrak{so}_6, [r]) \cong (\mathfrak{sl}_4, [r^2])$. Then a relation between the SO and SU type super-$A$-polynomials is given, deriving from a differential on Kauffman homology. Finally, a closed-form formula of SO($N$)($N \geq 4$) quantum $6j$-symbols for symmetric representations is given and some examples of SO($N$) fusion matrices for representations $R = \square, \square\square$ are computed. Chapter 6 summarizes the thesis and the appendices list some computation results of exact partition functions.

**Keywords:** Unitary/Orthosymplectic Duality; Line Defects; Knot Homology; Super-$A$-polynomial; Quantum $6j$-Symbols

**CLC number:** O413.4, O189.24

# Chapter 1 Introduction

## 1.1 Overview: Supersymmetric Gauge Theories and Magnetic Quivers

Supersymmetric gauge theories play very important roles in theoretical physics and mathematical physics, which bring many fruits to both physic and mathematics. In the studies of various supersymmetric gauge theories, people found that there exist various dualities between them which connect the strong-coupled theories and weak-coupled theories. Dualities can be checked by the computations of some physical observables, such as partition functions.

The first topic of this thesis mainly focuses on 3d $\mathcal{N} = 4$ and 5d $\mathcal{N} = 1$ supersymmetric gauge theories. Both of them have 8 supercharges. They have intricate moduli spaces of vacua depending on the dimension of the spacetime and both of them have one branch, called the Higgs branch which is a conical hyper-Kähler manifolds. Moreover, for 3d $\mathcal{N} = 4$ theories, they are distinguished by the existence of two branches that both are hyper-Kähler manifolds, which are called Higgs branch $\mathcal{M}_H$ and Coulomb branch $\mathcal{M}_C$. These two branches intersect at the origin which gives a superconformal fixed point. 3d mirror symmetry is an infrared intriguing duality [32] that interchanges the Higgs and Coulomb branch (also exchanges Fayet-Ilipoulous and mass parameters) of two theories that have completely different UV descriptions. Moreover, the Coulomb branch will be quantum corrected while the Higgs branch will be protected against the correction at a generic point of the parameter space [31].

It was observed that the Higgs branch of the theories with 8 supercharges suddenly changes at some special points of the parameter space. In various dimensions, these changes are caused by the presence of some new massless degrees of freedom and make the analysis of the moduli spaces becomes very difficult. To give a description of the Higgs branch $\mathcal{M}_H$ of a theory $T$ in a specific phase $P$, the technique of magnetic quivers was introduced [3–22] aiming to construct an auxiliary quiver gauge theory $Q$ whose quantum corrected Coulomb branch $\mathcal{M}_C$ [31] gives a description of this Higgs branch $\mathcal{M}_H$, i.e.

$$\mathcal{M}_H(T, P) = \mathcal{M}_C(Q(T, P)). \tag{1.1.1}$$

A magnetic quiver consists of nodes and edges. Circle nodes encode the 3d $\mathcal{N} = 4$ dynamical and background vector multiplets. These nodes are also called gauge nodes. Also, there are square nodes called flavor nodes.

Two neighboring nodes are connected by the edges which correspond to the 3d $\mathcal{N}=4$ hypermultiplets transform in the bi-fundamental representation of the adjacent nodes. It was discovered that a specific Higgs branch may admit several magnetic quivers $Q_i$ $(i=1,\ldots,n)$. In other words, for two distinct magnetic quivers $Q_i$ and $Q_j$, they satisfy $\mathcal{M}_C(Q_i)=\mathcal{M}_C(Q_j)$.

There exist two types of brane realizations of the Sp($k$) SQCD with 8 supercharges with orientifolds, these two realizations correspond to two different types of magnetic quivers which are a unitary and an orthosymplectic magnetic quiver. The unitary quiver is a D-type Dynkin quiver whose nodes are all unitary [33], and the term "orthosymplectic" indicates that the quiver is a linear chain composed of alternating orthogonal and symplectic nodes [34]. These two magnetic quivers will give the descriptions of the Higgs branch of the Sp($k$) SQCD. This thesis analyzes these two magnetic quivers as quantum field theories. As a typical example, the thesis discusses the 3d Sp($k$) SQCD and studies its two different mirror theories which are IR dual to each other by evaluating partition functions even taking the line defects into consideration. Also, the thesis studies the 5d Sp($k$) SQCD at infinite couplings, which also could be realized by two types of brane realizations that engender a unitary quiver and an orthosymplectic quiver, and the evidence for the duality between them are presented.

## 1.2 3d $\mathcal{N}=4$ Supersymmetric Gauge Theories

In this subsection, we give the basic of 3d $\mathcal{N}=4$ theories, which is essential to describe magnetic quivers.

### 1.2.1 Basic Data

In $\mathbb{R}^3$, the spin group is Spin(3) $\cong$ SU(2), the supersymmetric theories contain following data:

- Two components spinors $\psi^\alpha$ transform under the fundamental representation **2** of SU(2).
- Invariant tensors $\epsilon_{\alpha\beta}$ and $\epsilon^{\alpha\beta}$ which can raise and lower indices.
- Pauli matrices $(\sigma^\mu)^\alpha_\beta$.
- Momentum and angular momentum generators $P_\mu$ and $J^\mu_\nu$.

Furthermore, a supersymmetric theory has some additional odd generators called supercharges $Q^I_\alpha, I=1,\cdots,\mathcal{N}$ ($\alpha$'s are spinor indices) satisfying following anti-commutator:

$$\{Q^I_\alpha, Q^J_\beta\}=\delta^{IJ}(\sigma^\mu)_{\alpha\beta}P_\mu, \tag{1.2.1}$$

these supercharges transform as spinors in $\mathbb{R}^3$. The generators $P_\mu, J^\mu_\nu$ and $Q^I_\alpha$ generate the so-called $\mathcal{N}$-extend super-Poincaré algebra. One can act by rotations of index $I$ the supercharges ($I=1,\cdots,\mathcal{N}$), which will give the group of automorphism of the above algebra, i.e. O($\mathcal{N}$). The $\delta^{IJ}$ in (1.2.1) is the invariant tensor of O($\mathcal{N}$). There is a connected component SO($\mathcal{N}$) $\subset$ O($\mathcal{N}$) is known as the $R$-symmetry, which transforms the supercharges as

$$Q^I_\alpha \to R^I_J Q^J_\alpha. \tag{1.2.2}$$

Generally speaking, a supersymmetric gauge theory is specified by two data [82]:

- A compact Lie group $G$ as gauge group.
- A linear quaternionic representation $\rho : G \to \mathrm{Sp}(n)$ acting on the vector space $Q = \mathbb{H}^n$.

These data determine the field contents of a Lagrangian theory with $\mathcal{N}=4$ supersymmetry. It is common to use complex numbers rather than quaternions by using the isomorphism $\mathrm{Sp}(n) \cong \mathrm{USp}(2n,\mathbb{C}) := \mathrm{Sp}(2m,\mathbb{C}) \cap \mathrm{U}(n,n)$. Then a quaternionic representation acts by a symplectic-unitary transformation on $Q \cong \mathbb{C}^{2n}$. Moreover, if one restricts to quaternionic representation of "cotangent type", which means one specify a unitary representation $\rho : G \to \mathrm{U}(n)$ on $R \cong \mathbb{C}^n$, then $Q \cong R \oplus R^*$

- The vector multiplet only depends on the gauge group $G$, its field contents as follows:
  (a)A gauge connection $A_\mu$ on a principal $G$-bundle $P$ on $\mathbb{R}^3$.
  (b) Scalar field $\phi^{\dot{A}\dot{B}}$ transforming in the adjoint representation **3** of $\mathrm{SU}(2)_C$ R-symmetry and they can be treated as a section of adjoint bundle $Ad(P)$ of $P$. It has real component $\sigma \in \mathfrak{g} = \mathrm{Lie}(G)$ and complex component $\phi \in \mathfrak{g}_{\mathbb{C}} = \mathrm{Lie}(G_{\mathbb{C}})$
  $$\phi^{\dot{A}\dot{B}} = \begin{pmatrix} 2\phi & \sigma \\ \sigma & -2\bar{\phi} \end{pmatrix}$$
  (c) Complex gaugino $\lambda_\alpha^{A\dot{A}}$ in the bi-fundamental of $\mathrm{SU}(2)_H \times \mathrm{U}(2)_C$.
  (d)$D^{(AB)}$ denotes an auxiliary scalar field in the adjoint representation of $\mathrm{SU}(2)_H$.

- The hypermultiplet hinges on the quaternionic representation $\rho$. Usually, the hypermultiplet contains scalar field $\boldsymbol{\Phi}$ transforms in the fundamental representation of $\mathrm{SU}(2)_H$. $\boldsymbol{\Phi}$ can be viewed as the section of the associated vector bundle $P \times_G Q$. Its components $\boldsymbol{\Phi}^{AI}_{2n\times 2n}$ has $\mathrm{SU}(2)_H$ index $A$ and symplectic index $I = 1, \cdots, 2n$, also it satisfies the real condition

  $$(\boldsymbol{\Phi}^{AI})^\dagger = \epsilon_{AB}\Omega_{IJ}\boldsymbol{\Phi}^{BJ}$$

  where $\Omega_{IJ}$ is the invariant symplectic form of $\mathrm{USp}(2n)$. If one specializes to a cotangent type representation $Q \cong R \oplus R^*$, then one can decompose $2n \times 2n$ matrix $\boldsymbol{\Phi}^{AI}$ into $n$ $2\times 2$ blocks.

  $$\boldsymbol{\Phi}^{AI} = (\boldsymbol{\Phi}^1, \cdots, \boldsymbol{\Phi}^n)$$

  where

  $$\boldsymbol{\Phi}^i = \begin{pmatrix} X_i & Y_i \\ -\bar{Y}_i & \bar{X}_i \end{pmatrix} \tag{1.2.3}$$

  Here $(X_i, Y_i)$ are chiral fields and $(-\bar{Y}_i, \bar{X}_i)$ are anti-chiral fields. $X, Y$ transform under the unitary representation $R, R^*$ and the pair $(X, Y)$ parameterize a complex vector space $T^*R = R \oplus R^*$. $(X, \bar{Y})$ transform in the fundamental representation of $\mathrm{SU}(2)_H$ and unitary representation $R$ of the gauge group $G$ and $(Y_i, \bar{X}_i)$ in the dual.

### 1.2.2 Symmetries of 3d $\mathcal{N}=4$ Theories

The $3d$ $\mathcal{N}=4$ theories enjoy some symmetries which depend on the gauge group $G$ and its representation $\rho: G \to \mathrm{Sp}(n)$.

- *R-symmetry* For $3d$ $\mathcal{N}=4$ supersymmetry, it has 8 real supercharges and R-symmetry group is $\mathrm{SO}(4) \cong \mathrm{SU}(2)_H \times \mathrm{SU}(2)_C$. They rotate the scalars in hypermultiplet and vector multiplet respectively. If the spinor indices are denoted as $A, B, \cdots$ for $\mathrm{SU}(2)_H$ and $\dot{A}, \dot{B}, \cdots$ for $\mathrm{SU}(2)_C$. The supersymmetric algebra becomes

$$\{Q_\alpha^{A\dot{A}}, Q_\beta^{B\dot{B}}\} = \epsilon^{AB}\epsilon^{\dot{A}\dot{B}}(\sigma^\mu)_{\alpha\beta}P_\mu. \tag{1.2.4}$$

  Here the eight supercharges $Q^{A\dot{A}}$ transforms under the R-symmetry group $\mathrm{SU}(2)_H \times \mathrm{SU}(2)_C$. The super-Poincaré algebra admits so-called central extension which will introduce the additional generators that commute with $P_\mu$, $J_\nu^\mu$ and $Q_\alpha^{A\dot{A}}$. The deformed supersymmetry algebra is

$$\{Q_\alpha^{A\dot{A}}, Q_\beta^{B\dot{B}}\} = \epsilon^{AB}\epsilon^{\dot{A}\dot{B}}(\sigma^\mu)_{\alpha\beta}P_\mu + \epsilon_{\alpha\beta}\epsilon^{AB}Z^{\dot{A}\dot{B}} + \epsilon_{\alpha\beta}\epsilon^{\dot{A}\dot{B}}Z^{AB} \tag{1.2.5}$$

  where $Z^{AB}, Z^{\dot{A}\dot{B}}$ are scalar central charge associated to the flavor symmetry and they are charged under R-symmetry, and $A, B$ indices are symmetric. Here, $Z^{AB}$ transforms in the adjoint representation **3** of the $\mathrm{SU}(2)_H$ and $Z^{\dot{A}\dot{B}}$ transforms in the adjoint representation **3** of the $\mathrm{SU}(2)_C$. Usually one can use the $(\sigma^\mu)_{\alpha\beta}$'s components

$$(\sigma^\mu)_{\alpha\beta} = \left\{ \begin{pmatrix} -1 & 0 \\ 0 & 1 \end{pmatrix}, \begin{pmatrix} -i & 0 \\ 0 & -i \end{pmatrix}, \begin{pmatrix} 0 & 1 \\ 1 & 0 \end{pmatrix} \right\} \tag{1.2.6}$$

  and introduce the components of $P_{\alpha\beta} = (\sigma^\mu)_{\alpha\beta}P_\mu$ as

$$P_{\alpha\beta} = \begin{pmatrix} -2P_{\bar{z}} & P_t \\ P_t & 2P_z \end{pmatrix} \tag{1.2.7}$$

  then the supersymmetric algebra (1.2.5) could be rewritten as

$$\{Q_+^{A\dot{A}}, Q_+^{B\dot{B}}\} = -2\epsilon^{AB}\epsilon^{\dot{A}\dot{B}}P_{\bar{z}}, \qquad \{Q_-^{A\dot{A}}, Q_-^{B\dot{B}}\} = 2\epsilon^{AB}\epsilon^{\dot{A}\dot{B}}P_z, \tag{1.2.8}$$

$$\{Q_+^{A\dot{A}}, Q_-^{B\dot{B}}\} = \{Q_-^{A\dot{A}}, Q_+^{B\dot{B}}\} = \epsilon^{AB}\epsilon^{\dot{A}\dot{B}}P_t + \epsilon^{AB}Z^{\dot{A}\dot{B}} + \epsilon^{\dot{A}\dot{B}}Z^{AB}. \tag{1.2.9}$$

- *Flavor symmetry* Flavor symmetry commutes with the super-Poicaré algebra so it is a global symmetry. There are two types of global symmetries of $3d$ $\mathcal{N}=4$ theories, i.e. the Higgs branch global symmetry and the Coulomb branch global symmetry. For a generic quaternionic representation $\rho: G \to \mathrm{Sp}(n)$, the Higgs branch global symmetry is the normalizer $N_{\mathrm{Sp}(n)}(\rho(G))$ of the gauge group $G$ inside $\mathrm{Sp}(n)$ modulo

the action of the gauge group

$$G_H = N_{\mathrm{Sp}(n)}(\rho(G))/\rho(G). \tag{1.2.10}$$

For a theory of cotangent type specified by a unitary representation $\rho : G \to U(n)$, the Higgs branch global symmetry is

$$G_H = N_{\mathrm{U}(n)}(\rho(G))/\rho(G). \tag{1.2.11}$$

When there is an $U(1)$ factor in the gauge group $G$, there is a UV Coulomb branch global symmetry called *topological symmetry* manifests [35]. It rotates the periodic dual photon $\gamma$ defined by $d\gamma = *dA_{\mathrm{U}(1)}$ for each Abelian factor in $G$ . It is the Pontryagin dual of Abelian part of $G$ (which is also the center of GNO dual of $G$. )

$$G_C = Z(\hat{G}) = \mathrm{Hom}(\pi_1(G), U(1)) \cong U(1)^r, \tag{1.2.12}$$

if there are $r$ $U(1)$ factors in $G$. This symmetry is independent of the hypermultiplet representation and it only carries monopole operators. So this U(1) topological symmetry carries the magnetic charges of the gauge group, magnetic objects such as monopole operators and vortices in the following discussions carry nontrivial U(1) topological charges. Moreover, this U(1) topological symmetry may be enhanced to a non-abelian group in the IR region in a way that strongly depends on the hypermultiplet representation and the Coulomb branch global symmetry becomes its maximal torus $T_C$. As it has shown above, in $3d$ $\mathcal{N}=4$ gauge theory, the global flavor symmetry is $G_H \times G_C$ and its maximal torus is $T_H \times T_C$. The Cartan subalgebra of maximal torus will be denoted as $\mathfrak{t}_H \oplus \mathfrak{t}_C$, where $\mathfrak{t}_H = \mathrm{Lie}(T_H)$ and $\mathfrak{t}_C = \mathrm{Lie}(T_C)$. Here $G_H$ and $G_C$ are distinguished by their generators $J_H$ and $J_C$ contribute to the central extension of super-Poincaré algebra differently.

Apart from the vector multiplet and hypermultiplets, one needs the mass parameters and Fayet-Iliopoulos parameters to determine the Lagrangian of a $3d$ $\mathcal{N}=4$ gauge theory. One can assume that the scalar central charge $Z^{AB}$ and $Z^{\dot{A}\dot{B}}$ are proportional to $J_C$ and $J_H$ which are the generators of the Cartan subalgebra of the flavor symmetries of Coulomb and Higgs branch [83], i.e.

$$Z^{AB} = \eta^{AB} \cdot J_C \quad Z^{\dot{A}\dot{B}} = m^{\dot{A}\dot{B}} \cdot J_H. \tag{1.2.13}$$

$\eta^{AB}$ is called *Fayet-Iliopoulos parameter* (in short, FI parameter) and it takes value in $\mathfrak{t}_C$ and transforms in the adjoint representation $\mathbf{3}$ of $\mathrm{SU}(2)_H$. It associated with the $U(1)$ factor of the gauge group and can be viewed as the vacuum expectation value for scalar $\sigma^{AB}$ in a twisted vector multiplet for $G_C$ which is the vector multiplet with $\mathrm{SU}(2)_H$ and $\mathrm{SU}(2)_C$ interchanges. $m^{\dot{A}\dot{B}}$ is called *mass parameter* and it taks value in $\mathfrak{t}_H$ and transforms in the adjoint representation $\dot{\mathbf{3}}$ of $\mathrm{SU}(2)_C$. It can be viewed as the vacuum expectation value for scalar $\sigma^{\dot{A}\dot{B}}$ in a vector multiplet for $G_H$. Usually, one can make a simplication by focusing on real masses and real FI parameter. One can set the components $\eta^{11} = 0$ and $m^{\dot{1}\dot{1}} = 0$ and define

$$\eta = \eta^{12} \quad m = m^{\dot{1}\dot{2}}. \tag{1.2.14}$$

Because they are charged under R-symmetry, so one can take non-vanishing expectation values of $\eta$ and $m$, then the R-symmetry $\mathrm{SU}(2)_H \times \mathrm{SU}(2)_C$ will be broken down to the maximal torus $\mathrm{U}(1)_H \times \mathrm{U}(1)_C$ commuting with $m$ and $\eta$. If one pick the generic values of $m$ and $\eta$, then they will also break the flavor symmetry $G_H \times G_C$ down to a maximal torus $T_H \times T_C$.

### 1.2.3 The Supersymmetric Vacua

Supersymmetric vacua are configurations of the fields that are annihilated by all the supercharges, which also minimize the Euclidean action of the system. Classically, these are configurations of the vector multiplet field $(A, \sigma, \phi)$ and hypermultiplet fields $(X, Y)$ preserving all the supersymmetries. Hinging on the various parameters $m$ and $\eta$, there may exist perturbative as well as non-perturbative corrections. The supersymmetric vacua are the solutions of following two systems of equations,

The real set:

$$\mu_{\mathbb{R}} - \eta = 0 \tag{1.2.15}$$
$$(\sigma \cdot J + m \cdot J_H) \cdot X = 0 \tag{1.2.16}$$
$$(\sigma \cdot J + m \cdot J_H) \cdot Y = 0 \tag{1.2.17}$$
$$[\sigma, \varphi] = 0 \tag{1.2.18}$$

The complex set:

$$\mu_{\mathbb{C}} = 0 \tag{1.2.19}$$
$$(\varphi \cdot J) \cdot X = 0 \tag{1.2.20}$$
$$(\varphi \cdot J) \cdot Y = 0 \tag{1.2.21}$$
$$[\varphi, \varphi^\dagger] = 0 \tag{1.2.22}$$

Here (1.2.15) and (1.2.19) introduces the real moment map $\mu_{\mathbb{R}} : T^*R \to \mathfrak{g}^*$ and complex moment map $\mu_{\mathbb{C}} : T^*R \to \mathfrak{g}^* \otimes \mathbb{C}$ which are functions. Recall that $(X, Y)$ parameterizes a complex vector space $T^*R = R \oplus R^*$, this complex vector space has Kähler form $\omega$ and holomorphic symplectic forms $\Omega$ which are given by

$$\omega = dX \wedge d\bar{X} + dY \wedge d\bar{Y}, \qquad \Omega = dX \wedge dY. \tag{1.2.23}$$

Then $\mu_{\mathbb{R}}$ is the real moment map for $G$ associated to $\omega$ and $\mu_{\mathbb{C}}$ is the complex moment map for $G$ associated to $\Omega$. Equation (1.2.16), (1.2.17) and (1.2.20), (1.2.21) mean that if one act with gauge transformation and flavor transformation that generated by real or complex scalars on hypermultiplets, then it has to vanish. Finally, (1.2.18) and (1.2.22) means that all of the scalars in the vector multiplet commute among themselves.

The above vacua equations are critical points of the real superpotential $h$ and complex superpotential $\mathcal{W}$,

$$\begin{aligned} h &= \sigma \cdot (\mu_{\mathbb{R}} - \eta) + m \cdot \mu_{H,\mathbb{R}} \\ \mathcal{W} &= \varphi \cdot \mu_{\mathbb{C}} \end{aligned} \tag{1.2.24}$$

here $\mathcal{W}$ can be viewed as a $3d$ $\mathcal{N}=2$ superpotential, $\sigma \in \mathfrak{g}$, $\phi \in \mathfrak{g}_{\mathbb{C}}$ and $m$ is real mass. Also, $\mu_{H,\mathbb{R}}$ denotes the real moment map for the $G_H$ action on $T^*\mathbb{R}$. Here for simplicity, one can assume that $\sigma$ and $\phi$ are simultaneously diagonalized to a common Cartan subalgebra $\mathfrak{t} \subset \mathfrak{g}$.

- *Coulomb branch* The Coulomb branch $\mathcal{M}_C$ is characterized by the vacuum expectation value of the three real scalars, i.e. $\sigma, \phi$ in the vector multiplets together with the monopole operators. Due to the vacuum expectation values of these scalars being diagonal, thus the gauge group $G$ will be broken into the maximal torus at the classical level. The low-energy gauge fields can be dualized to dual photon which parameterize additional directions in the moduli space. So the classical description of Coulomb branch is given by [43]

$$\mathcal{M}_C = (\mathbb{R}^3 \times S^1)^{\mathrm{rk}(G)}/\mathcal{W}, \tag{1.2.25}$$

where $\mathbb{R}^3$ is parameterized by three scalars $\phi_i$ $(i = 1, 2, 3)$ and $S^1$ is parameterized by dual photon $\gamma$. $\mathcal{W}$ denotes the Weyl group of $G$. $\mathcal{M}$ receives both perturbative and non-perturbative quantum corrections [31, 84]. It is acted on by the $\mathrm{SU}(2)_C$ symmetry and can be found by setting the chiral fields in hypermultiplet $(X^i, Y_i) = 0$ and turning off the FI parameters、

Monopole operators imply that there exist singularities in the configuration of fundamental fields in the path integral. If one consider a 't Hooft monopole operator $V_m$, there will be some non-trivial Dirac monopole configuration in a small 2-sphere $S^2_p$ around an insertion point $p$,

$$A_\pm = \frac{m}{2}(\pm 1 - \cos\theta) d\phi \tag{1.2.26}$$

where $m \in \mathfrak{g} = \mathrm{Lie}(G)$. Meanwhile $m$ can also be viewed as a singled-valued transition function between two patches, i.e. $m : S^1 \to G$, $S^1$ is the equator of the $S^2_p$, $A_\pm$ denote the gauge field on the northern/southern regions $U_\pm \in S^2_p$. Because the transition function between these two regions has to be single-valued function, therefore one needs to impose

$$\exp(2\pi i m) = \mathbb{1}_G, \tag{1.2.27}$$

where $m \in \Gamma^*_{\hat{G}}$, which is the weight lattice of the GNO dual group of G. If one considers the gauge-invariant operators, then the fluxes $m \in \Gamma^*_{\hat{G}}/\mathcal{W}_{\hat{G}}$ [85]. Furthermore, monopole operators are charged under the center of GNO group $Z(\hat{G}) = \Gamma^*_{\hat{G}}/\Lambda_r(\hat{\mathfrak{g}})$ which can be viewed as topological symmetry, here $\Lambda_r(\mathfrak{g})$ is the root lattice of $\mathfrak{g} = \mathrm{Lie}(G)$. The monopole operator indices a $G$-bundle on $S^2_p$ with the connection, and this topological symmetry measures the topological degree $d \in \pi_1(G)$ of the $G$-bundle which is the homotopy class of the transition function $m : S^1 \to G$.

In 3d $\mathcal{N}=4$ theory, one should include supersymmetric monopole operators [86]. They are the singularities of the configurations space of fields that annihilates the supersymmetry variations of gauginos. Due to the presence of the GNO monopole flux $m$, $G$ is broken to its commutant $H_m \subset G$.

Furthermore, for the complex adjoint scalars $\phi$, one can also switch on a constant background. Depending on this background complex adjoint scalar $\phi = 0$ or $\phi \in \mathfrak{h}_m$, the $\mathcal{N}=2$ BPS monopole operators are called bare and dressed monopole operators respectively.

The R-charge of the BPS bare monopole operator of charge $m$ is [87–89]

$$\Delta(m) = -\sum_{\alpha\in\Delta_+}|\alpha(m)| + \frac{1}{2}\sum_{i=1}^{n}\sum_{\rho_i\in\mathcal{R}_i}|\rho_i(m)|, \tag{1.2.28}$$

this R-charge is defined in the infrared CFT. Here the first term comes from the $\mathcal{N}=4$ vector multiplets which sums over all positive roots $\alpha\in\Delta_+$ and the second term is contributed by $n$ $\mathcal{N}=4$ hypermultiplets. Here the $\mathcal{R}_i$ are the weights of the matter field representation under $G$. There was a criterion for classifying the 3d $\mathcal{N}=4$ theories [87]. A theory is named as *good* if *all* BPS monopole operators have $\Delta>\frac{1}{2}$; *ugly* if *all* BPS monopole operators satisfy the constraint $\Delta\geq\frac{1}{2}$ where $\Delta=\frac{1}{2}$ is called the unitary bound; *bad* if there *exist* BPS monopole operators satisfy $\Delta<\frac{1}{2}$ that contravening the unitary bound.

- *Higgs branch* $\mathcal{M}_H$ The Higgs branch of 3$d$ $\mathcal{N}=4$ theory with gauge group $G$ and matter $R\oplus R^*\cong\mathbb{C}^n\oplus\mathbb{C}^n$ is parameterized by the VEV of the scalars $X,Y$ in the hypermultiplets. The $\mathrm{SU}(2)_H$ symmetry will act on the Higgs branch. It is a hyper-Kähler quotient space

$$\mathcal{M}_H = (R\oplus R^*)///G = \{X,Y|\mu_{\mathbb{C}}=\mu_{\mathbb{R}}=0\}/G$$

which satisfies the superpotential constraint(F-term constraint) and D-term constraint

$$\mu_{\mathbb{C}} = \frac{\partial\mathcal{W}}{\partial\phi} = X\dot{Y} = 0 \quad \text{(Superpotential constraint)} \tag{1.2.29}$$

$$\mu_{\mathbb{R}} = X\cdot X^\dagger - Y^\dagger\cdot Y = 0 \quad \text{(D-term constraint)} \tag{1.2.30}$$

The Higgs branch is exempted from quantum corrections, so its classical geometry is exact.

### 1.2.4 Line Defects in 3d $\mathcal{N}=4$ Supersymmetric Gauge Theories

In principle, one can decompose the spacetime $\mathbb{R}^3$ as $\mathbb{C}_z\times\mathbb{R}_t$ where $z=x^1+ix^2$, $x^1,x^2$ are real Euclidean coordinates. Then there could have half-BPS line operators supported along $\mathbb{R}_t$ at the origin of the $\mathbb{C}$-plane. These line operators are preserved by two different types of 1d $\mathcal{N}=4$ SUSY subalgebra of the (1.2.8), which are called as $\mathrm{SQM}_A$ and $\mathrm{SQM}_B$ [49]. They preserve so-called vortex line operators and Wilson line operators respectively. $\mathrm{SQM}_A$ subalgebra is generated by the supercharges $Q^{\dot{a}}_A=\delta^\alpha_a Q^{a\dot{a}}_\alpha$, $\tilde{Q}^{\dot{a}}_A=(\sigma^3)^\alpha_a Q^{a\dot{a}}_\alpha$ and it preserve $\mathrm{SU}(2)_C$ R-symmetry and break $\mathrm{SU}(2)_H$ R-symmetry to its diagonal $\mathrm{U}(1)_H$ subgroup. Similarly, $\mathrm{SQM}_B$ subalgebra is generated by the supercharges $Q^a_B=\delta^\alpha_{\dot{a}}Q^{a\dot{a}}_\alpha$, $\tilde{Q}^a_B=(\sigma^3)^\alpha_{\dot{a}}Q^{a\dot{a}}_\alpha$ and it preserve $\mathrm{SU}(2)_H$ R-symmetry and break $\mathrm{SU}(2)_C$ R-symmetry to its diagonal $\mathrm{U}(1)_C$ subgroup.

- *Wilson line operator* Wilson line operators are preserved by $\mathrm{SQM}_B$. It can be thought of a theory of 1d $\mathcal{N}=4$ SQM preserve $\mathrm{SQM}_B$ symmetry living on the Wilson line to be coupled with the 3d $\mathcal{N}=4$ bulk

theory. One can introduce the complexified connection

$$\mathcal{A}_\mu = A_\mu - \frac{i}{2}(\sigma_\mu)_{\dot{A}\dot{B}}\phi^{\dot{A}\dot{B}}. \tag{1.2.31}$$

where the connection 1-form $\mathcal{A} \in \mathfrak{g}_{\mathbb{C}}$. Its component $\mathcal{A}_t = A_t - i\sigma$ is preserved by 1d $\mathrm{SQM}_B$. Let $V = \mathbb{C}^n$ is a complex-linear representation of complexified gauge group $G_{\mathbb{C}}$ and $\rho : \mathfrak{g}_{\mathbb{C}} \to \mathfrak{gl}(n)$. Then one can define a half-BPS Wilson line operator supported on line $\ell$ as

$$\mathcal{W} = \mathrm{Hol}_\ell(\rho(\mathcal{A})) = \boldsymbol{P}\exp\int_{\mathbb{R}_t}\rho(\mathcal{A}_t)dt \tag{1.2.32}$$

- *Vortex line* Vortex line operators are preserved by $\mathrm{SQM}_A$ which can be viewed as a 1d $\mathcal{N}=4$ SQM living on the line, coupled with the 3d $\mathcal{N}=4$ theory in the bulk by gauging 1d flavor symmetries with 3d background vector multiplets [35]. This gauging identifies the 1d $\mathcal{N}=4$ flavor symmetries with 3d $\mathcal{N}=4$ flavor symmetries by introducing a $\mathrm{SQM}_V$-invariant superpotential $\mathcal{W}$ which couples 1d chiral multiplets with 3d hypermultiplets. There are vortices carrying magnetic fluxes in the Higgs branch where the monopoles become the 1/2-BPS interfaces in 1d vortex quantum mechanics living on the vortex worldlines. For $\mathrm{U}(N)$ gauge theory with $N_f$ fundamental hypermultiplets and a real FI parameter $t_{\mathbb{R}} > 0$, there is a submanifold of the Higgs branch which admits vortex solutions is Grassmannian, the Higgs branch is the cotangent bundle of this Grassmannian $G(N, N_f)$ (assuming that $N_f \geq 2N$). On each point of Higgs vacuum $G(N, N_f)$, there are BPS vortices labeled by $\nu$. Then the family of vortex solutions form the moduli space of vortex $\mathcal{M}_\nu^n$ whose complex dimension is $nN_f$ which respect symmetry $\mathrm{U}(1)_z \times \mathrm{SU}(N) \times \mathrm{SU}(N_f - N)$, where $\mathrm{U}(1)_z$ is the Lorentz rotation around z-plane, and $\mathrm{SU}(N) \times \mathrm{SU}(N_f - N)$ is the isometries on Higgs branch.

## 1.3 Quiver Gauge Theory and Brane Realisation of 3d $\mathcal{N}=4$ Theories

### 1.3.1 Quiver Gauge Theory

The quiver gauge theory can be constructed as follows: for a gauge group $G$, one can embed its representation $\phi : G \to \mathrm{GL}(V)$ into a finite-dimensional vector space $V$. A quiver diagram encodes the vector multiplets of the SYM theory with vertices and hypermultiplets with links between the vertices. For each vertex $i$, there is a vector space $V_i$ associated with it which is acted by the semi-simple component of the gauge group. Generally, an oriented link from vertex $V_i$ to vertex $V_j$ represents a complex scalar transforming in the representation $\tilde{V}_i \otimes V_j \cong \mathrm{Hom}(V_i, V_j)$. Two links with opposite orientations will comprise a single hypermultiplet.

If there is a quiver gauge theory with gauge group $G$, then there is an electric 1-form symmetry $\ker\phi \subset G$ will act trivially on the matter content [37]. If there is a normal subgroup $H \subset \ker\phi$, then one can take the

quotient with respect to $H$, which physically equivalent to gauging the 1-form symmetry $H$ [10, 16, 38] that affects the spectrum of admissible line operators[37, 90, 91]. For the Wilson line operators that transform under the $G$-invariant but not $H$-invariant representations, they will be charged under the 1-form symmetry. After gauging this 1-form symmetry, the line defects will not survive because the corresponding representation is not permissible.

A quiver diagram for 3d $\mathcal{N}=4$ theories encodes the field contents as follows:

- Gauge nodes of a quiver ◯ encode the dynamical 3d $\mathcal{N}=4$ vector multiplets , while flavour nodes □ denote background vector multiplets. The notation are

$$\underset{k}{\circ} \longleftrightarrow \mathrm{U}(k) \qquad \underset{k}{\bullet} \longleftrightarrow \mathrm{SO}(k) \qquad \underset{2k}{\bullet} \longleftrightarrow \mathrm{Sp}(k) \tag{1.3.1}$$

  and the same colour-coding is used for flavour nodes. Here underlying gauge groups and flavor groups could be U($n$), SU($n$), SO($n$) and Sp($n$).
- An edge linking a pair of gauge nodes yields a hypermultiplet $H=(X,Y^\dagger)$, which consists of two $\mathcal{N}=2$ chiral multiplets $X,Y$. In a unitary quiver, an edge represents

$$\underset{k_1}{\circ}\!\!-\!\!\underset{k_2}{\circ} \longleftrightarrow \text{bi-fundamental hypermultiplet:} \quad H=(X,Y^\dagger)\in \mathbf{k_1}\otimes\overline{\mathbf{k_2}} \tag{1.3.2}$$

  *i.e.* each chiral multiplet transforms as bi-fundamental $X\in\mathbf{k_1}\otimes\overline{\mathbf{k_2}}$ and $Y\in\overline{\mathbf{k_1}}\otimes\mathbf{k_2}$. In an orthosymplectic quiver, an edge represents

$$\underset{k_1}{\bullet}\!\!-\!\!\underset{2k_2}{\bullet} \longleftrightarrow \text{half-hypermultiplet:} \quad h=(X,JY)\in \mathbf{k_1}\otimes\mathbf{2k_2} \tag{1.3.3}$$

  Here for each single chiral multiplet, it *does not* transform as $\mathbf{k_1}\otimes\mathbf{2k_2}$. One needs to use the Sp($k_2$) invariant tensor $J$ to define the half-hypermultiplet $h=(X,JY)$ that transforms appropriately.

Here let's introduce the criteria of classifying 3d $\mathcal{N}=4$ theories into *good*, *ugly*, or *bad* based on the *balance* of the gauge groups [87]. When there is a $G=\mathrm{U}(n),\mathrm{SO}(n),\mathrm{Sp}(n)$ gauge node in the quiver connecting to $N_f$ fundamental flavours, the *good* nodes satisfy

$$\text{for U}(n):\ N_f\geq 2n\,,\qquad \text{for SO}(n):\ N_f\geq n-1\,,\qquad \text{for Sp}(n):\ N_f\geq n+1\,. \tag{1.3.4}$$

Here if the equality is established, it corresponds to *balanced* node and the symmetry of $\mathcal{M}_C$ will be enhanced to a non-abelian group because of the presence of the monopole operators. Further, if the inequality strictly holds, then the corresponding node is called *over-balanced*.

### 1.3.2 Brane Realisation of 3d $\mathcal{N}=4$ Theories

The 3d $\mathcal{N}=4$ theories could be realized as a brane system in type IIB superstring theory [30]. There are 3 different types of brane as listed in Table 1.1, and their correspondences to the quiver diagrams are illustrated as follows

- D5-branes give rise to flavor symmetry in quiver diagrams.
- NS5-branes separate one gauge from another and give rise to those edges connecting the circle nodes in the quiver diagrams.
- D3-branes can give edge connecting the circle nodes and the square nodes when D3-branes and D5-branes are living in the same chamber in brane configurations.

The brane system will break the 10-dimensional spacetime symmetry into

$$\mathrm{SO}(1,9) \to \mathrm{SO}(1,2) \times \mathrm{SO}(3)_{3,4,5} \times \mathrm{SO}(3)_{7,8,9} \tag{1.3.5}$$

and the rotational symmetries $\mathrm{SO}(3)_{3,4,5} \subset \mathrm{SU}(2)_C$ and $\mathrm{SO}(3)_{7,8,9} \subset \mathrm{SU}(2)_H$ realise the 3d $\mathcal{N}=4$ R-symmetry $\mathrm{SO}(4)_R \cong \mathrm{SU}(2)_C \times \mathrm{SU}(2)_H$ geometrically. The configurations of branes in spacetime are depicted in 1-1. If one introduces one brane, half the supercharges would be broken; but if one puts the third brane into two 3-branes, the supersymmetry will not be further broken. Hence, the system preserves 8 supercharges. Here are the field contents of the effective theory on the 3-brane [30]:

- *Vector Multiplets* It will engender U(1) vector multiplet if a D3-brane has both ends on NS5 branes. Furthermore, if there are $n$ parallel D3-branes suspended between two NS5-branes, then there will be $n$ vector multiplets and preserve the $\mathrm{U}(1)^n$ gauge symmetry. When these $n$ parallel D3-branes coincide, the gauge symmetry would be enhanced to $\mathrm{U}(n)$ gauge symmetry via Chan-Paton factors. Under a low-energy limit, this will give a 3d $\mathrm{U}(N)$ theory living on the world-volume of D3 branes. The reason for 3d is because the D3 brane has a finite length along the $x^6$ direction between two NS5 branes and the $x^6$ direction becomes invisible under the low-energy limit.
- *Hypermultiplets* A hypermultiplet transforms under the fundamental representation of $\mathrm{U}(N)$ can be encoded in brane system by an intersection between a D5 and a D3-brane extended between two NS5-branes. When there is an open string extended between a D3 and D5-brane, it will engender a hypermultiplet. For a specific NS5-brane, if there are $N_1$ D3-branes attached to it from the left and $N_2$ D3-branes attached to it from the right, this configuration will be encoded as a hypermultiplet transforms in a bi-fundamental representation of $\mathrm{U}(N_1) \times \mathrm{U}(N_2)$.

Branes can be created or annihilated. When an NS5 brane pass through a D5-brane, then it will create a D3-brane connecting the D5-brane and NS5-brane [30]. This is called the Hanany-Witten move. As for the brane realizations of parameters in 3d $\mathcal{N}=4$ theories, the difference between the relative position of NS5 branes regards to the D3-brane in chamber $i$ corresponds to the triplet of FI parameters, and the difference between the relative position of D5 branes regards to the D3-brane in chamber $i$ corresponds to the triplet mass parameters.

The supersymmetric vacua are encoded in brane configuration and quiver diagram as follows

- *Coulomb Branch* $\mathcal{M}_C$ is the moduli space of D3-branes between NS5-branes, and the quaternionic dimension of $\mathcal{M}_C$ is equal to the total number of circle node in the quiver diagram.
- *Higgs Branch* $\mathcal{M}_H$ can be regarded as the hyper-Kähler quotient. One can introduce a complex matrix $A_{n_1\times n_2}$ for the hypermultiplet transforming in the bi-fundamental representation $\mathbf{n}_1 \otimes \bar{\mathbf{n}}_2$ of $GL(n_1)\times GL(n_2)$, then the matrix $A$ is equivalent to $g_1 A g_2^{-1}$ with $g_1 \in GL(n_1)$ and $g_2 \in GL(n_2)$. The hyper-Kähler quotient is the set of all matrices coming from edges that are subject to critical points of superpotential $\mathcal{W}$ and satisfy the equivalence relation. If there is a set of functions of this hyper-Kähler quotient, then these functions are going to transform under a representation of the corresponding symmetries associated to the flavour nodes.

The notations for various branes and orientifold are:

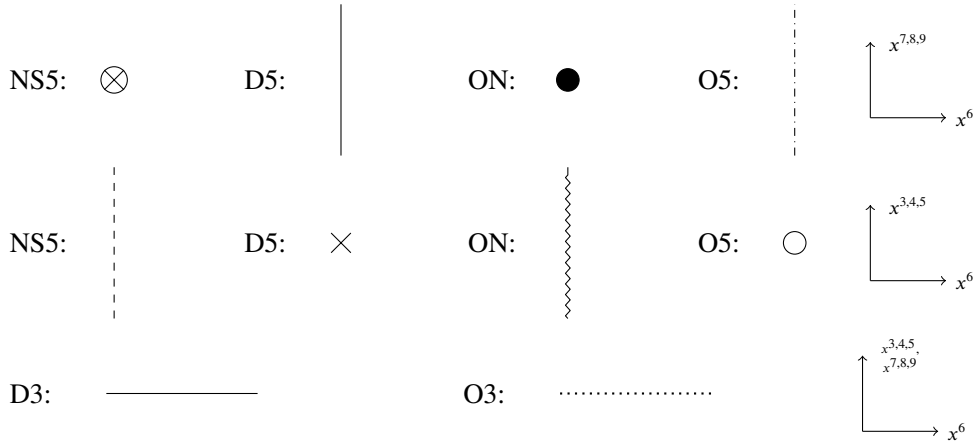


(1.3.6)

Besides the basic setup of the D3-D5-NS5 brane system in type IIB string theory, one can include various orientifolds and orbifold planes to enlarge the classes of 3d $\mathcal{N}=4$ quiver gauge theories. There are three types of them that need to be considered: O3, O5, and ON planes [33, 34, 87, 92–95].

| IIB | 0 | 1 | 2 | 3 | 4 | 5 | 6 | 7 | 8 | 9 |
|---|---|---|---|---|---|---|---|---|---|---|
| NS5/ON | × | × | × | × | × | × | | | | |
| D3/O3 | × | × | × | | | | × | | | |
| D5/O5 | × | × | × | | | | | × | × | × |
| | $\leftarrow \mathbb{R}^{1,2} \rightarrow$ | | | $\leftarrow \mathbb{R}^3_{3,4,5} \rightarrow$ | | | | $\leftarrow \mathbb{R}^3_{7,8,9} \rightarrow$ | | |
| | | | | $\circlearrowleft \mathrm{SU}(2)_C$ | | | | $\circlearrowleft \mathrm{SU}(2)_H$ | | |

**Table 1-1.** Space-time occupation of the D3-D5-NS5 setup in Hanany's paper [30]. Likewise, O3 or O5 planes occupy the same spacetime dimensions as D3 or D5 branes, respectively; while ON planes are parallel to NS5 branes.

The line operators are encoded in the brane system as follows:

- *Wilson loop* A supersymmetric Wilson loop can be obtained by an F1 string extended along the $x^5$ direction, one side of the string attaches to a stack of $N$ D3 branes. Because of the introduction of the F1 string, the rotational symmetry will be broken as

$$\mathrm{SO}(3)_{3,4,5}\times \mathrm{SO}(3)_{7,8,9} \rightarrow \mathrm{SO}(2)_{3,4}\times \mathrm{SO}(3)_{7,8,9} \subset \mathrm{U}(1)_C \times \mathrm{SU}(2)_H \tag{1.3.7}$$

But if an F1 string terminated on a D5 or D5' brane, then the supersymmetry would not be broken further, as shown in Figure 1-1, and the representation of the Wilson line would change depending on whether it ends on D5 or D5'.

For the case of an F1 string extended between N D3 branes and a D5' brane, there is the 1d massive complex fermion in the representation of $\mathrm{U}(1)\times\mathrm{U}(N)$. Its mass is proportional to the $x^5$ coordinate of the D5' brane. For $k$ F1 strings, one can integrate out the massive fermions then they can engender a supersymmetric Wilson loop operator transformed under the $k$-th anti-symmetric representation $\mathcal{A}^k$ of $\mathrm{U}(N)$. The weight of $\mathcal{A}^k$ is manifest in various ways of extending $k$ F1 strings between the D3 and D5' branes.

For the F1 string extended between N D3 branes and a D5 brane, it will give a heavy hypermultiplet transforms in $\mathrm{U}(1)\times\mathrm{U}(N)$. For $k$ F1 strings, one can integrate out the heavy hypermultiplets then they can engender the insertion of a supersymmetric Wilson line operator transforms under the $k$-th symmetric representation $\mathcal{S}^k$ of $\mathrm{U}(N)$. According to the s-rule, the weight of $\mathcal{S}^k$ is manifest in the brane configuration. Note that there is no restriction against the number of F1 strings extending between the same D3 and D5 pair.

| IIB | 0 | 1 | 2 | 3 | 4 | 5 | 6 | 7 | 8 | 9 |
|---|---|---|---|---|---|---|---|---|---|---|
| NS5 | × | × | × | × | × | × | | | | |
| D3 | × | × | × | | | | × | | | |
| D5 | × | × | × | | | | | × | × | × |
| F1 | × | | | | | × | | | | |
| D5′ | × | | | × | × | | | × | × | × |
| | ← $\mathbb{R}^{1,2}$ → | | | $\mathbb{R}^2_{3,4}$ $\circlearrowleft \mathrm{U}(1)_C$ | | | | ← $\mathbb{R}^3_{7,8,9}$ → $\circlearrowleft \mathrm{SU}(2)_H$ | | |

**(a)**

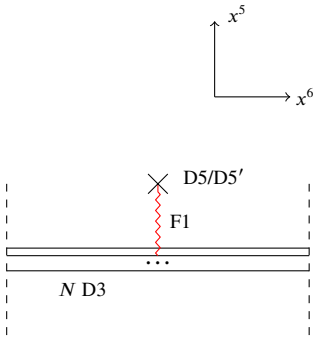


**(b)**

**Fig. 1-1.** Brane realisation of Wilson line defects.

- *Vortex loop* A supersymmetric vortex loop can be obtained by extending a D1 string along the $x^9$ direction, one end of the string adheres to a pile of D3 branes. Because of the introduction of the D1 string, the rotational symmetry will be broken as follows:

$$\mathrm{SO}(3)_{3,4,5}\times\mathrm{SO}(3)_{7,8,9}\to\mathrm{SO}(3)_{3,4,5}\times\mathrm{SO}(2)_{7,8}\subset\mathrm{SU}(2)_C\times\mathrm{U}(1)_H \tag{1.3.8}$$

But if a D1 string terminated on an NS5 or NS5' brane, then the supersymmetry would not be broken further, as shown in Figure 1-2, and the representation of the vortex line would change depending on whether it ends on NS5 or NS5'. One could derive a 1d $\mathcal{N}=4$ description of the vortex if one parallelizes a D1 brane and an extra fivebrane with a closet NS5-brane in the same brane configuration. This will define a 1d theory as shown in Fig 1-2b. The gauge coupling is given by the inverse of the distance between the NS5 and NS5' brane along $x^9$ direction, also the relative distance along $x^6$ coordinate corresponds to the 1d FI parameter $\eta$ which can be both positive and negative. Figure 1-2b will give a $\eta>0$ (respectively,

$\eta < 0$ ) deformation associated to the left (right, respectively) NS5-brane.

| IIB | 0 | 1 | 2 | 3 | 4 | 5 | 6 | 7 | 8 | 9 |
|---|---|---|---|---|---|---|---|---|---|---|
| NS5 | × | × | × | × | × | × | | | | |
| D3 | × | × | × | | | | × | | | |
| D5 | × | × | × | | | | | × | × | × |
| D1 | × | | | | | | | | | × |
| NS5′ | × | | | × | × | × | | × | × | |
| | $\leftarrow \mathbb{R}^{1,2} \rightarrow$ | | | $\underbrace{\leftarrow \mathbb{R}^3_{3,4,5} \rightarrow}_{\circlearrowleft \mathrm{SU}(2)_C}$ | | | | $\underbrace{\mathbb{R}^2_{7,8}}_{\circlearrowleft \mathrm{U}(1)_H}$ | | |

**(a)**

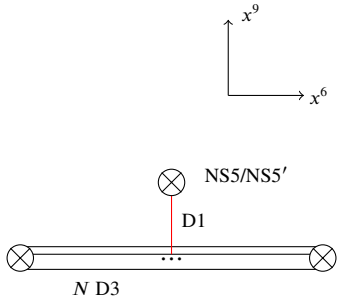


**(b)**

**Fig. 1-2.** Brane realisation of vortex line defects.

## 1.4 Mirror Symmetry of 3d $\mathcal{N}=4$ Supersymmetric Gauge Theories

The main topic of this thesis is an important duality—3d mirror symmetry. Duality in quantum field theory provides a powerful tool to deal with the strongly coupled phase where the traditional methods become useless. 3d mirror symmetry was firstly proposed by Intriligator and Seiberg in 1996 [32] as an IR duality that two different UV descriptions $\mathcal{T}$ and $\mathcal{T}'$ of 3d $\mathcal{N}=4$ gauge theories flow to the same infrared conformal fixed points. These two theories are related to each other by exchanging the moduli spaces of supersymmetric vacua, global symmetries, mass and FI parameters, i.e.

- *Moduli spaces* $\mathcal{M}_C \Longleftrightarrow \mathcal{M}'_H \qquad \mathcal{M}_H \Longleftrightarrow \mathcal{M}'_C$
- *Global symmetries* $G_C \Longleftrightarrow G'_H \qquad G_H \Longleftrightarrow G'_C$
- *Mass and FI parameters* $m_i \Longleftrightarrow \eta'_i \qquad \eta_i \Longleftrightarrow m'_i$

The R-symmetry for $\mathcal{N}=4$ theory is $\mathrm{SO}(4) \cong \mathrm{SU}(2)_C \times \mathrm{SU}(2)_H$, mirror symmetry will interchange these two SU(2) factors. Under the global $R$-symmetry, the vector multiplet transforms under the adjoint representation of $\mathrm{SU}(2)_C$ and keeps invariant under $\mathrm{SU}(2)_H$, and hypermultiplet transforms under the adjoint representation of $\mathrm{SU}(2)_H$ and keeps invariant under $\mathrm{SU}(2)_C$. Furthermore, mass parameter transforms under the representation $(\mathbf{3},\mathbf{1})$ of $\mathrm{SU}(2)_C \times \mathrm{SU}(2)_H$ and the FI parameter transforms under the representation $(\mathbf{1},\mathbf{3})$ of $\mathrm{SU}(2)_C \times \mathrm{SU}(2)_H$. Thus under 3d mirror symmetry, $(\mathcal{M}_C, m)$ of one theory maps to $(\mathcal{M}_H, \eta)$ of another theory.

The full 3d $\mathcal{N}=4$ superconformal algebra is OSp(4|4), and the vortex line defects and Wilson line defects will flow to superconformal defects in IR which preserve the $\mathrm{U}(1,1|2)_V$ and $\mathrm{U}1,1|2_W$ respectively. Note that the quantum corrections of one theory will convert into the classical effect in its mirror theory. Therefore the information of $\mathcal{M}_C$ with quantum correction will be encoded in the information of $\mathcal{M}_H$ of its mirror dual at the classical level.

In brane setup, $\mathcal{M}_C$ usually can be read off from the brane configurations, while $\mathcal{M}_H$ of the theory can be obtained by splitting the D3 brane between the NS5-branes and D5-branes [34]. Then the S-duality can

interchange the D5-brane and NS5-brane and keep D3-brane as it is, meanwhile the theory living inside the world-volume of the D3 branes will undergo the electric-magnetic duality transformation. The above descriptions are complete for the unitary quiver theory. However, when there are Sp($k$) or SO($2k$) gauge nodes get involved, one must introduce the orientifold planes, and S-duality will also act on them according to specific rules. In the end, one can obtain the dual theory from the dual brane configuration.

Furthermore, the 3d mirror symmetry will also map the Wilson line operators and vortex line operators into each other. This also provides one method to verify the 3d mirror symmetry.

## 1.5 Supersymmetric Localization

In order to check the 3d $\mathcal{N} = 4$ unitary and orthosymplectic duality, we need to evaluate the exact partition functions and study the spectra of line operators of two dual theories. Generally speaking, an exact partition function is given by an infinite-dimensional path integral over the field configurations. The supersymmetric localization technique provides a powerful tool to reduce this infinite-dimensional integral to a finite-dimensional integral. We give the general idea of this technique as follows. Consider the Euclidean path integral

$$Z_{\mathcal{M}} = \int_{\mathcal{M}} \mathcal{D}\Phi e^{-S[\varphi]}. \tag{1.5.1}$$

which integrates over all possible field configurations on a compact manifold $\mathcal{M}$. Suppose $\mathcal{Q}$ is a fermionic symmetry of the action. One can deform the partition function by adding an $\mathcal{Q}$-exact term $\mathcal{Q}V$ such that $Z_{\mathcal{M}}$ relies on the parameter $t$

$$Z_{\mathcal{M}}(t) = \int_{\mathcal{M}} \mathcal{D}\varphi e^{-S[\Phi]-t\mathcal{Q}V}. \tag{1.5.2}$$

Here, the compactness of the manifold ensures the above integral is convergent, and one can assume that $\mathcal{Q}^2 = 0$ such that $\mathcal{Q}^2 V = 0$ is automatically true. Then one can take differential of the partition function with respect to parameter $t$ which gives

$$\frac{\partial Z_{\mathcal{M}}(t)}{\partial t} = \int \mathcal{D}\Phi(\mathcal{Q}V)e^{-S-t\mathcal{Q}V} = \int \mathcal{D}\Phi\mathcal{Q}(Ve^{-S-t\mathcal{Q}V}) \tag{1.5.3}$$

where one assumes that the action is invariant under $\mathcal{Q}$ and $\mathcal{Q}$ is non-anomalous such that the measure is also $\mathcal{Q}$-invariant. Therefore $Z(t)$ is independent to $t$, so the value of $Z(t = \infty)$ is equal to the value of $Z(t = 0)$. When $t \to \infty$, the linear term of $t$ in the exponential of (1.5.2) should not disappear, which requires that

$$\mathcal{Q}V = 0 \tag{1.5.4}$$

The set of field configurations $\sigma(x)$ which satisfies (1.5.4) is called the saddle point, the corresponding partition function taking the values at saddle point is called $Z_{cl}(\sigma)$. All field configurations satisfied $\mathcal{Q}V > 0$ are infinitely impressed when $t \to \infty$, therefore the path integral *localizes* to the stationary points.

At the saddle point, the $\mathcal{O}(t^1)$ terms on the exponential of (1.5.2) vanishes, so one can expand the exponential around the saddle point, since the first-order term vanishes, then the perturbation of field configurations around the saddle point start from the second-order terms which will give a Gaussian integral. This part is called 1-loop partition function $Z_{1-loop}(\sigma)$. Thus the partition function (1.5.2) can be written as

$$Z = \int_{\text{saddle points}} \mathcal{D}\sigma Z_{cl}(\sigma) Z_{1-loop}(\sigma). \tag{1.5.5}$$

The above discussion holds for general $V$. However, one can choose some special $V$ to transform the path integral (1.5.2) into a finite dimensional integral on $\sigma$

$$Z = \int_{\text{saddle points}} d\sigma Z_{cl}(\sigma) Z_{1-loop}(\sigma). \tag{1.5.6}$$

Note that it is important to choose the manifold $\mathcal{M}$ appropriately, there are two reasons [96]: firstly, there exist some manifolds and backgrounds that will reduce the path integral to a much simpler problem which makes the moduli spaces more tractable; secondly, different manifolds and supersymmetric backgrounds will give different sectors of operators and correlators, including those between holomorphic and antiholomorphic operators and conserved currents.

## 1.6 Chern-Simons Theory and Knot Theory

This subsection mainly talks about another topic of this thesis–Knot theory.

### 1.6.1 Chern-Simons Theory and Knot Categorification

A knot $K$ is an embedding of $S^1$ into $\mathbb{R}^3$. In [50], the quantum invariants of 3-manifolds and knots can be beautifully interpreted under the framework of Chern-Simons theory. The Chern-Simons path integral on a 3-manifold $M$ with boundary is

$$Z(M, G) = \int_{\mathcal{A}/\mathcal{G}} \mathcal{D}\mathcal{A} e^{iS_{CS}} \tag{1.6.1}$$

here the path integral depends on manifold $M$ and a semi-simple compact Lie group $G$ as gauge group, integrating over the equivalence classes of gauge fields in the space $\mathcal{A}$ of gauge connections with respect to gauge transformations $g \in \mathcal{G}$. (1.6.1) is also called Witten-Reshetikhin-Turaev (WRT) invariant. $S_{CS}$ is Chern-Simons action which is metric-independent,

$$S_{CS} = \frac{k}{4\pi} \int_M \text{Tr}(A \wedge dA + \frac{2}{3} A \wedge A \wedge A) \tag{1.6.2}$$

where gauge field $A$ is the connection on the principal G-bundle $E \to M$, $k \in \mathbb{Z}$ is level.

Chern-Simons functional can be viewed as the Morse function of the space $\mathcal{A}$ and its critical points are given by the equation of motion

$$dA + A \wedge A = 0 \tag{1.6.3}$$

The gauge field $A$ which satisfies (1.6.3) is called a flat connection. Denote the moduli space of the flat connections on $M$ as $\mathcal{M}_{\text{flat}}(G, M)$. Then there is a natural mapping $\mathcal{M}_{\text{flat}}(G, M) \hookrightarrow \mathcal{M}_{\text{flat}}(G, \Sigma)$ by restricting to the boundary $\Sigma = \partial M$ which will result in a Lagrangian submanifold of $\mathscr{C} \subset \mathcal{M}_{\text{flat}}(G, \Sigma)$. If $\Sigma$ is a Riemann surface, then the moduli space of the flat connections on $\Sigma$ is given by the homomorphisms $\rho : \pi_1(\Sigma) \to G$ modulo the gauge transformations which act on $\rho$ by conjugation,

$$\mathcal{M}_{\text{flat}} = \text{Hom}(\pi_1(\Sigma) \to G)/G \tag{1.6.4}$$

where $G$ is the compact semi-simple gauge group. As shown by Atiyah and Bott [97], there is a natural symplectic form on $\mathcal{M}$

$$\omega = \frac{1}{4\pi^2} \int_\Sigma \text{Tr} \delta A \wedge \delta A \tag{1.6.5}$$

where $\delta$ is the exterior derivative on $\mathcal{M}$ which make $\delta A$ be one-form on $\mathcal{M}$ also on $\Sigma$.

In Chern-Simons theory, one can use some metric-independent and gauge invariant observables to construct the correlation functions which can be viewed as topological invariants. Wilson loop is this kind of observable. One can include a Wilson loop in the representation $R$ of $G$ along the knot $K \subset S^3$, then the expectation value of the Wilson loop $W_R(K) = \text{Tr}_R \text{Hol}_K(A) = \text{Tr}_R \exp(\oint_K A)$ is a quantum invariant of $K$, i.e.

$$\overline{J}^G_R(K; q) := \langle W_R(K) \rangle = \frac{\int [\mathcal{D}A]\, e^{iS} W_R(K)}{\int [\mathcal{D}A]\, e^{iS}}, \tag{1.6.6}$$

Here $q$ can be written in terms of the level $k$ and the dual Coxeter number $h^\vee$ of $G$ as

$$q = \exp\left(\frac{\pi i}{k + h^\vee}\right). \tag{1.6.7}$$

Specifically, when $M = S^3$, $G = \text{SU}(2)$ and $R$ is fundamental representation of SU(2), (1.6.6) is equal to the famous Jones polynomials $J(K, q)$ [98], which is a Laurent polynomial generally, $J(K, q) \in \mathbb{Z}[q^{\frac{1}{2}}, q^{-\frac{1}{2}}]$. Generally, $R$ could be any finite-dimensional representation of SU(2) which leads to $J_R(K; q)$. When $R$ is an $n$-dimensional irreducible representation [50, 99, 100], (1.6.6) will give the $n$-colored Jones polynomials $J_n(K, q)$. For $G = \text{SU}(N)$, (1.6.6) gives the two-variable colored HOMFLY-PT polynomials $P_R(K; a, q)$. Here $R$ denotes a representation of SU($N$) and $a = q^N$. For $G = \text{SO}(N)$, (1.6.6) give the colored Kauffman polynomial $F_R(K; a, q)$, $R$ denotes a representation of SO($N$) and $a = q^{N-1}$. For $G = \text{Sp}(N)$, (1.6.6) also give the colored Kauffman polynomial $F_R(K; a, q)$ but with $a = q^{N+1}$.

Now consider the concept of the categorification. Depending on the context, categorification has different meanings. Generally speaking, the categorification of a 3d TQFT will result in a 4d TQFT, and one can obtain the 3d TQFT from the 4d one by dimension reduction [101, 102]. Khovanov [103] constructed the categorification

of Jones polynomials by associating a chain complex to a link diagram $K$. He showed that the homology $H_{i,j}(K)$ of this chain complex is a knot invariant. The Poincaré polynomial of $H_{i,j}(K)$ is:

$$\mathrm{Kh}(K;q,t)=\sum_{i,j}t^i q^j \dim H_{i,j}(K)$$

when $t=-1$, one can recover the Jones polynomial

$$J(K;q)=\mathrm{Kh}(K;q,t=-1)=\sum_{i,j}(-1)^i q^j \dim H_{i,j}(K) \tag{1.6.8}$$

Later Khovanov and Rozansky proposed a triply-graded homology $\mathscr{H}_{ijk}$ whose graded Euler characteristic gives the the HOMFLY-PT polynomial [52]. The Poincaré polynomial of HOMFLY-PT homology is

$$\mathscr{P}(K;a,q,t)=\sum_{ijk}t^i q^j a^k \dim \mathscr{H}_{ijk} \tag{1.6.9}$$

when $t=-1$, one can recover the HOMFLY-PT polynomials:

$$P_{a,q}(K)=\mathscr{P}(K;a,q,t=-1)=\sum_{ijk}(-1)^i q^j a^k \dim \mathscr{H}_{ijk} \tag{1.6.10}$$

HOMFLY-PT homology is a stronger tool to distinguish knots and it is an interesting mathematical object [53]. Also, in [55], the $[r]$-colored triply-graded HOMFLY-PT homology $(\mathscr{H}_{[r]})_{i,j,k}(K)$ and its Poincaré polynomial called $[r]$-colored superpolynomial was proposed,

$$\mathscr{P}_{[r]}(K;a,q,t)=\sum_{ijk}t^i q^j a^k \dim(\mathscr{H}_{[r]}(K))_{ijk} \tag{1.6.11}$$

In the same way, the Kauffman homology can be obtained from the Kauffman polynomial by categorifying. In [54], the Kauffman homology was proposed and its structural properties were also studied. Later on, the quadruply-graded colored HOMFLY-PT homology was constructed in [55, 56]. The structures of this homology was studied thoroughly. One can define the $[r^s]$-colored Poincaré polynomial of the quadruply-graded HOMFLY-PT homology as

$$\mathscr{P}_{[r^s]}(K;a,q,t_r,t_c):=\sum_{i,j,k,l}a^i q^j t_r^k t_c^l \dim(\mathscr{H}^{\text{HOMFLY-PT}}_{[r^s]}(K))_{i,j,k,l} \tag{1.6.12}$$

Here $[r^s]$ denotes an $r\times s$ rectangular Young diagram. One can regrade the $\mathscr{H}^{\text{HOMFLY-PT}}_{[r^s]}(K)$ to define a tilde-version of colored quadruply-graded HOMFLY-PT homology as [57, 104]

$$\widetilde{\mathscr{H}}^{\text{HOMFLY-PT}}_{[r^s]}(K))_{i,j,k,l}:=\mathscr{H}^{\text{HOMFLY-PT}}_{[r^s]}(K))_{i,sj-k+l,k,l} \tag{1.6.13}$$

whose Poincaré polynomial is given by

$$\widetilde{\mathscr{P}}_{[r^s]}(K;a,Q,t_r,t_c) := \sum_{i,j,k,l} a^i Q^j t_r^k t_c^l \dim\left(\widetilde{\mathscr{H}}^{\text{HOMFLY-PT}}_{[r^s]}(K)\right)_{i,j,k,l} \tag{1.6.14}$$

In the above formula, for a generator $x$ and the representation specified by Young diagram $[r^s]$, the $Q$-grading is defined as

$$Q(x) := \frac{q(x)+t_r(x)-t_c(x)}{s} \tag{1.6.15}$$

Note that (1.6.12) and (1.6.14) have the relation

$$\widetilde{\mathscr{P}}_{[r^s]}(K;a,q,t_r,t_c) = \mathscr{P}_{[r^s]}(K;a,q,t_r,t_c) \tag{1.6.16}$$

Similarly, the triply-graded uncolored Kauffman homology was also proposed [54, 105]. And the existence of a quadruply-graded colored Kauffman homology was conjectured [57] and its structures were also discussed. The $[r^s]$-colored Poincaré polynomial of the quadruply-graded Kauffman homology can be defined as

$$\mathscr{F}_{[r^s]}(K;\lambda,q,t_r,t_c) := \sum_{i,j,k,l} \lambda^i q^j t_r^k t_c^l \dim(\mathscr{H}^{\text{Kauffman}}_{[r^s]}(K))_{i,j,k,l} \tag{1.6.17}$$

One can regrade the $\mathscr{F}^{\text{Kauffman}}_{[r^s]}(K)$ to define a tilde-version of colored quadruply-graded Kauffman homology as

$$\widetilde{\mathscr{H}}^{\text{Kauffman}}_{[r^s]}(K))_{i,j,k,l} := \mathscr{H}^{\text{Kauffman}}_{[r^s]}(K))_{i,sj-k+l,k,l} \tag{1.6.18}$$

whose Poincaré polynomial is given by

$$\widetilde{\mathscr{F}}_{[r^s]}(K;\lambda,Q,t_r,t_c) := \sum_{i,j,k,l} \lambda^i Q^j t_r^k t_c^l \dim\left(\widetilde{\mathscr{H}}^{\text{Kauffman}}_{[r^s]}(K)\right)_{i,j,k,l} \tag{1.6.19}$$

Here the definition of $Q$-grading is also given by (1.6.15). Analog to the HOMFLY-PT case, (1.6.17) and (1.6.19) have the relation

$$\widetilde{\mathscr{P}}_{[r^s]}(K;a,q,t_r,t_c) = \mathscr{P}_{[r^s]}(K;a,q,t_r,t_c) \tag{1.6.20}$$

There is a special case of Chern-Simons theory that is useful for the following discussion about the quantum $6j$-symbols, i.e. the Chern-Simons theory on three-sphere $S^3$. Consider a Chern-Simons theory on three-sphere $S^3$ with $\mathrm{U}(1)\times\mathrm{SU}(N)$ gauge group whose levels are $k_1$, $k_2$ respectively. The $\mathrm{U}(1)$ gauge connection is denoted as $B$, and the $\mathrm{SU}(N)$ gauge connection is denoted as $A$, then the Chern-Simons action can be written as

$$S = \frac{k_1}{4\pi}\int_{S^3} B\wedge dB + \frac{k_2}{4\pi}\int_{S^3} \mathrm{Tr}(A\wedge dA + \frac{2}{3}A\wedge A\wedge A) \tag{1.6.21}$$

Now the Wilson loop operator of a link $\mathcal{L}$ with $r$ components $\mathcal{K}_\alpha$ is

$$W_{\{(R_i,n_i)\}}[\mathcal{L}] = \prod_{\alpha=1}^{r} \mathrm{Tr}_{R_\alpha} U^A[\mathcal{K}_\alpha] \mathrm{Tr}_{n_\alpha} U^A[\mathcal{K}_\alpha] \tag{1.6.22}$$

where $R_\alpha$ are the representation carried by the component $\mathcal{K}_\alpha$ and $n_\alpha$ is the U(1)-charge carried by the component $\mathcal{K}_\alpha$. According to the (1.6.6), then the expectation value of the Wilson loop operator is

$$V^{\mathrm{U}(N)}_{\{(R_i,n_i)\}}[\mathcal{L}] := \left\langle W_{\{(R_i,n_i)\}}[\mathcal{L}] \right\rangle = \frac{\int [\mathcal{D}B]\mathcal{D}A e^{iS} W_{\{(R_i,n_i)\}}[\mathcal{L}]}{\int [\mathcal{D}B]\mathcal{D}A e^{iS}} = V^{\mathrm{SU}(N)}_{\{(R_i,n_i)\}}[\mathcal{L}] V^{\mathrm{U}(1)}_{\{(R_i,n_i)\}}[\mathcal{L}] \tag{1.6.23}$$

If the representation $R_\alpha$ of the component $\mathcal{K}_\alpha$ is given by a Young diagram with total number of boxes $l_\alpha$, then one can choose the U(1)-charge $n_\alpha = \frac{l_\alpha}{\sqrt{N}}$ and $k_1 = k_2 + N$, then the invariant (1.6.23) is a polynomial in $q = \exp\left(\frac{2\pi i}{k+N}\right)$ and $\lambda = q^N$.

### 1.6.2 Super-$A$-Polynomials

In Gukov's work [60], A-polynomial emerged as the algebraic curve described the classical and quantum properties of the theory when there is a Wilson loop in an infinite-dimensional representation of $\mathrm{SL}(2,\mathbb{C})$. The main idea is explained as follows.

Consider a knot $K$ in $S^3$, denote the open tubular neighborhood of $K$ as $N(K)$ which is homeomorphic to a solid torus, i.e. $N(K) \cong D^2 \times S^1$. Then the knot complement $M = S^3 \backslash N(K)$ is a compact 3-manifold with torus boundary $\partial M = \Sigma = T^2$. Then $\pi_1(M)$ is called knot group, and $\pi_1(\Sigma)$ is called peripheral group. Now the representaion of knot group is given by $\rho : \pi_1(M) \to \mathrm{SL}(2,\mathbb{C})$. One can restrict this representation to the boundary torus, i.e. $\pi_1(\Sigma) \to \mathrm{SL}(2,\mathbb{C})$. Since $\Sigma = T^2$, there are two generators of peripheral subgroup $\pi_1(\Sigma) = \mathbb{Z} \times \mathbb{Z}$, which are two cycles, called longitude $\gamma_l$ and $\gamma_m$. Since $\pi_1(\Sigma)$ is free Abelian group, therefore the matrices $\rho(\gamma_m)$ and $\rho(\gamma_l)$ commute and can be simultaneously brought into Jordan normal forms up to the conjugacy by $\mathrm{SL}(2,\mathbb{C})$ elements,

$$\rho(\gamma_m) = \begin{pmatrix} x & * \\ 0 & x^{-1} \end{pmatrix}, \qquad \rho(\gamma_l) = \begin{pmatrix} y & * \\ 0 & y^{-1} \end{pmatrix} \tag{1.6.24}$$

here $x, y \in \mathbb{C}^*$ which parameterizing the representation of peripheral subgroup $\pi_1(\Sigma)$ into $\mathrm{SL}(2,\mathbb{C})$. So there is a map assigns two complex numbers to each representation of knot group,

$$\begin{aligned} L = \mathrm{Hom}(\pi_1(M), \mathrm{SL}(2,\mathbb{C}))/\mathrm{SL}(2,\mathbb{C}) &\to \mathcal{P} = \mathrm{Hom}(\pi_1(\Sigma), \mathrm{SL}(2,\mathbb{C}))/\mathrm{SL}(2,\mathbb{C}) = (\mathbb{C}^* \times \mathbb{C}^*)/\mathbb{Z}_2 \\ \rho &\to (x, y) \end{aligned} \tag{1.6.25}$$

where $\mathbb{Z}_2$ is the Weyl group symmetry of $\mathrm{SL}(2,\mathbb{C})$ with the action $(x, y) \mapsto (x^{-1}, y^{-1})$. This is the representation variety of the $T = \partial M$. Moreover, a basis $(\gamma_m, \gamma_l)$ of $\pi_1(\Sigma)$ gives an embedding of $L$ into $\mathcal{P}$, and one can show

that the variety $L$ is the zero locus of a single polynomial $A(x, y)$, called A-polynomial [60, 106] which is an algebraic curve

$$L = \{(x, y) \in (\mathbb{C}^* \times \mathbb{C}^*)/\mathbb{Z}_2 | A(x, y) = 0\}. \tag{1.6.26}$$

which is a holomorphic Lagrangian sub-manifold of (1.6.4) and the symplectic form (1.6.5) turns into

$$\omega = \frac{i}{\hbar} d \log x \wedge d \log y. \tag{1.6.27}$$

The corresponding Liouville 1-form of above symplectic form is $\frac{i}{\hbar} \log y \frac{dx}{x}$, which satisfies the integrality condition

$$\oint_\Gamma \log y \frac{dx}{x} \in 2\pi^2 \mathbb{Q} \tag{1.6.28}$$

where $\Gamma$ is a closed cycle in the algebraic curve $L$.

For any knot complement $M = S^3 \backslash K$, there is an abelianization of $\pi_1(M)$ which is $H_1(M) \cong \mathbb{Z}$. Therefore the $A$-polynomial always contains a $(y-1)$ factor which encodes the information of the Abelian representation and other pieces encode the information of non-Abelian representations. Note that for hyperbolic knots, $A(x, y) \neq y - 1$ which means that it always contains information of non-Abelian representations. And it is possible for different knots to have the same $A$-polynomials [107], therefore it is *not* a complete knot invariant.

Now one can consider the generalized volume conjecture [60], which closely related to $A$-polynomial. Note that one can obtain the complexified gauge group $\mathrm{SL}(2, \mathbb{C})$ or $\mathrm{PSL}(2, \mathbb{C})$ by complexifying SU(2) or SO(3), respectively. The quantum knot invariants, colored by representations of $\mathfrak{g} = \mathfrak{sl}(2)$ or $\mathfrak{g} = \mathfrak{so}(3)$ which can be specified by a single row Young tableaux $[r]$ with length $r$, are denoted as $J^{\mathfrak{g}}_{[r]}(K; q)$. In the classical limit $q = e^{\hbar} \to 1$ and the large color limit $r \to \infty$ with $x = q^r$ fixed, the $[r]$-colored quantum knot invariant $J^{\mathfrak{g}}_{[r]}(K; q)$ behaves like

$$J^{\mathfrak{g}}_{[r]}(K; q) \underset{x=q^r}{\overset{r\to\infty, \hbar\to 0}{\sim}} \exp\left(\frac{1}{\hbar} S_0(x)) + \mathcal{O}(\hbar^0)\right) \tag{1.6.29}$$

where $S_0(x)$ is the classical $\mathrm{SL}(2, \mathbb{C})$ Chern-Simons action evaluated at point $x$ on the Riemann surface

$$S_0(x) = \int_{x_*}^{x} \log y \frac{dx}{x}, \tag{1.6.30}$$

and $\mathcal{O}(\hbar^0)$ represents the regular terms as $\hbar \to 0$, the integral is performed along the curve $A(x, y) = 0$ from some fixed base point $x_*$ to point $x$, and (1.6.30) makes sense only when integrality condition (1.6.28) holds. Because the change $\Delta S_0 \in 2\pi\mathbb{Z}$ when the integration path is an arbitrary closed cycle, so that $e^{iS_0}$ is well-defined and independent of path.

Fuji, Gukov and Sulkowski proposed [64] that there are two commutative deformations of the $A$-polynomial which can be parameterized by $a$ and $t$, called super-$A$-polynomial, denoted as $A^{\text{super}}(x, y, a, t)$. For super-$A$-polynomial, one have the following relations with $a$-deformed $A$-polynomial and $Q$-deformed $A$-polynomial

[108]:

$$A^{\text{super}}(x, y; a = 1, t) := A^{\text{ref}}(x, y; t) \tag{1.6.31}$$

$$A^{\text{super}}(x, y; a, t = -1) := A^{\text{Q-ref}}(x, y; t) \tag{1.6.32}$$

$$A^{\text{super}}(x, y; a = 1, t = -1) := A(x, y) \tag{1.6.33}$$

The volume conjecture for super-$A$-polynomial was proposed in [64]. The conjecture is in the classical limit $q = e^{\hbar} \to 1$ and the large color limit $r \to \infty$ with $a$, $t$ and $x = q^r$ fixed, then the $[r]$-colored superpolynomials $\mathscr{P}_{[r]}(a, q, t)$ behaves in the form

$$P_{[r]}(K; a, q, t) \underset{x=q^r}{\overset{r\to\infty,\hbar\to 0}{\sim}} \exp\left(\frac{1}{\hbar}\int \log y \frac{dx}{x} + \mathcal{O}(\hbar^0)\right) \tag{1.6.34}$$

where $\mathcal{O}(\hbar^0)$ represents the regular terms as $\hbar \to 0$ and the integral in the leading term on the right-hand side is performed on the zero locus of the super-$A$-polynomial $A^{\text{super}}(K; x, y; a, t) = 0$.

In [57], the super-$A$-polynomial of $[r]$-colored Kauffman homology was proposed. In the classical limit $q = e^{\hbar} \to 1$ and the large color limit $r \to \infty$ with $\lambda$, $t$ and $x = q^r$ fixed, then the Poincaré polynomial of $[r]$-colored Kauffman homology $\mathscr{F}(K; \lambda, q, t, 1)$ behaves in the form

$$\mathscr{F}_{[r]}(K; a, q, t, 1) \underset{x=q^r}{\overset{r\to\infty,\hbar\to 0}{\sim}} \exp\left(\frac{1}{\hbar}\int \log y \frac{dx}{x} + \mathcal{O}(\hbar^0)\right). \tag{1.6.35}$$

The integral is performed on the zero locus of the SO-type super-$A$-polynomial,

$$A^{\text{SO}}(K; x, y; \lambda, t) = 0 \tag{1.6.36}$$

### 1.6.3 Quantum $6j$-Symbols

Quantum knot invariants can also be computed via braiding and duality matrices in the Wess-Zumino-Novikov-Witten (WZNW) models [50]. In this method, a kind of important mathematical object called $6j$-symbol comes along, it has a deep relation with Hopf algebra and quantum group theory [65, 70–74]. The $6j$-symbol was proposed by Wigner [75, 76] and Racah [77] and it could be written in terms of a hypergeometric series ${}_4F_3$. Later on, Kirillov and Reshetikhin [78] obtained the expression of quantum $6j$-symbols for $U_q(\mathfrak{sl}_2)$ case. Let's focus on their ideas first.

A Hopf algebra $\mathcal{B}$ is an associative algebra with a comultiplication $\Delta : \mathcal{B} \to \mathcal{B} \otimes \mathcal{B}$, a counit $\epsilon : \mathcal{B} \to \mathbb{C}$ and an antipole $\gamma : B \to B$ such that they satisfy the following relations:

$$(\Delta \otimes 1)\Delta = (1 \otimes \Delta)\Delta, \qquad (\epsilon \otimes 1)\Delta = (1 \otimes \epsilon)\Delta, \qquad (\mathrm{Id} \otimes \gamma)\Delta = (\gamma \otimes \mathrm{Id})\Delta = \epsilon.$$

The universal enveloping algebra $U_q(\mathfrak{sl}_2)$ [78] is generated by the elements $H, X^{\pm}$. They satisfy the following

commutation relations

$$\left[X^{\pm}, H\right] = \mp 2X^{\pm}, \quad \left[X^{+}, X^{-}\right] = \frac{q^{\frac{H}{2}} - q^{-\frac{H}{2}}}{q^{\frac{1}{2}} - q^{-\frac{1}{2}}} \tag{1.6.37}$$

These generators define a Hopf algebra on $U_q(\mathfrak{sl}_2)$ under the following operations:

- Comulitplication $\Delta(X^{\pm}) = X^{\pm} \otimes q^{\frac{H}{4}} + q^{-\frac{H}{4}} \otimes X^{\pm}, \quad \Delta(H) = H \otimes 1 + 1 \otimes H$
- Antipole $S(X^{\pm}) = -q^{\pm\frac{1}{2}} X^{\pm}, \quad S(H) = -H$
- Counit $\epsilon(H) = \epsilon(X^{\pm}) = 0$

One can define a permutation operator $\sigma$ in $U_q(\mathfrak{sl}_2)^{\otimes 2}$ as $\sigma(a \otimes b) = b \otimes a,\ a, b \in U_q(\mathfrak{sl}_2)$. Then with comultiplication $\Delta' = \sigma \cdot \Delta$ and antipole $S' = S^{-1}$, another Hopf algebra structure denoted by $U_q'(\mathfrak{sl}_2)$ could be defined. One can tell that $U_q(\mathfrak{sl}_2) = U_q'(\mathfrak{sl}_2)$ but the comultiplications $\Delta$ and $\Delta'$ are related to each other by an automorphism [109]

$$\Delta'(a) = R\Delta(a)R^{-1}. \tag{1.6.38}$$

Here $R \in U_q(\mathfrak{sl}_2)$ is called universal $R$-matrix and it can be written as [78]

$$R = \exp\left(\frac{h}{4} H \otimes H\right) \sum_{n \geq 0} \frac{(1 - q^{-1})^n}{[n]!} e^n \otimes f^n \tag{1.6.39}$$

where $[n] := \frac{q^{\frac{n}{2}} - q^{-\frac{n}{2}}}{q^{\frac{1}{2}} - q^{-\frac{1}{2}}}$ is the quantum number, $e = \exp\left(\frac{h}{4} H\right) X^{+}$ and $f = \exp\left(-\frac{h}{4} H\right) X^{-}$. One can consider the embedding of $R$-matrices in $U_q(\mathfrak{sl}_2)^{\otimes 3}$ which is labeled by the indices, then the universal $R$-matrix satisfies

$$(\Delta \otimes \mathrm{Id})R = R_{12}R_{23}, \quad (\mathrm{Id} \otimes \Delta)R = R_{13}R_{12}, \quad (S \otimes \mathrm{Id})R = R^{-1} \tag{1.6.40}$$

and one can obtain the famous Yang-Baxter equation

$$R_{12}R_{13}R_{23} = R_{23}R_{13}R_{12}. \tag{1.6.41}$$

Next, one could consider the representations of $U_q(\mathfrak{sl}_2)$. It is worth to note that all irreducible representations of $U_q(\mathfrak{sl}_2)$ are finite-dimensional, thus they can be described in the weight basis $\{e_m^j\}$ where $j \in \mathbb{Z}$ or $j \in \mathbb{Z} \bigoplus \frac{1}{2}$. Denote the representation labeled by $j$ as $\pi^j$ and its dimension is $\dim \pi^j = 2j + 1$. Then the generators $H, X^{\pm}$ of $U_q(\mathfrak{sl}_2)$ act in weight basis $\{e_m^j\}$ in the following ways [78]:

$$\pi^j(X^{\pm})e_m^j = \sqrt{[j \mp m][j \pm m + 1]}\, e_{m+1}^j \tag{1.6.42}$$

$$\pi^j(H)e_m^j = 2me_m^j \tag{1.6.43}$$

where $-j \leq m \leq j$ and $2m \equiv 2j (mod 2)$.

Denote the representation space of the irreducible representation $\pi^j$ of $U_q(\mathfrak{sl}_2)$ as $V^j$, there exists a matrix $R^{j_1 j_2} = (\pi^{j_1} \otimes \pi^{j_2})R$ acts on the tensor product $V^{j_1} \otimes V^{j_2}$. One can consider the $q$-analog of Clebsch-Gordan coefficients as follows. Suppose $\pi^{j_1}$ and $\pi^{j_2}$ are irreducible representations of $U_q(\mathfrak{sl}_2)$. Then $V^{j_1} \otimes V^{j_2}$ can be decomposed into irreducible representations like

$$V^{j_1} \otimes V^{j_2} = \bigoplus_{\substack{|j_1-j_2|\leq j\leq j_1+j_2 \\ 2j\equiv 2j_1+2j_2 (\mathrm{mod}2)}} V^j \tag{1.6.44}$$

If the weight basis in the irreducible component $V^j$ is denoted as $e^j_m(j_1 j_2)$, then the components of $e^j_m(j_1 j_2)$ in the basis $e^{j_1} \otimes e^{j_2}$ are called the *Clebsh-Gordan coefficients* (in short, CG coefficients),

$$e^j_m(j_1 j_2) = \sum_{m_1 m_2} \begin{bmatrix} j_1 & j_2 & j \\ m_1 & m_2 & m \end{bmatrix}_q e^{j_1}_{m_1} \otimes e^{j_2}_{m_2} \tag{1.6.45}$$

conversely, one has

$$e^{j_1}_{m_1} \otimes e^{j_2}_{m_2} = \sum_{jm} \begin{bmatrix} j_1 & j_2 & j \\ m_1 & m_2 & m \end{bmatrix}_q e^j_m(j_1 j_2)\delta(j_1 j_2 j), \tag{1.6.46}$$

where

$$\delta(j_1 j_2 j) = \begin{cases} 1, & \text{if } |j_1 - j_2| \leq j \leq j_1 + j_2, 2j \equiv (2j_1 + 2j_2) \bmod 2 \\ 0, & \text{Otherwise} \end{cases} \tag{1.6.47}$$

Here these CG coefficients satisfy the following properties

$$\sum_{m_1 m_2} \begin{bmatrix} j_1 & j_2 & j \\ m_1 & m_2 & m \end{bmatrix}_q \begin{bmatrix} j_1 & j_2 & j' \\ m_1 & m_2 & m' \end{bmatrix}_q = \delta_{jj'}\delta_{mm'}\delta(j_1 j_2 j) \tag{1.6.48}$$

$$\sum_{\substack{|j_1-j_2|\leq j\leq j_1+j_2 \\ |m|\leq j}} \begin{bmatrix} j_1 & j_2 & j \\ m_1 & m_2 & m \end{bmatrix}_q \begin{bmatrix} j_1 & j_2 & j \\ m'_1 & m'_2 & m \end{bmatrix}_q = \delta_{mm'_1}\delta_{mm'_2}. \tag{1.6.49}$$

Along a similar path, one can construct the $q$-analog of the Wigner-Racah $6j$-symbols [78]. This case involves the tensor product of three irreducible representations of $U_q(\mathfrak{sl}_2)$, i.e. $V^{j_1} \otimes V^{j_2} \otimes V^{j_3}$. In principle, there are two possible orthogonal bases in $V^{j_1} \otimes V^{j_2} \otimes V^{j_3}$ for this case. One possible basis can be obtained by decomposing $V^{j_1} \otimes V^{j_2} = \bigoplus_{j_{12}} V^{j_{12}}$ at first, then take irreducible submodules in $V^{j_{12}} \otimes V^{j_3}$,

$$e^{j_{12}j}_m(j_1 j_2|j_3) = \sum_{m_1 m_2 m_3} \begin{bmatrix} j_{12} & j_3 & j \\ m_{12} & m_3 & m \end{bmatrix}_q \begin{bmatrix} j_1 & j_2 & j_{12} \\ m_1 & m_2 & m_{12} \end{bmatrix}_q e^{j_1}_{m_1} \otimes e^{j_2}_{m_2} \otimes e^{j_3}_{m_3}. \tag{1.6.50}$$

Another possible basis can be obtained by decomposing $V^{j_2} \otimes V^{j_3} = \bigoplus_{j_{23}} V^{j_{23}}$ at first, then take irreducible

submodules in $V^{j_1} \otimes V^{j_{23}}$.

$$e_m^{j_{23}j}(j_1|j_2j_3) = \sum_{m_1m_2m_3} \begin{bmatrix} j_1 & j_{23} & j \\ m_1 & m_{23} & m \end{bmatrix}_q \begin{bmatrix} j_2 & j_3 & j_{23} \\ m_2 & m_3 & m_{23} \end{bmatrix}_q e_{m_1}^{j_1} \otimes e_{m_2}^{j_2} \otimes e_{m_3}^{j_3}. \tag{1.6.51}$$

and the elements of the transformation matrix between these two bases is called *quantum* SU*(2)* 6$j$*-symbols*,

$$e_m^{j_{12}j}(j_1j_2|j_3) = \sum_{j_{23}} \begin{Bmatrix} j_1 & j_2 & j_{12} \\ j_3 & j & j_{23} \end{Bmatrix}_q e_m^{j_{23}j}(j_1|j_2j_3) \tag{1.6.52}$$

When $q = 1$, the quantum SU(2) 6$j$-symbol can be related to Racah-Wigner 6$j$-symbols as

$$\begin{Bmatrix} j_1 & j_2 & j_{12} \\ j_3 & j & j_{23} \end{Bmatrix}_{q=1} = \sqrt{[2j_{12}+1][2j_{23}+1]}(-1)^{j_1+j_2-j-j_3-2j_{12}} \begin{Bmatrix} j_1 & j_2 & j_{12} \\ j_3 & j & j_{23} \end{Bmatrix}^{\mathrm{RW}} \tag{1.6.53}$$

where the 6$j$-symbol on the right-hand side is the Racah-Wigner 6$j$-symbol. Generally, the Racah-Wigner 6$j$-symbol has the following expression:

$$\begin{aligned} \begin{Bmatrix} a & b & e \\ d & c & f \end{Bmatrix}^{\mathrm{RW}} &= \Delta(abe)\Delta(acf)\Delta(ced)\Delta(dbf) \\ &\times \sum_{z\geq 0}(-1)^z[z+1]!\,\{[z-a-b-e]![z-a-c-f]![z-b-d-f]![z-d-c-e]! \\ &[a+b+c+d-z]![a+d+e+f-z]![b+c+e+f-z]!\}^{-1} \end{aligned} \tag{1.6.54}$$

where the quantum number $[x]$ and quantum factorial $[n]!$ are defined as

$$[x] = \frac{q^{x/2} - q^{-x/2}}{q^{1/2} - q^{-1/2}}, \quad [n]! = [n][n-1]\cdots[2][1], \tag{1.6.55}$$

and also

$$\Delta(abc) = \sqrt{\frac{[-a+b+c]![a-b+c]![a+b-c]!}{[a+b+c+1]!}}. \tag{1.6.56}$$

For $\mathrm{SU}(2)_q$ Racah coefficients, one has

$$a = j_1,\ b = j_2,\ d = j_3,\ c = j_4,\ e = j_{12},\ f = j_{23} \tag{1.6.57}$$

and the spins are related to each other by

$$\vec{j_1} + \vec{j_2} + \vec{j_3} = \vec{j_4},\ \ \vec{j_1} + \vec{j_2} = \vec{j_{12}},\ \vec{j_2} + \vec{j_3} = \vec{j_{23}}. \tag{1.6.58}$$

The relation between quantum 6$j$-symbols and quantum knot invariant emerges from the researches of

$SU(2)_k$ WZNW model. For a three manifold $M_3$ with $r$ boundaries $\Sigma^{(1)}, \cdots, \Sigma^{(r)}$, there could be $l$ Wilson lines ($l = 1, 2, \cdots$) with carrying spins $j_l^{(i}$, begin or end on the boundary $\Sigma^{(i}$ at some punctures (marked points) $P_l^{(i} \in \Sigma^{(i)}$. Witten found that [50] one can associate a Hilbert space $\mathcal{H}^{(i}$ on each boundary $\Sigma^{(i)}$ and the properties of $\mathcal{H}^{(i}$ can be determined from the conformal blocks of $SU(2)_k$ WZNW model on $\Sigma^{(i)}$ with punctures $P_l^{(i)}$. The total Hilbert space on the $\Sigma = \bigcup_{i=1}^r \Sigma^{(i)}$ is $\mathcal{H} = \bigotimes_{i=1}^r \mathcal{H}^{(i)}$, and the Chern-Simons functional on $M_3$ can be viewed as a state on $\mathcal{H}$.

For $SU(2)_k$ WZNW model, there are two ways to combine four spins $j_1, j_2, j_3, j_4$ into a SU(2) singlet [68]:

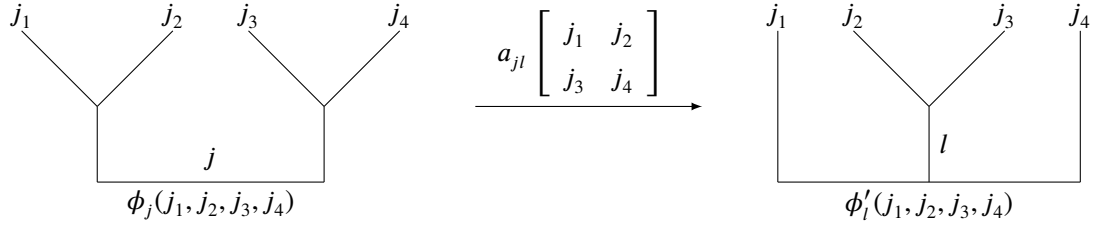


$(a)$ $(b)$

In the figure (a), the singlet is formed as follows: first $(j_1, j_2)$ and $(j_3, j_4)$ are combined into two common spin-$j$ representations separately by fusion rules of $SU(2)_k$ WZNW model, then these two spin-$j$ representations will combine into a $SU(2)_k$ singlet. In this way the allowed values of $j$ is $\max(|j_1 - j_2|, |j_3 - j_4|) \leq j \leq \min(j_1 + j_2, j_3 + j_4)$ if the level $k$ is sufficiently large enough. This representation is called as $\phi_j(j_1, j_2, j_3, j_4)$.

Whereas there is another way to form the singlet as shown in figure (b): first $(j_1, j_4)$ and $(j_2, j_3)$ are combined into two common spin-$l$ representations separately by fusion rules of $SU(2)_k$ WZNW model, then these two spin-$l$ representations will combine into a $SU(2)_k$ singlet. In this way the allowed values of $l$ is $\max(|j_1 - j_4|, |j_2 - j_3|) \leq l \leq \min(j_1 + j_4, j_2 + j_3)$ if the level $k$ is sufficiently large enough. This representation is called as $\phi'_l(j_1, j_2, j_3, j_4)$.

These two sets of representations are linearly independent and they can be related by so-called *duality matrix* or *fusion matrix* [68] as follows,

$$\phi_j(j_1, j_2, j_3, j_4) = \sum_l a_{jl} \begin{bmatrix} j_1 & j_2 \\ j_3 & j_4 \end{bmatrix} \phi'_l(j_1, j_2, j_3, j_4) \tag{1.6.59}$$

here the duality matrix relates to the quantum SU(2) $6j$-symbols

$$a_{jl} \begin{bmatrix} j_1 & j_2 \\ j_3 & j_4 \end{bmatrix} = (-1)^{j_1+j_2+j_3+j_4} \sqrt{[2j+1][2l+1]} \begin{Bmatrix} j_1 & j_2 & j \\ j_3 & j_4 & l \end{Bmatrix}_q \tag{1.6.60}$$

where the triplets $(jj_1j_2)$, $(jj_3j_4)$, $(lj_1j_4)$, $(lj_2j_3)$ satify the fusion rules

$$\max(|j_1 - j_2|, |j_3 - j_4|) \leq j \leq \min(j_1 + j_2, j_3 + j_4), \quad \max(|j_2 - j_3|, |j_1 - j_4|) \leq l \leq \min(j_1 + j_4, j_2 + j_3) \tag{1.6.61}$$

where $j_1+j_2+j \leq k$, $j_3+j_4+j \leq k$, $j_2+j_3+l \leq k$, $j_1+j_4+l \leq k$ also $j_1+j_2+j$, $j_3+j_4+j$, $j_2+j_3+l$, $j_1+j_4+l \in \mathbb{Z}$ needs to be satisfied. The phase in (1.6.60) is chosen such that $j_1 + j_2 + j_3 + j_4 \in \mathbb{Z}$.

Duality matrix satisfies the following properties:

- $\sum_j a_{jl} \begin{bmatrix} j_1 & j_2 \\ j_3 & j_4 \end{bmatrix} a_{jl'} \begin{bmatrix} j_1 & j_2 \\ j_3 & j_4 \end{bmatrix} = \delta_{ll'}$.
- $a_{jl} \begin{bmatrix} j_1 & j_2 \\ j_3 & j_4 \end{bmatrix} = a_{lj} \begin{bmatrix} j_1 & j_4 \\ j_3 & j_2 \end{bmatrix} = a_{lj} \begin{bmatrix} j_3 & j_2 \\ j_1 & j_4 \end{bmatrix} = a_{jl} \begin{bmatrix} j_3 & j_4 \\ j_1 & j_2 \end{bmatrix}$

Furthermore, there are also the following identities:

- $\sum_j a_{jl} \begin{bmatrix} j_1 & j_2 \\ j_3 & j_4 \end{bmatrix} = \sum_j a_{jl} \begin{bmatrix} j_2 & j_1 \\ j_4 & j_3 \end{bmatrix} = (-1)^{j_1+j_3-j-l} \sqrt{\frac{[2j+1][2l+1]}{[2j_1+1][2j_3+1]}} a_{j_1 j_3} \begin{bmatrix} j & j_2 \\ l & j_4 \end{bmatrix}$
- $a_{0l} \begin{bmatrix} j_1 & j_2 \\ j_3 & j_4 \end{bmatrix} = (-1)^{j_1+j_3-l} \sqrt{\frac{[2l+1]}{[2j_2+1][2j_3+1]}} \delta_{j_1 j_2} \delta_{j_3 j_4}$
- $a_{jl} \begin{bmatrix} 0 & j_2 \\ j_3 & j_4 \end{bmatrix} = \delta_{j_2 j} \delta_{j_4 l}$

Now let's discuss the SU($N$) quantum Racah coefficients which can be used to compute SU($N$) quantum link invariants. Note that the SU($N$) Chern-Simons field theory on $S^3$ is closely related to the SU$(N)_k$ WZNW conformal field theory on the boundary of $S^3$, which is similar to the SU$(2)_k$ case. One needs to note that any knot and link can be drawn in a braid representation [110]. As shown in Fig.1-3, the plat diagram of knots and links relate to the braids with four strands. Denote $b_i^{(+)}$ and $\{b_i^{(+)}\}^{-1}$ as the right-handed crossing and left-handed crossing between $i$-th and $(i+1)$-th strands in parallel orientation. In the same way,$b_i^{(-)}$ and $\{b_i^{(-)}\}^{-1}$ as the right-handed crossing and left-handed crossing between $i$-th and $(i+1)$-th strands in anti-parallel orientation.

Now introduce the method to obtain the quantum knot and link invariants from these ingredients. As shown in Fig.1-3, the Chern-Simons functional integral on the 3-ball $B_3$ with a $S^2$ boundary on the right will give the state in the Hilbert space $\mathcal{H}_R$ on $B_3$, i.e. $|\chi_0^{(2)}\rangle \in \mathcal{H}_R$, where the representation $R_i$ shows that the line going into the $S^2$ boundary of $B_3$ and the conjugate representation $\bar{R}_i$ shows that the line going out of the $S^2$ boundary of $B_3$. In the middle, a three-ball $B_2$ with two $S^2$ boundaries which contains a braid $\mathcal{B}$ represents a braiding operator $\mathcal{B}_\nu^{(1),(2)}$. On the left-handed side, another three-ball $B_1$ with a oppositely oriented $S^2$ boundary gives a state $\langle \Psi_0^{(1)}| \in \mathcal{H}_L = (\mathcal{H}_R)^*$ with conjugating all representations for $B_3$ correspondingly.

By gluing all the three-balls with 4-punctured $S^2$ boundaries, one can obtain the link. The gluing are performed along two opposite-oriented $S^2$-boundaries, then the SU($N$) quantum link invariants $V^{\mathrm{SU}(N)}_{\{(R_i,n_i)\}}[\mathcal{L}]$ in the (1.6.23) can be written as

$$V^{\mathrm{SU}(N)}_{\{(R_1,R_2)\}}[\mathcal{L}] = \langle \Psi_0^{(1)} | \mathcal{B}_\nu^{(1),(2)} | \chi_0^{(2)} \rangle \tag{1.6.62}$$

later when the Kauffman polynomials are computed from SO($N$) quantum 6$j$-symbols, the exactly similar method was utilized.

The 4-point conformal block in SU$(N)_k$ WZNW model has two sets of bases similar to SU(2) cases [1], i.e.

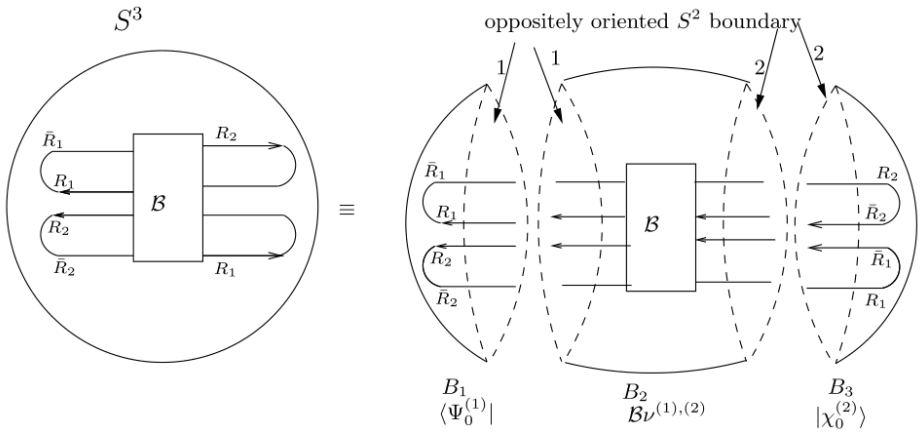


**Fig. 1-3.** A link in braid representation can be viewed as gluing of three-balls with 4-punctured $S^2$ boundaries [1].

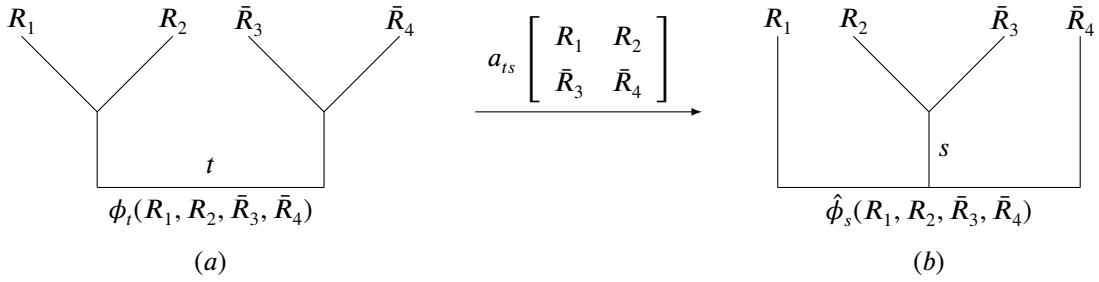


Here common representations of the final singlet are $t \in (R_1 \otimes R_2) \cap (\bar{R}_3 \otimes \bar{R}_4)$ and $s \in (R_1 \otimes \bar{R}_4) \cap (R_2 \otimes \bar{R}_3)$. These two sets of bases are related by *duality matrix* similar to SU(2) case discussed above.

$$|\phi_t(R_1, R_2, \bar{R}_3, \bar{R}_4) = \sum_s a_{ts} \begin{bmatrix} R_1 & R_2 \\ \bar{R}_3 & \bar{R}_4 \end{bmatrix} |\hat{\phi}_s(R_1, R_2, \bar{R}_3, \bar{R}_4) \tag{1.6.63}$$

here the SU($N$) duality matrix (also known as SU($N$) quantum Racah coefficients) can be expressed as

$$a_{ts} \begin{bmatrix} R_1 & R_2 \\ \bar{R}_3 & \bar{R}_4 \end{bmatrix} = \epsilon_{R_1} \epsilon_{R_2} \epsilon_{\bar{R}_3} \epsilon_{\bar{R}_4} \sqrt{\dim_q s} \sqrt{\dim_q t} \begin{Bmatrix} R_1 & R_2 & t \\ \bar{R}_3 & \bar{R}_4 & s \end{Bmatrix} \tag{1.6.64}$$

where $\epsilon_{R_i} = \epsilon_{\bar{R}_i} = \pm 1$ and $\epsilon_0 = 1$, and the curly brackets is similar to SU(2) quantum 6$j$-symbol with satisfying the following relations:

$$\begin{Bmatrix} R_1 & R_2 & t \\ \bar{R}_3 & \bar{R}_4 & s \end{Bmatrix} = \begin{Bmatrix} t & \bar{R}_2 & R_1 \\ s & \bar{R}_4 & \bar{R}_3 \end{Bmatrix} = \begin{Bmatrix} \bar{R}_1 & t & R_2 \\ \bar{R}_3 & \bar{s} & R_4 \end{Bmatrix} \tag{1.6.65}$$

The SU($N$) duality matrix has the following properties

- $a_{ts} \begin{bmatrix} R_1 & R_2 \\ \bar{R}_3 & \bar{R}_4 \end{bmatrix} = a_{st} \begin{bmatrix} \bar{R}_3 & R_2 \\ R_1 & \bar{R}_4 \end{bmatrix} = a_{\bar{s}\bar{t}} \begin{bmatrix} R_1 & \bar{R}_4 \\ \bar{R}_3 & R_2 \end{bmatrix} = a_{\bar{t}\bar{s}} \begin{bmatrix} \bar{R}_3 & \bar{R}_4 \\ R_1 & R_2 \end{bmatrix} = a_{ts} \begin{bmatrix} R_3 & R_4 \\ \bar{R}_1 & \bar{R}_2 \end{bmatrix}$

- If one of the representation is a singlet representation denoted by 0, then

$$a_{ts}\begin{bmatrix} R_1 & 0 \\ \bar{R}_3 & \bar{R}_4 \end{bmatrix} = \delta_{tR_1}\delta_{s\bar{R}_3}, \quad a_{ts}\begin{bmatrix} 0 & R_2 \\ \bar{R}_3 & \bar{R}_4 \end{bmatrix} = \delta_{tR_2}\delta_{sR_4} \tag{1.6.66}$$

$$a_{ts}\begin{bmatrix} R_1 & R_2 \\ 0 & \bar{R}_4 \end{bmatrix} = \delta_{tR_4}\delta_{sR_2}, \quad a_{ts}\begin{bmatrix} R_1 & R_2 \\ \bar{R}_3 & 0 \end{bmatrix} = \delta_{tR_3}\delta_{s\bar{R}_1} \tag{1.6.67}$$

These two sets of bases provide the eigenbasis of the braiding operators $b_i^{(\pm)}$. Apparently, for $b_1^{(\pm)}$ and $b_3^{(\pm)}$, one can use the conformal block $|\phi_t(R_1, R_2, \bar{R}_3, \bar{R}_4)\rangle$ as the eigenbasis. In these bases, the states $\langle\Psi_0^{(1)}|$, $|\chi_0^{(2)}\rangle$ and the braiding operator $\mathcal{B}_v^{(1),(2)}$ in (1.6.62) can be written as

$$\langle\Psi_0^{(1)}| = \sqrt{\dim_q R_1 \dim_q R_2}\langle\phi_0(\bar{R}_1, R_1, R_2, \bar{R}_2)^{(1)}| = \sum_{s\in R_1\otimes R_2}\epsilon_s^{(R_1R_2)}\sqrt{\dim_q s}\langle\hat{\phi}_s(\bar{R}_1, R_1, R_2, \bar{R}_2)^{(1)}| \tag{1.6.68}$$

$$\mathcal{B}_v^{(1),(2)} = \mathcal{B}|\phi_t(R_2, \bar{R}_2, \bar{R}_1, R_1)^{(1)}\rangle\langle\phi_t(\bar{R}_2, R_2, R_1, \bar{R}_1)^{(2)}| = \mathcal{B}|\hat{\phi}_s(R_2, \bar{R}_2, \bar{R}_1, R_1)^{(1)}\rangle\langle\hat{\phi}_s(R_2, \bar{R}_2, \bar{R}_1, R_1)^{(2)}| \tag{1.6.69}$$

$$|\chi_0^{(2)}\rangle = \sqrt{\dim_q R_1 \dim_q R_2}|\phi_0(R_2, \bar{R}_2, R_1, \bar{R}_1, R_1)^{(2)}\rangle = \sum_{s\in R_1\otimes R_2}\epsilon_s^{(R_1R_2)}\sqrt{\dim_q s}|\phi_0(R_2, \bar{R}_2, R_1, \bar{R}_1, R_1)^{(2)}\rangle \tag{1.6.70}$$

where $\epsilon_s^{(R_1,R_2)} = \pm 1$, and the quantum dimension $\dim_q R$ of representation $R$ is given by

$$\dim_q R = \prod_{\alpha>0}\frac{[\alpha\cdot(\rho+\Lambda_R)]}{[\alpha\cdot\rho]} \tag{1.6.71}$$

$\Lambda_R$ denotes the highest weight of representation $R$ and $\rho$ is the summation over all fundamental weights of SU($N$), also $\alpha > 0$ denotes the positive roots. Note that since

$$|\phi_0(R_1, R_2, \bar{R}_3, \bar{R}_4) = \sum_s a_{0s}\begin{bmatrix} R_1 & R_2 \\ \bar{R}_3 & \bar{R}_4 \end{bmatrix}|\hat{\phi}_s(R_1, R_2, \bar{R}_3, \bar{R}_4), \tag{1.6.72}$$

take inner product with $\langle\hat{\phi}_s(\bar{R}_1, \bar{R}_2, R_3, R_4)|$, one can find that

$$a_{0s}\begin{bmatrix} R_1 & R_2 \\ \bar{R}_3 & \bar{R}_4 \end{bmatrix} = \epsilon_s^{(R_1R_2)}\frac{\sqrt{\dim_q s}}{\sqrt{\dim_q R_1 \dim_q R_2}} \tag{1.6.73}$$

The conformal block $|\phi_t(R_1, R_2, \bar{R}_3, \bar{R}_4)\rangle$ can be treated as the eigenbasis of the braiding operators $b_1^{(\pm)}$ and $b_3^{(\pm)}$ and the conformal block $|\hat{\phi}_s(R_1, R_2, \bar{R}_3, \bar{R}_4)\rangle$ can be treated as the eigenbasis of the braiding operators $b_2^{(\pm)}$. They satisfy the following equations:

$$b_2^{(\pm)}|\hat{\phi}_s(R_1, R_2, \bar{R}_3, \bar{R}_4)\rangle = \lambda_s^{(\pm)}(R_2, \bar{R}_3)|\hat{\phi}_s(R_1, \bar{R}_3, , R_2, \bar{R}_4)\rangle \tag{1.6.74}$$

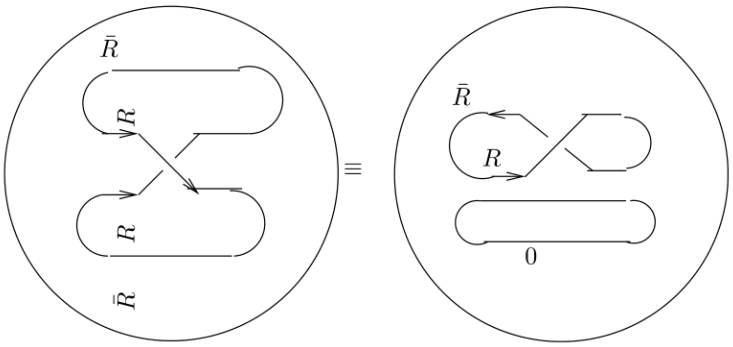


**Fig. 1-4.** Two ways to draw unknot in plat representation [1].

$$b_1^{(\pm)}|\phi_t(R_1,R_2,\bar{R}_3,\bar{R}_4)\rangle = \lambda_t^{(\pm)}(R_1,R_2)|\phi_t(R_2,R_1,\bar{R}_3,\bar{R}_4)\rangle \tag{1.6.75}$$

$$b_3^{(\pm)}|\phi_t(R_1,R_2,\bar{R}_3,\bar{R}_4)\rangle = \lambda_t^{(\pm)}(\bar{R}_3,\bar{R}_4)|\phi_t(R_1,R_2,\bar{R}_4,\bar{R}_3)\rangle \tag{1.6.76}$$

One can put the braid diagram in a vertical framing. In this framing, the braiding eigenvalues $\lambda_t^{(\pm)}(R_1,R_2) = \epsilon^{(\pm)}_{t;R_1,R_2}(q^{\frac{c_{R_1}+c_{R_2}-c_{R_t}}{2}})^{\pm 1}$ where $c_R$ is the quadratic Casimir operator of representation $R$, $c_R = \kappa_R - \frac{l^2}{2N}$, where $\kappa_R = \frac{1}{2}[(N+1)\,l + \sum_i (l_i^2 - 2il_i)]$, $l_i$ is the number of boxes in the $i$th row of the Young diagram of representation $R$ and $l = \sum_i l_i$. Moreover, $\epsilon^{(\pm)}_{t;R_1,R_2} = \pm 1$. Now one needs to fix the sign of the braiding eigenvalues as shown in the picture, there are two methods to draw the unknot in the plat representation of the braids, it can be expressed in following constraint equation:

$$\sum_s \dim_q s\ \lambda_s^{(+)}(R,R) = \lambda_0^{(-)}(R,\bar{R})\dim_q R. \tag{1.6.77}$$

here one can take $\epsilon^{(-)}_{0;R,\bar{R}} = 0$ and fix the signs $\epsilon^{(+)}_{s;R,R}$ satisfying (1.6.77). Consider the sign of the representations of type $R_n = \overleftarrow{\square\square\square\square\square\square}^{\,n}\overrightarrow{\ }$, Then for parallel strands under the large $k$ limit, the irreducible representation $\rho_l \in R_n \otimes R_n$ in $\mathrm{SU}(2)_k$ CFT would be

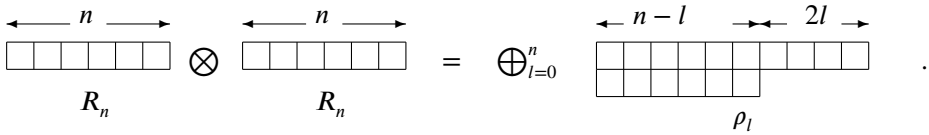


and $\epsilon^{(+)}_{\rho_l;R_n,R_n} = (-1)^{n-l}$. For anti-parallel strands under the large $k$ limit, the irreducible representation $\tilde{\rho}_l \in R_n \otimes \bar{R}_n$ are

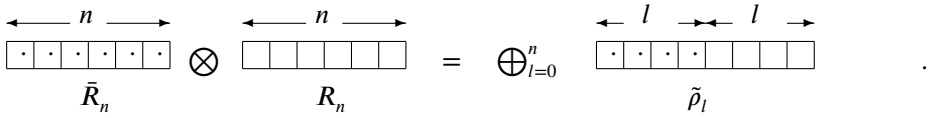


where the dots in the boxes indicate a column of length $N-1$. and the signs $\epsilon^{(-)}_{\tilde{\rho}_l;R_n,\bar{R}_n} = (-1)^l$.

# Chapter 2 Exact Partition Functions

In this chapter, we mainly discuss three kinds of exact partition functions: superconformal index, twisted indices, and $S^3$ partition function. These partition functions are powerful tools to check $3d$ $\mathcal{N}=4$ unitary/orthosymplectic duality because they are independent of coupling constants.

## 2.1 Superconformal Index

The 3d $\mathcal{N}=4$ superconformal index (SCI) [46] is the partition functions of 3d theory which is living on $S^1\times S^2$. It is defined as

$$\mathbb{I}(\mathfrak{q},\mathfrak{t})=\mathrm{Tr}(-1)^F\mathfrak{q}^{J+\frac{H+C}{4}}\mathfrak{t}^{H-C}\,, \tag{2.1.1}$$

Here $F$ is the Fermion number, $J$ is the $\mathrm{U}(1)_J$ rotational generator of the $S^2$, and $H$, $C$ represent the Cartan generators of the $\mathrm{SU}(2)_H\times\mathrm{SU}(2)_C$ R-symmetry, respectively. Note that the fugacities of global symmetries will not be considered. This superconformal index can be interpreted as the graded dimensions of the $\frac{1}{8}$-BPS states in an infrared conformal field theory.

The vector multiplet and an $\mathcal{N}=2$ chiral multiplet transformed in a representation $R$ of $G$ can be written as

$$Z_{\mathrm{vec}}(z,\mathfrak{m})=\prod_{\alpha\in\Delta}\left(\frac{\mathfrak{q}^{\frac{1}{2}}}{\mathfrak{t}^2}\right)^{-|\alpha(\mathfrak{m})|}\left(1-\mathfrak{q}^{\frac{|\alpha(\mathfrak{m})|}{2}}z^\alpha\right)\frac{\left(\mathfrak{t}^2\mathfrak{q}^{\frac{1+|\alpha(\mathfrak{m})|}{2}}z^\alpha;\mathfrak{q}\right)_\infty}{\left(\mathfrak{t}^{-2}\mathfrak{q}^{\frac{1+|\alpha(\mathfrak{m})|}{2}}z^\alpha;\mathfrak{q}\right)_\infty} \tag{2.1.2a}$$

$$Z_{\mathrm{chiral}}(z,\mathfrak{m})=\prod_{w\in R}\left(\frac{\mathfrak{q}^{\frac{1}{2}}}{\mathfrak{t}^2}\right)^{\frac{1}{4}|w(\mathfrak{m})|}\frac{\left(\mathfrak{t}^{-1}\mathfrak{q}^{\frac{3}{4}+\frac{1}{2}|w(\mathfrak{m})|}z^{-w};\mathfrak{q}\right)_\infty}{\left(\mathfrak{t}\mathfrak{q}^{\frac{1}{4}+\frac{1}{2}|w(\mathfrak{m})|}z^{w};\mathfrak{q}\right)_\infty}\,, \tag{2.1.2b}$$

where $G$ is the gauge group, $\Delta$ is the set of simple roots of $G$, and $\mathfrak{m}$ denotes the magnetic flux on $S^2$ which takes value in the cocharacter lattice of $G$. Here $(z;\mathfrak{q})_\infty:=\prod_{\ell=1}^{\infty}(1-z\mathfrak{q}^\ell)$ is the $\mathfrak{q}$-Pochhammer symbol. For unitary gauge groups, an $\mathcal{N}=4$ hypermultiplet can be decomposed into two $\mathcal{N}=2$ chiral multiplets with $R\oplus R^*$,

therefore

$$Z_{\text{hyp}}(z,\mathfrak{m}) \coloneqq Z_{\text{chiral}}(z,\mathfrak{m})Z_{\text{chiral}}(z^{-1},\mathfrak{m}) = \prod_{w\in R}\left(\frac{\mathfrak{q}^{\frac{1}{2}}}{\mathfrak{t}^2}\right)^{\frac{1}{2}|w(\mathfrak{m})|}\frac{\left(\mathfrak{t}^{-1}\mathfrak{q}^{\frac{3}{4}+\frac{1}{2}|w(\mathfrak{m})|}z^{\mp w};\mathfrak{q}\right)_\infty}{\left(\mathfrak{t}\mathfrak{q}^{\frac{1}{4}+\frac{1}{2}|w(\mathfrak{m})|}z^{\pm w};\mathfrak{q}\right)_\infty}. \tag{2.1.3}$$

The symbols $\pm,\mp$ in $\mathfrak{q}$-Pochhammer denote multiplication with both signs. Then the expression of a superconformal index for a given quiver gauge theory can be written in the following residue integration

$$\mathbb{I}(\mathfrak{q},\mathfrak{t}) = \sum_{\mathfrak{m}}\oint\prod_{\text{gauge}}\frac{1}{|W_G|}\left[\frac{dz}{2\pi i z}\right]Z_{\text{vec}}(z,\mathfrak{m})\prod_{\text{matter}}Z_{\text{chiral}}(z,\mathfrak{m}). \tag{2.1.4}$$

One can introducing the variables $t_h$ and $t_c$ as,

$$\mathfrak{q} = t_h t_c, \qquad \mathfrak{t} = \left(\frac{t_h}{t_c}\right)^{1/4}, \tag{2.1.5}$$

then the limits $t_h \to 0$ and $t_c \to 0$ engender the Hilbert series of the $\mathcal{M}_C$ and $\mathcal{M}_H$ of the 3d $\mathcal{N}=4$ theory, respectively [46].

Mathematically, the Hilbert series (also called the Hilbert-Poincaré series) is the generating function that counts the generators of graded pieces of polynomial rings. In supersymmetric gauge theories, the Hilbert series enumerate the bare and dressed gauge-invariant monopole operators which parameterize the Coulomb branch $\mathcal{M}_C$ and grade them by their quantum number under the topological symmetries and superconformal R-symmetry, modulo F-terms:

$$H_G(t) = \sum_{\mathfrak{m}\in\Gamma_{\hat{G}}^*/\mathcal{W}_{\hat{G}}} t^{\Delta(\mathfrak{m})}P_G(t,\mathfrak{m}). \tag{2.1.6}$$

The summation is performed over all sectors of GNO monopole operators in a Weyl chamber of the weight lattice of $G^\vee$ and $t^{\Delta(\mathfrak{m})}$ counts the BPS bare monopole operators with $R$-charge (1.2.28). After $G$ is broken into the residual gauge group $H_m$, there are still remain gauge invariants that are unbroken by GNO magnetic flux $\mathfrak{m}$ and $P_G(t,\mathfrak{m})$ numerate these gauge invariants.

$$P_G(t,\mathfrak{m}) = \prod_{i=1}^{r}\frac{1}{1-t^{d_i(\mathfrak{m})}}, \tag{2.1.7}$$

here $d_i(\mathfrak{m})$ $(i=1,\cdots,r)$ denote the degrees of the Casimir of $H_{\mathfrak{m}}$. Moreover, if $G$ is not simply-connected, then monopole operators may be charged under the topological symmetry (1.2.12), and a fugacity $z$ will emerge with topological charge $J(m)$. The Hilbert series (2.1.6) can be further refined

$$H_G(t,z) = \sum_{\mathfrak{m}\in\Gamma_{\hat{G}}^*/\mathcal{W}_{\hat{G}}} z^{J(\mathfrak{m})}t^{\Delta(\mathfrak{m})}P_G(t,\mathfrak{m}). \tag{2.1.8}$$

In particular, under the limit $t_c \to 0$ the SCI will reduce to the Molien-Weyl formula [39–41] which counts the algebraically independent single-trace gauge invariant operators that composed by the field operators. The limit $t_h \to 0$ of the SCI will engender the monopole formula [42]. Because of the 3d mirror symmetry, the Hilbert series of $\mathcal{M}_H$ ($\mathcal{M}_C$) will map to $\mathcal{M}_H$ ($\mathcal{M}_C$) of the mirror dual under $\mathfrak{t} \to \mathfrak{t}^{-1}$.

There also exist the extended BPS operators, i.e. Wilson line operators and vortex line operators. Note that they do not interchange under the 3d $\mathcal{N} = 4$ unitary/orthosymplectic duality. Alternatively, it is more interesting to study the gauge group that the same kind of line operators coupled in the dual theories. Under 3d $\mathcal{N} = 4$ unitary/orthosymplectic duality, there are no interchanges between the Wilson line operators and the vortex line operators. But it is interesting to study the correspondences between the gauge groups that the line defects coupled for the dual quiver gauge theory.

## 2.2 Twisted Indices

As we mentioned in the introduction, the 3d $\mathcal{N} = 4$ supersymmetry preserves 8 supercharges. One can preserve 4 supercharges on a 3-manifold $\mathcal{M}_3$ by twisting the factor of $\mathrm{SU}(2)_C$ or $\mathrm{SU}(2)_H$ R-symmetry [111]. Denote the generators of $\mathrm{U}(1)_H \subset \mathrm{SU}(2)_H$ and $\mathrm{U}(1)_C \subset \mathrm{SU}(2)_C$ as $H$ and $C$. One can define the integer-valued R-charges

$$R_A = 2H, \quad R_B = 2C. \tag{2.2.1}$$

If one consider a 3d theory on $\Sigma_g \times S^1$, where $\Sigma_g$ is a Riemann surface with genus $g$, then $R_A$ or $R_B$ can be identified with the $\mathrm{U}(1)_R$ charges of an $\mathcal{N} = 2$ sub-algebra. The $\mathrm{SU}(2)_C$ twist [111] preserves 4 scalar supercharges $Q_+^{1\dot{1}}$, $Q_+^{2\dot{1}}$, $Q_-^{1\dot{2}}$, $Q_-^{2\dot{2}}$ on $\mathcal{M}_3$ and the supersymmetry algebra

$$\{Q_+^{A\dot{1}}, Q_-^{B\dot{2}}\} = 2\epsilon^{AB}E$$

which preserves on $\Sigma_g \times S^1$ engenders an algebra of the $\mathcal{N} = 4$ SQM with $\mathrm{U}(1)_C \times \mathrm{SU}(2)_H$ R-symmetry, where $E$ is the generator of translation along $S^1$. This procedure is called the B-twist and it gives a topological twist along $\Sigma_g$ by $R_B$. The $\mathrm{SU}(2)_H$ twist preserves the 4 scalar supercharges $Q_+^{1\dot{1}}$, $Q_-^{2\dot{2}}$, $Q_+^{1\dot{2}}$, $Q_-^{2\dot{1}}$ on $\mathcal{M}_3$ and the supersymmetry algebra

$$\{Q_+^{1\dot{A}}, Q_-^{2\dot{B}}\} = 2\epsilon^{\dot{A}\dot{B}}E$$

preserves on $\Sigma_g \times S^1$ gives an algebra of the $\mathcal{N} = 4$ SQM with $\mathrm{U}(1)_H \times \mathrm{SU}(2)_C$ R-symmetry. This procedure is called the A-twist and it gives a topological twist along $\Sigma_g$ by $R_A$. A topological twist with the $\mathrm{SU}(2)_H$ (resp. $\mathrm{SU}(2)_C$) Cartan subgroup engenders the A-twisted (resp. B-twisted) index. Since under 3d $\mathcal{N} = 4$ mirror symmetry, $\mathrm{SU}(2)_H$ and $\mathrm{SU}(2)_C$ will interchange, so the A-twisted index of one theory must be equal to the B-twisted index of its mirror dual theory under the following relation

$$I_A^{[T]}(y, t) = I_B^{[\check{T}]}(\check{y}, t^{-1}), \tag{2.2.2}$$

where $y$ and $\check{y}$ are the flavor fugacities and their mirrors.

The following part of this section will consider the twisted partition functions [47, 112–116] on $S^1 \times S^2$ (i.e genus-0 case) with line operators. The topological twists will be carried out on the sphere $S^2$. These twisted indices in the genus-0 cases numerate the cohomologies of the topological charges. The topological twisted theory of A-twisted (B-twisted, respectively) will flow to a non-linear $\sigma$-model on the Coulomb (Higgs, respectively) branch of the 3d $\mathcal{N} = 4$ theory [47, 116].

In this thesis, in order to identify the correspondences of line operators for a specific pair of unitary and orthosymplectic quivers, the expectation value of the line defect operators are evaluated in a theory with topological twists [111]. Here the expectation values of the half-BPS vortex and Wilson lines operators on $S^1 \times S^2$ are considered because they preserve the A- and B-type topological supercharges separately. With using supersymmetric localization, the formula of evaluating the twisted indices (with line operators) can be expressed as the form of Jeffery-Kirwan contour integrals [47]. A vortex line expectation value in the A-twisted index is given by

$$\mathbb{I}^A = \sum_{\mathfrak{m}} \oint_{\text{JK}} \prod_{\text{gauge}} \frac{1}{|W_G|} \left[\frac{dz}{2\pi i z}\right] Z^A_{\text{vec}}(z, \mathfrak{m}) \prod_{\text{matter}} Z^A_{\text{chiral}}(z, \mathfrak{m})\, \mathcal{V}(z)\,, \tag{2.2.3}$$

with summation of magnetic fluxes $\mathfrak{m}$ supported on $S^2$. A vector multiplet and a chiral multiplet will contribute to the A-twisted indices:

$$Z^A_{\text{vec}}(z, \mathfrak{m}) = \left(t - t^{-1}\right)^{-\text{rk}(G)} \prod_{\alpha \in \Delta} \left(\frac{1 - z^\alpha}{t - z^\alpha t^{-1}}\right)^{\alpha(\mathfrak{m})+1}\,, \tag{2.2.4a}$$

$$Z^A_{\text{chiral}}(z, \mathfrak{m}) = \prod_{w \in R} \left(\frac{z^{\frac{w}{2}} t^{\frac{1}{2}}}{1 - z^w t}\right)^{w(\mathfrak{m})}\,. \tag{2.2.4b}$$

The vortex loop contribution can be computed from evaluating a 1d $\mathcal{N} = 4$ SQM [35]. For the U($k$) SQM with $N_1$ fundamental and $N_2$ anti-fundamental chiral multiplets

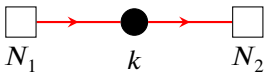


(2.2.5)

the contribution to the twisted indices becomes

$$\mathcal{V}(z) = \sum_{k=\sum_{i=1}^{N_1} k_i} \prod_{a=1}^{N_1} \left(\prod_{b \neq a}^{N_1} \frac{z_a t^{-1} - z_b t}{z_a - z_b} \left(\frac{1 - z_a t}{z_a - t}\right)^{N_2}\right)^{k_a}\,. \tag{2.2.6}$$

In this thesis, only $k = 1$ cases are considered. But it is uncomplicated to generalize the discussion to arbitrary $k$. For a general $\mathcal{N} = 4$ non-Abelian quiver gauge theory, the corresponding A-twisted index can be obtained by summing over all Bethe vacua [47, 112–116]. But in order to make it sufficient, one needs to refine (2.2.4) by switching on all deformation parameters of the theory to avoid missing some parts of the Bethe vacua. However, if

one turns on all deformation parameters, the Bethe ansatz equations become very difficult to solve algebraically. One can only solve them numerically for generic cases. In Appendix 2.1, another route was taken due to the difficulty to evaluate the A-twisted indices of Sp(1) SQCDs with vortex loops for a long and high-rank quiver. The B-twisted index with Wilson loops are computed whose computation formula is

$$\mathbb{I}^B = \oint_{\text{JK}} \prod_{\text{gauge}} \frac{1}{|W_G|} \left[\frac{dz}{2\pi i z}\right] Z^B_{\text{vec}}(z) \prod_{\text{matter}} Z^B_{\text{chiral}}(z)\, \mathcal{W}(z)\,, \tag{2.2.7}$$

where the contributions from a vector multiplet and a chiral multiplet are

$$Z^B_{\text{vec}}(z) = \left(t - t^{-1}\right)^{\text{rk}(G)} \prod_{\alpha\in\Delta} (1 - z^\alpha)\left(t - z^\alpha t^{-1}\right)\,, \tag{2.2.8a}$$

$$Z^B_{\text{chiral}}(z) = \prod_{w\in R} \frac{z^{\frac{w}{2}} t^{\frac{1}{2}}}{1 - z^w t}\,. \tag{2.2.8b}$$

The Wilson loop $\mathcal{W}(z)$ can be realized by inserting a character related to its representation. Note that for the B-twisted index, only the zero magnetic flux sector needs to be taken into account [47]. One can also expand the integrand into series in the neighborhood of the origin and only focus on the $z$-independent part. And it turns out that the evaluation of the expectation value of the Wilson loop (2.2.7) seems to be much easier compared to that of the vortex loop (2.2.3). Moreover, when one computes the SCIs and A-twisted indices, the magnetic lattices need to be shifted by a half except the weight lattices for unframed orthosymplectic quivers. This point is illustrated in §2.4 and §4.

## 2.3 Sphere Partition Function

$S^3$ partition functions can also be utilized to check the unitary/orthosymplectic duality by calculating the expectation value of line operators [35, 36]. The reason for considering the $S^3$ partition function is because $S^3$ is a compact manifold with a finite radius, so the IR divergence could be avoided when one calculates the path integral. Also, one can regularize the UV divergence properly to obtain a finite physical quantity.

A $S^3$ partition function has been computed by supersymmetric localization by Kapustin [48], which is given as

$$Z^{S^3} = \oint \prod_{\text{gauge}} \frac{1}{|W_G|} [ds]\, Z^{S^3}_{\text{vec}}(s) \prod_{\text{matter}} Z^{S^3}_{\text{hyp}}(s,m)\; Z_{\text{FI}}(s,\xi) Z^{S^3}_{\text{defect}}(s)\,. \tag{2.3.1}$$

A vector multiplet and a hypermultiplet contribute

$$Z^{S^3}_{\text{vec}}(s) = \prod_{\alpha\in\Delta} \text{sh}(\alpha\cdot s)\,, \tag{2.3.2a}$$

$$Z^{S^3}_{\text{hyp}}(s,m) = \prod_{w\in R} \frac{1}{\text{ch}(w\cdot s - m)}\,, \tag{2.3.2b}$$

where $m$ is a mass parameter and $\text{sh}(x) \equiv 2\sinh(\pi x)$ , $\text{ch}(x) \equiv 2\cosh(\pi x)$ . When the gauge group contains a

U(1) factor, the FI parameter $\xi$ will contribute to the $S^3$ partition function

$$Z_{\text{FI}}(s,\xi) = e^{2\pi i \xi \text{Tr}(s)} \,. \tag{2.3.3}$$

Note that for orthosymplectic quivers one needs to switch on an *unphysical* FI parameter (2.3.3) as a regulator [117], because in this case the quiver itself is not endowed with an FI parameter.Then its $S^3$ partition function can be evaluated by taking the limit $\xi \to 0$. As before, the Wilson loop is given by inserting a character

$$Z_{\text{Wilson}}(s) = \sum_{w\in R} e^{2\pi w\cdot s} \,. \tag{2.3.4}$$

The vortex loop which is encoded in the 1d SQM (2.2.5) engenders the following contribution:

$$Z_{\text{vortex}}(s) = \sum_{\substack{k_1,\cdots,k_N\in\{0,1\}\\ k=\sum_{i=1}^{N_1} k_i}} (-1)^{(N_1+N_2)k} \prod_{i<j}^{N_1} \frac{\text{sh}\left[s_i - s_j + i\left(k_i - k_j\right) z\right]}{\text{sh}\left[s_i - s_j\right]} \prod_{j=1}^{N_1}\prod_{a=1}^{N_2} \frac{\text{ch}\left(s_j - m_a\right)}{\text{ch}\left(s_j - m_a + i k_j z\right)} \,. \tag{2.3.5}$$

This thesis only focuses on $k = 1$ case.

## 2.4 Comments on Weight Lattice and Magnetic Lattice

As one can be seen from the previous discussion. The weight and magnetic lattices play crucial roles in the whole story of 3d unitary/orthosymplectic duality. For instance, one needs to sum over the magnetic lattice of the gauge group to compute the exact partition functions [85, 118, 119]. Meanwhile, the line operators are also sensitive to the weight lattice of the gauge group (not only its algebra). Thus, it is very necessary to discuss the weight and magnetic lattice a bit more. The following discussions follow Bourget's notation [38] and mainly focus on the cases of unitary and orthosymplectic quivers.

**Unitary quivers.** If the quiver explicitly contains flavor nodes, then $\ker\phi$ is trivial. For each U($n$) gauge node, the weight lattice is $\Lambda_w^{\text{U}(n)} = \mathbb{Z}^n$, while the magnetic lattice is $\Lambda_w^{\text{U}(n)^\vee} = \mathbb{Z}^n$. Thus, for a product gauge group $G = \prod_i \text{U}(n_i)$, the lattices are given by

$$\Lambda_w^G = \oplus_i \mathbb{Z}^{n_i} \,, \qquad \Lambda_w^{G^\vee} = \oplus_i \mathbb{Z}^{n_i} \,. \tag{2.4.1}$$

If the quiver theory is only comprised of unitary gauge nodes (i.e. without any flavour nodes), the group $\ker\phi = \text{U}(1)$ is non-trivial and continuous. The continuousness of the $\ker\phi$ would cause the partition functions to be divergent. Then one needs to remove this diagonally acting U(1). There are several ways:

- If there is a U(1) gauge node in the quiver, then this node could be turned into a flavor node. Now one can get a quiver with explicit flavor and the above discussion could be applied. This thesis only involves

| | group G | SO($2n+1$) | Sp($n$) | SO($2n$) |
|---|---|---|---|---|
| centre | $Z(G)$ | 1 | $\mathbb{Z}_2$ | $\mathbb{Z}_2$ |
| weight lattice of $G$ | $\Lambda_w^G$ | $\mathbb{Z}^n$ | $\mathbb{Z}^n$ | $\mathbb{Z}^n$ |
| magnetic lattice of $G$ | $\Lambda_w^{G^\vee}$ | $\mathbb{Z}^n$ | $\mathbb{Z}^n$ | $\mathbb{Z}^n$ |
| weight lattice of $G/\mathbb{Z}_2$ | $\Lambda_w^{G/\mathbb{Z}_2}$ | NA | $\mathbb{Z}^n$ | $\mathbb{Z}^n$ |
| magnetic lattice of $G/\mathbb{Z}_2$ | $\Lambda_w^{(G/\mathbb{Z}_2)^\vee}$ | NA | $\mathbb{Z}^n_{\sum\text{even}}$ | $\mathbb{Z}^n_{\sum\text{even}}$ |

**Table 2-1.** Lattices associated to different gauge group factors. $Z(G)$ denotes the centre of a group $G$. $\Lambda_w^G$ stands for the *weight lattice* of the group $G$, while $\Lambda_w^{G^\vee}$ is the *magnetic lattice* of $G$ (i.e. weight lattice of the GNO dual group $G^\vee$ [118]). $\mathbb{Z}^n$ denotes the standard integer lattice in $n$ dimensions. $\mathbb{Z}^n_{\sum|\text{even}}$ stands for the set of points $(a_1,\dots,a_n)\in\mathbb{Z}^n$ such that $\sum_i a_i=$ even. Likewise, $\mathbb{Z}^n_{\sum|\text{odd}}$ denotes the points $(a_1,\dots,a_n)\in\mathbb{Z}^n$ such that $\sum_i a_i=$ odd.

this case.

- One can get rid off the diagonal U(1) from any U($n$) node generally. The resulting gauge group can be chosen to be $G=\left[\mathrm{SU}(n)\times\prod_i \mathrm{U}(n_i)\right]/\mathbb{Z}_n^{\text{diag}}$. One should notice that this is not SU($n$) nor PSU($n$) [38]. The center of SU($n$) group is $\mathbb{Z}_n=Z(\mathrm{SU}(n))$. For each U($n_i$) factor, one can embed a $\mathbb{Z}_n$ into it and define a diagonally acting $\mathbb{Z}_n^{\text{diag}}$ group.

**Orthosymplectic quivers.** For orthosymplectic quivers, it was shown that if there exist explicit flavor nodes or at least one SO($2n+1$) factor in the quiver, then the ker $\phi$ is trivial. Table 2-1 summarises the weight and magnetic lattices of various factors for these cases. When the gauge group is $G=\prod_i \mathrm{SO}(2n_i+1)\times\prod_j \mathrm{Sp}(k_j)\times\prod_l \mathrm{SO}(2h_l)$, the lattices are

$$\Lambda_w^G=\bigoplus_i \Lambda_w^{\mathrm{SO}(2n_i+1)}\oplus\bigoplus_j \Lambda_w^{\mathrm{Sp}(k_j)}\oplus\bigoplus_l \Lambda_w^{\mathrm{SO}(2h_l)}, \tag{2.4.2a}$$

$$\Lambda_w^{G^\vee}=\bigoplus_i \Lambda_w^{\mathrm{SO}(2n_i+1)^\vee}\oplus\bigoplus_j \Lambda_w^{\mathrm{Sp}(k_j)^\vee}\oplus\bigoplus_l \Lambda_w^{\mathrm{SO}(2h_l)^\vee}. \tag{2.4.2b}$$

The group ker $\phi=\mathbb{Z}_2$ is non-trivial when the orthosymplectic quiver does not include flavor nodes nor SO($2n+1$) factors. One can choose to get rid off this discrete subgroup from the product gauge group or not, both options are physically reasonable. But from the viewpoint of the unframed orthosymplectic magnetic quivers [7, 8, 11, 17, 18, 27, 29], it would be better to remove the diagonal $\mathbb{Z}_2$ from the brane configurations perspective. One can consider a simple quiver

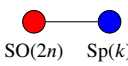


(2.4.3)

with $G=\mathrm{SO}(2n)\times\mathrm{Sp}(k)$. Then the $G/\mathbb{Z}_2$ will engender the following lattice

$$\Lambda_w^{G/\mathbb{Z}_2}=\left[\mathbb{Z}^n_{\sum|\text{even}}\oplus\mathbb{Z}^k_{\sum|\text{even}}\right]\cup\left[\mathbb{Z}^n_{\sum|\text{odd}}\oplus\mathbb{Z}^k_{\sum|\text{odd}}\right], \tag{2.4.4a}$$

$$\Lambda_w^{(G/\mathbb{Z}_2)^\vee} = \left[\mathbb{Z}^n \oplus \mathbb{Z}^k\right] \cup \left[\left(\mathbb{Z}+\tfrac{1}{2}\right)^n \oplus \left(\mathbb{Z}+\tfrac{1}{2}\right)^k\right], \tag{2.4.4b}$$

see Table 2-1 for notation. These magnetic lattices consist of the *integer* and *half-integer* lattice. Therefore, the set of the monopole operators that have contributions to the 3d quiver gauge theory is enlarged. Oppositely, the weight lattice displays the set of allowed representations is reduced. Specifically, the fundamental representations of SO($2n$) and Sp($k$) are not permitted because they live in $\mathbb{Z}^n_{\sum|\text{odd}}$ and $\mathbb{Z}^k_{\sum|\text{odd}}$, respectively. But the bi-fundamental hypermultiplet in (2.4.3) is still a permissible representation because it sits in $\mathbb{Z}^n_{\sum|\text{odd}} \oplus \mathbb{Z}^k_{\sum|\text{odd}}$ lattice.

# Chapter 3 3d Sp($k$) SQCD

This chapter is divided into two parts. The first part focuses on the duality between unitary and orthosymplectic quivers. They are mirror dual to Sp($k$) SQCDs from the viewpoint of branes and exact partition functions. This clears the way for studying the duality of the magnetic quivers in the next chapter. The second part investigates the dynamics of the brane systems under the existence of S-duality and O-planes. In order to study the dualities of 3d $\mathcal{N}=4$ theories, it is necessary to understand the D3-D5-NS5 brane dynamics in Type IIB string theory [30]. Meantime, the exact results obtained from the 3d $\mathcal{N}=4$ theories will disclose details of the type IIB brane systems [35, 36, 117, 120] Besides, the correspondences between Wilson lines on both unitary and orthosymplectic sides will be shown.

## 3.1 Duality of Unitary and Orthosymplectic Mirror Quivers

3d $\mathcal{N}=4$ low-energy theories with Sp($k$) gauge group and $N_f$ fundamental matter fields can be realised by type IIB brane configurations whose Lagrangian description can be summarized via the following quiver diagram:

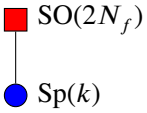


(3.1.1)

where the flavour number needs to satisfy the condition $N_f \geq 2k$ which guarantees the complete Higgsing. This means that the mirror theory can also be arised from Type IIB configurations [30, 34]. There is also another a bit more restrictive condition, i.e. $N_f \geq 2k+1$, which guarantees the Sp($k$) gauge node is *good* in the Gaiotto-Witten sense [87]. The gauge group is called balanced if $N_f = 2k+1$, see (1.3.4), then there will be an enhanced SO(2) topological symmetry emerges in IR. In [42], the Coulomb branch Hilbert series for Sp(1) with $N_f$ flavours is $H = \mathrm{PE}[t^2 + t^{N_f-2} + t^{N_f-1} - t^{2N_f-2}]$. Here each term has its specific meaning. The first three terms corresponds to the Casimir invariant, bare monopole operator, and dressed monopole operator of charge 2, $N_f-2$, and $N_f-1$, separately. The last term is a constraint relation at order $2N_f-2$. When $N_f=3$, the IR global symmetry of $\mathcal{M}_C$ will emerge because of the monopole operators. In this case, the bare monopole operator can be viewed as a component of the global symmetry multiplet of R-charge 1. This discussion still holds for the case of Sp($k$) with $N_f = 2k+1$ [42]. When $N_f = 2k$, the theory is called *bad* which indicates that there is one monopole

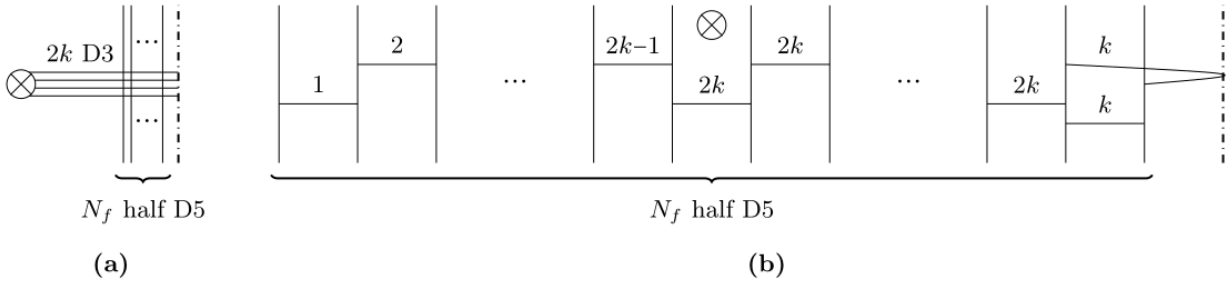


**Fig. 3-1.** Brane configuration for 3d Sp($k$) with $N_f$ fundamental flavours. (See (1.3.6) for notations.) In (a), the brane configuration is in the electric phase in which all D3 branes are extended between NS5-branes. In order to transit to the magnetic phase as shown in (b), $2k$ half D5s are moved through the half NS5 towards the left-hand-side. The mirror theory can be derived from (b) through S-duality, *i.e.* interchanging D5 and NS5, and replacing the O5$^-$ with an ON$^-$.

operator at the fewest that contravenes the unitary bound.

Hence, the IR theory needs to be carefully evaluated [121]. The examples discussed in this thesis are *not* bad theories unless otherwise stated. Intriguingly, there exist two different realizations that correspond to the same effective theory:

- The first realization is composed of a stack of $k$ D3 branes which are intersected by $2N_f$ half D5 branes on top of an O3$^+$ orientifold plane [34].
- The second realization is composed of $k$ D3 branes crossing an O5$^-$ orientifold, along with $2N_f$ half D5 branes parallel to the orientifold [33, 95].

Here let's briefly discuss $Op$-planes. For general case when $p \leq 5$, there are four types of orientifolds denoted as $Op^+, Op^-, \widetilde{Op^+}, \widetilde{Op^-}$ [122, 123]. The $\pm$ denotes two kinds of orientifold projections $\Omega$'s according to the different choices of $\Omega$ on the Chan-Paton factors and world-sheet. Here, both the $Op^+$ and $Op^-$ planes only permit one to put an even number of $\frac{1}{2}Dp$-brane. $\widetilde{Op^-}$ planes permit one to put an odd number of $\frac{1}{2}Dp$-branes, because there must be one $\frac{1}{2}Dp$-brane gets stuck into the orientifold, so $\widetilde{Op^-}$ planes can be viewed as the bound state of $Op^-$ planes also the $\frac{1}{2}Dp$-brane. These four kinds of $Op$-planes will convert into one another when they go through the $\frac{1}{2}$NS-branes or $\frac{1}{2}$D-branes [33, 124, 125]. $Op^-$ ($\widetilde{Op^-}$) will change into $Op^+$ ($\widetilde{Op^+}$) when they passes through the $\frac{1}{2}$NS-branes, and vice versa. And $Op^-$ ($Op^+$) will change into $\widetilde{Op^-}$ ($\widetilde{Op^+}$) when they passes through the $\frac{1}{2}D(p+2)$-branes and vice versa.

For O3-planes mentioned here, there are also four types of them according to above general discussion, i.e $O3^+, O3^-, \widetilde{O3^+}, \widetilde{O3^-}$ [34]. Here the charge of $O3^-$ is $-\frac{1}{4}$ but the charges of the other three types are $\frac{1}{4}$ and they can convert into each other via $SL(2,\mathbb{Z})$ duality symmetry in type IIB string theory. Furthermore, the $O3^+$ and $O3^-$ can transform into each other via S-duality, and $\widetilde{O3^+}$ and $O3^-$ keep invariant under S-duality. Here one can conclude that the changes of $O3$-planes when they cross the $\frac{1}{2}$-NS brane are S-dual to that of $O3$-planes when they cross the $\frac{1}{2}D5$-branes [34].

**Unitary mirror quiver.** Firstly consider the brane configuration for 3d Sp($k$) with $N_f$ fundamental flavours 3-1. Its mirror quiver [33] is presented as follows:

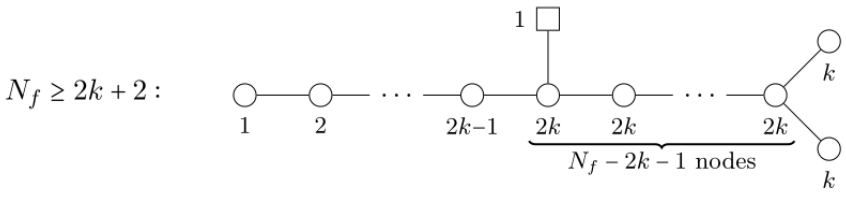


(3.1.2)

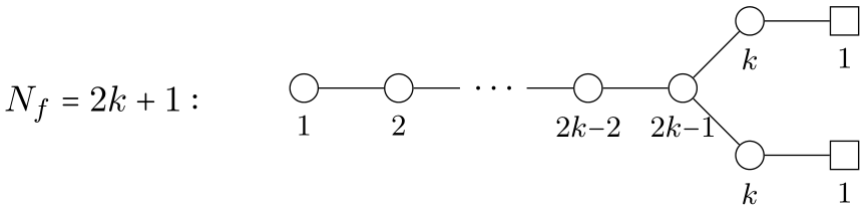


(3.1.3)

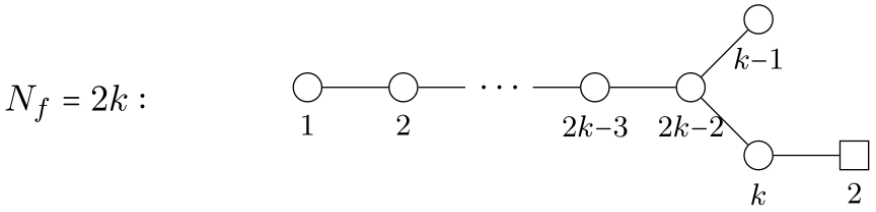


(3.1.4)

Each case above has $N_f$ balanced nodes. Moreover, the $N_f = 2k+1$ case exhibits a U(1) flavor symmetry, which shows that there exists a non-trivial $\mathrm{U}(1)_J$ symmetry in the Coulomb branch of the balanced mirror Sp($k$) gauge theory.

**Orthosymplectic mirror quiver.** Secondly consider the brane configuration for 3d Sp($k$) with $N_f$ fundamental flavors using $O3$ planes, as shown in Figure 3-2. Its corresponding mirror quiver [34] is given by

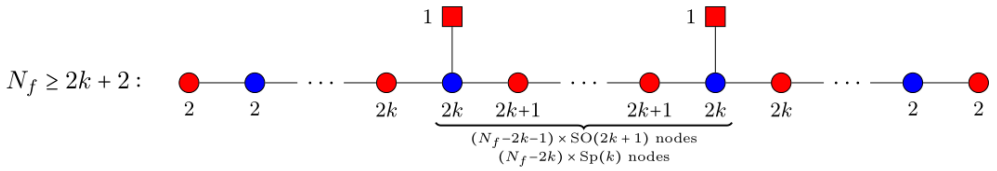


(3.1.5)

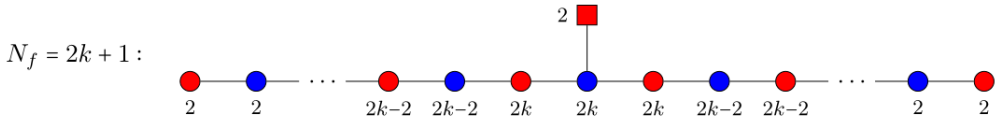


(3.1.6)

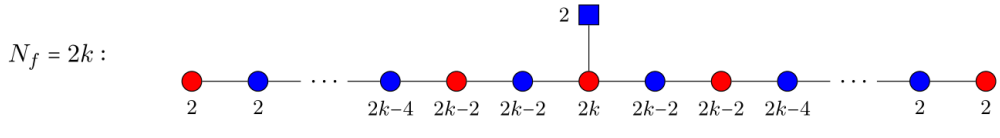


(3.1.7)

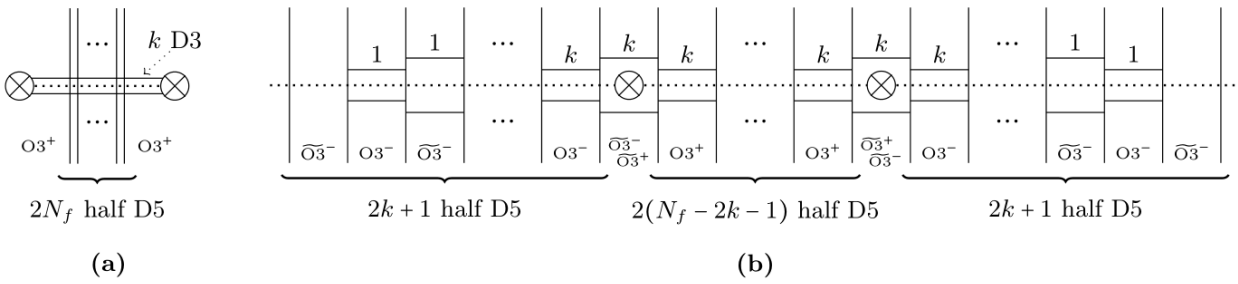


**Fig. 3-2.** Brane configuration for 3d Sp($k$) with $N_f$ fundamental flavours by utilizing O3 planes. (See (1.3.6) for notations.) Figure (a) shows the electric phase of the brane system. The stack of $k$ full D3-branes on top of an O3$^+$ plane engenders the Sp($k$) gauge group. The figure (b) shows the magnetic phase could be achieved by moving 2k half D5 through each of the half NS5s. Generally, one can move an extra half D5-brane through each half NS5-brane when $N_f \geq 2k+2$. Then, one can obtain the mirror brane system via S-duality, where D5-brane and NS5-branes. O3$^+$ and $\widetilde{\text{O3}}^-$ are interchanged, whereas O3$^-$ and $\widetilde{\text{O3}}^+$ keep invariant.

There is a linear quiver of $p = 2N_f - 3$ balanced SO(2) nodes on the both ends will bring about an enhanced SO($p+3$) = SO($2N_f$) symmetry of $\mathcal{M}_C$ [87]. Similar to the unitary counterpart, the $N_f = 2k+1$ case exhibits a SO(2) $\cong$ U(1) flavour symmetry implying the existence of a non-trivial U(1)$_J$ topological symmetry on the mirror side.

It's expected that the 3d $\mathcal{N} = 4$ unitary/orthosymplectic mirror quiver pairs that can be obtained from the Sp($k$) SQCD flow to the same IR fixed point [33, 34]. One can compute a superconformal index for both sides in the given order of perturbative expansion to verify it. The results when $k = 1$ with $N_f = 3, 4, 5, 6$ and $k = 2$ with $N_f = 4, 5, 6$ are listed in Table 1. Furthermore, under the limits (2.1.5), the computed SCIs will engender the known Hilbert series of $\mathcal{M}_C$ and $\mathcal{M}_H$ [126–128], this provides a convincing consistent check of the computation.

## 3.2 Matches of Wilson Line Defects in the Two Mirror Quivers

It is natural to consider whether the mirror duality between unitary and orthosymplectic quivers still holds when they are equipped with the same set of line defects. If this is true, then one could ask how they map to each other under the duality. In this section, a dictionary for the Wilson lines is presented under the mirror duality. Note that when one compares the Wilson line operators on the unitary and orthosymplectic sides, they have to arise from an equal number of brane systems. In the brane system, the F1 strings can end on a stack of D3 branes for both sides of mirror pairs with the same possibilities. These F1 strings engender the Wilson line defects. One can infer that the total dimension of the representations of Wilson lines remains the same under the unitary/orthosymplectic duality. If one compute the B-twisted indices for $k = 1$ with $N_f = 3, 4, 5, 6$ – see Tables 3, 4, 5, 6– and $k = 2$ with $N_f = 4, 5, 6$ – see Tables 7, 8, 9 – an intriguing pattern between the Wilson lines in (3.1.2) and in (3.1.5) will emerge. Here are a few observations.

**Observation 1:** When there is a fundamental Wilson line at the Sp($r$) node, for $1 \leq r \leq k$

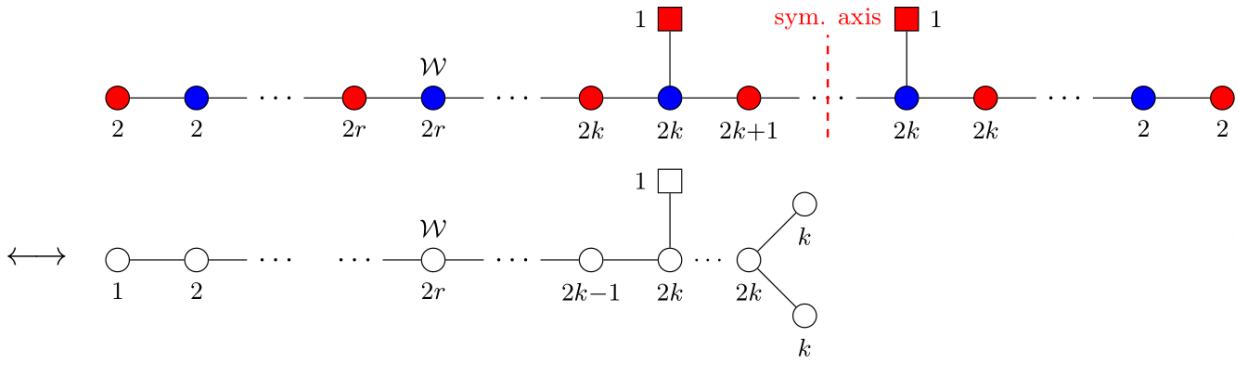


(3.2.1)

Here Wilson line of the U($2r$) gauge node marked in the second line is in the fundamental representation.

**Observation 2:** When there is a fundamental Wilson line at the SO($2r$) node, for $1 \leq r \leq k$

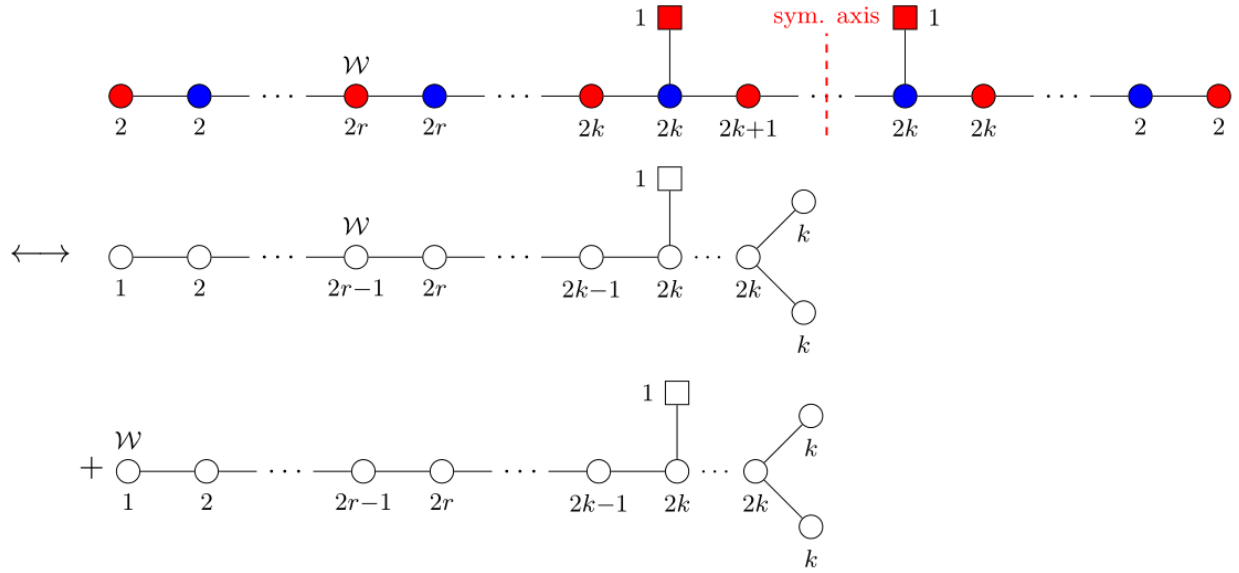


(3.2.2)

Here the Wilson lines transform in the fundamental representations for the unitary nodes. The above quiver diagram (similar cases for the following diagrams) means that the expectation value of a single Wilson line in the orthosymplectic quiver matches that of a linear combination of two Wilson lines on the unitary side.

**Observation 3:** When the Wilson line inserted at the Sp($k$) node which is at the position $l \geq 2k$ (not the

central node):

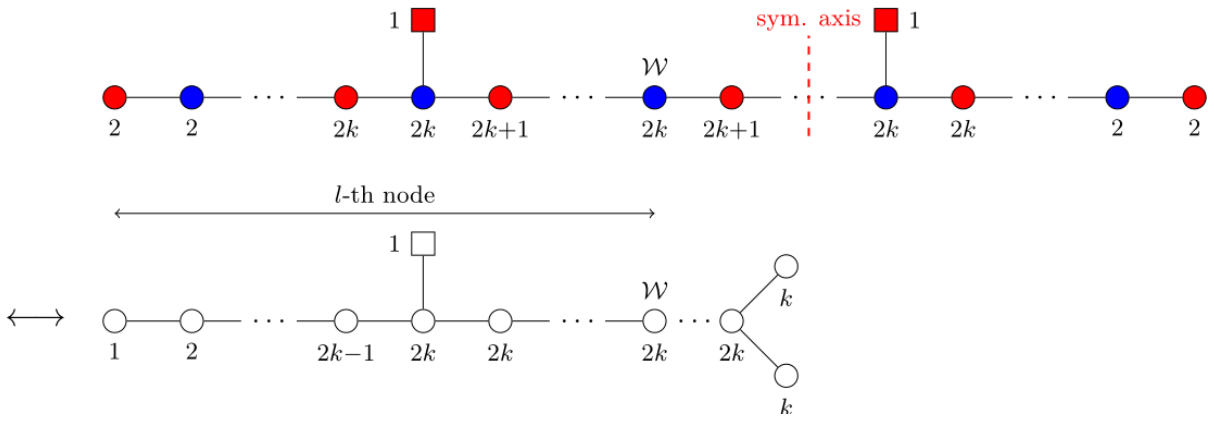


(3.2.3)

and the Wilson lines attached to the unitary nodes will transform under the fundamental representation.

**Observation 4:** When SO($2k+1$) node is inserted at the $l$-th node ( which is not at the center) and $l > 2k$:

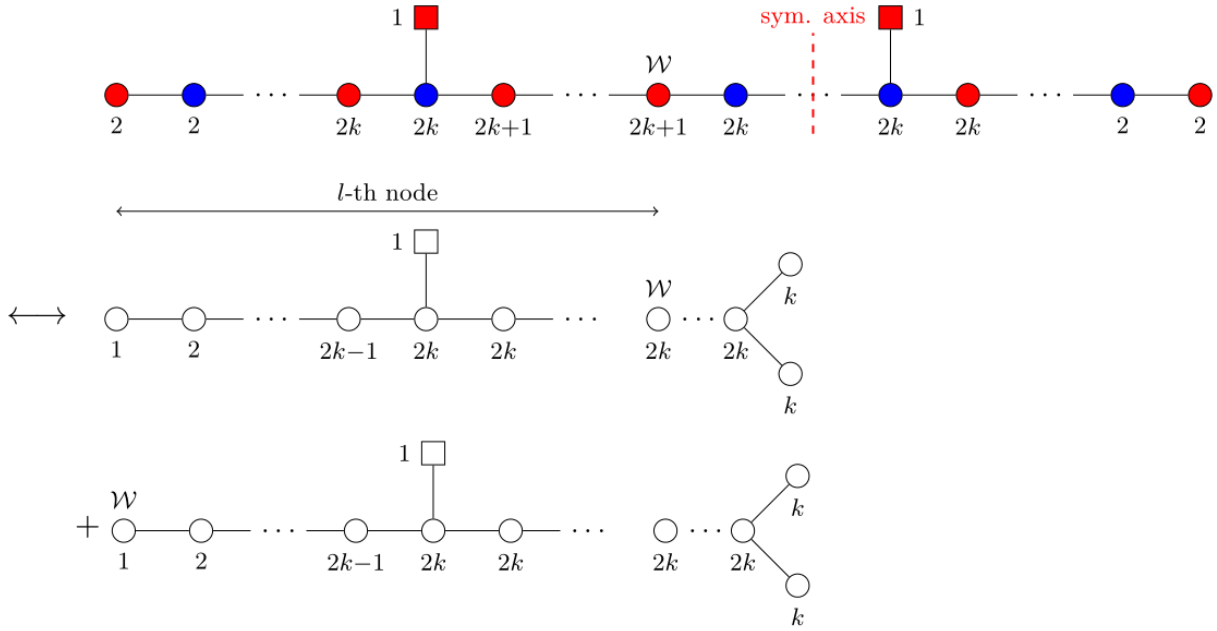


(3.2.4)

Here the Wilson lines attached to the unitary nodes will transform under the fundamental representation.

**Observation 5:** When a fundamental Wilson line is inserted at the central Sp($k$) node

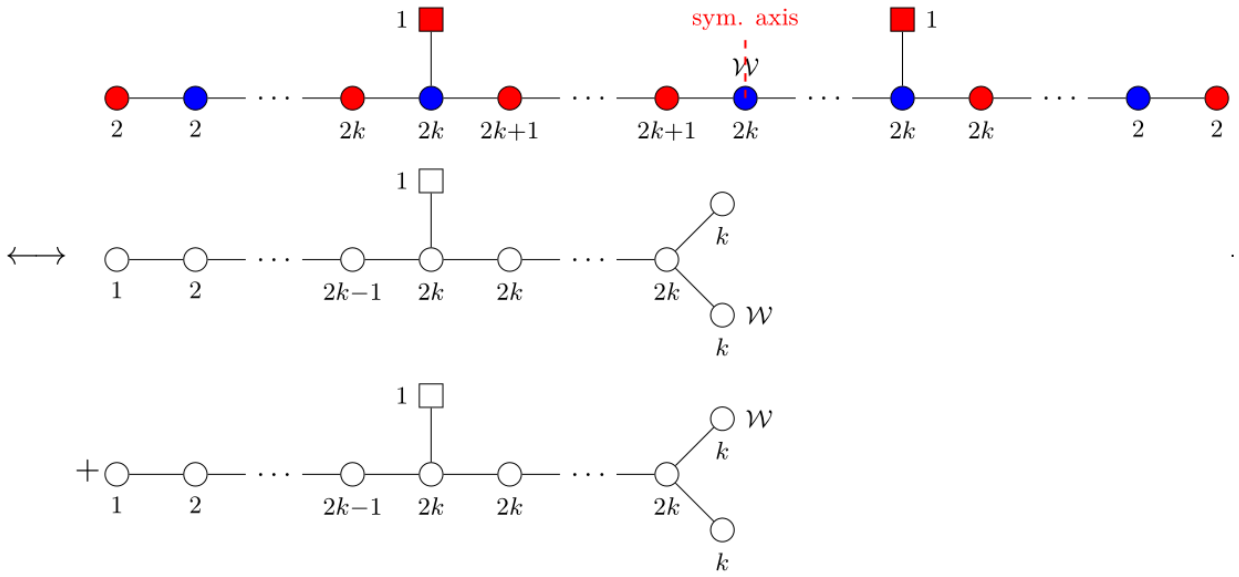


(3.2.5)

Note that the Wilson lines attached to the unitary nodes will transform under the fundamental representations.

**Observation 6:** When a fundamental Wilson line is inserted at the central SO($2k+1$) node and a fundamental Wilson line inserted at the unitary nodes

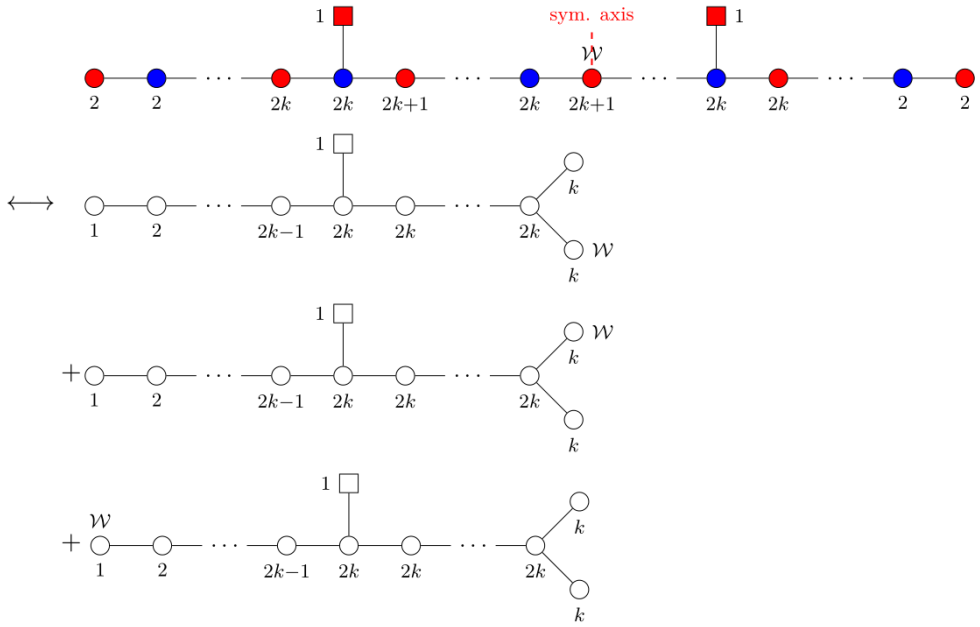


(3.2.6)

From observations 1, 3, one can notice that a Wilson line attached to an Sp gauge node is dual to a Wilson line inserted at the corresponding unitary node from the left in the quiver. From observations 2, 4, 6, a Wilson

line at a non-Abelian SO gauge node matches to a combination of one(s) at the unitary node(s) and one at the left U(1) node. From observation 5, one can conclude that a Wilson line inserted at the middle Sp gauge node matches with a linear combination of the Wilson lines inserted at the two spinor nodes. Finally, one can check that the total dimensions of the representation on both sides are equal.

The above observations also suit for balanced case $N_f = 2k + 1$. Because the flavour nodes are inserted at the spinor nodes in (3.1.3) or the central Sp node in (3.1.6), Observations 1 and 2 suit for all SO($2l$) nodes ($1 \leq l \leq k$) and all Sp($l$) nodes ($1 \leq l \leq k-1$) separately. Likewise, Observation 5 are applied to the Wilson line attached to the central Sp($k$) node.

## 3.3 Mirror Symmetry for Wilson and Vortex Defect

This section mainly discusses the properties of line operators under 3d $\mathcal{N} = 4$ mirror symmetry. In this case, Wilson and vortex line defect will interchange [35, 36, 49]. In the Sp($k$) SQCD with $N_f$ flavours case, a vortex defect can be described by an Sp($k$) representation $R$ and a flavor splitting $N_f = L + (N_f - L)$. It is expected to obtain the mirror Wilson lines from the Sp($k$) vortex lines by utilizing the brane realizations and confirming the exact partition functions match. Firstly, consider the brane system of Sp($k$) SQCD with a vortex line defect:

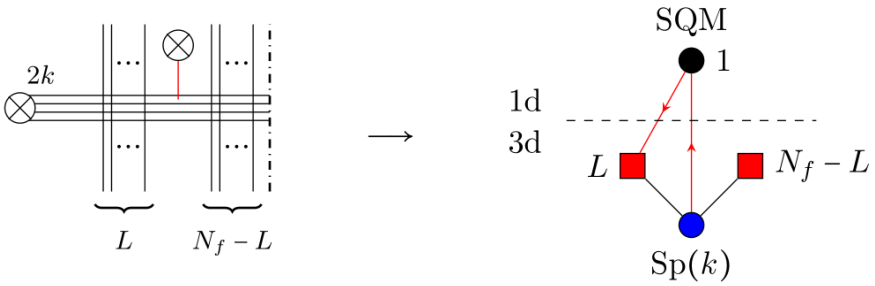


(3.3.1)

with the notations of (1.3.6). In this case, the D1-brane can terminate on any of the $2k$ D3-branes, therefore the vortex defect can be described by the fundamental representation of Sp($k$). The $S^3$ partition function for Sp($k$) SQCD with $N_f$ fundamental hypermultiplets of mass parameters $m_i$ ($i = 1, \ldots, N_f$) is

$$Z^{S^3}_{\mathrm{Sp}(k),N_f}(m) = \sum_{I \in C_k^{N_f}} \prod_{j=1}^{k} \frac{m_{I_j} \,\mathrm{sh}(2m_{I_j})}{\prod_{\ell \notin I} \mathrm{sh}(m_\ell \pm m_{I_j})} \tag{3.3.2}$$

here the index $I$ runs over all possible combinations $C_k^{N_f}$ of $k$ different integers out of the set $\{1, \ldots, N_f\}$. If there exists the vortex of type $L + (N_f - L)$ in (3.3.1) where the vortex couple to $L$ fundamental hypermultiplets, the partition function can be written as

$$Z^{S^3}_{(L,N_f-L),\mathbf{2k}} = (2k - L) \cdot Z^{S^3}_{\mathrm{Sp}(k),N_f}(m) + \sum_{j=1}^{L} Z^{S^3}_{\mathrm{Sp}(k),N_f}(m_j \to m_j - i)\,. \tag{3.3.3}$$

Now the mass parameters of hypermultiplets are charged under the vortex. In the Appendix 3, the computations of the $S^3$ partition functions (3.3.2)–(3.3.3) and a proof of the correspondences between the $S^3$ partition functions with line defects under the mirror symmetry when $k = 1$ are presented. The formula (3.3.3) indicates that there are 2k configurations of D1-brane ending on the D3 brane. It also shows a splitting of the flavors. After performing the S-duality, then these $2k$ brane configurations would bring about a linear combination of Wilson lines in the mirror dual. The following flavor splitting will show this. First let's pay attention to the $N_f > 2k+1$ case (3.1.2).

**Splitting $L+(N_f-L)$, $1 \le L \le 2k-1$.** If one performs S-duality, (3.3.1) would engender two different kinds of brane configurations. The first one contains the F1 string stretched between the defect D5-brane and one of the $L$ D3 branes in the following brane system

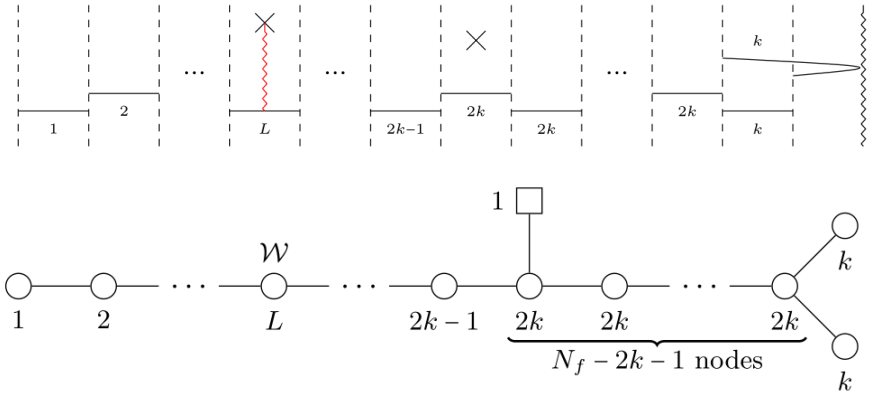


(3.3.4a)

The F1 string would result in a fundamental Wilson line in the U($L$) gauge group.

Another brane configuration is sourced from the so-called D3-brane spike [129], which means that the F1 sliding off the D5-branes because there are different numbers of D3 branes connecting on the two sides. There exists an F1 string extended between the defect D5-brane and flavor D5-brane. Actually, there exist $(2k - L)$ configurations that can engender the same brane system, and the flavor Wilson line defects that they produce comes with multiplicity $2k - L$.

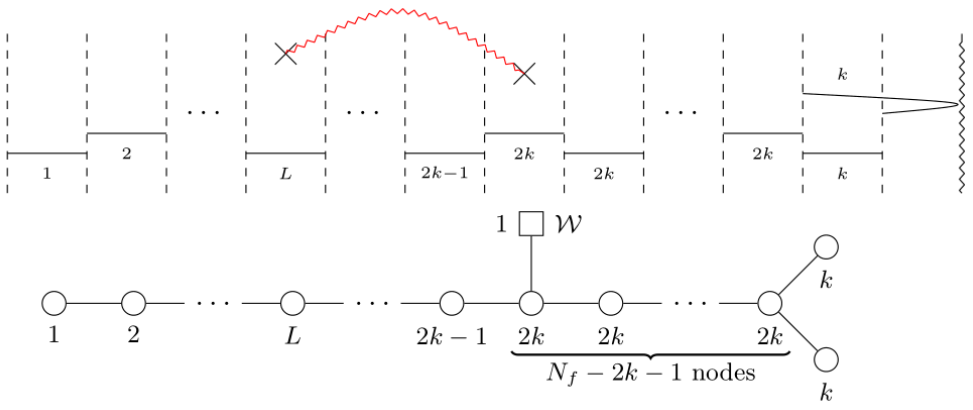


(3.3.4b)

For the unitary mirror quiver case (3.1.2), (3.1.3) and (3.1.4), the FI parameter $\xi_l - \xi_{l+1}$ is assigned to the $l$-th node counting from the left. Moreover, for the balanced $D$-type diagram, one can assign $\xi_{N_f-1} \pm \xi_{N_f}$ as the FI parameters to the two spinor nodes. The $S^3$ partition function of the corresponding mirror dual unitary quiver equals to (3.3.2) under interchanging the FI and mass parameters $\xi_i \longleftrightarrow m_i$. There is the $T[\mathrm{SU}(2k)]$ tail [87] in the mirror unitary counterpart (3.3.4), therefore the fundamental Wilson loop attached to the $L$-th node ($L \leq 2k-1$) will engender the shifts of the FI parameters [35] in the $S^3$ partition function as follows,

$$Z^{S^3}_{\mathcal{W}\text{ at U}(L)} = \sum_{j=1}^{L} Z^{S^3}(\xi_j \to \xi_j - i)\,.$$

Therefore, (3.3.3) turns into

$$Z^{S^3}_{(L,N_f-L),\mathbf{2k}}\big|_{m_i\to\xi_i} = Z^{S^3}_{\mathcal{W}\text{ at U}(L)} + (2k-L)\cdot Z^{S^3}(\xi) \tag{3.3.5}$$

where the first term gives a fundamental Wilson loop at the $L$-th node, the second term gives the $(2k-L)$ flavour Wilson loops on the unitary mirror side with interchanging the FI and mass parameters $\xi_i \longleftrightarrow m_i$.

One can also verify that there is also an similar relation holds for twisted indices

$$\mathbb{I}^{A}_{(L,N_f-L),\mathbf{2k}} = \mathbb{I}^{B}_{\mathcal{W}\text{ at U}(L)} + (2k-L)\cdot \mathbb{I}^{B} \tag{3.3.6}$$

The index $\mathbb{I}^B$ without defect operators on the right-hand side contributed by the flavour Wilson line because of the unrefined computation. The results of B-twisted indices for $k=1$ case are listed in Tables 4, 5, 6 and the results of A-twisted indices are listed in Table 2.

**Splitting $L+(N_f-L)$ for $2k \leq L \leq N_f-1$.** In this range of $L$, the S-duality of (3.3.1) only produce the following brane configuration:

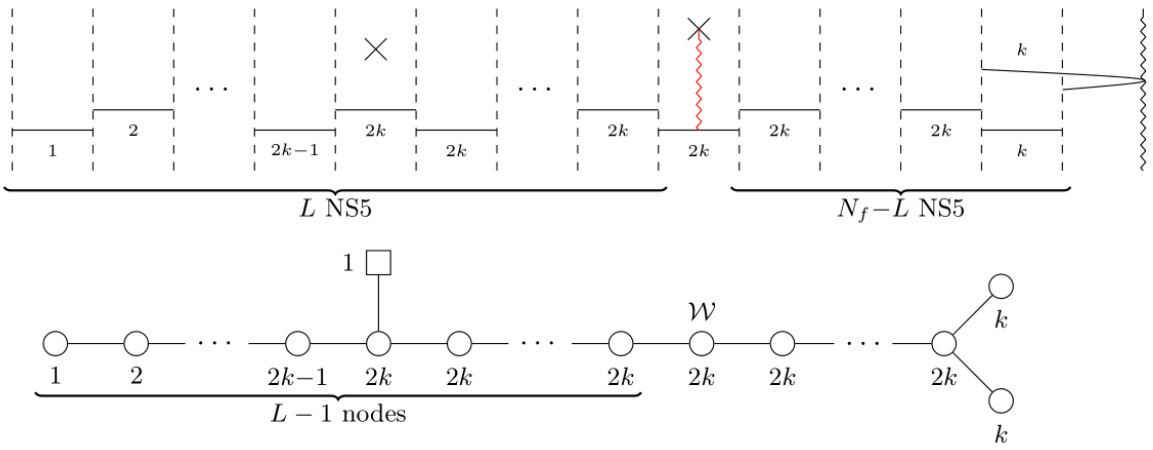


(3.3.7)

This brane configuration leads to a fundamental Wilson line attached to an U($2k$) node in the linear chain of the quiver theory. The result of (3.13) which engenders the $S^3$ partition function with the Wilson loop for the $k = 1$ case matches with the $S^3$ partition function with vortex in the mirror theory.

Similarly, (3.3.7) indicates the twisted indices satisfies:

$$\mathbb{I}^A_{(L,N_f-L),\mathbf{2}} = \mathbb{I}^B_{\mathcal{W} \text{ at } [0,\ldots,0,1,0,\ldots,0]} \tag{3.3.8}$$

where $[0,\ldots,0,1,0,\ldots,0]$ represents the $L$-th gauge node in the $D_{N_f}$-type Dynkin quiver. The B-twisted index are listed in Tables 4, 5 for $k = 1$, 6 and the A-twisted index are listed in Table 2.

**Splitting $(N_f-1)+1$.** As mentioned previously, after one performs S-duality, (3.3.1) would give two different types of brane configurations hinging on which D3 branes the F1 would terminate. Firstly, if there is an F1 extended between the defect D5-brane and the stack of $k$ D3-branes that does not move across the ON plane, the brane configuration is given as:

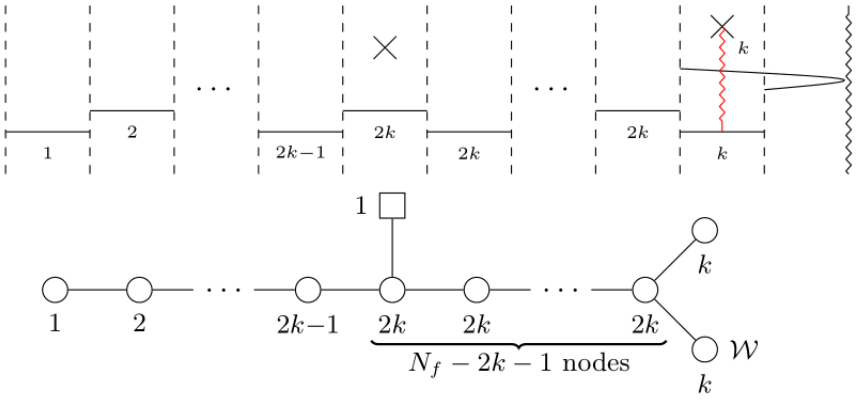


(3.3.9)

which produces a fundamental Wilson line in one of the spinor nodes of the balanced $D$-type diagram, it is a U($k$) node with FI parameter $\xi_{N_f-1} - \xi_{N_f}$. The F1 string could also extend between a defect D5 brane and $k$ D3 branes that move across the ON plane. This gives

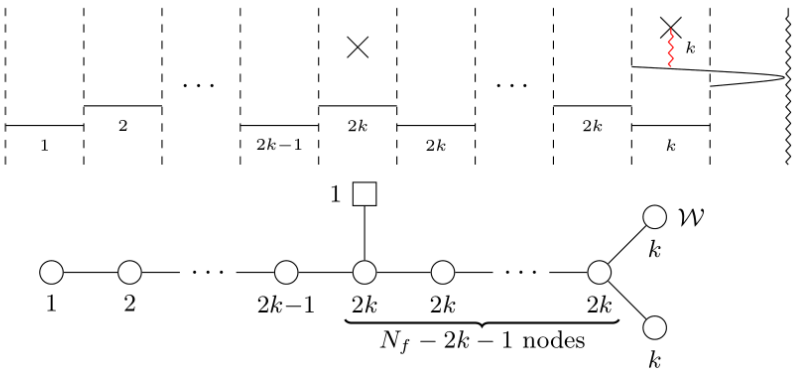


(3.3.10)

which induces a fundamental Wilson line on another spinor node of the balanced $D$-type diagram whose corresponding FI parameter is $\xi_{N_f-1}+\xi_{N_f}$. The summation of the $S^3$ partition functions in the presence of the $k=1$ Wilson loops was calculated as (3.16) shown, which matches with the mirror vortex. In terms of twisted indices, this implies

$$\mathbb{I}^{A}_{(N_f-1,1),\mathbf{2k}} = \mathbb{I}^{B}_{\mathcal{W}\text{ at }[0,\ldots,0,1,0]} + \mathbb{I}^{B}_{\mathcal{W}\text{ at }[0,\ldots,0,0,1]} \tag{3.3.11}$$

where $[0,\ldots,0,1,0]$ and $[0,\ldots,0,0,1]$ label the spinor nodes in the $D_{N_f}$-type quiver. The B-twisted indices for $k=1$ are listed in Tables 4, 5, 6 and the A-twisted indices are listed in Table 2.

**Splitting $N_f+0$.** In this case, the mirror symmetry between vortex defects becomes more subtle. Here the defect D5 brane appears between the NS5 brane and the ON plane, however, F1 has two different choices to terminate on the $D3$-branes stack hinging on whether $D3$ passes through the ON plane.

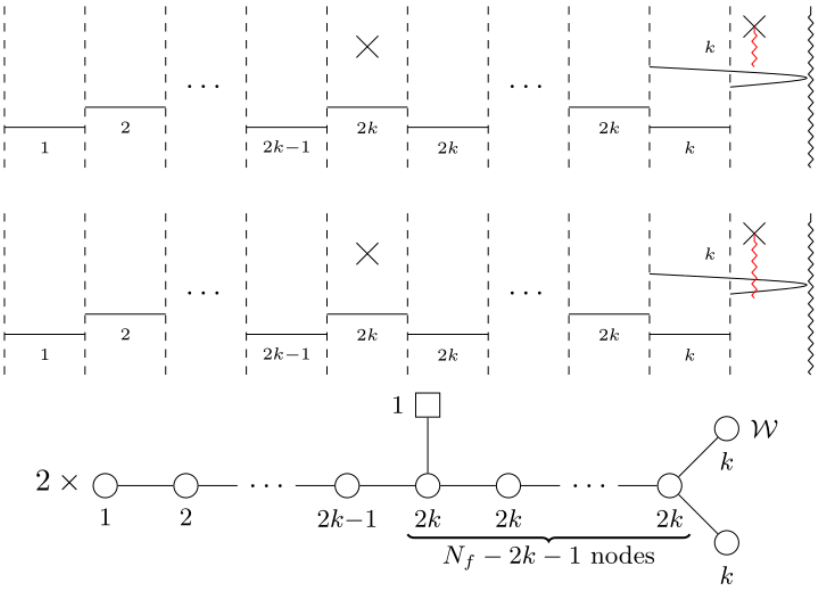


(3.3.12)

Here there will produce a multiplicity two of the Wilson line with FI parameter $\xi_{N_f-1}+\xi_{N_f}$ at the spinor node of type $[0,\ldots,0,1]$.

The $S^3$ partition functions satisfy the relation

$$Z^{S^3}_{(N_f,0),\mathbf{2k}} = 2\cdot Z^{S^3}_{\mathcal{W}\text{ at }[0,\ldots,0,1]}\,. \tag{3.3.13}$$

This relation has been checked for $k=1$ case in (3.17) and the result matches with the mirror vortex. For twisted indices, the relation under mirror symmetry is

$$\mathbb{I}^{A}_{(N_f,0),\mathbf{2k}} = (t+t^{-1})\cdot \mathbb{I}^{B}_{\mathcal{W}\text{ at }[0,\ldots,0,1]}\,. \tag{3.3.14}$$

Note that the factor $t + t^{-1}$ in (3.3.14) can be verified by computation, but the origination of this factor remains ambiguous. The results of the B-twisted index are listed in Tables 4, 5, 6 and for the A-twisted index are listed in Table 2.

**Balanced case.** This case satisfies the relation $N_f = 2k + 1$. As it is shown in (3.1.3), there are two flavor nodes reside at the two spinor nodes, so one can apply the pattern of (3.3.4) for all splittings of $L + (N_f - L)$, $1 \leq L \leq 2k - 1 = N_f - 2$. There are still two remaining splittings: $L = 2k = N_f - 1$ will engender the vortex defect which is dual to the summation of the expectation values of the Wilson lines inserted at the two spinor nodes, just as same as the case shown in (3.3.9)–(3.3.10). And the logic of $L = 2k + 1 = N_f$ case is similar to (3.3.12), i.e. there exists a Wilson line inserted at a spinor node with a multiplicity two.

**Comment on orthosymplectic mirror quiver.** One can utilize mirror symmetry to study the behaviors of Wilson lines as in §3.2 by studying the corresponding behaviors of vortex lines defects in the Sp($k$) SQCD. But since there are two different brane configurations for vortex defects, then this way is actually not straightforward.

For example, one can insert a D1 defect among any two half D5 branes for an O3 configuration

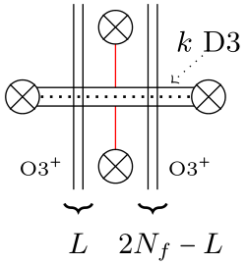


This configuration will engender a vortex of $L + (2N_f - L)$ splitting. Here the $2N_f$ half-hypermultiplets correspond to $2N_f + 2$ splittings. Half of these splittings can be got rid of once one takes the symmetry along the $x^6$ direction into consideration, then the 1d supersymmetric quantum mechanics and the coupling between this 1d SQM and the 3d theory would become more subtle. When $L$ is odd, the SQM coupled to the Sp($k$) gauge symmetry in the bulk and an SO($L$) flavour symmetry will give the vortex defect that does not appear in (3.3.1). Moreover, it is difficult to calculate the expectation value of the A-twisted index and $S^3$ partition function of such a vortex defect. This requires a detailed understanding of the 1d/3d coupled system which will be studied in future work.

## 3.4 A Comment on Vortex Line Defects in the Two Mirrors

In view of §3.2, it is also very intriguing to consider whether one can match the vortex line defects between the two different mirrors of Sp($k$) theory. One kind of intriguing vortex defect can be realized as 3d mirrors of a Wilson line in the fundamental representation in the Sp($k$) gauge symmetry.

**Unitary mirror quiver.** In this case, the position of the F1 string relative to the flavor D5 branes is unphysical. Because there is the same number of D3 branes on both sides of any D5 branes, the F1 string can freely move across these D5 branes. The brane realization for a Wilson line in the fundamental representation is

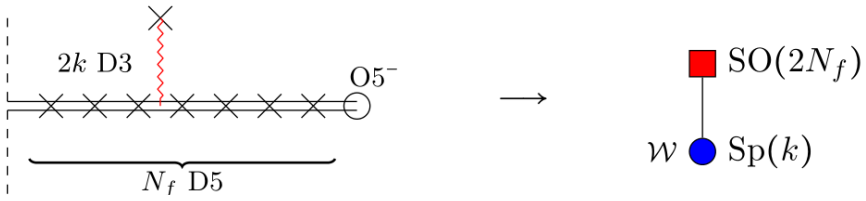


**Fig. 3-3.** The brane construction for a fundamental Wilson line

According to 3-3 and with the condition $N_f > 2k+1$, the mirror vortex defect is given by the following brane system:

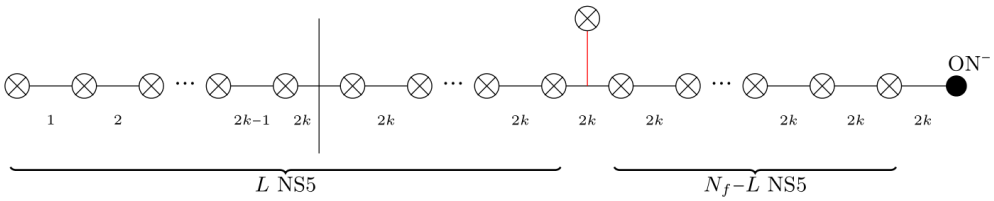


**Fig. 3-4.** Sp(k) mirror vortex brane configuration Nf>2k+1

One can move the D1-string to the closet NS5-brane on the left, which leads to the following insertion:

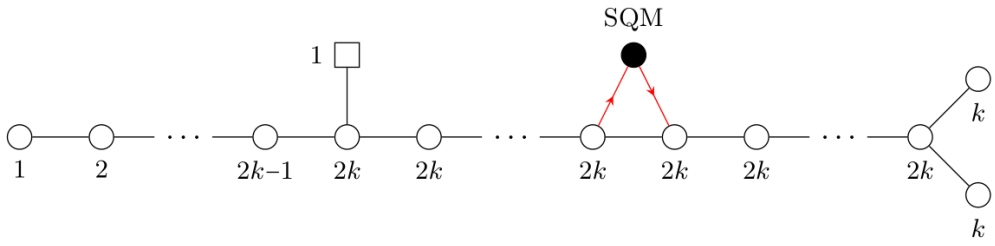


(3.4.1)

while the following defect insertion is realized by moving the D1-string to the closest NS5 brane on the right:

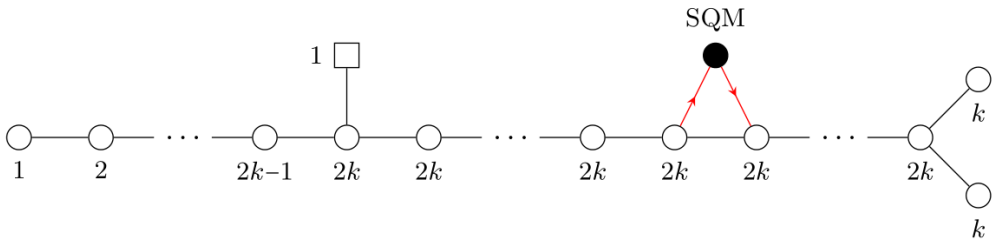


(3.4.2)

For brane configuration (3-4), it is straightforward to see that the above two defects are equivalent since the D-string can move across any of the NS5-branes provided that there is the same number of D3 branes on both sides

of NS5 branes. Put differently, the vortex defects are equivalent to each other if they are defined by two adjacent U($2k$) gauge nodes. In [35], this was also been proved in terms of $S^3$ partition function.

Similarly, the following configurations also describe dual defects according to hopping duality

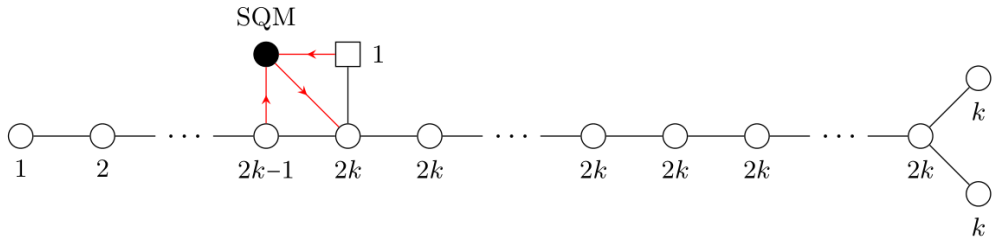


(3.4.3)

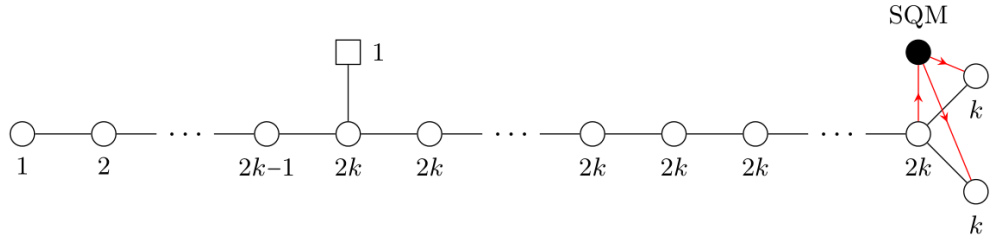


(3.4.4)

Their equivalency can be derived directly from the discussions in [35]. For the case of $k = 1$ $N_f > 3$, one can show that the vortex loop included in the $D$-type quiver is mirror dual to the Wilson loop included in the Sp(1) SQCD by evaluating the $S^3$ partition functions (3.20).

**Orthosymplectic mirror quiver.** Now considering the brane system of a Sp($k$) gauge theory with a Wilson line in fundamental representation with utilizing an O3 plane as shown in Figure 3-5. One should note that the

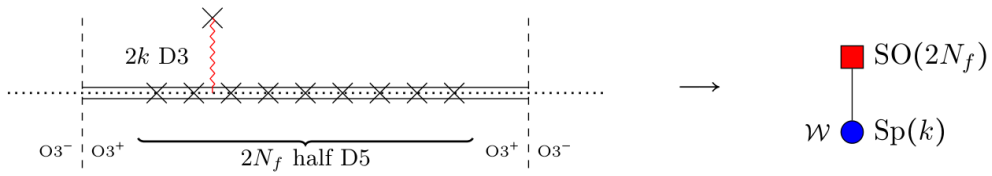


**Fig. 3-5.** Brane configuration of a Sp($k$) gauge theory with a fundamental Wilson line with utilizing an O3 plane

F1's position relative to the flavor D5 branes is not physical. Because there is the same number of D3 branes on both sides of any half D5 branes, the F1 string can freely move across these half D5 branes.

According to Figure 3-5 and with the condition $N_f > 2k + 1$, the mirror configuration is the following system Because here is same number of D3-branes on both sides, D1 string can freely move through any central half NS5-branes. The following defect insertion can be realized by moving the D1-string in 3-6 to the closet NS5

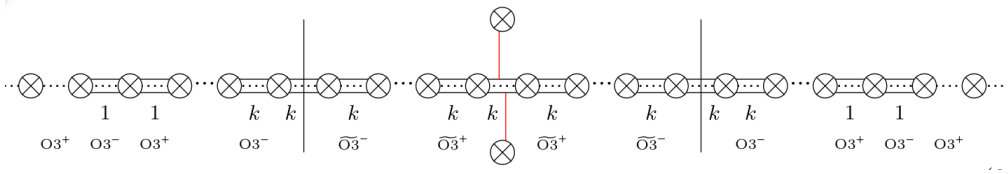


**Fig. 3-6.** The mirror configuration of 3-5 with condition $N_f > 2k+1$.

brane on the left:

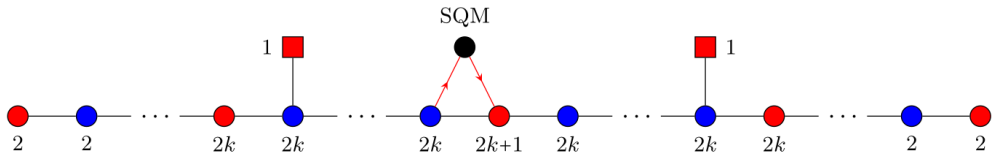


(3.4.5)

while the following defect insertion can be realized by moving the D1-string in 3-6 to the closet NS5 brane on the right:

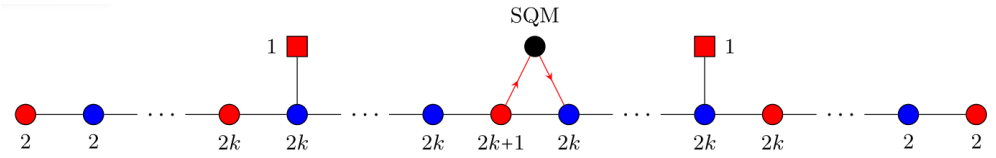


(3.4.6)

Same as the above cases, one can check that these two defects are equivalent according to the generalization of the hopping duality to the brane systems with O3 planes. Therefore, the vortex defects defined by two successive Sp($k$) and SO($2k+1$) nodes should be the same, which is mirror dual to a Wilson line defect in the fundamental representation.

Furthermore, there exists another mirror pair of the Wilson lines in the fundamental representations which can be realised in the Sp($k$) theories:

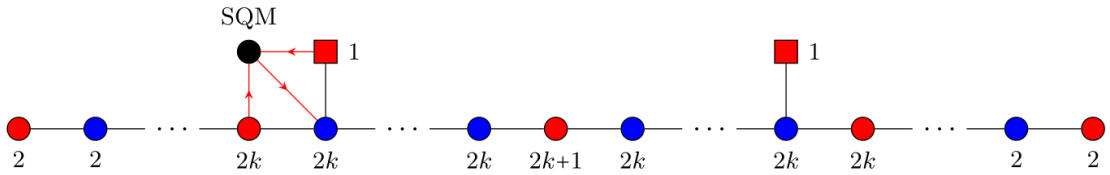


(3.4.7)

This can be obtained by moving the D1 string in 3-6 to the left of the interval including the half D5 flavour brane. However, the verification of these predictions by using the A-twisted index or $S^3$ partition function is still unclear yet.In the future, it is possible to use squashed sphere partition function [130, 131] to verify these predictions.

**Comments on the balanced case $N_f = 2k+1$.** One may conjecture the following statements along the above logic: a fundamental Wilson line in Sp($k$) SQCD with $N_f = 2k+1$ flavours is expected to be mirror dual to

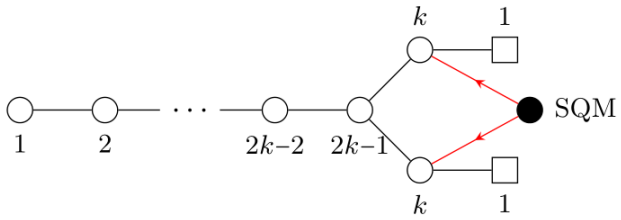


(3.4.8)

Furthermore, the expectation value of Wilson line ought to be mirror dual to the following orthosymplectic quiver with inserting vortex defect:

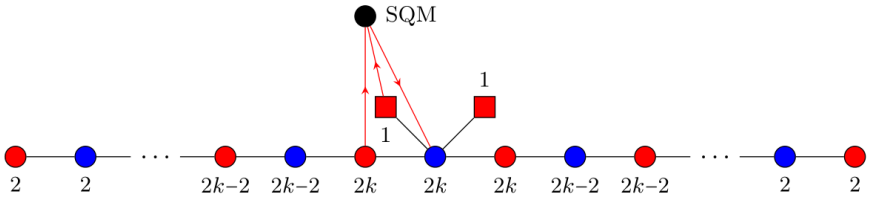


(3.4.9)

But up to now, it is still a puzzle about how to describe the coupling between 1d SQM and the half-hypermultiplet exactly. This remains for future research.

## 3.5 The Main Results of Chapter 3

This chapter mainly discussed the various behaviors of the Wilosn and vortex line defects in 3d Sp($k$) SQCD. The main results of this chapter can be summarized as follows:

- By evaluating the superconformal indices to the given order of perturbative expansion, a pair of 3d $\mathcal{N} = 4$ unitary and orthosymplectic mirror quivers were obtained from the Sp($k$) SQCD and they have been verified to flow to the same IR fixed point. Furthermore, under the limit $t_h \to 0$ and $t_c \to 0$, the superconformal indices reproduce the know Coulomb and Higgs branch Hilbert series of 3d $\mathcal{N} = 4$ theory.

- By evaluating the B-twisted indices, a dictionary for Wilson line operators that originate from an equal number of brane configurations was created under the unitary/orthosymplectic duality. The total dimensions of the representations for Wilson lines keep invariant under the duality. Several observations were provided as examples of the dictionary.

- The vortex defects in the Sp($k$) SQCD with $N_f$ flavors were included by splitting the $N_f$ flavors as $N_f = L + (N_f - L)$. This kind of vortex can be realized by $2k$ configurations of the D1 ending on D3 branes. These $2k$ configurations would engender a linear combination of the Wilson line defects in the mirror theory under S-duality. This chapter also analyzed various flavor splitting and checked the

mirror symmetry for Wilson and vortex defects by evaluating the $S^3$ partition function and twisted index, including $N_f > 2k+1$ and $N_f = 2k+1$ cases.

- This chapter also discussed the matches between the vortex line defects between two different mirrors of Sp($k$) gauge theory. It was found that the vortex defects defined by two adjacent U($2k$) nodes are equivalent from the perspective of the brane system and the $S^3$ partition functions on the unitary side. Meanwhile, the vortex defect defined by two consecutive Sp($k$) and SO($2k+1$) gauge nodes could also be viewed as the same defect that mirror dual to a fundamental Wilson line defect.

# Chapter 4 5d Sp($k$) SQCD

This chapter mainly consider the 5d $\mathcal{N}=1$ theory with Sp($k$) gauge group and $N_f$ fundamental flavours. If the low-energy description admits a UV completion into 5d $\mathcal{N}=1$ superconformal field theory, then it must satisfy $N_f \leq 2k+5$. Although the restraint was used to be $N_f \leq 2k+4$ from the perspective of field theory [132] and 5-brane web [133], but this condition could be relaxed to the case $N_f = 2k+5$ in [134].

When the Higgs branch of a 5d $\mathcal{N}=1$ theory varies from the IR range at the finite coupling to the UV range at infinite coupling, there will be new massless instantons appear. And the magnetic quiver technique [3, 8, 24, 25] can give the descriptions for both cases. Following the same logic in §3, there are two different string theory realizations for the cases of Sp($k$) gauge groups which will engender two kinds of magnetic quivers:

- Unitary quivers obtained from the 5-brane webs with the existence of an O7$^-$ plane [8].
- (unitary-)orthosymplectic magnetic quivers obtained from 5-brane webs with an O5$^+$ plane [8, 11].

Note that for the finite coupling case, the magnetic quivers are the same as 3d Sp($k$) mirror quivers in §3. Therefore, one should pay attention to the case of the Higgs branch at infinite coupling whose related unitary and orthosymplectic quivers are presented in the Table 1 of [8]. At the strong coupling fixed point, the unitary magnetic quivers derived from 5d or 6d brane systems have no explicit flavour nodes, which are also called *unframed quivers*. To render a well-defined theory, one needs to remove an overall U(1) from the quiver gauge group. In Table 1 of [8], this diagonal U(1) can be removed by ungauging a U(1) gauge node first and then choosing a U(1) gauge node which is not balanced if there is such a node. Because the magnetic quivers only contain good nodes, therefore the appropriate U(1) gauge node is always over-balanced. Due to the presence of the Dynkin diagram of the enhanced symmetry of the Coulomb branch provided by the collection of balanced nodes, it is injudicious to discard this pattern. A detailed explanation is given in Appendix 2.3.

The orthosymplectic quivers are unframed if they correspond to $\mathcal{M}_H$ of 5d / 6d theories at the strong coupling fixed point, except for the fact that one needs to sum over the *integer + half-intege* magnetic lattice due to a diagonal $\mathbb{Z}_2$. This fact is important when one evaluates such as SCIs, A-twisted indices, and the Hilbert series of the Coulomb branch.

## 4.1 Duality of Unitary and Orthosymplectic Magnetic Quivers

It was proposed that the 3d $\mathcal{N} = 4$ unitary and orthosymplectic magnetic quiver shares both the same Coulomb and Higgs branch [38], resulting in the corresponding Hilbert series equal. This part of the thesis will provide the evidence that they flow to the same IR fixed points by computing the exact results, which shows that they are dual at the QFT level.

**$E_4$ quiver.** First considering the case $k = 1$, $N_f = 3$. The $E_4 \cong \mathfrak{su}(5)$ quiver is given by the $\mathfrak{su}(5)$ Dynkin diagram. Here the wiggly line on the right-hand side denotes a charge 2 hypermultiplet under the U(1) gauge

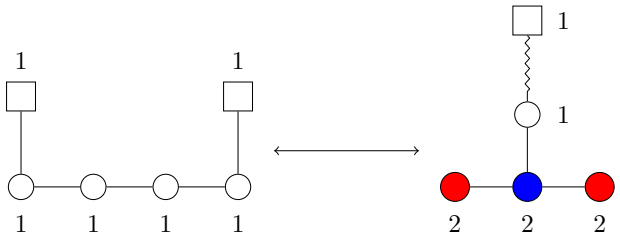


**Fig. 4-1.** $E_4$ quiver

node. Remark that here the index for the orthosymplectic case needs to be computed as mentioned in §2.4. By perturbative computation, one can show that these two quivers give the equal superconformal indices

$$\begin{aligned}\mathbb{I} = 1 &+ \sqrt{\mathfrak{q}}\left(\frac{24}{\mathfrak{t}^2} + \mathfrak{t}^2\right) + \mathfrak{q}\left(-26 + \frac{200}{\mathfrak{t}^4} + \mathfrak{t}^4\right) + 2\mathfrak{q}^{\frac{5}{4}}\mathfrak{t}^5 + \mathfrak{q}^{\frac{3}{2}}\left(\frac{1000}{\mathfrak{t}^6} - \frac{451}{\mathfrak{t}^2} + \mathfrak{t}^6\right) + \mathfrak{q}^{\frac{7}{4}}\left(-2\mathfrak{t}^3 + 2\mathfrak{t}^7\right) \\ &+ \mathfrak{q}^2\left(373 + \frac{3675}{\mathfrak{t}^8} - \frac{2824}{\mathfrak{t}^4} + \mathfrak{t}^8\right) + \ldots \end{aligned} \tag{4.1.1}$$

up to order $\mathcal{O}(\mathfrak{q}^2)$.

**$E_5$ quiver.** Then consider the $N_f = 4$ case. The unitary quiver has been given by the $k = 1$, $N_f = 5$ case in §3, the orthosymplectic case is presented in the following diagram. Since the orthosymplectic quiver is unframed, one needs to sum over both integer and half-integer lattice. Then one can show that both quivers give the same superconformal indices by perturbative expansion, which is same as $k = 1$, $N_f = 5$ case of Table 1 up to $\mathcal{O}(\mathfrak{q}^{3/2})$.

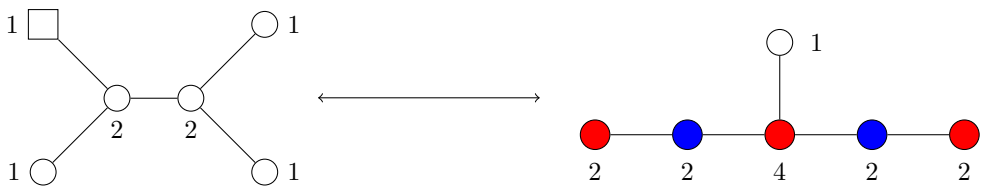


**Fig. 4-2.** $E_5$ quiver

**$E_6$ quiver.**　Consider the unitary quiver (4-3): whose Coulomb branch is given by the closure of the $E_6$ minimal

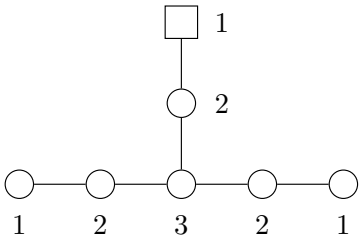


**Fig. 4-3.** $E_6$ quiver

nilpotent orbit $\overline{\mathcal{O}}_{\text{min}}^{\mathfrak{E}_6}$. Moreover, for the unitary-orthosymplectic quiver, the Coulomb branch is also given by $\overline{\mathcal{O}}_{\text{min}}^{\mathfrak{E}_6}$ takes the following form [8] (see also A.1.5 of [135] for class $\mathcal{S}$ description):


Due the computation abilities of computer, the superconformal indices of these theories can only be expanded to order $\mathcal{O}(\mathfrak{q})$. which yields the same result as follows:

$$\mathbb{I} = 1 + \frac{78\sqrt{\mathfrak{q}}}{\mathfrak{t}^2} + \mathfrak{q}\left(-79 + \frac{2430}{\mathfrak{t}^4}\right) + \dots \,. \tag{4.1.2}$$

**$E_7$ quiver.**　Then considering the unitary-orthosymplectic quiver whose Coulomb branch is $\overline{\mathcal{O}}_{\text{min}}^{\mathfrak{E}_7}$.

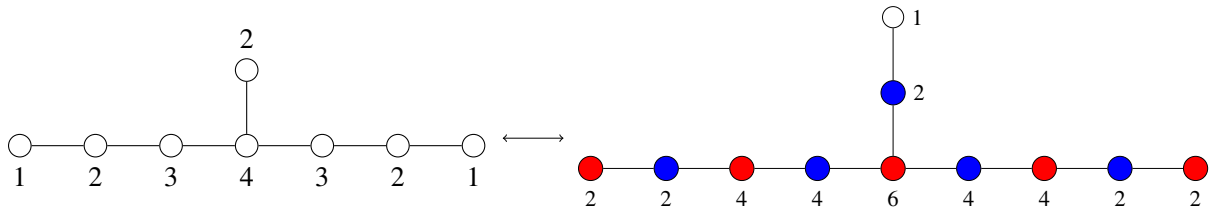


(4.1.3)

Here the unitary quiver is unframed, the orthosymplectic quiver was also known [8] (the viewpoint of class $\mathcal{S}$ is given in the section 3.2.2 of [136]). Now it is very difficult to evaluate the superconformal indices because of the high rank of gauge groups. However, one can use the $S^3$ partition function since they are equivalence for these theories on the level of the various legs in the two star-shaped quivers (4.1.3). In order to implement the computation, one can decouple a U(1) factor from the middle U(4) gauge node to turn it into a SU(4) gauge node, this can be done because the computation of sphere partition function is irrelevant to the magnetic lattice (Refer to §2.4.).

The two tails of both the quivers in (4.1.3) are $T[\text{SU}(4)] \simeq T[\text{SO}(6)]$ [87]. For a general $T[G]$ theory, the

corresponding partition function is represented in (3.26). For $T[\mathrm{SU}(4)] \simeq T[\mathrm{SO}(6)]$, one can check that

$$Z^{S^3}_{T[\mathrm{SU}(4)]} = Z^{S^3}_{T[\mathrm{SO}(6)]} = \frac{1}{12} \prod_{1\le i<j\le 3} \frac{(m_i \pm m_j)}{\mathrm{sh}(m_i \pm m_j)} \,. \tag{4.1.4}$$

By computing residues, the $S^3$ partition function of the other tail is

$$Z^{S^3}\left[\begin{array}{ccc} 2 & & \mathrm{SU}(4) \\ \circ & - & \square \end{array}\right] = Z^{S^3}\left[\begin{array}{ccccc} 1 & & 2 & & 6 \\ \circ & - & \bullet & - & \blacksquare \end{array}\right] = \sum_{i=1}^{3} \frac{m_i^2}{\prod_{j\neq i} \mathrm{sh}(m_j \pm m_i)} \,. \tag{4.1.5}$$

Note that (4.1.5) is given by the result of the (3.24) with imposing the equality $m_4 = m_1 + m_2 + m_3$ due to the SU(4) flavor symmetry. Thus, the equalities of (4.1.4) and (4.1.5) indicate that the $S^3$ partition functions of the both side of (4.1.3) match.

## 4.2 Wilson lines and Unframed Quivers

**Admissible Wilson lines for unframed unitary quivers.** There are several ways to realize the quotient $\prod_i \mathrm{U}(n_i)/\ker\phi$ (refer to §2.4 ), where $\ker\phi \cong \mathrm{U}(1)$ is continuous. One needs to treat the allowed line defects carefully, even if these theories have been alleged to engender the same moduli spaces:

- If $n_i = 1$ for some $i$ which corrresponds to over-balanced gauge nodes, then one can ungauge the group and the resulting quotient is $G' = G/\ker\phi \cong \prod_{j\neq i} \mathrm{U}(n_j)$. Because there is the U(1) flavor nodes for $i$, $G'$ do not have trivially acting subgroup. Then the representations under which the Wilson lines transform could be arbitrary product representation of $\mathrm{U}(n_j)|_{j\neq i}$, *i.e.*

$$\mathcal{W} \in \Lambda_w^{G'} = \bigoplus_{j\neq i} \mathbb{Z}^{n_j} \,. \tag{4.2.1}$$

- For the case $n_i \geq 2$, one can also remove $\ker\ \phi$ from $\mathrm{U}(n_i)$ node. Then the gauge group will turn into $G^{\mathrm{naive}} = \mathrm{SU}(n_i) \times \prod_{j\neq i} \mathrm{U}(n_j)$. However, there are still remain a non-trivial $\mathbb{Z}_{n_i}^{\mathrm{diag}} = Z(\mathrm{SU}(n_i)) \subset \mathrm{U}(1) = Z(\mathrm{U}(n_j))$ for $j \neq i$. This $\mathbb{Z}_{n_i}$ will acts trivially on the matter content and give an electric 1-form symmetry for $G^{\mathrm{naive}}$ gauge theory [37]. Nonetheless, from the perspective of brane configuration, the proper gauge group should be $G' = G^{\mathrm{naive}}/\mathbb{Z}_{n_i}^{\mathrm{diag}}$ which will define the allowed Wilson line representation $\mathcal{R}$ to be $\mathrm{SU}(n_i) \times \prod_{j\neq i} \mathrm{U}(n_j)$. In this way, the representation $\mathcal{R}$ is $\mathbb{Z}_{n_i}^{\mathrm{diag}}$ invariant therefore its charge under this diagonal U(1) is 0 mod $n_i$.

As an example, one can check the following affine $E_6$ unitary quiver with the charges $q^{(I)}$ for $\mathrm{U}(1)_I$, $\{a_i^{(I)}\}_{i=1,2}$ for the $\mathrm{U}(2)_I$ fugacities and $\{b_j\}_{j=1,2,3}$ for the U(3) fugacities. In Figure 4-5a, one can see that the diagonal U(1) subgroup for $\mathrm{U}(1)_3$ node has been ungauged, therefore it is definitely able to consider the non-trivial Wilson line:

$$\mathcal{R} = q^{(1)} \otimes \prod_I [0,0]_{a_i^{(I)}} \otimes [0,0,0]_{b_j} \tag{4.2.2}$$

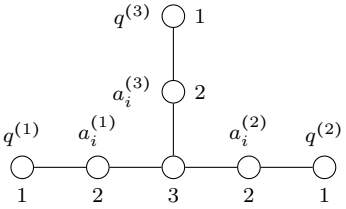


**Fig. 4-4.** affine $E_6$ quiver

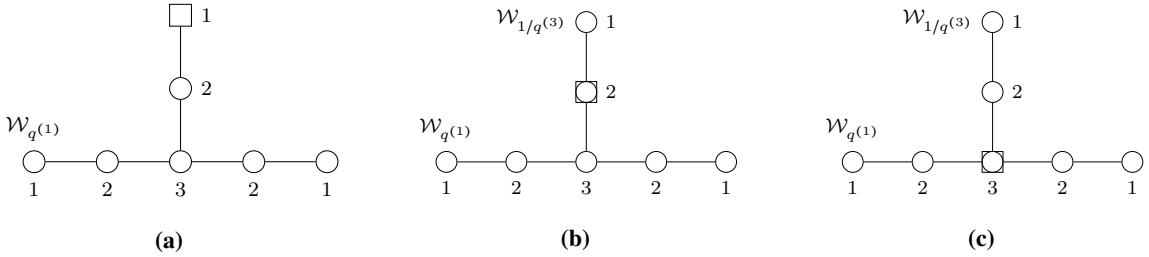


**Fig. 4-5.** Affine $E_6$ Dynkin quiver and various choices of ungauging. The superposition of a circle and a square is called a squircle, it stands for the node whose diagonal U(1) is ungauged. The Wilson lines defined in each theory have the same B-twisted indices, see Table 15.

Then in Figure 4-5b, one can see that the diagonal U(1) subgroup for $\mathrm{U}(2)_3$ node has been ungauged. Therefore, the Wilson lines are demanded to be $\mathbb{Z}_2^{\text{diag}}$-invariant. Therefore, the representation $\mathcal{R}$ (4.2.2) need to be modified by $\mathbb{Z}_2$ invariance by introducing an extra $q^{(3)}$ charge:

$$\begin{aligned} \mathcal{R}' &= q^{(1)} \otimes \left(q^{(3)}\right)^x \otimes \prod_{I\neq 3} [0,0]_{a_i^{(I)}} \otimes [0]_{\mathrm{SU}(2)_{(3)}} \otimes [0,0,0]_{b_j} \\ \mathbb{Z}_2 - \text{invariance} \quad &\Rightarrow \quad 1 + x = 0 \bmod 2 \end{aligned} \tag{4.2.3}$$

Similarly, in Figure 4-5c there will yield $\mathbb{Z}_3$ invariant Wilson line after ungauging the central U(3) node by introducing the $q^{(3)}$ charge:

$$\begin{aligned} \mathcal{R}'' &= q^{(1)} \otimes \left(q^{(3)}\right)^x \otimes \prod_{I} [0,0]_{a_i^{(I)}} \otimes [0,0]_{\mathrm{SU}(3)} \\ \mathbb{Z}_3 - \text{invariance} \quad &\Rightarrow \quad 1 + x = 0 \bmod 3 \end{aligned} \tag{4.2.4}$$

The simplest case which is in agreement with (4.2.2), (4.2.3),(4.2.4) is $x = -1$. Moreover, the computation results of the B-twisted indices agree in Figure 4-5. The result is listed in Table 15.

**Admissible Wilson lines for unframed orthosymplectic quivers.** In this case, one needs to remove the diagonal $\ker \phi = \mathbb{Z}_2$ for both magnetic lattice and weight lattice of the gauge group, refer to (2.4.4). Since the fundamental representation of a single SO($2n$) node or single Sp($k$) node is not included in the weight lattice, therefore one is not permitted to admit the Wilson line transforming in these representations. If one pursues the Wilson line operators in "simple" representation, there are two ways as follows:

- Insert the Wilson line operator which transforms according to the product of two fundamental representations of two different gauge nodes. This matches to the $\mathbb{Z}^n_{\sum|\text{odd}} \oplus \mathbb{Z}^k_{\sum|\text{odd}}$ factor in (2.4.4).
- Insert the Wilson line operator which transforms according to a representation on the root lattice of a SO($2n$) or Sp($k$) gauge node, which matches to the $\mathbb{Z}^n_{\sum|\text{even}} \oplus \mathbb{Z}^k_{\sum|\text{even}}$ factor in (2.4.4).

## 4.3 General Observations and Conjectures

This section will find a pattern between the permissible Wilson lines of various magnetic quiver constructions, which is prompted by the observation of the two different mirror quivers in Chapter 3. There are two kinds of exceptional families [8]:

- The $E_{8,7,6,5}$ families who are classified by the rank $k$ of the 5d Sp($k$) gauge group.
- The $E_{4-2l}$ and $E_{3-2l}$ families hinge on the rank $k$ and an integer $0 \leq l \leq k$.

Due to the 5-branes which are unaffected by the orientifold projection, except $E_8$ family, there is a single U(1) in all orthosymplectic quivers for exceptional $E_n$ families. And since this U(1) will not increase the dimension of the representation, one can study the Wilson lines in $q \otimes [1,0,\ldots,0]_{C/D}$ of U(1) representation with charges 1 and a fundamental representation of a Sp($2n$) or SO($k$) gauge node.

For $E_{7,6,5}$ with $k = 1$, the B-twisted indices with Wilson loops have been listed in Tables 5, 15, 16. Also, the results for $E_4$ with $k = 1, 2$ and $E_3$ with $k = 1, 2, 3$ are listed in Tables 10, 11, 12, 13. These indices present a structural pattern of the Wilson lines in unitary and orthosymplectic quivers[①]. The pattern shows the conjectures as follows based on the results and with assuming the regularity of the behavior:

**$E_7$ family.** For a Wilson line which transforms under $q \otimes [1,0,\ldots,0]_{C_r}$ of the U(1) gauge node and an Sp($r$) gauge node ($1 \leq r \leq k+1$)

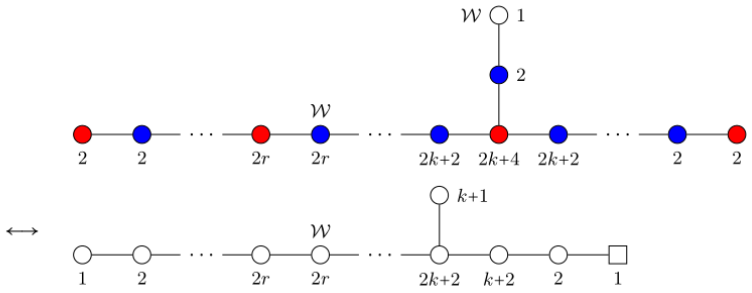


(4.3.1)

① For $E_n$ families, one can derive the unframed unitary quivers from brane webs. In order to fix the center of mass of the brane configuration, one need to ungauge an overall U(1) factors. Appendix 2.3 further explains how to choose the ways of ungauging.

The Wilson line transforming in $q \otimes [1,0,\ldots,0]_{D_r}$ of the U(1) and an SO($2r$) gauge node, here $1 \leq r \leq k+2$

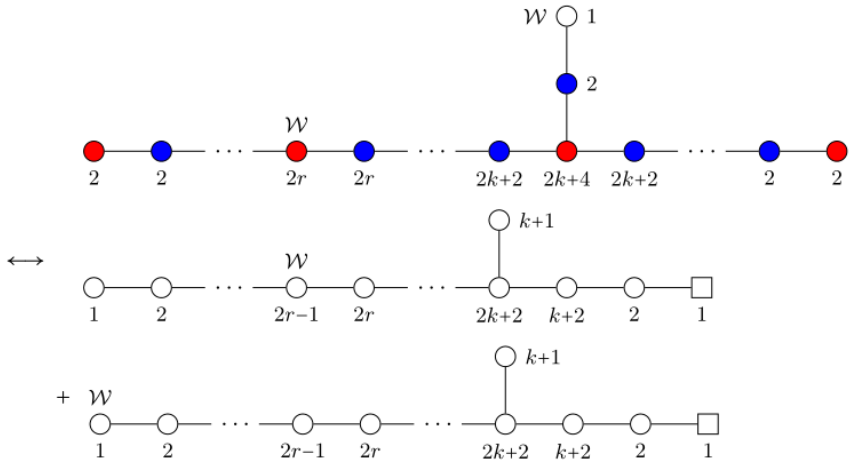


(4.3.2)

Note that for $r = 1$ case, there only exists a single Wilson line in the unitary quiver. The Wilson line transforming in $q \otimes [1,0,\ldots,0]_{D_{k+2}}$ of the U(1) and an SO($2k+4$) gauge node

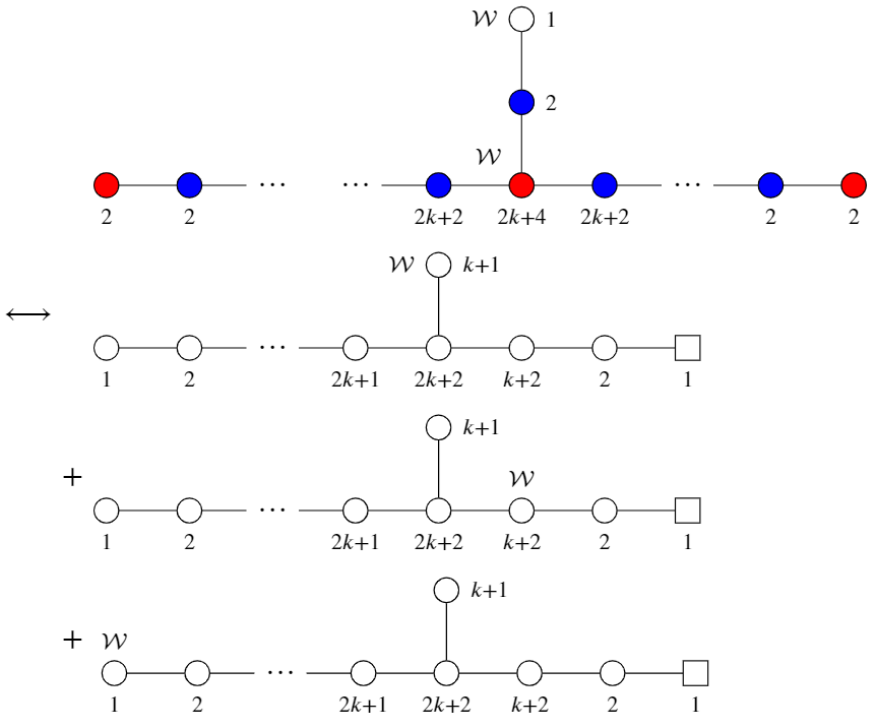


(4.3.3)

**$E_6$ family.** The Wilson line transforming in $q \otimes [1,0,\ldots,0]_{C_r}$ of the U(1) and an Sp($r$) gauge node, here $1 \le r \le k+1$

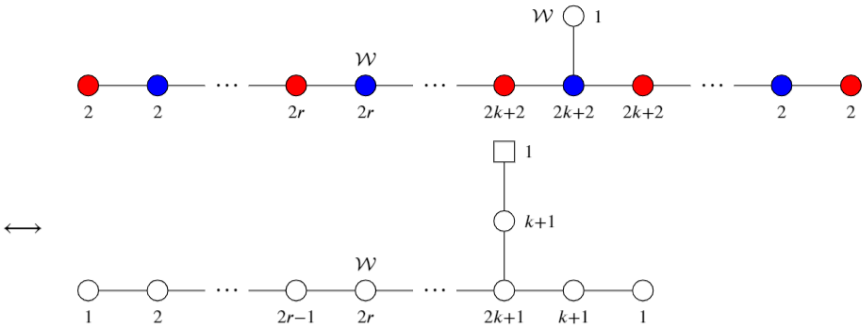


(4.3.4)

The Wilson line transforming in $q \otimes [1,0,\ldots,0]_{D_r}$ of the U(1) and an SO($2r$) gauge node, here $1 \le r \le k+3$

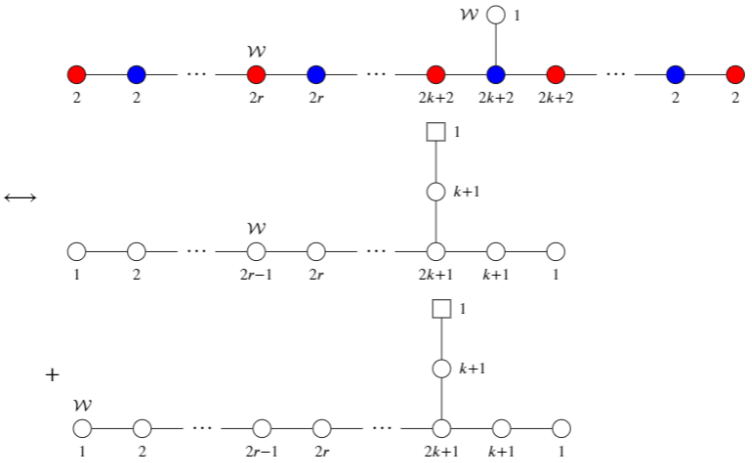


(4.3.5)

Note that for $r = 1$ case, there only exists one Wilson line in the unitary quiver. The Wilson line transforming in $q \otimes [1,0,\ldots,0]_{C_{k+1}}$ of the U(1) and the central Sp($k+1$) gauge node

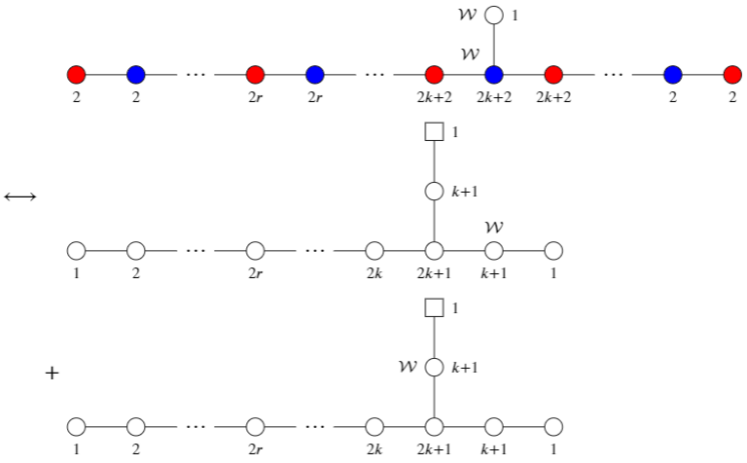


(4.3.6)

**$E_5$ family.**　For a Wilson line which transforms in $q \otimes [1, 0, \dots, 0]_{C_r}$ of the U(1) gauge node and an Sp($r$) gauge node ($1 \le r \le k$)

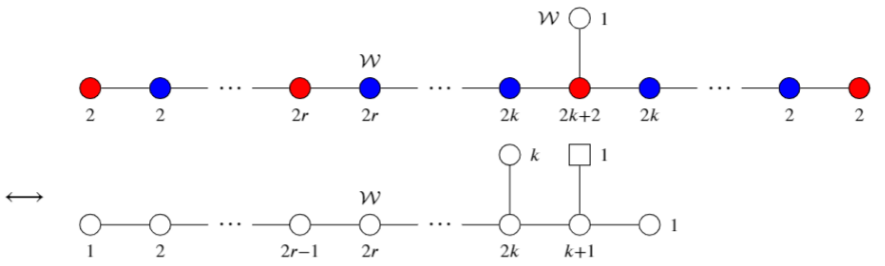


(4.3.7)

The Wilson line transforming in $q \otimes [1, 0, \dots, 0]_{D_r}$ of the U(1) and an SO($2r$) gauge node ($1 \le r \le k$)

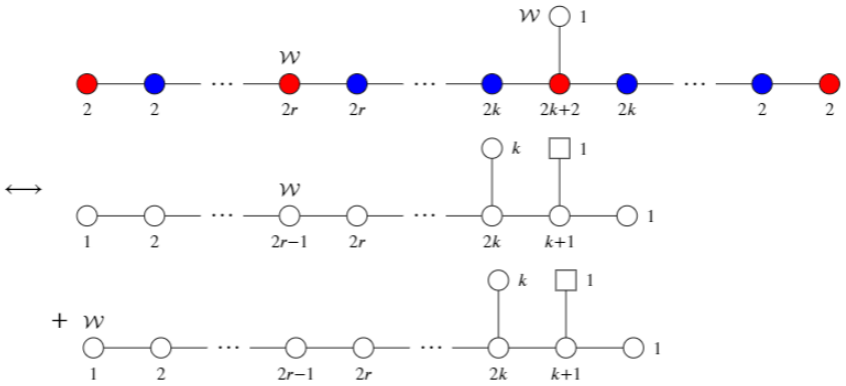


(4.3.8)

The Wilson line transforming in $q \otimes [1, 0, \dots, 0]_{D_{k+1}}$ of the U(1) and the central SO($2k + 2$) gauge node

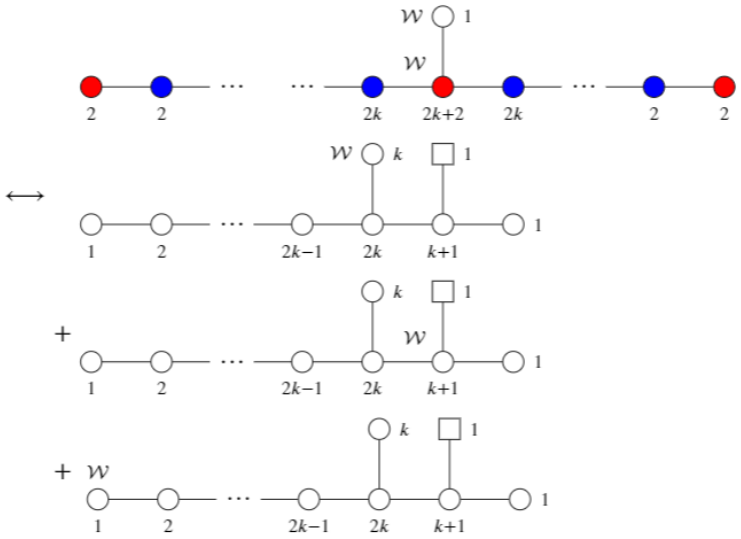


(4.3.9)

**$E_4$ family.** The Wilson line transforming in $q\otimes[1,0,\dots,0]_{C_r}$ of the U(1) and an Sp($r$) gauge node ($1 \le r \le k-l$)

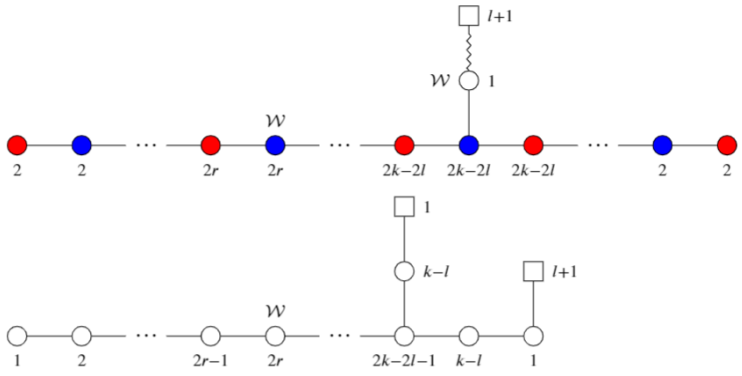


(4.3.10)

The Wilson line transforming in $q \otimes [1,0,\dots,0]_{D_r}$ of the U(1) and an SO($2r$) gauge node, ($1 \le r \le k-l$)

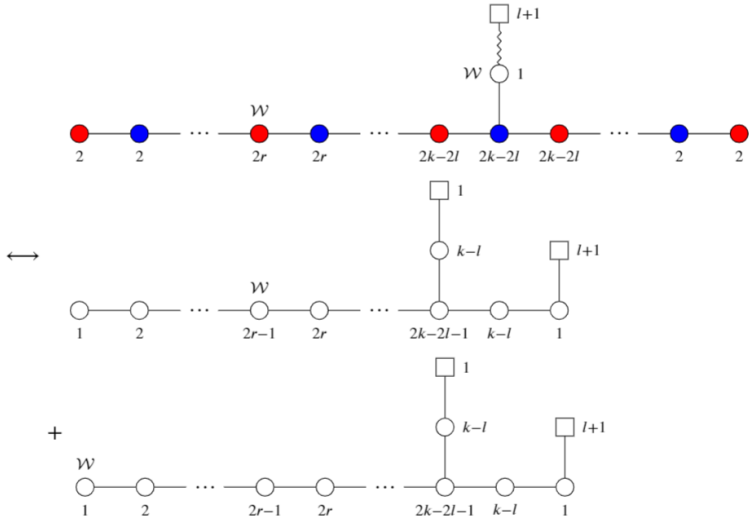


(4.3.11)

The Wilson line transforming in $q \otimes [1,0,\dots,0]_{C_{k-l}}$ of the U(1) and the central Sp($k-l$) node

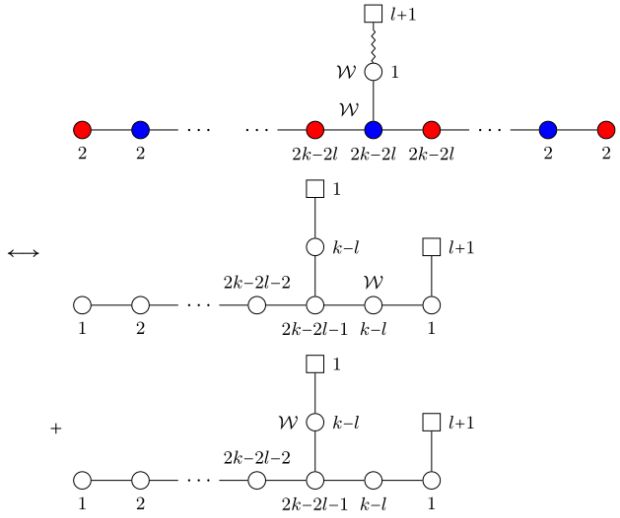


(4.3.12)

**$E_3$ family.** The Wilson line transforming in $q \otimes [1,0,\ldots,0]_{C_r}$ of the U(1) and an Sp($r$) node ($1 \le r \le k-l-1$)

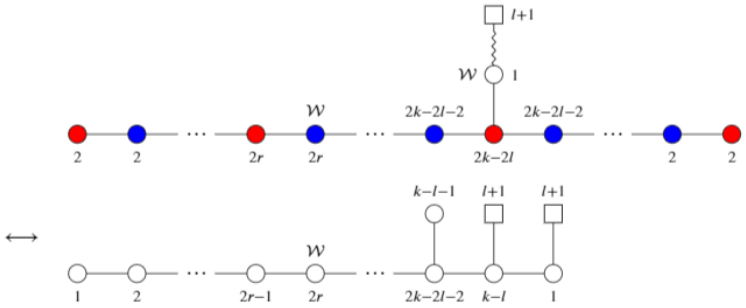


(4.3.13)

The Wilson line transforming in $q \otimes [1,0,\ldots,0]_{D_r}$ of the U(1) and an SO($r$) node ($1 \le r \le k-l-1$)

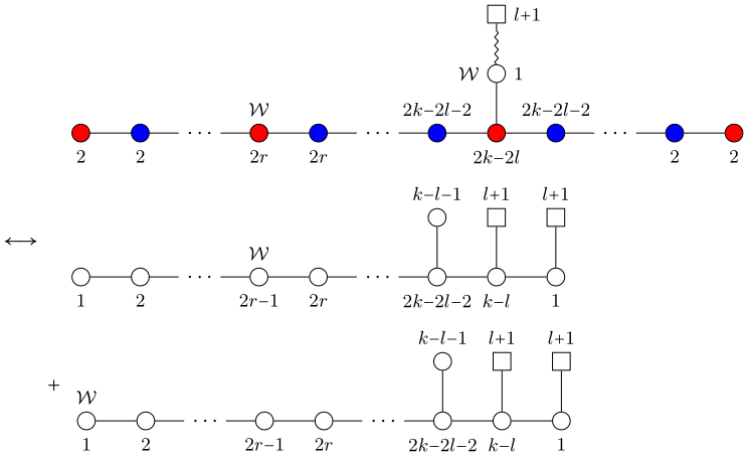


(4.3.14)

The Wilson line transforming in $q \otimes [1,0,\ldots,0]_{D_{k-l}}$ of the U(1) and the central SO($2k-2l$) node.

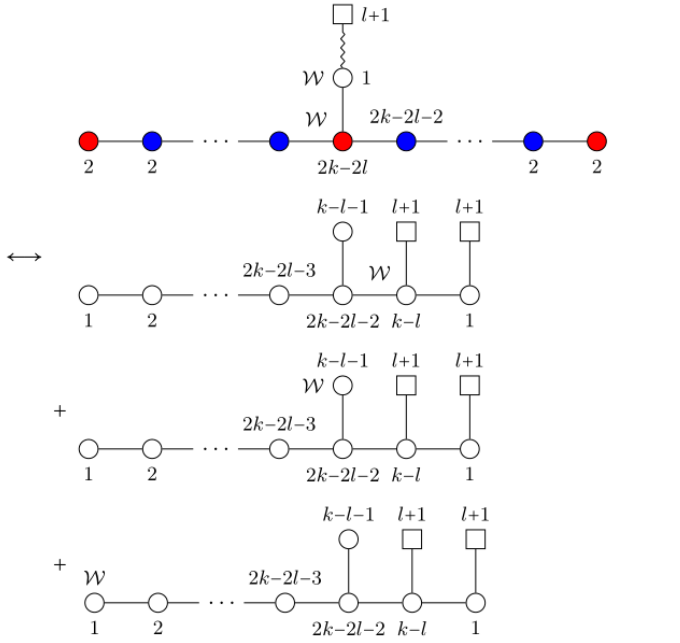


(4.3.15)

**$E_8$ family and 6d Sp($k$) SQCD.**　$E_8$ family discussed in [8] is given by the infinite coupling limit of 5d $\mathcal{N}=1$ Sp($k$) with the number of flavors constraint by $N_f \leq 2k+5$. Due to the high rank of the gauge group, the current desktop could not compute the partition functions with defects. Furthermore, due to the lack of a U(1) node, it is difficult to give a clear prediction about how the Wilson lines will match. The same situation occurs when one studies the 6d $\mathcal{N}=(1,0)$ Sp($k$) SQCD with $N_f = 2k+8$ flavors case, in which there are also a unitary magnetic quiver [4] and an orthosymplectic magnetic quiver [7].

**Wilson line transforming in other representations.**　Also, one can show that for the $E_4$ orthosymplectic quiver, the Wilson lines transforming under charge-2 and symmetric representations coincide with the Wilson lines for $E_4$ unitary quivers.

First of all, one can insert a Wilson line with charge 2 at SO(2) with character $q^2$ on the orthosymplectic side:

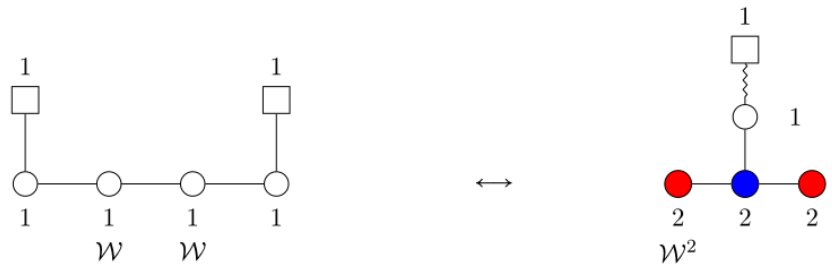


(4.3.16a)

and the corresponding Wilson line on the unitary side will transform under two adjacent U(1) nodes in the charges $(+1,+1)$. Then one should pick the second symmetric representation [2] of Sp(1)

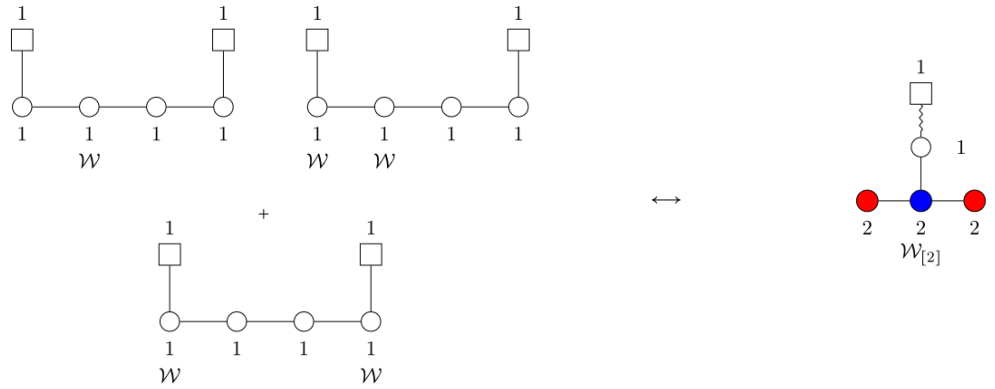


(4.3.16b)

In this case, the line operator on the unitary side will become a linear combination of 3 distinct Wilson lines. Two of these Wilson lines are charged under two U(1) nodes and the remaining one is only charged under one U(1) gauge node, here all U(1) charges are +1.

Finally, one could consider the charge-2 representation of the U(1)


(4.3.16c)

In this case, the Wilson line will be charged under one U(1) node on the unitary side with a charge +1.

The above three instances describe the correspondence of Wilson lines under the unitary-orthosymplectic duality on the right, and the charge-1 Wilson lines on the unitary side inserted at one gauge group or the product of two gauge groups are described on the left-hand side. Moreover, it is more difficult to check the unitary-orthosymplectic duality since the dimension of the representation in which a Wilson line transforms for the orthosymplectic case gets greater.

## 4.4 Refining Symmetries

There is still a question about matching the global symmetries after restoring the fugacities in the partition function. Especially, a corresponding 0-form symmetry would be introduced once one gauges the 1-form symmetry $\mathbb{Z}_2^{\text{diag}}$ [37]. Theoretically, one can evaluate the SCIs by turning on all fugacities of the global symmetries. However, in practice, one only needs to pay attention to the Coulomb branch operators since the 1-form symmetry $\mathbb{Z}_2^{\text{diag}}$ does not act on the Higgs branch operators. Then one can compute the Coulomb branch Hilbert series by using the monopole formula rather than computing the full superconformal index [42], given that the computation of the latter is much more difficult. One can turn on the following fugacities to refine the Coulomb branch Hilbert series:

- For U($k$) gauge group, one can turn on the fugacity $z$ by inserting the factor $z^{\sum_{i=1}^{k} m_i}$, which corresponding to the U(1) topological symmetry.
- For SO($2N$) gauge group, one can turn on the fugacity $y$ by inserting the factor $y^{\sum_{i=1}^{N} m_i}$ with $y^2 = 1$, which corresponding to the central $\mathbb{Z}_2$ symmetry.

here SO(2) $\cong$ U(1) is the continuous center symmetry. There exists the zero-form symmetry $\mathbb{Z}_\ell$ resulting from gauging the one-form symmetry $\mathbb{Z}_\ell$, which will contribute to the Hilbert series as follows:

$$\text{HS} = \sum_{\kappa=0}^{\ell-1} q^{\kappa} \sum_{\mathbf{m}\in\left(\mathbb{Z}+\frac{\kappa}{\ell}\right)^{\text{rk}}} P(t,\mathbf{m})\, \mathbf{z}^{\mathbf{m}}\, t^{\Delta(\mathbf{m})} \tag{4.4.1}$$

where $\left(\mathbb{Z}+\frac{\kappa}{\ell}\right)^{\text{rk}}$ denotes an appropriate lattice shifted by $+\frac{\kappa}{\ell}$ in every component. See §2.4 and [38]. In the

following, one would see that the global symmetries of the orthosymplectic quivers that emerge in the UV can be identified as the subgroups of the larger symmetries of the unitary counterparts. The residual symmetry cannot be addressed and it only appears at IR.

**$E_4$ quiver.** For the $E_4$ quiver, one could switch on the fugacities as depicted in the following quivers:

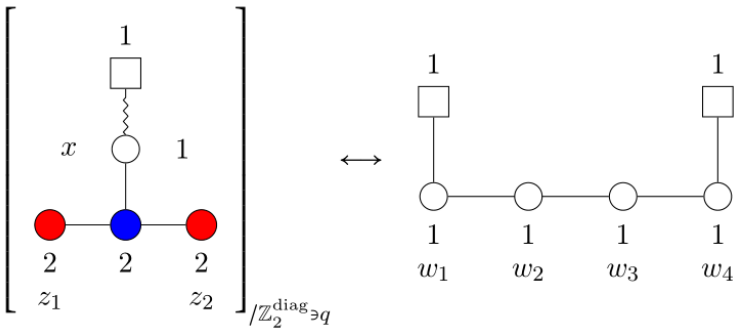


(4.4.2)

Computing the monopole formula will give the following match of partially refined Hilbert series.

$$
\begin{aligned}
&\mathrm{HS}^{\mathrm{OSp}}(z_i = z, x = w^2, q) = \mathrm{H}_{\mathbb{Z}}(z_i = z, x = w^2) + q \cdot \mathrm{H}_{\mathbb{Z}+\frac{1}{2}}(z_i = z, x = w^2) \\
&= \mathrm{HS}^{(\mathrm{A})}\left(w_1 = w_4 = z, w_2 = \tfrac{q}{w}, w_3 = qw\right)|_{q^2=1} \\
&= 1 + t\left(6 + \frac{1}{z^2} + \frac{4}{z} + 4z + z^2 + q\left(\frac{2}{w} + 2w + \frac{1}{wz} + \frac{w}{z} + \frac{z}{w} + wz\right)\right) \\
&\quad + t^2\Big(26 + \frac{4}{w^2} + 4w^2 + \frac{1}{z^4} + \frac{4}{z^3} + \frac{12}{z^2} + \frac{1}{w^2z^2} + \frac{w^2}{z^2} + \frac{20}{z} + \frac{2}{w^2z} + \frac{2w^2}{z} + 20z + \frac{2z}{w^2} + 2w^2z \\
&+ 12z^2 + \frac{z^2}{w^2} + w^2z^2 + 4z^3 + z^4 + q\Big(\frac{12}{w} + 12w + \frac{1}{wz^3} + \frac{w}{z^3} + \frac{4}{wz^2} + \frac{4w}{z^2} + \frac{9}{wz} + \frac{9w}{z} \\
&+ \frac{9z}{w} + 9wz + \frac{4z^2}{w} + 4wz^2 + \frac{z^3}{w} + wz^3\Big)\Big) + t^3\Big(78 + \frac{20}{w^2} + 20w^2 + \frac{1}{z^6} + \frac{4}{z^5} + \frac{12}{z^4} + \frac{1}{w^2z^4} \\
&+ \frac{w^2}{z^4} + \frac{28}{z^3} + \frac{4}{w^2z^3} + \frac{4w^2}{z^3} + \frac{48}{z^2} + \frac{9}{w^2z^2} + \frac{9w^2}{z^2} + \frac{68}{z} + \frac{16}{w^2z} + \frac{16w^2}{z} + 68z + \frac{16z}{w^2} + 16w^2z \\
&+ 48z^2 + \frac{9z^2}{w^2} + 9w^2z^2 + 28z^3 + \frac{4z^3}{w^2} + 4w^2z^3 + 12z^4 + \frac{z^4}{w^2} + w^2z^4 + 4z^5 + z^6 \\
&+ q\Big(\frac{6}{w^3} + \frac{44}{w} + 44w + 6w^3 + \frac{1}{wz^5} + \frac{w}{z^5} + \frac{4}{wz^4} + \frac{4w}{z^4} + \frac{1}{w^3z^3} + \frac{12}{wz^3} + \frac{12w}{z^3} + \frac{w^3}{z^3} + \frac{2}{w^3z^2} \\
&+ \frac{24}{wz^2} + \frac{24w}{z^2} + \frac{2w^3}{z^2} + \frac{4}{w^3z} + \frac{37}{wz} + \frac{37w}{z} + \frac{4w^3}{z} + \frac{4z}{w^3} + \frac{37z}{w} + 37wz + 4w^3z + \frac{2z^2}{w^3} + \frac{24z^2}{w} \\
&+ 24wz^2 + 2w^3z^2 + \frac{z^3}{w^3} + \frac{12z^3}{w} + 12wz^3 + w^3z^3 + \frac{4z^4}{w} + 4wz^4 + \frac{z^5}{w} + wz^5\Big) + \mathcal{O}(t^4)
\end{aligned}
\tag{4.4.3}
$$

By evaluating the Hilbert series perturbatively up to order $t^{10}$, the two global symmetries are identified beside $\mathbb{Z}_2^{\text{diag}}$.

**$E_5$ quiver.** Due to the dependence on the U(1) ungauging scheme of the unitary counterparts (A) and (B) as shown in (4.4.4) , the global symmetries of $E_5$ quivers could be identified in a much intriguing way. One can

turn on the fugacities as follows:

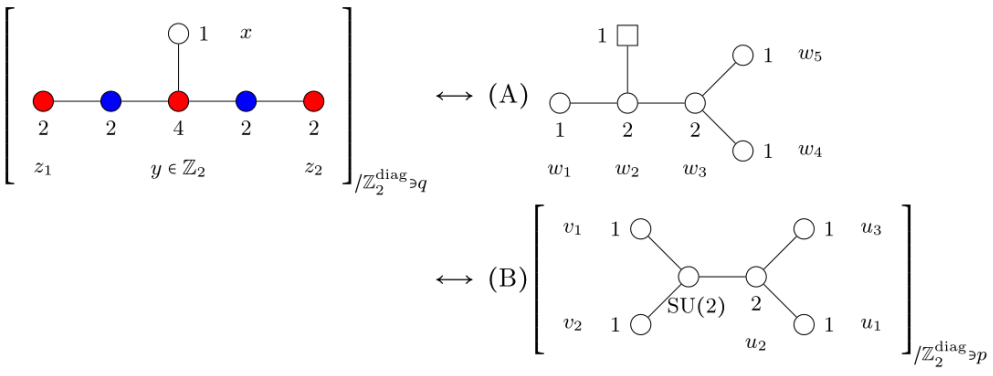


(4.4.4)

By computing the Hilbert series, one can obtain that

$$
\begin{aligned}
&\mathrm{HS}^{\mathrm{OSp}}(z_i = z, y = 1, x = 1, q) = \mathrm{H}_{\mathbb{Z}}(z_i = z, y = 1, x = 1) + q \cdot \mathrm{H}_{\mathbb{Z}+\frac{1}{2}}(z_i = z, y = 1, x = 1) \\
&= \mathrm{HS}^{(\mathrm{A})}(w_1 = w_4 = w_5^{-1} = z, w_2 = w_3 = q)|_{q^2=1} \\
&= \mathrm{HS}^{(\mathrm{B})}(u_1 = u_3^{-1} = z, u_2 = q, v_1 = v_2^{-1} = z, p = 1)|_{q^2=1} \\
&= 1 + t\left(11 + 8z + \frac{8}{z} + z^2 + \frac{1}{z^2} + q\left(4z + \frac{4}{z} + 8\right)\right) \\
&+ t^2\left(130 + 96z + \frac{96}{z} + 47z^2 + \frac{47}{z^2} + 8z^3 + \frac{8}{z^3} + z^4 + \frac{1}{z^4} + q\left(4z^3 + \frac{4}{z^3} + 32z^2 + \frac{32}{z^2} + 80z + \frac{80}{z} + 104\right)\right) \\
&+ t^3\big(942 + 808z + \frac{808}{z} + 487z^2 + \frac{487}{z^2} + 208z^3 + \frac{208}{z^3} + 47z^4 + \frac{47}{z^4} + 8z^5 + \frac{8}{z^5} + z^6 + \frac{1}{z^6} \\
&+ q\left(4z^5 + \frac{4}{z^5} + 32z^4 + \frac{32}{z^4} + 168z^3 + \frac{168}{z^3} + 432z^2 + \frac{432}{z^2} + 724z + \frac{724}{z} + 864\right)\big) \\
&+ t^4\big(5350 + 4744z + \frac{4744}{z} + 3381z^2 + \frac{3381}{z^2} + 1856z^3 + \frac{1856}{z^3} + 772z^4 + \frac{772}{z^4} + 208z^5 + \frac{208}{z^5} + 47z^6 + \frac{47}{z^6} + 8z^7 \\
&+ \frac{8}{z^7} + z^8 + \frac{1}{z^8} + q\big(4z^7 + \frac{4}{z^7} + 32z^6 + \frac{32}{z^6} + 168z^5 + \frac{168}{z^5} + 672z^4 + \frac{672}{z^4} + 1712z^3 + \frac{1712}{z^3} + 3152z^2 + \frac{3152}{z^2} \\
&+ 4500z + \frac{4500}{z} + 5056\big)\big) + t^5\big(24218 + 22264z + \frac{22264}{z} + 17199z^2 + \frac{17199}{z^2} + 11168z^3 + \frac{11168}{z^3} + 5900z^4 \\
&+ \frac{5900}{z^4} + 2480z^5 + \frac{2480}{z^5} + 772z^6 + \frac{772}{z^6} + 208z^7 + \frac{208}{z^7} + 47z^8 + \frac{47}{z^8} + 8z^9 + \frac{8}{z^9} + z^{10} + \frac{1}{z^{10}} \\
&+ q\big(23488 + 21516z + \frac{21516}{z} + 16592z^2 + \frac{16592}{z^2} + 10656z^3 + \frac{10656}{z^3} + 5568z^4 + \frac{5568}{z^4} + 2264z^5 + \frac{2264}{z^5} \\
&+ 672z^6 + \frac{672}{z^6} + 168z^7 + \frac{168}{z^7} + 32z^8 + \frac{32}{z^8} + 4z^9 + \frac{4}{z^9}\big)\big) + \mathcal{O}(t^6)
\end{aligned}
\tag{4.4.5}
$$

The results of perturbative computation are same up to order $t^5$. Thus the GNO lattice are divided into $\mathbb{Z}$ and $\mathbb{Z}+\frac{1}{2}$ lattice in different ways for the orthosymplectic quiver and unitary quiver (B). Furthermore, for the realization of $\mathbb{Z}_2^{\text{diag}}$ in the unitary quiver, one need to embed the $\mathbb{Z}_2$ into a diagonal $\mathrm{U}(1) \subset \mathrm{U}(1)_{\text{top}} \times \mathrm{U}(1)_{\text{top}}$ for (A) and a single $\mathrm{U}(1)_{\text{top}}$ for (B). Also one can identify all continuous global symmetries between the unitary quiver (A) and the orthosymplectic quiver as follows

$$
\begin{aligned}
&\mathrm{HS}^{\mathrm{OSp}}(z_i, y = 1, x, q) = \mathrm{HS}^{(\mathrm{A})}(w_1 = z_1^{-1}, w_2 = q\sqrt{z_1 z_2 x}, w_3 = \tfrac{q}{\sqrt{z_1 z_2 x}}, w_4 = z_1, w_5 = z_2)|_{q^2=1} \\
&= 1 + t\Big(9 + 4z_1 + \frac{4}{z_1} + 4z_2 + \frac{4}{z_2} + z_1 z_2 + \frac{z_1}{z_2} + \frac{1}{z_1 z_2} + \frac{z_2}{z_1} + 2q z_1^{-\frac{1}{2}} z_2^{-\frac{1}{2}} (\sqrt{x} + 1/\sqrt{x})\left(1 + z_1 + z_2 + z_1 z_2\right)\Big) \\
&+ \mathcal{O}(t^2)
\end{aligned}
\tag{4.4.6}
$$

which has been verified up to order $t^5$.

**$E_6$ quiver.** One can turn on the following fugacities for the $E_6$ magnetic quivers

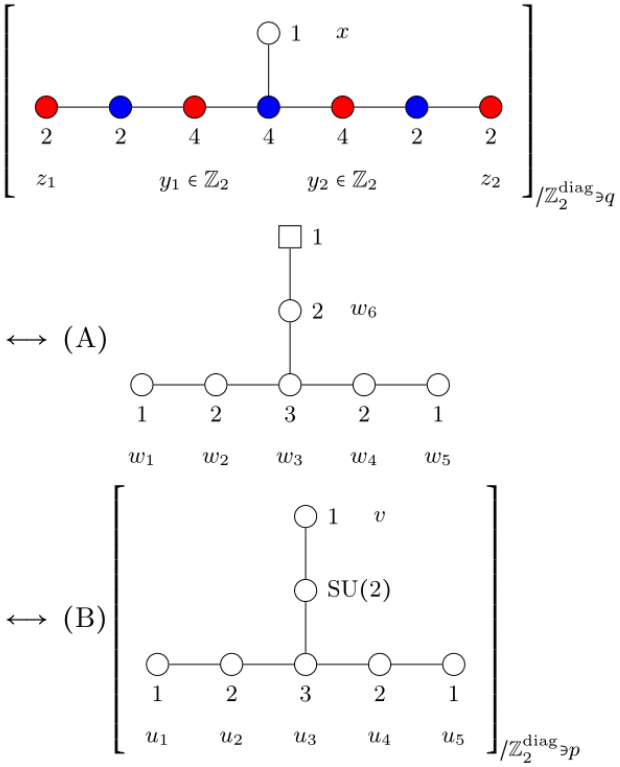


$\longleftrightarrow$ (A)

$\longleftrightarrow$ (B) (4.4.7)

By computing the Hilbert series, one can obtain that

$$
\begin{aligned}
&\mathrm{HS}^{\mathrm{OSp}}(z_i = z, y_i = x = 1, q) = \mathrm{H}_{\mathbb{Z}}(z_i = z, y_i = x = 1) + q \cdot \mathrm{H}_{\mathbb{Z}+\frac{1}{2}}(z_i = z, y_i = x = 1) \\
&= \mathrm{HS}^{(\mathrm{A})}(w_1 = w_5 = 1, w_2 = w_4 = q, w_3 = w_6^{-1} = z)|_{q^2=1} \\
&= \mathrm{HS}^{(\mathrm{B})}(u_1 = u_5 = z, u_2 = u_4 = q, u_3 = v = p = 1)|_{q^2=1} \\
&= \mathrm{HS}^{(\mathrm{B})}(u_1 = u_5 = 1, u_2 = u_4 = q, u_3 = v^{-1} = z, p = 1)|_{q^2=1} \\
&= 1 + t\left(20 + 12z + \frac{12}{z} + z^2 + \frac{1}{z^2} + q\left(16 + 8z + \frac{8}{z}\right)\right) \\
&+ t^2\left(422 + 300z + \frac{300}{z} + 115z^2 + \frac{115}{z^2} + 12z^3 + \frac{12}{z^3} + z^4 + \frac{1}{z^4} + q\left(384 + 280z + \frac{280}{z} + 96z^2 + \frac{96}{z^2} + 8z^3 + \frac{8}{z^3}\right)\right) \\
&+ t^3\left(5834 + 4756z + \frac{4756}{z} + 2518z^2 + \frac{2518}{z^2} + 808z^3 + \frac{808}{z^3} + 115z^4 + \frac{115}{z^4} + 12z^5 + \frac{12}{z^5} + z^6 + \frac{1}{z^6}\right. \\
&\left. + q\left(5696 + 4616z + \frac{4616}{z} + 2432z^2 + \frac{2432}{z^2} + 752z^3 + \frac{752}{z^3} + 96z^4 + \frac{96}{z^4} + 8z^5 + \frac{8}{z^5}\right)\right) \\
&+ t^4\left(60006 + 51688z + \frac{51688}{z} + 33050z^2 + \frac{33050}{z^2} + 15104z^3 + \frac{15104}{z^3} + 4618z^4 + \frac{4618}{z^4}\right. \\
&+ 808z^5 + \frac{808}{z^5} + 115z^6 + \frac{115}{z^6} + 12z^7 + \frac{12}{z^7} + z^8 + \frac{1}{z^8} + q\left(59344 + 51184z + \frac{51184}{z} + 32576z^2 + \frac{32576}{z^2}\right. \\
&\left.\left. + 14848z^3 + \frac{14848}{z^3} + 4448z^4 + \frac{4448}{z^4} + 752z^5 + \frac{752}{z^5} + 96z^6 + \frac{96}{z^6} + 8z^7 + \frac{8}{z^7}\right)\right) \\
&+ t^5\left(479893 + 429036z + \frac{429036}{z} + 305471z^2 + \frac{305471}{z^2} + 170968z^3 + \frac{170968}{z^3} + 72650z^4 + \frac{72650}{z^4}\right.
\end{aligned}
\tag{4.4.8}
$$

$$
\begin{aligned}
&+22240z^5+\frac{22240}{z^5}+4618z^6+\frac{4618}{z^6}+808z^7+\frac{808}{z^7}+115z^8+\frac{115}{z^8}+12z^9+\frac{12}{z^9}+z^{10}+\frac{1}{z^{10}}\\
&+q\big(477888+427016z+\frac{427016}{z}+303920z^2+\frac{303920}{z^2}+169744z^3+\frac{169744}{z^3}+71936z^4+\frac{71936}{z^4}\\
&+21824z^5+\frac{21824}{z^5}+4448z^6+\frac{4448}{z^6}+752z^7+\frac{752}{z^7}+96z^8+\frac{96}{z^8}+8z^9+\frac{8}{z^9}\big)\big)+\mathcal{O}(t^6)
\end{aligned}
$$

The results of perturbative computation coincide up to order $t^5$. Same as the previous case, the splitting of GNO lattice into integer and half-integer lattice for unitary quiver (B) is different from the splitting in the orthosymplectic quiver.

**$E_7$ quiver.** For this case, one can focus on the following quivers and their symmetry refinement:

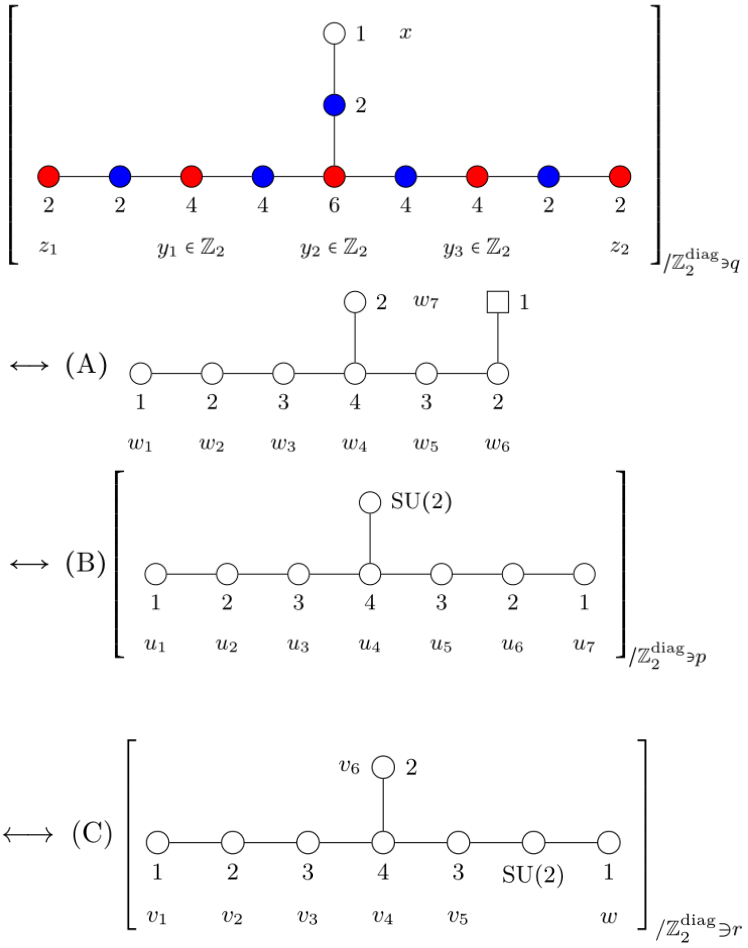


(4.4.9)

The relation of the Hilbert series of Coulomb branch on both sides is:

$$
\begin{aligned}
\mathrm{HS}^{\mathrm{OSp}}(z_i=z,y_i=x=1,q)&=\mathrm{H}_{\mathbb{Z}}(z_i=z,y_i=x=1)+q\cdot\mathrm{H}_{\mathbb{Z}+\frac{1}{2}}(z_i=z,y_i=x=1)\\
&=\mathrm{HS}^{(\mathrm{A})}(w_1=w_7=w_4^{-1}=z,w_2=w_6=q,w_3=w_5=1)|_{q^2=1}\\
&=\mathrm{HS}^{(\mathrm{B})}(u_1=u_7=z,u_2=u_6=q,u_{3,4,5}=p=1)|_{q^2=1}\\
&=\mathrm{HS}^{(\mathrm{C})}(v_1=v_5=v_6^{-1}=z,v_{2,3,4,5}=w=1,r=q)
\end{aligned}
\tag{4.4.10}
$$

$$
\begin{aligned}
&= \mathrm{H}^{(\mathrm{C})}_{\mathbb{Z}}(v_1 = v_5 = v_6^{-1} = z, v_{2,3,4,5} = w = 1) + r|_{r=q} \cdot \mathrm{H}^{(\mathrm{C})}_{\mathbb{Z}+\frac{1}{2}}(v_1 = v_5 = v_6^{-1} = z, v_{2,3,4,5} = w = 1) \\
&= 1 + t\left(35 + 16z + \frac{16}{z} + z^2 + \frac{1}{z^2} + q\left(32 + 16z + \frac{16}{z}\right)\right) + t^2\Big(1351 + 896z + \frac{896}{z} + 273z^2 \\
&+ \frac{273}{z^2} + 16z^3 + \frac{16}{z^3} + z^4 + \frac{1}{z^4} + q\big(1312 + 896z + \frac{896}{z} + 256z^2 + \frac{256}{z^2} + 16z^3 + \frac{16}{z^3}\big)\Big) + \mathcal{O}(t^3)
\end{aligned}
$$

The results of perturbative computation coincide up to order $t^3$. Furthermore, the splitting of the GNO lattice into integer lattice and half-integer lattice *does* coincide with the separation in the unitary quiver (C), whereas it *does not* coincide with the separation in (B).

The two global $\mathrm{U}(1)_{z_i}$ symmetries and the $\mathbb{Z}_2^{\mathrm{diag}}$ can be identified by verifying the following relation:

$$
\begin{aligned}
&\mathrm{HS}^{\mathrm{OSp}}(z_i, y_i = x = 1, q) = \mathrm{HS}^{(\mathrm{C})}(v_1 = z_1, v_5 = v_6^{-1} = z_2, v_{2,3,4,5} = w = 1, r = q) \\
&= 1 + t\big( + 33 + 8z_1 + \frac{8}{z_1} + 8z_2 + \frac{8}{z_2} + z_1 z_2 + \frac{z_1}{z_2} + \frac{1}{z_1 z_2} + \frac{z_2}{z_1} 16q\sqrt{z_1 z_2}\left(1 + z_1 + z_2 + z_1 z_2\right)\big) + \mathcal{O}(t^2)
\end{aligned}
\tag{4.4.11}
$$

**Remarks.** This section gives a demonstration that the discrete zero-form symmetry $\mathbb{Z}_2^{\mathrm{diag}}$ in orthosymplectic quiver, which coming from gauging the one-form symmetry $\mathbb{Z}_2^{\mathrm{diag}}$ can be restored in their unitary counterparts $T^{(\alpha)}$. And the embedding of the discrete zero-form symmetry $\mathbb{Z}_2^{\mathrm{diag}}$ hinges on a U(1) ungauging scheme ($\alpha$). Although it is much more difficult to refine global symmetries for orthosymplectic quivers compared to unitary quivers, one can still study the problems of embedding the symmetries visible in the orthosymplectic quiver into that of the unitary counterpart.

## 4.5 The Main Results of Chapter 4

This chapter mainly discussed the 5d $\mathcal{N} = 1$ theory with Sp($k$) gauge group and $N_f$ fundamental flavours. The main results of this chapter can be summarized as follows:

- By computing the superconformal indices and the $S^3$ partition function of $E_{4,5,6}$ and $E_7$ unitary and orthosymplectic quivers respectively, both quivers give the same results which provide the evidence that they flow to the same IR fixed points and dual at the QFT level.

- The admissible Wilson lines for unframed unitary and orthosymplectic quivers were discussed according to the ranks of the gauge groups of the gauge nodes. In general, for the unframed unitary quivers, one needs to quotient the electric 1-form symmetry $\ker \phi$ and a non-trivial diagonally acting $\mathbb{Z}_n^{\mathrm{diag}}$ symmetry from the gauge group $G$; for the unframed orthosymplectic quivers, one can insert the Wilson line operators which transforms according to the product of two fundamental representations of two different gauge nodes or to a representation on the root lattice of a SO($2n$) (or Sp($k$)) gauge node.

- The structural patterns between the Wilson lines in unitary and orthosymplectic quivers for various cases were listed, which can be verified by computing the B-twisted indices with Wilson loops. The $k = 1$ $E_{5,6,7}$, $k = 1, 2$ $E_4$ and $k = 1, 2, 3$ $E_3$ families were analysed. Also, the Wilson lines transforming under charge-2 and symmetric representations $E_4$ orthosymplectic quiver matches with the Wilson lines for $E_4$ unitary quivers.

- In order to find the match patterns between the global symmetries if the fugacities are (partially) included in the partition functions, the corresponding refined Coulomb branch Hilbert series were computed via monopole formula for $E_{4,5,6,7}$ quivers and they match, and the global symmetries of the orthosymplectic quivers apparent at UV were identified as the subgroups of the (much larger) symmetries of the unitary counterparts.

# Chapter 5 On Knot Theory

## 5.1 Knot Homology and Super-$A$-Polynomial

### 5.1.1 An Isomorphism Between Colored HOMFLY-PT and Kauffman Homology for Thin Knots

As mentioned in Chapter 1, one can define the quadruply-graded HOMFLY-PT homology $(\mathscr{H}_R^{\text{HOMFLY-PT}})_{i,j,k,l}$ with $(a, q, t_r, t_c)$-grading whose Poincaré polynomial is given by (1.6.13). Define a $\delta$-grading to every generator $x$ of the $[r]$-colored HOMFLY-PT homology

$$\delta(x) := a(x) + \frac{q(x)}{2} - \frac{t_r(x) + t_c(x)}{2}. \tag{5.1.1}$$

For a knot $K$, if all generators of its $[r]$-colored HOMFLY-PT homology are endowed with the same $\delta$-grading which is $\frac{r}{2}S(K)$, where $S(K)$ is the Rasmussen $s$-invariant of the knot $K$ [137], then the knot $K$ is called homologically thin. Otherwise, the knot is called homologically thick. Here we only focus on thin knots. Similarly, for $[r]$-colored Kauffman homology, one can also define the $\delta$-grading as follows [57]:

$$\delta(x) := \frac{3\lambda(x)}{2} + \frac{q(x)}{2} - \frac{t_r(x) + t_c(x)}{2}. \tag{5.1.2}$$

For homologically-thin knots $K$, all generators have the same $\delta$-grading $rS(K_{\text{thin}})$.

The colored Kauffman homology is endowed with rich differential structures and relations between the homological invariants can be deduced from the isomorphisms of the representations [57]. One useful isomorphism for this study is the isomorphism of the representations $(\mathfrak{so}_6, [r]) \cong (\mathfrak{sl}_4, [r^2])$ [57], which give the isomorphism between the bi-graded homologies

$$\mathscr{H}_{\mathfrak{so}_6,[r]}(K) \cong \mathscr{H}_{\mathfrak{sl}_4,[r^2]}(K). \tag{5.1.3}$$

For thin knots, (5.1.3) can be written in terms of the Poincaré polynomials [57]

$$\widetilde{\mathscr{F}}_{[r]}(K_{\text{thin}}; a=q^5, Q=q, t_r=q^{-1}, t_c=qt) = \widetilde{\mathscr{P}}_{[r^2]}(K_{\text{thin}}; a=q^4, Q=q^2, t_r=q^{-1}, t_c=qt) \tag{5.1.4}$$

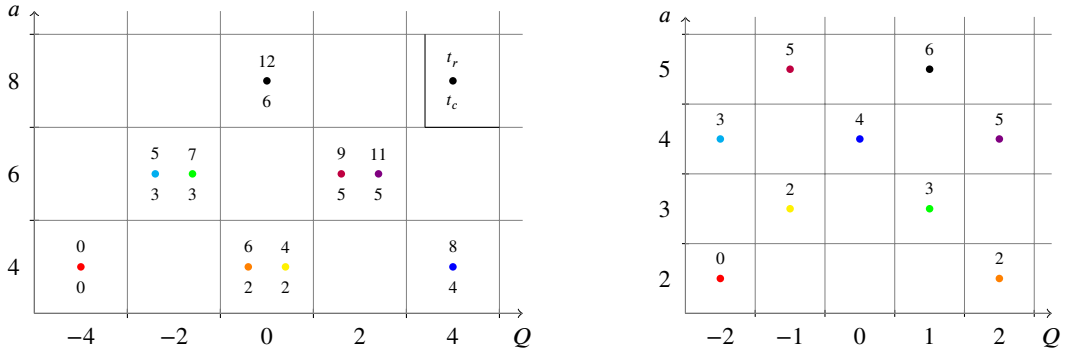


**Fig. 5-1.** This figure shows the correspondence of generators of $[1^2]$-colored HOMFLY-PT homology (left) and uncolored Kauffman homology (right) for knot $\mathbf{3_1}$. The same color indicates the identifications of generators under (5.1.5)

It can be found that there exists an isomorphism between the $[1^2]$-colored HOMFLY-PT homology and the uncolored Kauffman homology for the cases of knots $3_1$ and $4_1$. Therefore, one can uplift (5.1.3) to the following isomorphism between HOMFLY-PT and Kauffman homologies for $K_{\text{thin}}$ with changing the gradings

$$\left(\widetilde{\mathscr{H}}^{\text{Kauffman}}_{[r]}(K_{\text{thin}})\right)_{i,j,k,l} \cong \left(\widetilde{\mathscr{H}}^{\text{HOMFLY-PT}}_{[r^2]}(K_{\text{thin}})\right)_{\frac{3}{2}i+\frac{3}{4}j-\frac{1}{2}k,-\frac{5}{2}i-\frac{5}{4}j+\frac{3}{2}k,i+\frac{1}{2}j,l}, \tag{5.1.5}$$

The above isomorphism holds up to some grading shifts which is proportional to $\frac{rS(K)}{2}$ in $(a, Q, t_r)$ degrees. (5.1.5) gives the following identity of Poincaré polynomials

$$\widetilde{\mathcal{F}}_{[r]}(K_{\text{thin}}; a, Q, t_r, t_c) = \left(\frac{Q^3}{at_r^2}\right)^{\frac{rS(K)}{2}} \widetilde{\mathcal{P}}_{[r^2]}(K_{\text{thin}}; a^{\frac{3}{2}}Q^{-\frac{5}{2}}t_r, a^{\frac{3}{4}}Q^{-\frac{5}{4}}t_r^{\frac{1}{2}}, a^{-\frac{1}{2}}Q^{\frac{3}{2}}, t_c)\,. \tag{5.1.6}$$

Note that the grading shifts of variables in (5.1.6) are linearly dependent, therefore one *cannot* utilize (5.1.6) from right to the left to obtain the Poincaré polynomials of $[r^2]$-colored HOMFLY-PT homology from that of $[r]$-colored Kauffman homology for a thin knot.

The Poincaré polynomials of quadruply-graded HOMFLY-PT homology for the double twist knots $K_{m,n}$, which are homologically-thin, colored by rectangular Young tableau $[r^s]$ is presented in [138, 139]. By checking the differentials and all properties of the corresponding colored Kauffman homologies [57] obtain from the HOMFLY-PT homologies by using the relations (5.1.5) and (5.1.6) for double twist knots, (5.1.5) and (5.1.6) have been verified.

### 5.1.2 Differential on Super-$A$-polynomials of SO type

In this section, following the notions in the introduction, the Poincaré polynomial of triply-graded homology $\mathcal{Q}_{[r]}(K; a, q, t)$ only with $t_r$-grading is called the superpolynomial which are denoted as

$$\mathcal{Q}_{[r]}(K; a, q, t) := \mathcal{Q}_{[r]}(K; a, q, t_r = t, t_c = 1)\,, \tag{5.1.7}$$

Herr the notation $\mathcal{Q} = \mathcal{P}$ or $\mathcal{F}$ represents Poincaré polynomials of either HOMFLY-PT or Kauffman homology for the convenience of discussion.

In [55, 140], it was proposed that for some specific knots, like thin knots and torus knots, their $[r]$-colored superpolynomials are endowed with so-called *exponential growth properties*

$$\mathcal{Q}_{[r]}(K; a, q = 1, t) = \left[\mathcal{Q}_{[1]}(K; a, q = 1, t)\right]^r . \tag{5.1.8}$$

Then the superpolynomial colored by a symmetric representation was conjectured [141] to satisfy the following identity,

$$\mathcal{Q}_{[r]}(K; a, q, t) = \sum_{l_1+l_2+\cdots+l_n=r} \begin{bmatrix} r \\ l_1, l_2, \ldots, l_n \end{bmatrix}_{q^2} a^{\sum_{i=1}^n a_i l_i} t^{\sum_{i=1}^n t_i l_i} q^{\sum_{i,j=1}^n Q_{i,j} l_i l_j + \sum_{i=1}^n q_i l_i}, \tag{5.1.9}$$

Here $(a_i, q_i, t_i)$ are constants and $Q_{i,j}$ is a matrix which encodes the information of a quiver related to the given knot under the knot-quiver correspondence [141]. The coefficient on the right hand side is the $q$-multibinomial

$$\begin{bmatrix} r \\ l_1, l_2, \ldots, l_n \end{bmatrix}_q := \frac{(q;q)_r}{(q;q)_{l_1}(q;q)_{l_2}\cdots(q;q)_{l_n}} \tag{5.1.10}$$

In the large color limit

$$q = e^{\hbar} \to 1, \quad r \to \infty, \quad a = \text{fixed}, \quad t = \text{fixed}, \quad x = q^{2r} = \text{fixed}, \tag{5.1.11}$$

the asymptotic behavior of superpolynomial takes the form

$$\mathcal{Q}_{[r]}(K; a, q, t) \underset{x=q^{2r}}{\overset{r\to\infty,\hbar\to 0}{\sim}} \exp\left(\frac{1}{2\hbar}\int \log y \frac{dx}{x} + \mathcal{O}(\hbar)\right) . \tag{5.1.12}$$

Similar to the case of $A$-polynomial, the integral in the leading term on the right-hand side is performed on the zero locus of the super-$A$-polynomial

$$\mathcal{A}(K; x, y, a, t) = 0 . \tag{5.1.13}$$

and $\mathcal{O}(\hbar)$ still represents the regular term as $\hbar \to 0$.

For the superpolynomials in the form of (5.1.9), the large color behavior (5.1.12) can be rewritten as the following integral form approximately,

$$\mathcal{Q}_{[r]}(K; a, q, t) \sim \int e^{\frac{1}{2\hbar}\left(\widetilde{\mathcal{W}}(K; z_1, \cdots, z_n; x, a, t) + \mathcal{O}(\hbar)\right)} dx \prod_{i=1}^n dz_i , \tag{5.1.14}$$

where $z_i = q^{2l_i}$, $x = q^{2r}$. Then (5.1.12) can be captured from the saddle point equations

$$\exp\left(z_i \frac{\partial \widetilde{\mathcal{W}}(K; z_1, \cdots, z_n; x, a, t)}{\partial z_i}\right)\Big|_{z_i = z_i^*} = 1 \tag{5.1.15}$$

and the zero locus of the super-$A$-polynomial

$$\exp\left(x\frac{\partial\widetilde{\mathscr{W}}(K;z_1^*,\cdots,z_n^*;x,a,t)}{\partial x}\right)=y \tag{5.1.16}$$

In the section 4.5 of the [57], there exists a universal differential $d_{\rightarrow}^{\text{univ}}$ with $(a,q,t)$-degree $(0,2,1)$, which gives an identity between the Poincaré polynomial of $[r]$-colored Kauffman homology and HOMFLY-PT homology as

$$\mathscr{F}_{[r]}(K;a,q,t)=q^{rS(K)}\mathscr{P}_{[r]}(K;aq^{-1},q,t)+(1+q^2t)f(a,q,t), \tag{5.1.17}$$

where $f(a,q,t)$ is a complicated polynomial of $a,q,t$ with integer coefficients depending on the knot $K$. One can kill the last term on the right-hand side by imposing $t=-q^{-2}$, then

$$\mathscr{F}_{[r]}(K;a,q,-q^{-2})=q^{rS(K)}\mathscr{P}_{[r]}(K;aq^{-1},q,-q^{-2})\,. \tag{5.1.18}$$

If a knot satisfies the exponential growth property, then it admits a superpolynomial expressed as (5.1.9) and it is easy to check the leading order of the large color behavior can be identified with that of the colored HOMFLY-PT polynomial up to the non-trivial variable changes $a\to aq^{-1}$ with $t=-q^{-2}$. Then, in the large color limit, the Poincaré polynomial of the $[r]$-colored Kauffman homology behaves as

$$\mathscr{F}_{[r]}(K;a,q,-q^{-2})\sim\int e^{\frac{1}{2\hbar}\left(\widetilde{\mathscr{W}}^{\text{SU}}(K;z_i;x,a)+\mathscr{O}(\hbar)\right)}dxdz_i\,. \tag{5.1.19}$$

In the above formula, one can extract the $a$-deformed $A$-polynomial of SU type $A^{\text{SU}}(K;x,y,a)$ from the right-hand side in the large color limit (5.1.11) . Meanwhile, one can also obtain the $a$-deformed $A$-polynomial of $SO$-type $A^{\text{SO}}(K;x,y,a)$. Therefore, one can have the following conjecture:

**Conjecture** For a knot satisfying the exponential growth property, the zero locus of the super-$A$-polynomial of SO-type at $t=-1$

$$\mathscr{A}^{\text{SO}}(K;x,y,a,t=-1)=0$$

includes two branches $A^{\text{SO}}(K;x,y,a)=0$ and $A^{\text{SU}}(K;x,y,a)=0$.

Now let's take the trefoil $\mathbf{3_1}$ as an instance. In this case, the super-$A$-polynomial can be evaluated. The colored superpolynomial of trefoil is given by eq.(5.8) in [57]

$$\begin{aligned}&\mathscr{F}_{[r]}(\mathbf{3_1};a,q,t)\\&=\sum_{k=0}^{r}\sum_{j=0}^{k}\sum_{i=0}^{r-k}a^{i-k+3r}q^{3k-2j(1+r)+r(2r-3)+i(2j+2r-1)}t^{2(i-j+r)}\begin{bmatrix}r\\k\end{bmatrix}_{q^2}\begin{bmatrix}k\\j\end{bmatrix}_{q^2}\begin{bmatrix}r-k\\i\end{bmatrix}_{q^2}\\&\qquad\times(-a^2t^3q^{2r-2};q^2)_j(-q^2t;q^2)_{r-k}(-aq^{-1}t;q^2)_i\,.\end{aligned} \tag{5.1.20}$$

The corresponding twisted superpotential is given by [57]

$$\begin{aligned}\widetilde{\mathscr{W}^{\mathrm{SO}}}(\mathbf{3_1};x,w,v,z,a,t) = &\log\left(\frac{wx^3}{z}\right)\log a - \log v\log x + (\log x)^2 + \log w\log(vx)\\ &+ 2\log\left(\frac{wx}{v}\right)\log t - \frac{3\pi^2}{6} - \mathrm{Li}_2(x) + \mathrm{Li}_2(v) + \mathrm{Li}_2(zv^{-1})\\ &+ \mathrm{Li}_2(w) + \mathrm{Li}_2(xz^{-1}w^{-1}) + \mathrm{Li}_2(-a^2t^3x) - \mathrm{Li}_2(-a^2t^3xv)\\ &+ \mathrm{Li}_2(-t) - \mathrm{Li}_2(-txz^{-1}) + \mathrm{Li}_2(-at) - \mathrm{Li}_2(-atw)\,,\end{aligned} \tag{5.1.21}$$

here $w = q^{2i}$, $v = q^{2j}$ and $z = q^{2k}$. Here the asymptotic property of Q-Pochhammer $(x;q)_k = \prod_{i=1}^{k}(1-xq^{i-1}) \sim e^{\frac{1}{\hbar}(\mathrm{Li}_2(x)-\mathrm{Li}_2(xz))}$ was used. Follow the discussion above, when $t=-1$, one can obtain the large color behavior of colored Kauffman polynomial

$$\widetilde{\mathscr{W}^{\mathrm{SO}}}(\mathbf{3_1};x,w,v,z,a,t=-1) = \widetilde{\mathcal{W}^{\mathrm{SO}}}(\mathbf{3_1};x,w,v,z,a) \tag{5.1.22}$$

Meanwhile, when $t = q^{-2}$, one can check that the summation over $k$ and $i$ on the right-hand side of (5.1.20) will collapse to $k = r$ and $i = 0$ due to the factor $(-q^2t;q^2)_{r-k}$. Therefore, one have

$$\widetilde{\mathscr{W}^{\mathrm{SO}}}(\mathbf{3_1};x,w=1,v,z=x,a,t=-1) = \widetilde{\mathcal{W}^{\mathrm{SO}}}(\mathbf{3_1};x,v,a) \tag{5.1.23}$$

From the equations (5.1.14) and (5.1.15), one can obtain the super-$A$-polynomial of SO-type of $\mathbf{3_1}$ [57], and the $t=-1$ specialization yields

$$\mathscr{A}^{\mathrm{SO}}(\mathbf{3_1};x,y,a,t=-1) = (1-ax)A^{\mathrm{SO}}(\mathbf{3_1};x,y,a)A^{\mathrm{SU}}(\mathbf{3_1};x,y,a) \tag{5.1.24}$$

where

$$\begin{aligned}A^{\mathrm{SO}}(\mathbf{3_1};x,y,a) &= a^7x^7 - a^7x^6 - a^2xy + y\,,\\ A^{\mathrm{SU}}(\mathbf{3_1};x,y,a) &= y^2 - ya^2 + xya^2 - 2x^2ya^2 - xy^2a^2 - x^3a^4 + x^4a^4 + 2x^2ya^4 + x^3ya^4 - x^4ya^6.\end{aligned} \tag{5.1.25}$$

This result satisfies the Conjecture proposed above.

Note that one can evaluate super-$A$-polynomials of SO-type for $K_{m,n}$ by utilizing the rules of changing the variable proposed in the last section. But it is usually difficult to solve the saddle point equations (5.1.14) and (5.1.15) for general double twist knots. Nevertheless, the colored Kauffman homologies of $K_{m,n}$ are equipped with the universal differential $d_{\rightarrow}^{\mathrm{univ}}$, one can still confirm the above Conjecture by verifying the relations corresponding to the (5.1.22) and (5.1.23) for double twist knots.

## 5.2 SO($N$) Quantum 6$j$-Symbols

As it has been explained in the introduction that the quantum knot invariants could be computed via braiding operation by utilizing quantum 6$j$-symbols. Actually, 6$j$-symbols play important roles in revealing the symmetries in various aspects of mathematics and physics [75, 142–145]. However, it is quite hard to calculate them for higher rank cases. In order to study their properties more carefully, it is essential to obtain a closed-form expression of quantum 6$j$-symbols. Since the quantum SU($N$) knot invariants, i.e. colored HOMFLY-PT polynomials (homology), can be computed from the quantum SU($N$) 6$j$-symbols. Therefore, the quantum SO($N$) knot invariants, i.e. colored Kauffman polynomials should also be computed by using quantum SO($N$) 6$j$-symbols in principle, and it should be equal to the results obtained in §5.1.1. In the following part, the quantization of SO($N$) 6$j$-symbols with all symmetric representations is presented. The classical SO($N$) 6$j$-symbol was proposed by Ališauskas [80, 81]. Then some proofs of the validity of the proposed quantized SO($N$) 6$j$-symbols are presented via representation theory and the computations of the Kauffman polynomials.

### 5.2.1 SO($N$) Quantum 6$j$-Symbols for Symmetric Representations

In [80, 81], the expression of the classical 6$j$-symbol of SO($N$) ($n \geq 4$) with all representations symmetric was given:

$$\begin{aligned}
\begin{Bmatrix} a & b & e \\ d & c & f \end{Bmatrix}_{\mathrm{SO}(N)} = & \left( \frac{(2c+N-2)(2d+N-2)(2e+N-2)}{8 d_c^{(N)} d_d^{(N)} d_e^{(N)}} \right)^{1/2} \\
& \times \begin{pmatrix} c & d & e \\ 0 & 0 & 0 \end{pmatrix}_N^{-1} \sum_{l'} (-1)^{(c+d-e)/2+f+N+l'} (2l'+N-3) \\
& \times \begin{Bmatrix} \frac{1}{2}b & \frac{1}{2}f+\frac{1}{4}N-1 & \frac{1}{2}d+\frac{1}{4}N-1 \\ \frac{1}{2}f+\frac{1}{4}N-1 & \frac{1}{2}(b+N)-2 & l'+\frac{1}{2}N-2 \end{Bmatrix} \\
& \times \begin{Bmatrix} \frac{1}{2}a & \frac{1}{2}f+\frac{1}{4}N-1 & \frac{1}{2}c+\frac{1}{4}N-1 \\ \frac{1}{2}f+\frac{1}{4}N-1 & \frac{1}{2}(a+N)-2 & l'+\frac{1}{2}N-2 \end{Bmatrix} \\
& \times \begin{Bmatrix} \frac{1}{2}a & \frac{1}{2}b+\frac{1}{4}N-1 & \frac{1}{2}e+\frac{1}{4}N-1 \\ \frac{1}{2}b+\frac{1}{4}N-1 & \frac{1}{2}(a+N)-2 & l'+\frac{1}{2}N-2 \end{Bmatrix} \\
& \times \left( \frac{l'!(N-3)!}{(l'+N-4)!} \right)^{1/2},
\end{aligned} \tag{5.2.1}$$

Where dimension of the SO($N$) symmetric irreducible representations $l$ are given as

$$d_l^{(N)} = \frac{(2l+N-2)!(l+N-3)!}{l!(N-2)!} \tag{5.2.2}$$

and the special 3$j$-symbols is given by

$$\begin{aligned}\begin{pmatrix} l_1 & l_2 & l_3 \\ 0 & 0 & 0 \end{pmatrix}_N =&(-1)^{\psi_N}\frac{1}{\Gamma(\frac{N}{2})}\left(\frac{(J+N-3)!}{(N-3)!\Gamma(J+N/2)}\right.\\ &\left.\times\prod_{i=1}^{3}\frac{(l_i+N/2-1)\Gamma(J-l_i+N/2-1)}{d_{l_i}^{(N)}(J-l_i)!}\right)^{1/2},\end{aligned} \tag{5.2.3}$$

where $J=\frac{1}{2}(l_1+l_2+l_3)$. When $N$ is even, the curly braces on the right represent the SU(2) 6$j$-symbols. But when $N$ is odd, it will involve the linear combination of parameters in the expression and the summation range will be restricted under certain conditions [81]. In the following quantized SO($N$) 6$j$-symbol case, only even $N$ cases will be considered.

A natural quantized version of the above Ališauskas' results can be written in following closed-form expression of quantum SO($N$) ($N\geq 4$) 6$j$-symbols for all symmetric representations,

$$\begin{aligned}\begin{Bmatrix} a & b & e \\ d & c & f \end{Bmatrix}_{\mathrm{SO}(N)} =&\left(\frac{[2c+N-2]_q[2d+N-2]_q[2e+N-2]_q}{[2]_q^3\dim_q[c]\dim_q[d]\dim_q[e]}\right)^{1/2}\\ &\times\begin{pmatrix} c & d & e \\ 0 & 0 & 0 \end{pmatrix}_N^{-1}\sum_{l'}(-1)^{(c+d-e)/2+f+N+l'}\left[2l'+N-3\right]_q\\ &\times\begin{Bmatrix} \frac{1}{2}b & \frac{1}{2}f+\frac{1}{4}N-1 & \frac{1}{2}d+\frac{1}{4}N-1 \\ \frac{1}{2}f+\frac{1}{4}N-1 & \frac{1}{2}(b+N)-2 & l'+\frac{1}{2}N-2 \end{Bmatrix}_{\mathrm{SU}(2)}\\ &\times\begin{Bmatrix} \frac{1}{2}a & \frac{1}{2}f+\frac{1}{4}N-1 & \frac{1}{2}c+\frac{1}{4}N-1 \\ \frac{1}{2}f+\frac{1}{4}N-1 & \frac{1}{2}(a+N)-2 & l'+\frac{1}{2}N-2 \end{Bmatrix}_{\mathrm{SU}(2)}\\ &\times\begin{Bmatrix} \frac{1}{2}a & \frac{1}{2}b+\frac{1}{4}N-1 & \frac{1}{2}e+\frac{1}{4}N-1 \\ \frac{1}{2}b+\frac{1}{4}N-1 & \frac{1}{2}(a+N)-2 & l'+\frac{1}{2}N-2 \end{Bmatrix}_{\mathrm{SU}(2)}\\ &\times\left(\frac{[l']_q![N-3]_q!}{[l'+N-4]_q!}\right)^{1/2},\end{aligned} \tag{5.2.4}$$

Here the curly brace still the SU(2) quantum 6$j$-symbols [78]. In the current discussion, only the symmetric representations will be involved. Therefore, $a,b,c,d,e,f$ are the number of boxes in the corresponding single row Young tableau. The definition of quantum number is same as (1.6.55). But the definition of quantum factorial needs to be modified as

$$[x]_q!=[x]_q[x-1]_q\cdots[x-\lfloor x\rfloor]_q\,, \tag{5.2.5}$$

where $\lfloor x\rfloor$ denotes the floor of $x$ to make sure that this definition suits for both integer and half-integer. Then the quantum dimension of SO($N$) symmetric representation $[l]$ and the special quantum 3$j$-symbols can be obtained by quantizing (5.2.2) and (5.2.3) in following way:

$$\dim_q[l] = \frac{[l+N-3]_q!}{[l]_q![N-2]_q!}\left([l+N-2]_q + [l]_q\right), \tag{5.2.6}$$

$$\begin{aligned}\begin{pmatrix} l_1 & l_2 & l_3 \\ 0 & 0 & 0 \end{pmatrix}_N &= \frac{1}{[N/2-1]_q!}\left(\frac{[J+N-3]_q!}{[N-3]_q![J+N/2-1]_q!}\right. \\ &\left.\times\prod_{i=1}^{3}\frac{\left[2l_i+N-2\right]_q\left[J-l_i+N/2-2\right]_q!}{[2]_q\dim_q[l_i]\left[J-l_i\right]_q!}\right)^{1/2},\end{aligned} \tag{5.2.7}$$

where $J = \frac{1}{2}(l_1+l_2+l_3)$.

In the introduction, the multiplicity-free 6$j$-symbols for a Lie group $G$ are defined as

$$\begin{Bmatrix} R_1 & R_2 & R_{12} \\ R_3 & R_4 & R_{23} \end{Bmatrix}_G, \tag{5.2.8}$$

where all $R$'s denote the representation of Lie group $G$. As explained in the introduction, here $R_{12} \in (R_1 \otimes R_2) \cap (\bar{R}_3 \otimes \bar{R}_4)$ and $R_{23} \in (R_2 \otimes R_3) \cap (\bar{R}_1 \otimes \bar{R}_4)$. Then, according to the fusion rules, even though $R_1, R_2, R_3, R_4$ are all symmetric representations, $R_{12}$ and $R_{23}$ could be non-symmetric. Furthermore, for two identical SO($N$) symmetric representations $[r]$, their fusion rule is

$$[r] \otimes [r] = \bigoplus_{l=0}^{r}\bigoplus_{j=0}^{l}[2l-j, j], \tag{5.2.9}$$

which yields the non-symmetric representations. Note that the notation of the representation $R$ corresponding to a Young diagram with $r_1 \geq r_2 \geq \cdots$ is $R = [r_1, r_2, \cdots]$. Moreover, one can obtain the following identities of quantum 6$j$-symbols.

- The isomorphism $(\mathfrak{so}_6, [r]) \simeq (\mathfrak{sl}_4, [r, r])$ will yields

$$\begin{Bmatrix} [r] & [r] & [2l-j, j] \\ [r] & [r] & [2l'-j', j'] \end{Bmatrix}_{\text{SO(6)}} = \begin{Bmatrix} [r,r] & [r,r] & [2l, 2l-j, j] \\ [r,r] & [r,r] & [2l', 2l'-j', j'] \end{Bmatrix}_{\text{SU(4)}}, \tag{5.2.10}$$

  Here $0 \leq j \leq l, 0 \leq j' \leq l', 0 \leq l, l' \leq r$, and it has been verified that this relation holds by utilizing the SU(4) quantum 6$j$-symbols [146]. Here $j$ and $j'$ are set to be 0, since there is only a closed-form formula of SO($N$) quantum 6$j$-symbols for symmetric representations. Therefore, (5.2.10) reduces to

$$\begin{Bmatrix} [r] & [r] & [2l] \\ [r] & [r] & [2l'] \end{Bmatrix}_{\text{SO(6)}} = \begin{Bmatrix} [r,r] & [r,r] & [2l, 2l] \\ [r,r] & [r,r] & [2l', 2l'] \end{Bmatrix}_{\text{SU(4)}}, \tag{5.2.11}$$

  where $0 \leq l \leq r$. Then it is quite easy to obtain this kind of SU(4) quantum 6$j$-symbols by using (5.2.4).

- As Lie algebra, $\mathfrak{so}_4$ and $\mathfrak{sl}_2 \oplus \mathfrak{sl}_2$ are isomorphic. When all representations are symmetric, there is

$$\left\{\begin{matrix}[r] & [r] & [2l] \\ [r] & [r] & [2l']\end{matrix}\right\}_{\mathrm{SO}(4)} = \left(\left\{\begin{matrix}[r] & [r] & [2l] \\ [r] & [r] & [2l']\end{matrix}\right\}_{\mathrm{SU}(2)}\right)^2, \tag{5.2.12}$$

  here $0 \leq l, l' \leq r$.

- The above discussions only suit for the case of $N \geq 4$. But there exists the isomorphism $(\mathfrak{so}_3, [r]) \simeq (\mathfrak{sl}_2, [2r])$ yields

$$\left\{\begin{matrix}[r] & [r] & [2l] \\ [r] & [r] & [2l']\end{matrix}\right\}_{\mathrm{SO}(3)}\Big|_{q\to q^2} = \left\{\begin{matrix}[2r] & [2r] & [4l] \\ [2r] & [2r] & [4l']\end{matrix}\right\}_{\mathrm{SU}(2)}, \tag{5.2.13}$$

  where $0 \leq l, l' r$.

### 5.2.2 SO($N$) Duality Matrices for Symmetric Representations

The fusion rule of SO($N$) symmetric representations (5.2.9) would yield the non-symmetric representations $R_{12}$ and $R_{23}$. This section will present a way to compute the Kauffman polynomials colored by SO($N$) symmetric representations. The relation of SO($N$) fusion matrix and SO($N$) quantum 6$j$-symbols is almost same as (1.6.64) for SU($N$) case. But one needs to notify that SO($N$) representations are real, therefore one only needs to consider the fusion matrix in the form of $a_{ts}\left[\begin{smallmatrix} R & R \\ R & R\end{smallmatrix}\right]$, where $t, s \in R \otimes R$. The properties of this SO($N$) fusion matrix is given by

- Symmetric:

$$a_{ts}\begin{bmatrix} R & R \\ R & R\end{bmatrix} = a_{st}\begin{bmatrix} R & R \\ R & R\end{bmatrix} \tag{5.2.14}$$

- Orthogonality:

$$\sum_s a_{ts}\begin{bmatrix} R & R \\ R & R\end{bmatrix} a_{sm}\begin{bmatrix} R & R \\ R & R\end{bmatrix} = \delta_{tm}. \tag{5.2.15}$$

- Similar to (1.6.73), the SO($N$) fusion matrix satisfy

$$a_{0s}\begin{bmatrix} R & R \\ R & R\end{bmatrix} = \epsilon_s^R \frac{\sqrt{\dim_q s}}{\dim_q R} \tag{5.2.16}$$

When $t$ and $s$ are symmetric and the entries are trivial representations, the entries in (5.2.4) are known. Then one can obtain the whole fusion matrix by solving the equations according to the orthonormality and symmetry of the fusion matrix. Here the results of SO($N$) fusion matrices for $R =$ $\square$, $\square\square$ are listed,

1. $R =$ 

$$\begin{Bmatrix} R & R & t \\ R & R & s \end{Bmatrix} = \frac{1}{\dim_q R} \left( \begin{array}{c|ccc} & s=\varnothing & \begin{array}{|c|}\hline\\\hline\\\hline\end{array} & \begin{array}{|c|c|}\hline\\\hline\end{array} \\ \hline t=\varnothing & 1 & 1 & 1 \\ \begin{array}{|c|}\hline\\\hline\\\hline\end{array} & 1 & \frac{[N]_q}{[N-1]_q([N-2]_q+[2]_q)} & -\frac{1}{[N-1]_q} \\ \begin{array}{|c|c|}\hline\\\hline\end{array} & 1 & -\frac{1}{[N-1]_q} & \frac{[N-2]_q}{[N-1]_q([N]_q+[2]_q)} \end{array} \right) \tag{5.2.17}$$

where the quantum dimension $\dim_q R = [N-1]_q + 1$.

2. $R =$ 

$$\begin{Bmatrix} R & R & t \\ R & R & s \end{Bmatrix} = \frac{1}{\dim_q R} \left( \begin{array}{c|cccccc} & s=\varnothing & \begin{array}{|c|}\hline\\\hline\\\hline\end{array} & \begin{array}{|c|c|}\hline\\\hline\end{array} & \begin{array}{|c|c|}\hline\\\hline\\\hline\end{array} & \begin{array}{|c|c|c|}\hline\\\hline\\\cline{1-1}\end{array} & \begin{array}{|c|c|c|c|}\hline\\\hline\end{array} \\ \hline t=\varnothing & 1 & 1 & 1 & 1 & 1 & 1 \\ \begin{array}{|c|}\hline\\\hline\\\hline\end{array} & 1 & b_{11} & b_{12} & b_{13} & b_{14} & b_{15} \\ \begin{array}{|c|c|}\hline\\\hline\end{array} & 1 & b_{21} & b_{22} & b_{23} & b_{24} & b_{25} \\ \begin{array}{|c|c|}\hline\\\hline\\\hline\end{array} & 1 & b_{31} & b_{32} & b_{33} & b_{34} & b_{35} \\ \begin{array}{|c|c|c|}\hline\\\hline\\\cline{1-1}\end{array} & 1 & b_{41} & b_{42} & b_{43} & b_{44} & b_{45} \\ \begin{array}{|c|c|c|c|}\hline\\\hline\end{array} & 1 & b_{51} & b_{52} & b_{53} & b_{54} & b_{55} \end{array} \right), \tag{5.2.18}$$

where the quantum dimension $\dim_q R = [N-1]_q + [N-1]_q[N]_q/[2]_q$, and

$$\begin{aligned}
b_{11} &= \frac{-q^4 - q^N - q^{2+N} + q^{4+N} - q^{2+2N} + q^{4+2N} + q^{6+2N} + q^{2+3N}}{(1+q^2)(-1+q^N)(q^4+q^N+q^{2N}+q^{4+N})}, \\
b_{12} = b_{21} &= \frac{q^{N+2}+1}{q^{N+2}+q^N+q^2+1}, \\
b_{13} = b_{31} &= \frac{q^N\left(q^2-1\right)\left(q^{N+2}+1\right)}{q^{3N}+q^{2N+4}-q^N-q^4}, \\
b_{14} = b_{41} &= \frac{\left(q^2-1\right)^2 q^N}{q^{2N}+q^{N+4}+q^N+q^4}, \\
b_{15} = b_{51} &= \frac{\left(q^4-1\right)q^{N-2}}{1-q^{2N}}, \\
b_{22} &= \frac{-q^{2N}+q^{N+2}+3q^{N+4}-2q^{N+6}-q^{N+8}-2q^{2N+2}+3q^{2N+4}+q^{2N+6}-2q^{2N+8}+q^{3N+6}-2q^N+q^2}{(q^2+1)(q^N+1)(q^N-q^2)(q^{N+4}-1)}, \\
b_{23} = b_{32} &= -\frac{\left(q^2-1\right)q^N}{(q^N+1)(q^N-q^2)}, \\
b_{24} = b_{42} &= \frac{q^N\left(q^2-1\right)^2\left(q^{N+2}+1\right)}{(q^2-q^N)(q^{N+4}+q^{2N+4}-q^N-1)}, \\
b_{25} = b_{52} &= \frac{\left(q^4-1\right)q^N}{q^{N+4}+q^{2N+4}-q^N-1}, \\
b_{33} &= \frac{q^{2N}\left(q^2-1\right)^2\left(q^2+1\right)\left(q^{2N}-q^{N+2}+q^{N+6}-q^{2N+2}-2q^{2N+4}-q^{2N+6}+q^{2N+8}+q^{3N+2}-q^{3N+6}+q^{4N+4}+q^4\right)}{(q^N-1)(q^N+1)(q^N-q^2)(q^N+q^4)\left(q^{2N}-q^6\right)(q^{2N+2}-1)},
\end{aligned}$$

$$
\begin{aligned}
b_{34} = b_{43} &= -\frac{q^{2N}\left(q^2-1\right)^2\left(q^2+1\right)\left(q^{N+2}+1\right)}{\left(q^N+1\right)\left(q^{2N}-q^{N+2}+q^{N+4}-q^6\right)\left(q^{2N+2}-1\right)},\\
b_{35} = b_{53} &= \frac{\left(q^2-1\right)^2\left(q^2+1\right)q^{2N-2}}{\left(q^{2N}-1\right)\left(q^{2N+2}-1\right)},\\
b_{44} &= \frac{q^{2N}\left(q^2-1\right)^2\left(q^2+1\right)\left(2q^{N+2}-2q^{N+4}+q^{N+6}+q^{2N+4}-q^N-q^2\right)}{\left(q^{2N}-q^{N+2}+q^{N+4}-q^6\right)\left(q^{2N+2}-1\right)\left(q^{N+4}+q^{2N+4}-q^N-1\right)},\\
b_{45} = b_{54} &= -\frac{\left(q^2-1\right)^2\left(q^2+1\right)q^{2N}}{\left(q^{2N+2}-1\right)\left(q^{N+4}+q^{2N+4}-q^N-1\right)},\\
b_{55} &= \frac{q^{2N+2}\left(q^2-1\right)^2\left(q^2+1\right)\left(q^N-q^2\right)}{\left(q^{N+6}-1\right)\left(q^{2N+2}-1\right)\left(q^{N+4}+q^{2N+4}-q^N-1\right)}.
\end{aligned}
$$

By using these two SO($N$) fusion matrices and the braiding procedures which were introduced in the introduction, one can evaluated the colored Kauffman polynomials for $K_{m,n}$ when $R=$ $\square$ , $\square\square$. The results of this braiding computations match with $\mathcal{F}_{[r]}(K; a=q^{N-1}, q, t=-1)$ obtained in §5.1.1 which was derived from Poincaré polynomial of $[r^2]$-colored HOMFLY-PT homology [139] via (5.1.6).

## 5.3 The Main Results of Chapter 5

This chapter mainly focuses on the knot theory. The main results of this chapter can be summarized as follows:

- A simple rule of grading change that transforms the $[r^2]$-colored quadruply-graded HOMFLY-PT homology to $[r]$-colored quadruply-graded Kauffman homology for thin knots is proposed. The obtaining Kauffman homologies satisfy all the differentials and symmetries for colored Kauffman homology of double twist knots.

- From the universal differential which relates the $[r]$-colored Kauffman homology and $[r]$-colored HOMFLY-PT homology, it was found that the super-$A$-polynomials of SO-types contain both $a$-deformed $A$-polynomials of SO and SU type at $t=-1$.

- With natural quantizing the SO($N$)($N \geq 4$) $6j$-symbols for symmetric representation proposed by Ališauskas, the SO($N$) fusion matrices for $R=$ $\square$, $\square\square$ and the corresponding colored Kauffman polynomials were computed. This quantization was verified from the perspectives of the representation theory and the Kauffman polynomials.

# Chapter 6 Summary and Discussions

This thesis focuses on two main topics which are all related to three-dimensional field theories: the unitary/orthosymplectic mirror symmetry of 3d $\mathcal{N} = 4$ theories and knot theory from 3d Chern-Simons theory. For the first topic, the key point is how to judge whether two magnetic quivers engender the same moduli space descriptions that are dual as 3d $\mathcal{N} = 4$ theories. For the second one, the key point is how to capture the characteristics of colored Kauffman polynomials more precisely from different perspectives.

For the unitary/orthosymplectic mirror symmetry, the thesis includes several kinds of supersymmetric partition functions to verify it: superconformal index, twisted index, and $S^3$ partition function. As a first probe, the thesis calculated the SCIs for both unitary and orthosymplectic counterparts by perturbative expansion. For the 5d Sp($k$) theories of §4, these results also holds for the finite coupling quivers. Also, the SCIs for a pair of 5d Sp($k$) infinite coupling magnetic quivers have been calculated in §4.1 and the results match with each other up to the given order expansion. Also under the Coulomb and Higgs limit, it reproduces the known Hilbert series of Coulomb and Higgs branch separately. Moreover in §4.4, there are some zero-form symmetries that can be identified. Also by introducing two kinds of topological twists of $R$-symmetry, one can obtain so-called A-twisted and B-twisted indices. Here, the half-BPS line defects also play the role as a probe in the 3d Sp($k$) and 5d Sp($k$) theories. In §3, a 3d setup was established which admits a type IIB brane system realisation entirely. Also, the dictionary for Wilson lines between two 3d $\mathcal{N} = 4$ Sp($k$) mirror theories also have been presented in §3.2 by computing the B-twisted indices including the Wilson lines. Due to the mirror symmetry of the Wilson line and vortex line in §3.3, these two kinds of line defects were also been included in §3.4. Next, the thesis focused on the 5d Sp($k$) theories at infinite coupling and studied the magnetic quivers in this case. Here, the line operators are included under QFT framework rather than underlying brane configurations. In §4.2, the admissible Wilson lines defects has been discussed. In §4.3, the patterns of matching between the Wilson lines in two kinds of magnetic quivers are revealed. These results are proved by the calculations of the B-twisted indices.

It has been shown that the unitary/orthosymplectic mirror symmetry is reflected both in their moduli spaces and the exact partition functions for a pair of magnetic quivers. They have the same SCIs and their Wilson lines also match. In (4.3.16), the matching of Wilson lines with higher representations for the $E_4$ quivers has been presented. Then it is natural to ask whether there exists a rule to match the Wilson lines with higher representations generally for a pair of magnetic quivers. §3.4 put forward a matching between vortex lines on both unitary and orthosymplectic sides, which are dual to the fundamental Wilson line defects in Sp($k$) SQCD, therefore it is necessary to find the correspondences between the vortex line defects in two magnetic quivers in §4 henceforward. In order to do this, the vortex line defects in orthosymplectic quivers need to be further understood

and A-twisted indices for various cases needs to be computed.

Here is another intriguing question arises. As discussed in §3.1,for Sp(1) theory with 3 flavors, one can obtain the unitary/orthosymplectic mirror theories in (3.1.3) and (3.1.6) respectively. Meanwhile, the $k = 1$ $A_3$ quiver theory in (3.1.3) on the unitary side is mirror dual to U(1) theory with 4 flavors. And it has already known that the $A_3$ and $D_3$ unitary quiver are coincide [95, 147]. Therefore, one can obtain a 3d $\mathcal{N} = 4$ dualities web:

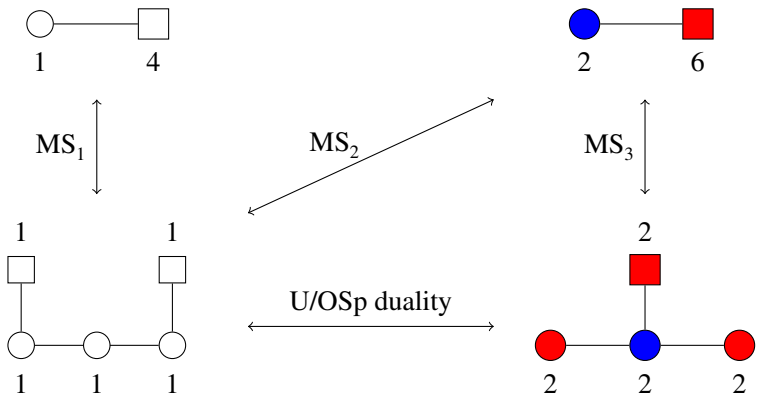


(6.0.1)

As Table 1 indicates, these theories have the same superconformal indices. Then one can compute their $S^3$ partition functions. First, the $S^3$ partition function of supersymmetric QED U(1) theory with 4 flavors has already been given in [117]

$$\begin{aligned} Z^{S^3}_{(1)-[4]} &= \int ds \frac{e^{2\pi i(\xi_1-\xi_2)s}}{\mathrm{ch}(s-m_1)\,\mathrm{ch}(s-m_2)\,\mathrm{ch}(s-m_3)\,\mathrm{ch}(s-m_4)} \\ &= \frac{i}{i^3(e^{\pi(\xi_1-\xi_2)}-e^{-\pi(\xi_1-\xi_2)})} \sum_{i=1}^{4} \frac{e^{2\pi i m_i(\xi_1-\xi_2)}}{\prod_{j\neq i}\mathrm{sh}(m_i-m_j)}\,, \end{aligned} \tag{6.0.2}$$

where the FI parameter is $\xi_1 - \xi_2$ and $m_i$ $(i = 1, \ldots, 4)$ are the mass parameters. The $S^3$ partition function of the unitary $A_3$ quiver gauge theory is

$$\begin{aligned} Z^{S^3}_{A_3} &= \int \prod_{j=1}^{3} ds_j \frac{e^{2\pi i \sum_{j=1}^{3}(\xi_j-\xi_{j+1})s_i}}{\mathrm{ch}(m_1-s_1)\,\mathrm{ch}(s_1-s_2)\,\mathrm{ch}(s_2-s_3)\,\mathrm{ch}(s_3-m_2)} \\ &= \int \prod_{j=1}^{3} ds_j \prod_{k=1}^{4} dt_k \frac{e^{2\pi i \sum_{j=1}^{3}(\xi_j-\xi_{j+1})s_i} e^{-2\pi i(t_1(m_1-s_1)+t_2(s_1-s_2)+t_3(s_2-s_3)+t_4(s_3-m_2))}}{\prod_{k=1}^{4}\mathrm{ch}(t_k)} \\ &= e^{2\pi i(-m_1\xi_1+m_2\xi_4)} \int dt_1 \frac{e^{2\pi i(m_1-m_2)t_1}}{\mathrm{ch}(t_1-\xi_1)\,\mathrm{ch}(t_1-\xi_2)\,\mathrm{ch}(t_1-\xi_3)\,\mathrm{ch}(t_1-\xi_4)}\,, \end{aligned} \tag{6.0.3}$$

where $\xi_i - \xi_{i+1}$ $(i = 1, 2, 3)$ denote the FI parameter of the $i$-th U(1) node counting from the left-hand side, and $m_{1,2}$ denote the mass parameters of the flavors. The last line is obtained as follows: the integration over $ds_j (j = 1, 2, 3)$ will yield the delta functions that impose the following relations:

$$t_2 = t_1 + \xi_1 - \xi_2\,, \quad t_3 = t_1 + \xi_1 - \xi_3\,, \quad t_4 = t_1 + \xi_1 - \xi_4\,.$$

Then one can integrate over $dt_k$ ($k = 2, 3, 4$). It is obvious that the final line of the (6.0.3) is the same as (6.0.2) with interchanging the mass and FI parameters. This implies the mirror symmetry $\mathrm{MS}_1$ shown in (6.0.1).

Now let's focus on the $S^3$ partition function of the Sp(1) with 3 flavors. In this case, one has to introduce a UV regulator $\xi$ to perform the integral and then take $\xi \to 0$ limit by utilizing the L'Hospital rule as:

$$Z^{S^3}_{\mathrm{SQCD}} = \lim_{\xi\to 0} \int ds \frac{e^{2\pi i \xi s} \operatorname{sh}^2(2s)}{\prod_{i=1}^{3} \operatorname{ch}(\pm s - m_i)} = \sum_{i=1}^{3} \frac{m_i \operatorname{sh}(2m_i)}{\prod_{j\neq i} \operatorname{sh}(m_j \pm m_i)} \,. \tag{6.0.4}$$

This result is same as (6.0.3) if one take the limit $m_i \to 0$ and let $\xi_4 = \xi_1 + \xi_2 + \xi_3$, up to $\xi_i \leftrightarrow m_i$ under the mirror symmetry. This implies the mirror symmetry $\mathrm{MS}_2$ in (6.0.1). But in order to obtain (6.0.4), one needs to send regulator $\xi \to 0$, therefore $\xi$ cannot capture the emergent IR SO(2) symmetry. Then the mirror symmetry $\mathrm{MS}_3$ can be shown by sending $\xi_j \to 0$ for $A_3$ $S^3$ partition function

$$\lim_{\xi_j\to 0} Z^{S^3}_{A_3} = \frac{(m_1 - m_2)\left(1 + (m_1 - m_2)^2\right)}{6 \operatorname{sh}(m_1 - m_2)} \,. \tag{6.0.5}$$

and the the $S^3$ partition function of the orthosymplectic quiver can be computed by introducing the regulators $\xi, \eta$ and send them to 0, i.e.

$$Z^{S^3}_{\mathrm{OSp}} = \lim_{\xi,\eta\to 0} \int ds dt_1 dt_2 \frac{e^{2\pi i(\xi_1 t_1 + \xi_2 t_2 + \eta s)} \operatorname{sh}^2(2s)}{\operatorname{ch}(\pm s - m) \prod_{i=1,2} \operatorname{ch}(t_i \pm s)} = \frac{m\left(1 + 4m^2\right)}{3 \operatorname{sh}(2m)} \,. \tag{6.0.6}$$

This coincides with (6.0.5) if identifying the mass parameters of these two theories as:

$$m = \frac{m_1 - m_2}{2} \,. \tag{6.0.7}$$

Then one can include the line operators. In SQED (6.0.2), the Wilson loop with charge $q$ will shift the FI parameter as $\xi_1 \to \xi_1 - iq$. It is mirror dual to the vortex defect in the unitary $A_3$ quiver which can be realized by a 1d SQM that couples to two neighboring $U(1)$ gauge nodes in 3d theory. In (6.0.8), one possible case is presented. Another configuration is its dual under hopping duality. One needs to pay attention that in unitary $A_3$ quiver of (6.0.8), the directions of the arrows for 1d chiral are for $q < 0$. For $q > 0$, the direction would be opposite. This vortex defect would cause a shift in mass parameter $m_1$ as $m_1 \to m_1 - iq$ in the $S^3$ partition function. When $q < 0$ and even, the vortex in the orthosymplectic quiver of (6.0.8) will turn into the dual configuration because of (6.0.7), and it will yield a shift of mass parameter as $m \to m + i|q|/2$ in the $S^3$ partition function. For the odd $q$ case, the corresponding description is still a puzzle. Furthermore, for any charge $q$, it is also a question to give a description about the B-type defect in the Sp(1) SQCD with 3 flavors since this theory doesn't have an

explicit FI parameter.

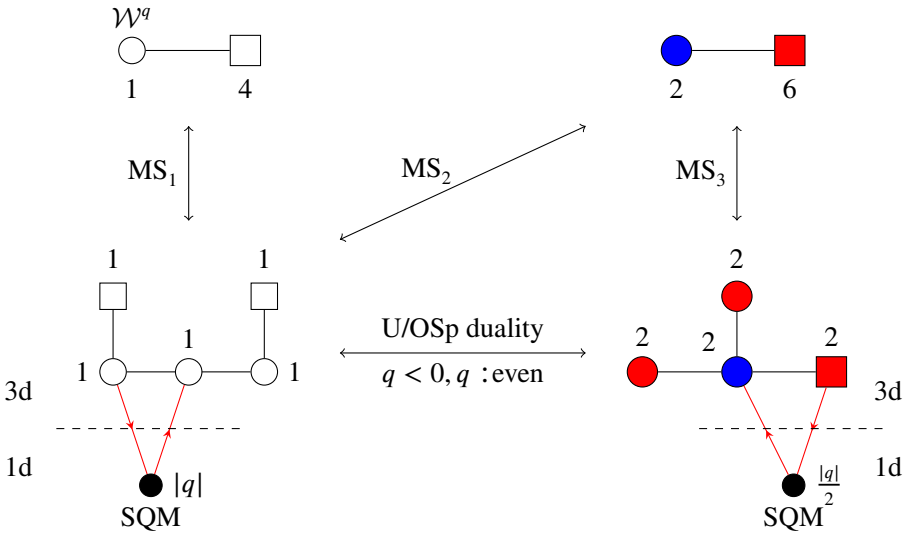


(6.0.8)

Also in §3.3 and Appendix 3, it proposed the vortex defects in the two theories which are mirror dual to the fundamental Wilson line of the Sp(1) SQCD with $N_f > 3$. But it's also still a problem about how to give the elucidations of A-type line operators in the two mirror theories dual to the fundamental Wilson line of the Sp(1) SQCD for $N_f = 3$ case. Because in this case, the integral kernel (6.0.4) of the Sp(1) SQCD cannot transform into the integral kernel (6.0.3) of the unitary mirror quiver due to one $\text{sh}^2$ factor cannot be eliminated by the Cauchy determinant formula. It needs further study in the future.

As for the knot theory, the thesis mainly focuses on colored Kauffman homology and quantum SO($N$) $6j$-symbols. In Chapter 5, first, there exists a simple rule of changing variables to obtain $[r]$-colored quadruply-graded Kauffman homologies from $[r^2]$-colored quadruply-graded HOMFLY-PT homologies for thin knots. And the properties of the resulting $[r]$-colored quadruply-graded Kauffman homology have been checked by using differentials and symmetries proposed in the paper [57]. Also it has been shown that the super-$A$-polynomials of SO type contain both $a$-deformed $A$-polynomials of SO and SU type at $t = -1$.

Then by quantizing the SO($N$)($N \geq 4$) $6j$-symbols for symmetric representations given by Ališauskas, the SO($N$) fusion matrices for $R = \square, \square\square$ also the Kauffman polynomials colored by corresponding representations are computed. The resulting colored Kauffman polynomials coincide with the one obtained by changing variables from colored HOMFLY-PT polynomials. However, there still remain some unsolved questions. First, the volume conjecture only concerns the large color behavior of symmetric representations. But for the large color behavior of arbitrary colors, one also needs to formulate the volume conjecture which characterizes the moduli space of the flat SL$(2, \mathbb{C})$ connections over the knot complement. Second, one needs to find a closed-form expression of SO($N$) $6j$-symbols when $R_{12}$ and $R_{23}$ are non-symmetric for both classical and quantized cases. Moreover, the $6j$-symbol in AdS is proved to be the Lorentzian inversion of a crossing-symmetric tree-level exchange amplitude and the one-loop vertex correction for $\phi^3$-theory in $AdS_{d+1}$ background is given by a spectral integral over the $6j$-symbol for SO$(d+1, 1)$. The study of quantum SO$(6j)$-symbols may bring some enlightenment to the calculation of $6j$-symbols in the AdS background.

# Appendices

# 1 Superconformal Index

The two theories mirror dual to the 3d $\mathcal{N}=4$ Sp($k$) SQCD with $N_f$ flavours are discussed in §3. Therefore, by using the same method one can compute the SCIs of the 3d unitary and orthosymplectic mirror quivers in §3.1. It has been verified that they are match which are listed in Table 1.

| $k$ | $N_f$ | **superconformal index** |
|---|---|---|
| 1 | 3 | $1+\sqrt{q}\left(\frac{15}{t^2}+t^2\right)+q\left(-17+\frac{84}{t^4}+3t^4\right)+q^{3/2}\left(\frac{300}{t^6}-\frac{173}{t^2}-2t^2+3t^6\right)$ $+q^2\left(138+\frac{825}{t^8}-\frac{707}{t^4}-2t^4+5t^8\right)+\cdots$ |
| 1 | 4 | $1+\frac{28\sqrt{q}}{t^2}+q\left(-29+\frac{300}{t^4}+2t^4\right)+q^{3/2}\left(\frac{1925}{t^6}-\frac{649}{t^2}-t^2+t^6\right)$ $+q^2\left(376+\frac{8918}{t^8}-\frac{5643}{t^4}-t^4+3t^8\right)+\cdots$ |
| 1 | 5 | $1+\frac{45\sqrt{q}}{t^2}+q\left(-46+\frac{770}{t^4}+t^4\right)+q^{3/2}\left(\frac{7644}{t^6}-\frac{1714}{t^2}+t^6\right)$ $+q^2\left(988+\frac{52920}{t^8}-\frac{24574}{t^4}-t^4+2t^8\right)+\cdots$ |
| 1 | 6 | $1+\frac{66\sqrt{q}}{t^2}+q\left(-67+\frac{1638}{t^4}+t^4\right)+4q^{3/2}\left(\frac{5775}{t^6}-\frac{929}{t^2}\right)$ $+q^2\left(\frac{222156}{t^8}-\frac{78299}{t^4}+2143+2t^8\right)+\cdots$ |
| 2 | 4 | $1+\sqrt{q}\left(\frac{28}{t^2}+3t^2\right)+q\left(\frac{335}{t^4}+52+6t^4\right)+q^{3/2}\left(\frac{2492}{t^6}+\frac{104}{t^2}+48t^2+13t^6\right)$ $+q^2\left(\frac{13524}{t^8}-\frac{2524}{t^4}-96+40t^4+23t^8\right)+\cdots$ |
| 2 | 5 | $1+\sqrt{q}\left(\frac{45}{t^2}+t^2\right)+q\left(-2+\frac{980}{t^4}+3t^4\right)+\cdots.$ |
| 2 | 6 | $1+\frac{66\sqrt{q}}{t^2}+\cdots$ |

**Table 1.** Superconformal index for the unitary and orthosymplectic mirrors of Sp($k$) with $N_f$ flavours.

# 2 Twisted Indices

3d $\mathcal{N}=4$ twisted indices have been discussed in §2.2. This part lists some results which advocate the statements in the thesis.

## 2.1 A-twisted Index Sp(1), $N_f=3,4,5,6$ Flavours and Vortex Defect

The vortex line defect can be realized by coupling 1d SQM to the 3d bulk theory as shown in (3.3.1), similar to the discussions in [35]. Table 2 lists the A-twisted indices of Sp(1) theory with $N_f=3,\ldots,6$ in presence of

vortex lines. Here splitting $L+(N_f-L)$ denotes that $L$ flavours couple to the 1d SQM.

Note that one needs to bear the prefactor issue in mind when comparing the A-twisted indices in 2 and the B-twisted indices of the mirror theories with Wilson lines. In §3.2, the B-twisted indices were evaluated from the Higgs branch Hilbert series by inserting Wilson lines. The twisted indices and Hilbert series coincide up to overall factors, see [47]. Likewise, the A-twisted indices coincide with the Hilbert series of Coulomb branches, which are shown in Table 2

| Vortex line | A-twisted index |
|---|---|
| 3+0 | $-\frac{t(1+t^2)}{(-1+t^2)^2(1+t)^2}$ |
| 2+1 | $-\frac{2t^2}{(-1+t)^2(1+t)^2}$ |
| 1+2 | $-\frac{t(1+t^2)}{(-1+t^2)^2}$ |
| 0+3 | $\frac{(1+t^2)^2}{2(-1+t^2)^2}$ |

**(a)** $N_f=3$

| Vortex line | A-twisted index |
|---|---|
| 4+0 | $-\frac{t^2(1+t^2)}{(-1+t^2)^2(1+t^2)}$ |
| 3+1 | $\frac{2t^3}{(-1+t^2)^2(1+t^2)}$ |
| 2+2 | $\frac{t^2}{(-1+t)^2(1+t)^2}$ |
| 1+3 | $\frac{t(1+t^4)}{(-1+t)^2(1+t)^2(1+t^2)}$ |
| 0+4 | $\frac{-(1+t^4)}{2(-1+t^2)^2}$ |

**(b)** $N_f=4$

| Vortex line | A-twisted index |
|---|---|
| 5+0 | $\frac{t^3(1+t^2)}{(-1+t)^2(1+t)^2(1-t+t^2)(1+t+t^2)}$ |
| 4+1 | $-\frac{2t^4}{(-1+t)^2(1+t)^2(1-t+t^2)(1+t+t^2)}$ |
| 3+2 | $\frac{t^3(1+t^2)}{(-1+t)^2(1+t)^2(1-t+t^2)(1+t+t^2)}$ |
| 2+3 | $-\frac{t^2(1+t^4)}{(-1+t)^2(1+t)^2(1-t+t^2)(1+t+t^2)}$ |
| 1+4 | $\frac{t(1+t^2)(1-t^2+t^4)}{(-1+t)^2(1+t)^2(1-t+t^2)(1+t+t^2)}$ |
| 0+5 | $-\frac{(1+t^2)^2(1-t^2+t^4)}{2(-1+t)^2(1+t)^2(1-t+t^2)(1+t+t^2)}$ |

**(c)** $N_f=5$

| Vortex line | A-twisted index |
|---|---|
| 6+0 | $-\frac{t^4(1+t^2)}{(-1+t)^2(1+t)^2(1+t^2)(1+t^4)}$ |
| 5+1 | $\frac{2t^5}{(-1+t)^2(1+t)^2(1+t^2)(1+t^4)}$ |
| 4+2 | $-\frac{t^4}{(-1+t)^2(1+t)^2(1+t^4)}$ |
| 3+3 | $\frac{t^3}{(-1+t)^2(1+t)^2(1+t^2)}$ |
| 2+4 | $-\frac{t^2(1-t^2+t^4)}{(-1+t)^2(1+t)^2(1+t^4)}$ |
| 1+5 | $\frac{t(1+t^8)}{(-1+t)^2(1+t)^2(1+t^2)(1+t^4)}$ |
| 0+6 | $-\frac{1+t^8}{2(-1+t)^2(1+t)^2(1+t^4)}$ |

**(d)** $N_f=6$

**Table 2.** A-twisted index for Sp(1) with $N_f$ flavours with a vortex line defect characterised by a splitting of flavour $L+(N_f-L)$ and the fundamental representation of Sp(1).

## 2.2 B-twisted Index for Mirrors of Sp($k$) and Wilson Defect

The B-twisted indices for the 3d mirrors of Sp($k$) SQCD with Wilson lines are listed in (3)–(9)

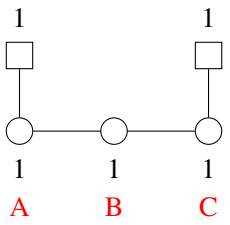


| | |
|---|---|
| A,C | $\frac{t}{(1-t)^2(1+t)^2}$ |
| B | $\frac{2t^2}{(-1+t)^2(1+t)^2(1+t^2)}$ |

**Table 3.** Sp(1) with $N_f = 3$. B-twisted index in the presence of Wilson lines inserted at the marked position in the quiver.

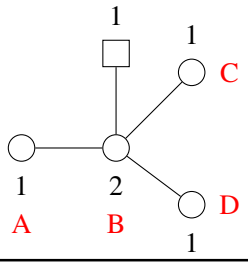


| | |
|---|---|
| A,C,D | $\frac{t^2}{(-1+t)^2(1+t)^2(1+t^2)}$ |
| B | $\frac{t}{(-1+t)^2(1+t)^2}$ |

**Table 4.** Sp(1) with $N_f = 4$. B-twisted index in the presence of Wilson lines inserted at the marked position in the quiver.

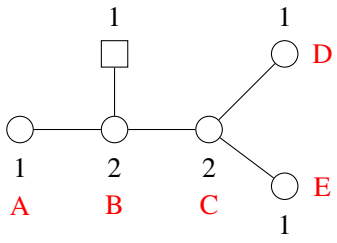


| | |
|---|---|
| A | $\frac{t^2(1-t^8)}{(1-t^4)^2(1-t^6)}$ |
| B | $\frac{t(1-t^8)}{(1-t^2)(1-t^4)(1-t^6)}$ |
| C | $\frac{t^2(1-t^4)}{(1-t^2)^2(1-t^6)}$ |
| D, E | $\frac{t^3}{(1-t^2)(1-t^6)}$ |

**Table 5.** Sp(1) with $N_f = 5$. B-twisted index in the presence of Wilson lines inserted at the marked position in the quiver. This quiver is also the $E_5$ family for $k = 1$ case.

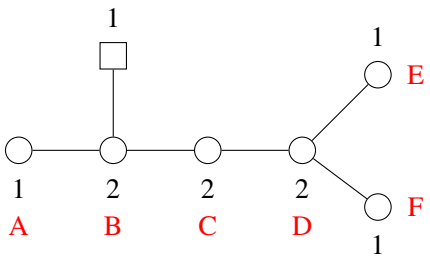


| | |
|---|---|
| A | $\frac{t^2(t^4-t^2+1)}{(t-1)^2(t+1)^2(t^2+1)(t^4+1)}$ |
| B | $\frac{t(t^4-t^2+1)}{(t-1)^2(t+1)^2(t^4+1)}$ |
| C | $\frac{t^2}{(t-1)^2(t+1)^2(t^2+1)}$ |
| D | $\frac{t^3}{(t-1)^2(t+1)^2(t^4+1)}$ |
| E,F | $\frac{t^4}{(t-1)^2(t+1)^2(t^2+1)(t^4+1)}$ |

**Table 6.** Sp(1) with $N_f = 6$. B-twisted index in the presence of Wilson lines inserted at the marked position in the quiver

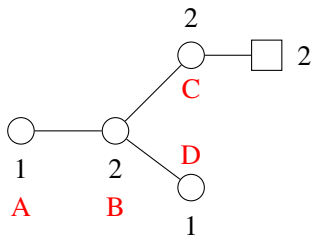


| | |
|---|---|
| A,D | $\frac{2t^3(1+t^2)(1+t^4)}{(-1+t)^4(1+t)^4(1-t+t^2)^2(1+t+t^2)^2}$ |
| B | $\frac{2t^2(1+t^2)^2(1+t^4)}{(-1+t)^4(1+t)^4(1-t+t^2)^2(1+t+t^2)^2}$ |
| C | $\frac{2t(1+t^2)(1+t^4)^2}{(-1+t)^4(1+t)^4(1-t+t^2)^2(1+t+t^2)^2}$ |

**Table 7.** There are two identical cones for the Higgs branch of Sp(2) SQCD with $N_f = 4$. And one of these two cones is the Coulomb branch of the quiver. B-twisted index with Wilson lines are inserted at the marked position.

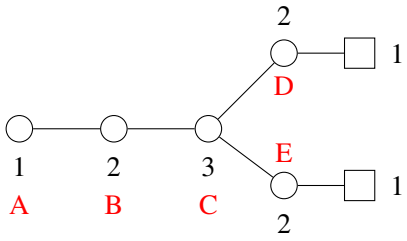


| | |
|---|---|
| A | $\frac{2t^4(1-t^2+t^4)}{(-1+t)^4(1+t)^4(1+t^2)^2(1+t^4)}$ |
| B | $\frac{2t^3(1-t^2+t^4)}{(-1+t)^4(1+t)^4(1+t^2)(1+t^4)}$ |
| C | $\frac{2t^2(1-t+t^2)(1+t+t^2)(1-t^2+t^4)}{(-1+t)^4(1+t)^4(1+t^2)^2(1+t^4)}$ |
| D,E | $\frac{t(1-t^2+t^4)}{(-1+t)^4(1+t)^4(1+t^2)}$ |

**Table 8.** Sp(2) with $N_f = 5$. B-twisted index with Wilson lines at the labelled position in the quiver.

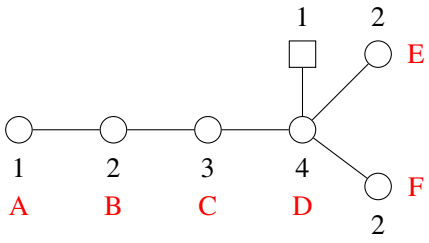


| | |
|---|---|
| A | $\frac{t^4(t^8+1)}{(t-1)^4(t+1)^4(t^2+1)^2(t^2-t+1)(t^2+t+1)(t^4+1)}$ |
| B | $\frac{t^3(t^8+1)}{(t-1)^4(t+1)^4(t^2+1)(t^2-t+1)(t^2+t+1)(t^4+1)}$ |
| C | $\frac{t^2(t^8+1)}{(t-1)^4(t+1)^4(t^2+1)^2(t^4+1)}$ |
| D | $\frac{t(t^8+1)}{(t-1)^4(t+1)^4(t^2+1)(t^2-t+1)(t^2+t+1)}$ |
| E, F | $\frac{t^2(t^8+1)}{(t-1)^4(t+1)^4(t^2+1)^2(t^2-t+1)(t^2+t+1)}$ |

**Table 9.** Sp(2) with $N_f = 6$. B-twisted index with Wilson lines at the labelled position in the quiver.

## 2.3 Wilson Lines for Exceptional Families

The unitary 3d mirrors of Sp($k$) SQCD theories are encoded in the D5-D3-NS5 brane system with O5 orientifold planes. In this brane system, the NS5 branes are viewed as flavor nodes in the quiver due to the existence of non-dynamical degrees of freedom on NS5 branes. However, $E_{6,7,8}$ unitary quivers are obtained from $(p, q)$ 5-brane, $[p, q]$ 7-brane settings where all these 5-branes occupy dynamical degrees of freedom. Therefore, one can only obtain an unframed magnetic quiver from the brane webs. Moreover, one needs to make a choice to decide where to gauge an overall U(1) factor. Physically, this will fix the center of mass of the system. If there exist two different ungauging methods, a Wilson line inserted at the same position in the quiver would engender two different B-twisted indices.

In order to endow an explicit flavor group to the resulting quiver, one needs to ungauge on an U(1). Otherwise, a fundamental Wilson line of a single gauge group in an unframed quiver is not invariant under the discrete 1-form symmetry and the corresponding B-twisted index is 0. This thesis mainly paid attention to the $E_n (n \leq 7)$ families. Depending on $k$, situations are different. When $k = 1$, all unitary quivers are affine Dynkin diagram of $\mathfrak{e}_n$, then ungauging any of the U(1)'s will engender exactly the same B-twisted index due to the symmetry of the quivers. When $k > 1$, one of the tails of the quiver is extended though the quiver itself is not affine Dynkin diagram anymore. This tail is named as $T[\mathrm{SU}(N)]$ tail which is a chain of gauge nodes with increasing ranks by one, which starts with U(1) and terminate with U($N$) for a given $N$. As shown in §3, for a Wilson line on a SO($2n$) node of the orthosymplectic quiver, it is always necessary to insert a Wilson line operator on the U(1) gauge node in the $T[\mathrm{SU}(N)]$ tail. For this reason, the U(1) gauge node in the $T[\mathrm{SU}(N)]$ tail should not be gauged. Hence, the U(1) nodes which are away from the extended tail will be ungauged for the $E_7$ family. For $E_{n\leq 6}$, there exist two U(1) gauge nodes far from the tail, and one can ungauge any of them due to the symmetry of the quivers. By ungauging in this way, one would obtain a delicate pattern of matching between the Wilson lines inserted in the unframed orthosymplectic quivers, as illustrated in §4.3. In the following Table (10)–(16), some instances of B-twisted indices with Wilson lines in the above ungauging scheme for several families are listed.

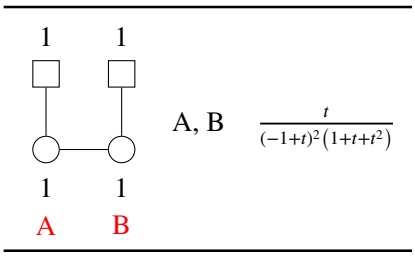


**Table 10.** $E_3$ family for $k = 1$. B-twisted index with Wilson lines inserted at the marked position in the quiver.

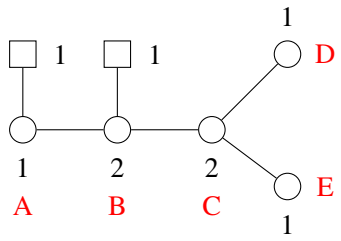


| | |
|---|---|
| A | $\frac{t(1+t^4)(1+t^3-t^4+t^5+t^8)}{(-1+t)^4(1+t)^2(1+t^2)(1-t+t^2)(1+t+t^2)(1+t+t^2+t^3+t^4+t^5+t^6)}$ |
| B | $\frac{t(1+t^4)(1+t^3+t^6)}{(-1+t)^4(1+t)^2(1-t+t^2)(1+t+t^2)(1+t+t^2+t^3+t^4+t^5+t^6)}$ |
| C | $\frac{t^2(1+t^2)(1+t^3+t^6)}{(-1+t)^4(1+t)^2(1-t+t^2)(1+t+t^2)(1+t+t^2+t^3+t^4+t^5+t^6)}$ |
| D, E | $\frac{t^3(1+t^3+t^6)}{(-1+t)^4(1+t)^2(1-t+t^2)(1+t+t^2)(1+t+t^2+t^3+t^4+t^5+t^6)}$ |

**Table 11.** $E_3$ family for $k = 2$. B-twisted index with Wilson lines at the labelled position in the quiver.

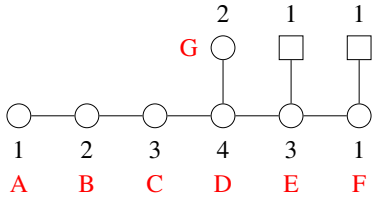


| | |
|---|---|
| A | $\frac{(1-t)\left(\begin{array}{c}t^5(1+2t+3t^2+4t^3+5t^4+6t^5+8t^6+10t^7+12t^8+13t^9+14t^{10}+15t^{11}+17t^{12}\\+18t^{13}+19t^{14}+19t^{15}+19t^{16}+18t^{17}+17t^{18}+15t^{19}+14t^{20}+13t^{21}\\+12t^{22}+10t^{23}+8t^{24}+6t^{25}+5t^{26}+4t^{27}+3t^{28}+2t^{29}+t^{30})\end{array}\right)}{(1-t^2)(1-t^3)(1-t^6)(1-t^7)(1-t^8)(1-t^{10})(1-t^{11})}$ |
| B | $\frac{(1-t)(1-t^4)\left(\begin{array}{c}t^4(1+2t+3t^2+4t^3+5t^4+6t^5+8t^6+10t^7+12t^8+13t^9+14t^{10}+15t^{11}+17t^{12}\\+18t^{13}+19t^{14}+19t^{15}+19t^{16}+18t^{17}+17t^{18}+15t^{19}+14t^{20}+13t^{21}\\+12t^{22}+10t^{23}+8t^{24}+6t^{25}+5t^{26}+4t^{27}+3t^{28}+2t^{29}+t^{30})\end{array}\right)}{(1-t^2)^2(1-t^3)(1-t^6)(1-t^7)(1-t^8)(1-t^{10})(1-t^{11})}$ |
| C | $\frac{(1-t)\left(\begin{array}{c}t^3(1+2t+3t^2+4t^3+5t^4+6t^5+8t^6+10t^7+12t^8+13t^9+14t^{10}+15t^{11}+17t^{12}\\+18t^{13}+19t^{14}+19t^{15}+19t^{16}+18t^{17}+17t^{18}+15t^{19}+14t^{20}+13t^{21}\\+12t^{22}+10t^{23}+8t^{24}+6t^{25}+5t^{26}+4t^{27}+3t^{28}+2t^{29}+t^{30})\end{array}\right)}{(1-t^2)^2(1-t^3)(1-t^7)(1-t^8)(1-t^{10})(1-t^{11})}$ |
| D | $\frac{(1-t)\left(\begin{array}{c}t^2(1+2t+3t^2+4t^3+5t^4+6t^5+8t^6+10t^7+12t^8+13t^9+14t^{10}+15t^{11}+17t^{12}\\+18t^{13}+19t^{14}+19t^{15}+19t^{16}+18t^{17}+17t^{18}+15t^{19}+14t^{20}+13t^{21}\\+12t^{22}+10t^{23}+8t^{24}+6t^{25}+5t^{26}+4t^{27}+3t^{28}+2t^{29}+t^{30})\end{array}\right)}{(1-t^2)^2(1-t^3)(1-t^6)(1-t^7)(1-t^{10})(1-t^{11})}$ |
| E | $\frac{(1-t)\left(\begin{array}{c}t(1-t^2+t^4)(1+2t+3t^2+4t^3+5t^4+6t^5+8t^6+10t^7+12t^8+13t^9+14t^{10}+15t^{11}+17t^{12}\\+18t^{13}+19t^{14}+19t^{15}+19t^{16}+18t^{17}+17t^{18}+15t^{19}+14t^{20}+13t^{21}\\+12t^{22}+10t^{23}+8t^{24}+6t^{25}+5t^{26}+4t^{27}+3t^{28}+2t^{29}+t^{30})\end{array}\right)}{(1-t^2)^2(1-t^3)(1-t^7)(1-t^8)(1-t^{10})(1-t^{11})}$ |
| F | $\frac{t(1-t)\left(1-t^3+t^6\right)\left(\begin{array}{c}1+2t+3t^2+5t^3+6t^4+8t^5+9t^6+10t^7+12t^8+13t^9+14t^{10}+15t^{11}\\+16t^{12}+17t^{13}+17t^{14}+17t^{15}+17t^{16}+17t^{17}+16t^{18}+15t^{19}+14t^{20}+13\\t^{21}+12t^{22}+10t^{23}+9t^{24}+8t^{25}+6t^{26}+5t^{27}+3t^{28}+2t^{29}+t^{30}\end{array}\right)}{(1-t^3)(1-t^4)^2\left(1-t^6\right)(1-t^7)(1-t^{10})(1-t^{11})}$ |
| G | $\frac{(1-t)t^3\left(\begin{array}{c}(1+2t+3t^2+4t^3+5t^4+6t^5+8t^6+10t^7+12t^8+13t^9+14t^{10}\\+15t^{11}+17t^{12}+18t^{13}+19t^{14}+19t^{15}+19t^{16}+18t^{17}+17t^{18}+15t^{19}\\+14t^{20}+13t^{21}+12t^{22}+10t^{23}+8t^{24}+6t^{25}+5t^{26}+4t^{27}+3t^{28}+2t^{29}+t^{30})\end{array}\right)}{(1-t^2)(1-t^3)(1-t^4)(1-t^6)(1-t^7)(1-t^{10})(1-t^{11})}$ |

**Table 12.** $E_3$ family for $k = 3$. B-twisted index with Wilson lines at the labelled position in the quiver.

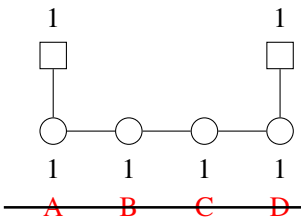


| | |
|---|---|
| A, D | $\frac{t(1-t+t^2)}{(-1+t)^2(1+t+t^2+t^3+t^4)}$ |
| B, C | $\frac{t^2}{(-1+t)^2(1+t+t^2+t^3+t^4)}$ |

**Table 13.** $E_4$ family for $k = 1$. B-twisted index with Wilson lines at the labelled position in the quiver.

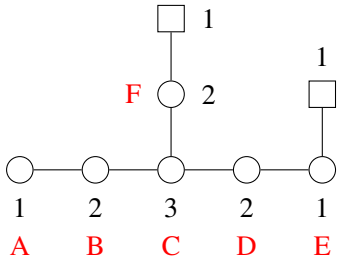


| | |
|---|---|
| A | $\frac{t^4(1+t+t^2+t^3+t^4+t^5+t^6+t^7+t^8+t^9+t^{10}+t^{11}+t^{12})}{(-1+t)^4(1+t)^2(1+t^2)(1-t+t^2)(1+t+t^2)^2(1+t+t^2+t^3+t^4)(1+t^3+t^6)}$ |
| B | $\frac{t^3(1+t+t^2+t^3+t^4+t^5+t^6+t^7+t^8+t^9+t^{10}+t^{11}+t^{12})}{(-1+t)^4(1+t)^2(1-t+t^2)(1+t+t^2)^2(1+t+t^2+t^3+t^4)(1+t^3+t^6)}$ |
| C | $\frac{t^2(1+t+t^2+t^3+t^4+t^5+t^6+t^7+t^8+t^9+t^{10}+t^{11}+t^{12})}{(-1+t)^4(1+t)^2(1+t^2)(1+t+t^2)(1+t+t^2+t^3+t^4)(1+t^3+t^6)}$ |
| D | $\frac{t^2(1+t+t^3+t^4+t^5+t^6+t^7+t^8+t^9+t^{10}+t^{11}+t^{13}+t^{14})}{(-1+t)^4(1+t)^2(1-t+t^2)(1+t+t^2)^2(1+t+t^2+t^3+t^4)(1+t^3+t^6)}$ |
| E | $\frac{t(1+t^2+t^3+t^5+t^7+t^8+t^9+t^{10}+t^{11}+t^{13}+t^{15}+t^{16}+t^{18})}{(-1+t)^4(1+t)^2(1+t^2)(1-t+t^2)(1+t+t^2)^2(1+t+t^2+t^3+t^4)(1+t^3+t^6)}$ |
| F | $\frac{t(1-t^2+t^4)(1+t^2+t^3+t^4+2t^5+t^6+2t^7+t^8+t^9+t^{10}+t^{12})}{(-1+t)^4(1+t)^2(1-t+t^2)(1+t+t^2)^2(1+t+t^2+t^3+t^4)(1+t^3+t^6)}$ |

**Table 14.** $E_4$ family for $k = 2$. B-twisted index with Wilson lines inserted at the marked position in the quiver.

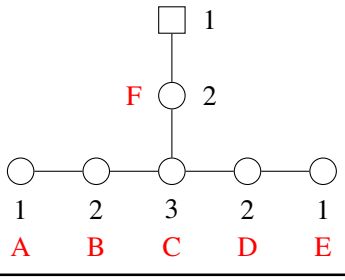


| | |
|---|---|
| A, E | $\frac{t^4}{(1-t^4)(1-t^6)}$ |
| B, D | $\frac{t^3}{(1-t^2)(1-t^6)}$ |
| C | $\frac{t^2}{(1-t^2)(1-t^4)}$ |
| F | $\frac{t(1-t^{12})}{(1-t^4)(1-t^6)^2}$ |

**Table 15.** $E_6$ family for $k = 1$. B-twisted index with Wilson lines at the labelled position in the quiver.

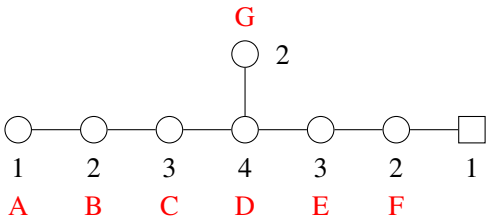


| | |
|---|---|
| A | $\frac{t^6}{(1-t^6)(1-t^8)}$ |
| B | $\frac{t^5(1-t^4)}{(1-t^2)(1-t^6)(1-t^8)}$ |
| C | $\frac{t^4}{(1-t^2)(1-t^8)}$ |
| D | $\frac{t^3}{(1-t^2)(1-t^6)}$ |
| E | $\frac{t^2(1-t^{12})}{(1-t^4)(1-t^6)(1-t^8)}$ |
| F | $\frac{t(1-t^{20})}{(1-t^6)(1-t^8)(1-t^{10})}$ |
| G | $\frac{t^4}{(1-t^4)(1-t^6)}$ |

**Table 16.** $E_7$ family for $k = 1$. B-twisted index with Wilson lines at the labelled position in the quiver.

# 3 Sphere Partition Function

In this section, some results of $S^3$ partition functions in the presence/absence of line defects for 3d $\mathcal{N}=4$ theories are listed. These results are relevant to the statements in the thesis.

## 3.1 Sp($k$) SQCDs and Their Mirrors

**Sp($k$) SQCD.** The $S^3$ partition function for Sp($k$) SQCD with $N_f$ fundamental hypermultiplets can be written as

$$\begin{aligned} Z^{S^3}_{\mathrm{Sp}(k),N_f}(m) &= \lim_{\xi\to 0}\int [d\mathbf{s}]\frac{e^{2\pi i\xi\sum_{i=1}^k s_i}\prod_{\alpha\in\Delta}\mathrm{sh}(\alpha\cdot s)}{\prod_{j=1}^{N_f}\prod_{w\in\square}\mathrm{ch}(w\cdot s-m_j)} \\ &= \sum_{I\in C_k^{N_f}}\prod_{j=1}^{k}\frac{m_{I_j}\,\mathrm{sh}(2m_{I_j})}{\prod_{\ell\notin I}\mathrm{sh}(m_\ell\pm m_{I_j})}\,. \end{aligned} \tag{3.1}$$

Here $I$ runs over all $C_k^{N_f}$ combinations of $k$ distinct integers in $\{1,\dots,N_f\}$. In order to compute the residue in the first line, one can take poles at

$$s_j=\pm m_{I_j}+i\frac{2k_j+1}{2}\,,\quad k_j\in\mathbb{Z}_{\geq 0} \tag{3.2}$$

and their permutations $S_k$ on $I$. Then, the second line can be obtained by evaluating the limit $\xi\to 0$ with utilizing the L'Hospital's rule.

**Vortex loops in Sp($k$) SQCD.** The $S^3$ partition function of the U(1) SQM for a vortex loop of type $N_f = L+\left(N_f-L\right)$ in (3.3.1) can be written as

$$Z_{(L,N_f-L),\mathbf{2k}}(z)=\sum_{w_i\in\square}\prod_{j\neq i}\frac{\mathrm{sh}(w_i\cdot s-w_j\cdot s+iz)}{\mathrm{sh}(w_i\cdot s-w_j\cdot s)}\prod_{\ell=1}^{L}\frac{\mathrm{ch}(w_i\cdot s-m_\ell)}{\mathrm{ch}(w_i\cdot s-m_\ell+iz)}\,. \tag{3.3}$$

There are $2k$ terms in the summation because the dimension of the fundamental representation of Sp($k$) is $2k$. The $\mathrm{ch}(w_i\cdot s-m_k+iz)$ in the denominator will shift some of the poles in (3.2) by $-i$. After evaluating the residue, one can obtain

$$\begin{aligned} Z^{S^3}_{(L,N_f-L),\mathbf{2k}} &= \lim_{\xi\to 0,z\to 1}\int [d\mathbf{s}]\frac{e^{2\pi i\xi\sum_{i=1}^k s_i}\prod_{\alpha\in\Delta}\mathrm{sh}(\alpha\cdot s)}{\prod_{j=1}^{N_f}\prod_{w\in\square}\mathrm{ch}(w\cdot s-m_j)}Z_{(L,N_f-L),\mathbf{2k}}(z)\,, \\ &= (2k-L)\cdot Z^{S^3}_{\mathrm{Sp}(k),N_f}(m)+\sum_{j=1}^{L}Z^{S^3}_{\mathrm{Sp}(k),N_f}(m_j\to m_j-i)\,. \end{aligned} \tag{3.4}$$

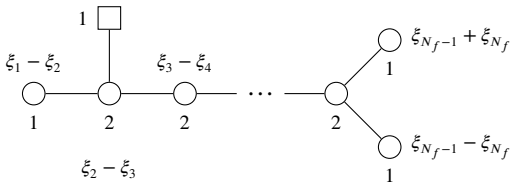


(3.5)

The mirror unitary quiver is the $D_{N_f}$-type quiver (3.5), one can obtain the equivalence between the $k=1$ $S^3$ partition functions. In this case, (3.4) turns into

$$Z^{S^3}_{(L,N_f-L),\mathbf{2}} = \sum_{j=1}^{L} \frac{(2m_j - i)\,\mathrm{sh}(2m_j)}{\prod_{\ell\neq j}\mathrm{sh}(m_\ell \pm m_j)} + \sum_{k=L+1}^{N_f} \frac{(2m_k)\,\mathrm{sh}(2m_k)}{\prod_{\ell\neq k}\mathrm{sh}(m_\ell \pm m_k)}\,. \tag{3.6}$$

The derivation is nearly identical to the §3.2 in [117].

***D*-type quiver.** For thisc case, the $S^3$ partition function is

$$\begin{aligned} Z^{S^3}_D =& \frac{1}{2^{N_f-3}}\int dz^{(1)}dz_\pm \prod_{j=2}^{N_f-2} dz_1^{(j)}dz_2^{(j)} \frac{e^{2\pi i(\xi_1-\xi_2)z^{(1)}}e^{2\pi i\sum_{j=2}^{N_f-2}(\xi_j-\xi_{j+1})(z_1^{(j)}+z_2^{(j)})}e^{2\pi i(\xi_{N_f-1}\pm\xi_{N_f})z_\pm}}{\prod_{i=1,2}\mathrm{ch}(z_i^{(2)}-z^{(1)})\,\mathrm{ch}(z_i^{(2)}-m)\,\mathrm{ch}(z_i^{(N_f-2)}-z_\pm)} \\ &\times \frac{\prod_{j=2}^{N_f-2}\mathrm{sh}^2(z_1^{(j)}-z_2^{(j)})}{\prod_{j=2}^{N_f-3}\prod_{k,\ell=1,2}\mathrm{ch}(z_k^{(j)}-z_\ell^{(j+1)})} \end{aligned} \tag{3.7}$$

$$\begin{aligned} =& \frac{1}{2}\frac{1}{\mathrm{sh}(\xi_1-\xi_2)\,\mathrm{sh}(\xi_{N_f-1}-\xi_{N_f})}\int dz_+ \prod_{j=2}^{N_f-2} dz_1^{(j)}dz_2^{(j)} \frac{e^{2\pi i\sum_{j=2}^{N_f-2}(\xi_j-\xi_{j+1})(z_1^{(j)}+z_2^{(j)})}e^{2\pi i(\xi_{N_f-1}+\xi_{N_f})z_+}}{\prod_{i=1,2}\mathrm{ch}(z_i^{(2)}-m)\,\mathrm{ch}(z_i^{(N_f-2)}-z_+)} \\ &\times \frac{(e^{2\pi i(\xi_1-\xi_2)z_1^{(2)}}-e^{2\pi i(\xi_1-\xi_2)z_2^{(2)}})(e^{2\pi i(\xi_{N_f-1}-\xi_{N_f})z_1^{(N_f-2)}}-e^{2\pi i(\xi_{N_f-1}-\xi_{N_f})z_2^{(N_f-2)}})}{\prod_{j=2}^{N_f-3}\prod_{i=1,2}\mathrm{ch}(z_i^{(j)}-z_i^{(j+1)})}\,. \end{aligned} \tag{3.8}$$

By using the Cauchy determinant formula, one can obtain the second line from the first line. Then, one can take the Fourier transformation of *ch*:

$$\begin{aligned} Z^{S^3}_D =& \frac{1}{2}\frac{1}{\mathrm{sh}(\xi_1-\xi_2)\,\mathrm{sh}(\xi_{N_f-1}-\xi_{N_f})}\int dz_+ \prod_{j=2}^{N_f-2} dz_1^{(j)}dz_2^{(j)}e^{2\pi i\sum_{j=2}^{N_f-2}(\xi_j-\xi_{j+1})(z_1^{(j)}+z_2^{(j)})}e^{2\pi i(\xi_{N_f-1}+\xi_{N_f})z_+} \\ &(e^{2\pi i(\xi_1-\xi_2)z_1^{(2)}}-e^{2\pi i(\xi_1-\xi_2)z_2^{(2)}})(e^{2\pi i(\xi_{N_f-1}-\xi_{N_f})z_1^{(N_f-2)}}-e^{2\pi i(\xi_{N_f-1}-\xi_{N_f})z_2^{(N_f-2)}}) \\ &\int \frac{ds_1ds_2}{\mathrm{ch}\,s_1\,\mathrm{ch}\,s_2}e^{2\pi i(s_1(z_1^{(2)}-m)+s_2(z_2^{(2)}-m))}\int \frac{dp_1dp_2}{\mathrm{ch}\,p_1\,\mathrm{ch}\,p_2}e^{2\pi i(p_1(z_1^{(N_f-2)}-z_+)+p_2(z_2^{(N_f-2)}-z_+))} \\ &\int \prod_{j=2}^{N_f-3}\frac{dt_1^{(j)}dt_2^{(j)}}{\mathrm{ch}\,t_1^{(j)}\,\mathrm{ch}\,t_2^{(j)}}e^{2\pi i\sum_{j=2}^{N_f-3}(t_1^{(j)}(z_1^{(j)}-z_1^{(j+1)})+t_2^{(j)}(z_2^{(j)}-z_2^{(j+1)}))}\,. \end{aligned} \tag{3.9}$$

One can expand the product in the second line which will give four terms. Then focus on the term proportional to $e^{2\pi i(\xi_1-\xi_2)z_1^{(2)}+2\pi i(\xi_{N_f-1}-\xi_{N_f})z_1^{(N_f-2)}}$. Integrating over the variables $z_+$ and $z_i^{(j)}$ $(i=1,2\ j=2,\ldots,N_f-2)$, it will

engender the delta functions that give the following relations:

$$s_2 = -\xi_2 - s_1\,, \quad p_1 = \xi_{N_f} - s_1\,, \quad p_2 = \xi_{N_f-1} + s_1\,, \quad t_1^{(j)} = s_1 - \xi_{j+1}\,, \quad t_2^{(j)} = -s_1 - \xi_{j+1}\,, \tag{3.10}$$

which gives the shift $s_1 \to s_1 - \xi_1$. There are also other 3 terms that lead to similar relations by exchanging $\xi_1 \leftrightarrow \xi_2$ and $\xi_{N_f-1} \leftrightarrow \xi_{N_f}$. Finally, the result can be written as

$$\begin{aligned} Z_D^{S^3} =& \frac{e^{2\pi i(\xi_1+\xi_2)m}}{\mathrm{sh}(\xi_2-\xi_1)\,\mathrm{sh}(\xi_{N_f-1}-\xi_{N_f})} \int ds_1 \frac{1}{\prod_{j=2}^{N_f-2}\mathrm{ch}(s_1\pm\xi_j)} \\ &\times\left(\frac{1}{\mathrm{ch}(s_1-\xi_1)\,\mathrm{ch}(s_1+\xi_2)} - \frac{1}{\mathrm{ch}(s_1+\xi_1)\,\mathrm{ch}(s_1-\xi_2)}\right)\frac{1}{\mathrm{ch}(s_1-\xi_{N_f-1})\,\mathrm{ch}(s_1+\xi_{N_f})} \\ =& e^{2\pi i(\xi_1+\xi_2)m}\sum_{i=1}^{N_f}\frac{\xi_i\,\mathrm{sh}(2\xi_i)}{\prod_{k\neq i}\mathrm{sh}(\xi_k\pm\xi_i)}\,. \end{aligned} \tag{3.11}$$

Taking the limit $m \to 0$, it matches with the $S^3$ partition function of the Sp(1) SQCD with $N_f$ flavours by interchanging the FI parameters and mass parameters $\xi_i \leftrightarrow m_i$.

**Wilson loops in $D$-type quiver.** One can insert a Wilson loop in the fundamental representation at the $L$-th node counting from the left in (3.5). If $L = 1$, the Wilson loop will shift $\xi_1 \to \xi_1 - i$. Then, the summation of the Wilson loop inserted in the left U(1) (3.3.4) and the flavor Wilson loop (3.3.4b) is given by:

$$Z^{S^3}_{\mathcal{W}\text{ at }[1,0,\ldots,0,0]} + Z_D^{S^3} = \frac{(2\xi_1-i)\,\mathrm{sh}(2\xi_1)}{\prod_{\ell\neq1}\mathrm{sh}(\xi_\ell\pm\xi_1)} + \sum_{j=2}^{N_f}\frac{(2\xi_j)\,\mathrm{sh}(2\xi_j)}{\prod_{\ell\neq j}\mathrm{sh}(\xi_\ell\pm\xi_j)}\,, \tag{3.12}$$

This result equals to the vortex (3.6) of the $1+(N_f-1)$ splitting under $\xi \leftrightarrow m$. When $2 \le L \le N_f - 2$, then (3.10) are modified such that

$$\begin{aligned} & Z^{S^3}_{\mathcal{W}\text{ at }[0,\ldots,0,1,0,\ldots,0]} \\ =& \frac{1}{\mathrm{sh}(\xi_2-\xi_1)\,\mathrm{sh}(\xi_{N_f-1}-\xi_{N_f})}\int ds_1 \frac{1}{\prod_{k=L+1}^{N_f-2}\mathrm{ch}(s_1\pm\xi_k)\prod_{j=2}^{L}\mathrm{ch}(s_1-\xi_j-i)\,\mathrm{ch}(s_1+\xi_j)} \\ &\times\left(\frac{1}{\mathrm{ch}(s_1-\xi_1-i)\,\mathrm{ch}(s_1+\xi_2)} - \frac{1}{\mathrm{ch}(s_1+\xi_1)\,\mathrm{ch}(s_1-\xi_2-i)}\right)\frac{1}{\mathrm{ch}(s_1-\xi_{N_f-1})\,\mathrm{ch}(s_1+\xi_{N_f})} \\ &+ \frac{1}{\mathrm{sh}(\xi_2-\xi_1)\,\mathrm{sh}(\xi_{N_f-1}-\xi_{N_f})}\int ds_1 \frac{1}{\prod_{k=L+1}^{N_f-2}\mathrm{ch}(s_1\pm\xi_k)\prod_{j=2}^{L}\mathrm{ch}(s_1-\xi_j)\,\mathrm{ch}(s_1+\xi_j-i)} \\ &\times\left(\frac{1}{\mathrm{ch}(s_1-\xi_1)\,\mathrm{ch}(s_1+\xi_2-i)} - \frac{1}{\mathrm{ch}(s_1+\xi_1-i)\,\mathrm{ch}(s_1-\xi_2)}\right)\frac{1}{\mathrm{ch}(s_1-\xi_{N_f-1})\,\mathrm{ch}(s_1+\xi_{N_f})} \\ =& \sum_{j=1}^{L}\frac{(2\xi_j-i)\,\mathrm{sh}(2\xi_j)}{\prod_{\ell\neq j}\mathrm{sh}(\xi_\ell\pm\xi_j)} + \sum_{k=L+1}^{N_f}\frac{(2\xi_k)\,\mathrm{sh}(2\xi_k)}{\prod_{\ell\neq k}\mathrm{sh}(\xi_\ell\pm\xi_k)}\,. \end{aligned} \tag{3.13}$$

which is equal to (3.6) under $\xi \leftrightarrow m$. There are two possible spinor nodes for fundamental Wilson loop to impose. For the node with with FI parameter $\xi_{N_f-1} - \xi_{N_f}$, the Wilson loop will give the shift

$$\xi_j \to \xi_j - \frac{i}{2}\,(j = 1, \dots, N_f - 1)\,, \quad \xi_{N_f} \to \xi_{N_f} + \frac{i}{2}\,. \tag{3.14}$$

For the other node with FI parameter $\xi_{N_f-1} + \xi_{N_f}$, the Wilson loop will give the shift

$$\xi_j \to \xi_j - \frac{i}{2}\,, \quad (j = 1, \dots, N_f)\,. \tag{3.15}$$

Therefore the summation of the fundamental Wilson loops at spinor nodes (3.3.9) and (3.3.10) is given by

$$Z^{S^3}_{\mathcal{W}\text{ at }[0,\dots,1,0]} + Z^{S^3}_{\mathcal{W}\text{ at }[0,\dots,0,1]} = \sum_{j=1}^{N_f-1} \frac{(2\xi_j - i)\,\mathrm{sh}(2\xi_j)}{\prod_{\ell\neq j}\mathrm{sh}(\xi_\ell \pm \xi_j)} + \frac{(2\xi_{N_f})\,\mathrm{sh}(2\xi_{N_f})}{\prod_{\ell\neq N_f}\mathrm{sh}(\xi_\ell \pm \xi_{N_f})}\,, \tag{3.16}$$

this corresponds to the $(N_f - 1) + 1$ splitting vortex in the mirror dual. For the Wilson loop with multiplicity 2 as shown in (3.3.12) inserted at the node with the FI parameter $\xi_{N_f-1} + \xi_{N_f}$ is

$$2 \cdot Z^{S^3}_{\mathcal{W}\text{ at }[0,\dots,0,1]} = \sum_{j=1}^{N_f} \frac{(2\xi_j - i)\,\mathrm{sh}(2\xi_j)}{\prod_{\ell\neq j}\mathrm{sh}(\xi_\ell \pm \xi_j)}\,, \tag{3.17}$$

this corresponds to the $N_f + 0$ splitting vortex line defect in the mirror dual

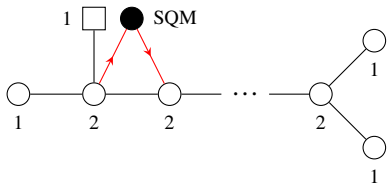


(3.18)

**Vortex loops in $D$-type quiver.** For the vortex contribution (3.18), the partition function is

$$Z^{\mathrm{SQM}} = \sum_{\ell=1,2} \frac{\mathrm{sh}(z^{(2)}_1 - z^{(2)}_2 - (-1)^\ell iz)}{\mathrm{sh}(z^{(2)}_1 - z^{(2)}_2)} \prod_{j=1,2} \frac{\mathrm{ch}(z^{(2)}_\ell - z^{(3)}_j)}{\mathrm{ch}(z^{(2)}_\ell - z^{(3)}_j + iz)}\,. \tag{3.19}$$

The vortex acts on the integrand of (3.9) by multiplying a factor $(e^{-2\pi t^{(2)}_1 z} + e^{-2\pi t^{(2)}_2 z})$. Since the relations (3.10) will not change, the vortex expectation value becomes

$$\begin{aligned} Z^{S^3}_{D,\mathcal{V}} =& \frac{1}{\mathrm{sh}(\xi_2 - \xi_1)\,\mathrm{sh}(\xi_{N_f-1} - \xi_{N_f})} \int ds_1 \frac{(e^{2\pi s_1} + e^{-2\pi s_1})}{\prod_{j=2}^{N_f-2}\mathrm{ch}(s_1 \pm \xi_j)} \\ &\times \left( \frac{1}{\mathrm{ch}(s_1 - \xi_1)\,\mathrm{ch}(s_1 + \xi_2)} - \frac{1}{\mathrm{ch}(s_1 + \xi_1)\,\mathrm{ch}(s_1 - \xi_2)} \right) \frac{1}{\mathrm{ch}(s_1 - \xi_{N_f-1})\,\mathrm{ch}(s_1 + \xi_{N_f})} \end{aligned}$$

$$= \sum_{i=1}^{N_f} \frac{\xi_i \,\mathrm{sh}(2\xi_i)(e^{2\pi\xi_i} + e^{-2\pi\xi_i})}{\prod_{k\neq i} \mathrm{sh}(\xi_k \pm \xi_i)} \,. \tag{3.20}$$

One can check that this matches with the expectation value of the Wilson line defect in the fundamental representation in the Sp(1) SQCD. In [35], they presented the derivation of hopping duality, therefore the vortex defects (3.4.1), (3.4.2), (3.4.3) are equivalent.

***D*-type quiver of higher rank.** This paragraph will explain the derivation of the closed-form formula of the $S^3$ partition function of the $D$-type quiver in (3.1.2) which is mirror dual to the Sp($k$) SQCD with $N_f$ flavours. Since the $S^3$ partition function of $T[\mathrm{U}(2k)]$ has been given in [117] which corresponds to the left tail in (3.1.2). Furthermore, the contribution of the spinor nodes can be obtained form the $S^3$ partition function of the U($k$) SQCD with $2k$ flavours (3.23). Combining above pieces, one can obtain

$$\begin{aligned} Z =& \frac{1}{(k!)^{N_f-2k-1}} \int \prod_{j=1}^{N_f-2k-1} d\mathbf{z}^{(j)} \frac{e^{2\pi i \sum_{j=1}^{N_f-2k-1}(\xi_{2k-1+j}-\xi_{2k+j})(\sum_{k=1} z_k^{(j)})} \prod_{j=1}^{N_f-2k-1} \prod_{n\neq\ell} \mathrm{sh}^2(z_n^{(j)} - z_\ell^{(j)})}{\prod_{n=1}^{2k} \mathrm{ch}(z_n^{(1)} - m) \prod_{j=1}^{N_f-2k-2} \prod_{n,\ell=1}^{2k} \mathrm{ch}(z_n^{(j)} - z_\ell^{(j+1)})} \\ & Z^{S^3}_{T[\mathrm{U}(2k)]}(\mathbf{z}^{(1)}, \xi) Z^{S^3}_{\mathrm{U}(k),N_f}(z^{(N_f-2k-1)}, \xi_{N_f-1} - \xi_{N_f}) Z^{S^3}_{\mathrm{U}(k),N_f}(z^{(N_f-2k-1)}, \xi_{N_f-1} + \xi_{N_f}) \,. \end{aligned} \tag{3.21}$$

Again one can use the Cauchy determinant identity repeatedly to obtain

$$\begin{aligned} Z =& \frac{1}{\mathrm{sh}^k(\xi_{N_f-1} \pm \xi_{N_f}) \prod_{n\neq\ell}^{2k} \mathrm{sh}(\xi_n - \xi_\ell)} \int \prod_{j=1}^{N_f-2k-1} d\mathbf{z}^{(j)} \frac{e^{2\pi i \sum_{j=1}^{N_f-2k-1}(\xi_{2k-1+j}-\xi_{2k+j})(\sum_{k=1} z_k^{(j)})}}{\prod_{n=1}^{2k} \mathrm{ch}(z_n^{(1)} - m) \prod_{j=1}^{N_f-2k-2} \prod_{n=1}^{2k} \mathrm{ch}(z_n^{(j)} - z_n^{(j+1)})} \\ & \sum_{J\in C_k^{N_f}} \frac{e^{2\pi i(\xi_{N_f-1}-\xi_{N_f})(\sum_{j=1}^k m_{J_j})}}{\prod_{j=1}^k \prod_{\ell\notin I} \mathrm{sh}(m_\ell - m_{I_j})} \sum_{I\in C_k^{N_f}} \frac{e^{2\pi i(\xi_{N_f-1}+\xi_{N_f})(\sum_{j=1}^k m_{I_j})}}{\prod_{j=1}^k \prod_{\ell\notin I} \mathrm{sh}(m_\ell - m_{I_j})} \,. \end{aligned} \tag{3.22}$$

To get rid off the *sh* factor in the numerator of the integral kernel, one can utilize the Cauchy determinant formula repeatedly. And by performing Fourier transformation to $\frac{1}{ch}$ and $\frac{1}{sh}$ and integrating over the gauge fugacities, one can obtain the delta functions which impose similar relations as above. After performing Fourier transformation further and using the identity $\mathrm{sh}(x) = -i\,\mathrm{ch}(x+\frac{i}{2})$ , one can turn the formula into a combination of products of the U(1) integral formula as shown in §2.2 of [117]. In this way, the $S^3$ partition function of the $D$-type higher-rank quivers was computed and be verified that it equals to (3.1) up to a factor under interchange $\xi_i \leftrightarrow m_i$ when $k = 2$.

## 3.2 Other Theories

In this part, the closed-form formulae of $S^3$ partition functions for 3d $\mathcal{N} = 4$ theories are listed. Note that the $S^3$ partition function of SQCDs for other types of gauge groups can be computed as (3.1).

U($k$) **SQCD.** The $S^3$ partition function of U($k$) SQCD with $N_f$ flavours and the FI parameter $\xi$ is

$$Z^{S^3}_{\mathrm{U}(k),N_f}(m,\xi) = \sum_{I\in C_k^{N_f}} \frac{e^{2\pi i\xi(\sum_{j=1}^k m_{I_j})}}{\mathrm{sh}^k(\xi)\prod_{j=1}^k\prod_{\ell\notin I}\mathrm{sh}(m_\ell - m_{I_j})}\,. \tag{3.23}$$

If one turns off the FI parameter, it becomes

$$Z^{S^3}_{\mathrm{U}(k),N_f}(m) = \lim_{\xi\to 0} Z^{S^3}_{\mathrm{U}(k),N_f}(m,\xi) = \sum_{I\in C_k^{N_f}} \frac{(\sum_{j=1}^k m_{I_j})^k}{\prod_{j=1}^k\prod_{\ell\notin I}\mathrm{sh}(m_\ell - m_{I_j})}\,. \tag{3.24}$$

SO(2$k$) **SQCD.** For SO($k$) SQCD, there is no FI parameter. Therefore, one needs to introduce a regulator for evaluating $S^3$ partition function and take the zero limit of regulator as in (3.1). The results is

$$Z^{S^3}_{\mathrm{SO}(2k),N_f}(m) = \sum_{I\in C_k^{N_f}} \frac{(\sum_{j=1}^k m_{I_j})^k}{\prod_{j=1}^k \mathrm{sh}(m_{I_j})\prod_{\ell\notin I}\mathrm{sh}(m_\ell \pm m_{I_j})}\,. \tag{3.25}$$

$T[G]$ **theory.** For the $T[G]$ theory, the $S^3$ partition function is given as [87]

$$Z^{S^3}_{T[G]} = \mathrm{const}\cdot\prod_{\alpha\in\Delta^+}\frac{\alpha\cdot m}{\mathrm{sh}(\alpha\cdot m)}\,. \tag{3.26}$$

A closed-form formula with FI parameter for $A$-type was presented in [117]. After taking the limit which send FI parameters to 0, and the constant equals to

$$\frac{1}{G(1+N)} = \frac{1}{\prod_{k=1}^{N-1}k!}\,,$$

where $G(x)$ is the Barnes gamma function. For $C$ and $D$ types, the $S^3$ partition function can also be computed by introducing regulators repeatedly. The (3.26) was checked up to $T[\mathrm{SO}(6)]$.

# Acknowledgement

During my Ph.D. period at Fudan University, I have received much support regardless of academic aspects and daily-life aspects.

First I would like to thank my supervisor Satoshi Nawata from the bottom of my heart. His rigorous scholarship and hard-working attitude toward research set an example for me and I learned a lot from him. He also gave me countless assistance when I encounter difficulties in my life. Then I also would like to thank my collaborators Marcus Sperling and Zhenghao Zhong, they also gave me a lot of help when I researched on the 3d $\mathcal{N} = 4$ unitary/orthosymplectic dualities. And Marcus also helped me a lot when I visited YMSC at Tsinghua University. I also thank YMSC for providing me a precious opportunity to communicate with lots of top researchers in mathematical physics.

I would like to thank Zhang Hao and Yang Yuanzhe. Zhang Hao and I collaborated to carry out the research on the project of knot homology and quantum $6j$-symbols together, under the guidance of Satoshi during 2019-2020. Yang Yuanzhe also gave me lots of help during my Ph.D. period.

Thanks Fudan University provides me with good conditions to study and research. The environment in Jiangwan Campus is beautiful. When I am tired, walking around campus makes me feel relaxed.

I would like to thank my parents for encouraging me to chase my dream. The home is always my harbor. And also thanks to my girlfriend Li Wanqi, she is always with me no matter what difficulties I encounter.

# 攻读博士学位期间研究成果

- [1] **Hao Wang**, Yuanzhe Jack Yang, Hao Derrick Zhang, Satoshi Nawata. On Knots, Complements, and $6j$-Symbols. Annales Henri Poincaré volume 22, pages 2691–2720 (2021).
- [2]Satoshi Nawata, Marcus Sperling, **Hao Wang**, Zhenghao Zhong, Magnetic quivers and line defects —On a duality between 3d $\mathcal{N} = 4$ unitary and orthosymplectic quivers, J. High Energ. Phys. 2022, 174 (2022).

# 参考文献


[1] Zodinmawia and P. Ramadevi, SU($N$) *quantum Racah coefficients & non-torus links*, *Nucl. Phys. B* **870** (2013) 205 [1107.3918].

[2] N. Seiberg and E. Witten, *Electric - magnetic duality, monopole condensation, and confinement in N=2 supersymmetric Yang-Mills theory*, *Nucl. Phys. B* **426** (1994) 19 [hep-th/9407087].

[3] S. Cabrera, A. Hanany and F. Yagi, *Tropical Geometry and Five Dimensional Higgs Branches at Infinite Coupling*, *JHEP* **01** (2019) 068 [1810.01379].

[4] S. Cabrera, A. Hanany and M. Sperling, *Magnetic quivers, Higgs branches, and 6d N=(1,0) theories*, *JHEP* **06** (2019) 071 [1904.12293].

[5] A. Bourget, S. Cabrera, J.F. Grimminger, A. Hanany, M. Sperling, A. Zajac et al., *The Higgs mechanism — Hasse diagrams for symplectic singularities*, *JHEP* **01** (2020) 157 [1908.04245].

[6] A. Bourget, S. Cabrera, J.F. Grimminger, A. Hanany and Z. Zhong, *Brane Webs and Magnetic Quivers for SQCD*, *JHEP* **03** (2020) 176 [1909.00667].

[7] S. Cabrera, A. Hanany and M. Sperling, *Magnetic Quivers, Higgs Branches, and 6d N=(1,0) Theories – Orthogonal and Symplectic Gauge Groups*, *JHEP* **02** (2020) 184 [1912.02773].

[8] A. Bourget, J.F. Grimminger, A. Hanany, M. Sperling and Z. Zhong, *Magnetic Quivers from Brane Webs with O5 Planes*, *JHEP* **07** (2020) 204 [2004.04082].

[9] A. Bourget, J.F. Grimminger, A. Hanany, M. Sperling, G. Zafrir and Z. Zhong, *Magnetic quivers for rank 1 theories*, *JHEP* **09** (2020) 189 [2006.16994].

[10] C. Closset, S. Schafer-Nameki and Y.-N. Wang, *Coulomb and Higgs Branches from Canonical Singularities: Part 0*, *JHEP* **02** (2021) 003 [2007.15600].

[11] M. Akhond, F. Carta, S. Dwivedi, H. Hayashi, S.-S. Kim and F. Yagi, *Five-brane webs, Higgs branches and unitary/orthosymplectic magnetic quivers*, *JHEP* **12** (2020) 164 [2008.01027].

[12] M. van Beest, A. Bourget, J. Eckhard and S. Schafer-Nameki, *(Symplectic) Leaves and (5d Higgs) Branches in the Poly(go)nesian Tropical Rain Forest*, *JHEP* **11** (2020) 124 [2008.05577].

[13] A. Bourget, S. Giacomelli, J.F. Grimminger, A. Hanany, M. Sperling and Z. Zhong, *S-fold magnetic quivers*, *JHEP* **02** (2021) 054 [2010.05889].

[14] M. Van Beest, A. Bourget, J. Eckhard and S. Schäfer-Nameki, *(5d RG-flow) Trees in the Tropical Rain Forest*, *JHEP* **03** (2021) 241 [2011.07033].

[15] J. Eckhard, S. Schäfer-Nameki and Y.-N. Wang, *Trifectas for $T_N$ in 5d*, *JHEP* **07** (2020) 199 [2004.15007].

[16] C. Closset, S. Giacomelli, S. Schafer-Nameki and Y.-N. Wang, *5d and 4d SCFTs: Canonical Singularities, Trinions and S-Dualities*, *JHEP* **05** (2021) 274 [2012.12827].

[17] M. Akhond, F. Carta, S. Dwivedi, H. Hayashi, S.-S. Kim and F. Yagi, *Factorised 3d $\mathcal{N} = 4$ orthosymplectic quivers*, *JHEP* **05** (2021) 269 [2101.12235].

[18] A. Bourget, J.F. Grimminger, A. Hanany, R. Kalveks, M. Sperling and Z. Zhong, *Folding Orthosymplectic Quivers*, 2107.00754.

[19] M. Akhond and F. Carta, *Magnetic quivers from brane webs with O7$^+$-planes*, 2107.09077.

[20] M. van Beest and S. Giacomelli, *Connecting 5d Higgs Branches via Fayet-Iliopoulos Deformations*, 2110.02872.

[21] A. Bourget, J.F. Grimminger, M. Martone and G. Zafrir, *Magnetic quivers for rank 2 theories*, 2110.11365.

[22] M. Sperling and Z. Zhong, *Balanced B and D-type orthosymplectic quivers – Magnetic quivers for product theories*, 2111.00026.

[23] M. Del Zotto and A. Hanany, *Complete Graphs, Hilbert Series, and the Higgs branch of the 4d $\mathcal{N} = 2$ ($A_n$, $A_m$) SCFTs*, *Nucl. Phys. B* **894** (2015) 439 [1403.6523].

[24] S. Cremonesi, G. Ferlito, A. Hanany and N. Mekareeya, *Instanton Operators and the Higgs Branch at Infinite Coupling*, *JHEP* **04** (2017) 042 [1505.06302].

[25] G. Ferlito, A. Hanany, N. Mekareeya and G. Zafrir, *3d Coulomb branch and 5d Higgs branch at infinite coupling*, *JHEP* **07** (2018) 061 [1712.06604].

[26] N. Mekareeya, K. Ohmori, Y. Tachikawa and G. Zafrir, *$E_8$ instantons on type-A ALE spaces and supersymmetric field theories*, *JHEP* **09** (2017) 144 [1707.04370].

[27] A. Hanany and N. Mekareeya, *The small $E_8$ instanton and the Kraft Procesi transition*, *JHEP* **07** (2018) 098 [1801.01129].

[28] A. Hanany and G. Zafrir, *Discrete Gauging in Six Dimensions*, *JHEP* **07** (2018) 168 [1804.08857].

[29] A. Hanany and M. Sperling, *Discrete quotients of 3-dimensional $\mathcal{N} = 4$ Coulomb branches via the cycle index*, *JHEP* **08** (2018) 157 [1807.02784].

[30] A. Hanany and E. Witten, *Type IIB superstrings, BPS monopoles, and three-dimensional gauge dynamics*, *Nucl. Phys.* **B492** (1997) 152 [hep-th/9611230].

[31] N. Seiberg and E. Witten, *Gauge dynamics and compactification to three-dimensions*, in *Conference on the Mathematical Beauty of Physics (In Memory of C. Itzykson)*, pp. 333–366, 6, 1996 [hep-th/9607163].

[32] K.A. Intriligator and N. Seiberg, *Mirror symmetry in three-dimensional gauge theories*, *Phys. Lett. B* **387** (1996) 513 [hep-th/9607207].

[33] A. Hanany and A. Zaffaroni, *Issues on orientifolds: On the brane construction of gauge theories with SO(2n) global symmetry*, *JHEP* **07** (1999) 009 [hep-th/9903242].

[34] B. Feng and A. Hanany, *Mirror symmetry by O3 planes*, *JHEP* **11** (2000) 033 [hep-th/0004092].

[35] B. Assel and J. Gomis, *Mirror Symmetry And Loop Operators*, *JHEP* **11** (2015) 055 [1506.01718].

[36] A. Dey, *Line Defects in Three Dimensional Mirror Symmetry beyond Linear Quivers*, 2103.01243.

[37] D. Gaiotto, A. Kapustin, N. Seiberg and B. Willett, *Generalized Global Symmetries*, *JHEP* **02** (2015) 172 [1412.5148].

[38] A. Bourget, J.F. Grimminger, A. Hanany, R. Kalveks, M. Sperling and Z. Zhong, *Magnetic Lattices for Orthosymplectic Quivers*, *JHEP* **12** (2020) 092 [2007.04667].

[39] S. Benvenuti, B. Feng, A. Hanany and Y.-H. He, *Counting BPS Operators in Gauge Theories: Quivers, Syzygies and Plethystics*, *JHEP* **11** (2007) 050 [hep-th/0608050].

[40] B. Feng, A. Hanany and Y.-H. He, *Counting gauge invariants: The Plethystic program*, *JHEP* **03** (2007) 090 [hep-th/0701063].

[41] J. Gray, A. Hanany, Y.-H. He, V. Jejjala and N. Mekareeya, *SQCD: A Geometric Apercu*, *JHEP* **05** (2008) 099 [0803.4257].

[42] S. Cremonesi, A. Hanany and A. Zaffaroni, *Monopole operators and Hilbert series of Coulomb branches of 3d $\mathcal{N} = 4$ gauge theories*, *JHEP* **01** (2014) 005 [1309.2657].

[43] M. Bullimore, T. Dimofte and D. Gaiotto, *The Coulomb Branch of 3d $\mathcal{N} = 4$ Theories*, *Commun. Math. Phys.* **354** (2017) 671 [1503.04817].

[44] J.F. Grimminger and A. Hanany, *Hasse diagrams for 3d $\mathcal{N} = 4$ quiver gauge theories — Inversion and the full moduli space*, *JHEP* **09** (2020) 159 [2004.01675].

[45] A. Bourget, J.F. Grimminger, A. Hanany, M. Sperling and Z. Zhong, *Branes, Quivers, and the Affine Grassmannian*, 2102.06190.

[46] S.S. Razamat and B. Willett, *Down the rabbit hole with theories of class $\mathcal{S}$*, *JHEP* **10** (2014) 099 [1403.6107].

[47] C. Closset and H. Kim, *Comments on twisted indices in 3d supersymmetric gauge theories*, *JHEP* **08** (2016) 059 [1605.06531].

[48] A. Kapustin, B. Willett and I. Yaakov, *Exact Results for Wilson Loops in Superconformal Chern-Simons Theories with Matter*, *JHEP* **03** (2010) 089 [0909.4559].

[49] T. Dimofte, N. Garner, M. Geracie and J. Hilburn, *Mirror symmetry and line operators*, *JHEP* **02** (2020) 075 [1908.00013].

[50] E. Witten, *Quantum Field Theory and the Jones Polynomial*, *Commun. Math. Phys.* **121** (1989) 351.

[51] N. Reshetikhin and V. Turaev, *Invariants of three manifolds via link polynomials and quantum groups*, *Invent. Math.* **103** (1991) 547.

[52] M. Khovanov and L. Rozansky, *Matrix factorizations and link homology II*, *Geom. Topol.* **12** (2008) 1387 [math/0505056].

[53] N.M. Dunfield, S. Gukov and J. Rasmussen, *The Superpolynomial for knot homologies*, *Exp. Math.* **15** (2006) 129 [math/0505662].

[54] S. Gukov and J. Walcher, *Matrix factorizations and Kauffman homology*, hep-th/0512298.

[55] S. Gukov and M. Stošić, *Homological Algebra of Knots and BPS States*, *Proc. Symp. Pure Math.* **85** (2012) 125 [1112.0030].

[56] E. Gorsky, S. Gukov and M. Stosic, *Quadruply-graded colored homology of knots*, *Fund. Math.* **243** (2018) 209 [1304.3481].

[57] S. Nawata, P. Ramadevi and Zodinmawia, *Colored Kauffman Homology and Super-A-polynomials*, *JHEP* **01** (2014) 126 [1310.2240].

[58] R. Kashaev, *The Hyperbolic volume of knots from quantum dilogarithm*, *Lett. Math. Phys.* **39** (1997) 269 [q-alg/9601025].

[59] H. Murakami and J. Murakami, *The Colored Jones Polynomials and the Simplicial Volume of a Knot*, *Acta Math.* **186** (2001) 85 [math/9905075].

[60] S. Gukov, *Three-dimensional quantum gravity, Chern-Simons theory, and the A-polynomial*, *Commun. Math. Phys.* **255** (2005) 577 [hep-th/0306165].

[61] S. Gukov and H. Murakami, *SL(2,C) Chern–Simons Theory and the Asymptotic Behavior of the Colored Jones Polynomial*, *Lett. Math. Phys.* **86** (2008) 79 [math/0608324].

[62] H. Awata, S. Gukov, P. Sulkowski and H. Fuji, *Volume Conjecture: Refined and Categorified*, *Adv. Theor. Math. Phys.* **16** (2012) 1669 [1203.2182].

[63] M. Aganagic and C. Vafa, *Large N Duality, Mirror Symmetry, and a Q-deformed A-polynomial for Knots*, 1204.4709.

[64] H. Fuji, S. Gukov and P. Sulkowski, *Super-A-polynomial for knots and BPS states*, *Nucl. Phys. B* **867** (2013) 506 [1205.1515].

[65] G.W. Moore and N. Seiberg, *LECTURES ON RCFT*, in *1989 Banff NATO ASI: Physics, Geometry and Topology*, 9, 1989.

[66] R. Kaul and T. Govindarajan, *Three-dimensional Chern-Simons theory as a theory of knots and links*, *Nucl. Phys. B* **380** (1992) 293 [hep-th/9111063].

[67] R. Kaul and T. Govindarajan, *Three-dimensional Chern-Simons theory as a theory of knots and links. 2. Multicolored links*, *Nucl. Phys. B* **393** (1993) 392.

[68] R. Kaul, *Chern-Simons theory, colored oriented braids and link invariants*, *Commun. Math. Phys.* **162** (1994) 289 [hep-th/9305032].

[69] P. Ramadevi, T. Govindarajan and R. Kaul, *Three-dimensional Chern-Simons theory as a theory of knots and links. 3. Compact semisimple group*, *Nucl. Phys. B* **402** (1993) 548 [hep-th/9212110].

[70] G.W. Moore and N. Seiberg, *Classical and Quantum Conformal Field Theory*, *Commun. Math. Phys.* **123** (1989) 177.

[71] D. Kazhdan and G. Lusztig, *Tensor structures arising from affine Lie algebras. I*, *J. Amer. Math. Soc.* **6** (1993) 905.

[72] D. Kazhdan and G. Lusztig, *Tensor structures arising from affine Lie algebras. II*, *J. Amer. Math. Soc.* **6** (1993) 949.

[73] D. Kazhdan and G. Lusztig, *Tensor structures arising from affine Lie algebras. III*, *J. Amer. Math. Soc.* **7** (1994) 335.

[74] D. Kazhdan and G. Lusztig, *Tensor structures arising from affine Lie algebras. IV*, *J. Amer. Math. Soc.* **7** (1994) 383.

[75] L. Biedenharn and H. Van Dam, *Quantum theory of angular momentum : a collection of reprints and original papers*, Academic Press, New York (1965).

[76] E.P. Wigner, *On the matrices which reduce the Kronecker products of representations of SR groups*, in *The Collected Works of Eugene Paul Wigner*, pp. 608–654, Springer (1993).

[77] G. Racah, *Theory of Complex Spectra. II*, *Phys. Rev.* **62** (1942) 438.

[78] A. Kirillov and N. Reshetikhin, *Representations of the Algebra $U_q(sl_2)$, q-Orthogonal Polynomials and Invariants of Links*, in *New Developments In The Theory Of Knots.*, pp. 202–256, 1990, DOI.

[79] S. Nawata, P. Ramadevi and Zodinmawia, *Multiplicity-free quantum 6j-symbols for $U_q(\mathfrak{sl}_N)$*, *Lett. Math. Phys.* **103** (2013) 1389 [1302.5143].

[80] S. Ališauskas, *Some coupling and recoupling coefficients for symmetric representations of* SO($n$), *J. Phys. A: Math. Gen.* **20** (1987) 35.

[81] S. Ališauskas, *6j-symbols for symmetric representations of* SO($n$) *as the double series*, *J. Phys. A: Math. Gen.* **35** (2002) 10229–10246 [math-ph/0206044].

[82] D. Gaiotto and T. Okazaki, *Sphere correlation functions and Verma modules*, *JHEP* **02** (2020) 133 [1911.11126].

[83] M. Bullimore, A. Ferrari and H. Kim, *Twisted indices of 3d $\mathcal{N} = 4$ gauge theories and enumerative geometry of quasi-maps*, *JHEP* **07** (2019) 014 [1812.05567].

[84] N. Seiberg, *IR dynamics on branes and space-time geometry*, *Phys. Lett. B* **384** (1996) 81 [hep-th/9606017].

[85] A. Kapustin, *Wilson-'t Hooft operators in four-dimensional gauge theories and S-duality*, *Phys. Rev. D* **74** (2006) 025005 [hep-th/0501015].

[86] V. Borokhov, A. Kapustin and X.-k. Wu, *Monopole operators and mirror symmetry in three-dimensions*, *JHEP* **12** (2002) 044 [hep-th/0207074].

[87] D. Gaiotto and E. Witten, *S-Duality of Boundary Conditions In N=4 Super Yang-Mills Theory*, *Adv. Theor. Math. Phys.* **13** (2009) 721 [0807.3720].

[88] D. Bashkirov and A. Kapustin, *Supersymmetry enhancement by monopole operators*, *JHEP* **05** (2011) 015 [1007.4861].

[89] M.K. Benna, I.R. Klebanov and T. Klose, *Charges of Monopole Operators in Chern-Simons Yang-Mills Theory*, *JHEP* **01** (2010) 110 [0906.3008].

[90] O. Aharony, N. Seiberg and Y. Tachikawa, *Reading between the lines of four-dimensional gauge theories*, *JHEP* **08** (2013) 115 [1305.0318].

[91] D. Tong, *Line Operators in the Standard Model*, *JHEP* **07** (2017) 104 [1705.01853].

[92] A.M. Uranga, *Towards mass deformed N=4 SO(n) and Sp(k) gauge theories from brane configurations*, *Nucl. Phys. B* **526** (1998) 241 [hep-th/9803054].

[93] E.G. Gimon and J. Polchinski, *Consistency conditions for orientifolds and d manifolds*, *Phys. Rev. D* **54** (1996) 1667 [hep-th/9601038].

[94] A. Hanany and A. Zaffaroni, *Branes and six-dimensional supersymmetric theories*, *Nucl. Phys. B* **529** (1998) 180 [hep-th/9712145].

[95] A. Kapustin, *D(n) quivers from branes*, *JHEP* **12** (1998) 015 [hep-th/9806238].

[96] F. Benini, *Localization in supersymmetric field theories*, *YITP Kyoto School* (2016) .

[97] M.F. Atiyah and R. Bott, *The Yang-Mills equations over Riemann surfaces*, *Phil. Trans. Roy. Soc. Lond. A* **308** (1982) 523.

[98] V.F. Jones, *A polynomial invariant for knots via von Neumann algebras*, in *Fields Medallists' Lectures*, pp. 448–458, World Scientific (1997), DOI.

[99] N. Reshetikhin and V.G. Turaev, *Invariants of 3-manifolds via link polynomials and quantum groups*, *Inventiones mathematicae* **103** (1991) 547.

[100] R. Kirby and P. Melvin, *The 3-manifold invariants of Witten and Reshetikhin-Turaev for sl (2, C)*, *Inventiones mathematicae* **105** (1991) 473.

[101] L. Crane and I. Frenkel, *Four-dimensional topological field theory, Hopf categories, and the canonical bases*, *J. Math. Phys.* **35** (1994) 5136 [hep-th/9405183].

[102] S. Gukov, *Gauge theory and knot homologies*, *Fortsch. Phys.* **55** (2007) 473 [0706.2369].

[103] M. Khovanov, *A categorification of the Jones polynomial*, *Duke Math. J.* **101** (2000) 359 [math/9908171].

[104] S. Gukov, S. Nawata, I. Saberi, M. Stošić and P. Sułkowski, *Sequencing BPS Spectra*, *JHEP* **03** (2016) 004 [1512.07883].

[105] M. Khovanov and L. Rozansky, *Virtual crossings, convolutions and a categorification of the* SO*(2N) Kauffman polynomial*, math/0701333.

[106] C. Daryl, S. Peter, B, C. Marc, G. Henri and L. D, D, *Plane curves associated to character varieties of 3-manifolds*, *Invent. Math.* **118** (1994) 47.

[107] W.D. Neumann and D. Zagier, *Volumes of hyperbolic three-manifolds*, *Topology* **24** (1985) 307.

[108] M. Aganagic and C. Vafa, *Large N Duality, Mirror Symmetry, and a Q-deformed A-polynomial for Knots*, 1204.4709.

[109] V.G. Drinfeld, *Hopf algebras and the quantum Yang-Baxter equation*, *Sov. Math. Dokl.* **32** (1985) 254.

[110] J.S. Birman, *Braids, Links, and Mapping Class Groups.(AM-82), Volume 82*, Princeton University Press (2016).

[111] L. Rozansky and E. Witten, *HyperKahler geometry and invariants of three manifolds*, *Selecta Math.* **3** (1997) 401 [hep-th/9612216].

[112] N.A. Nekrasov and S.L. Shatashvili, *Bethe/Gauge correspondence on curved spaces*, *JHEP* **01** (2015) 100 [1405.6046].

[113] S. Gukov and D. Pei, *Equivariant Verlinde formula from fivebranes and vortices*, *Commun. Math. Phys.* **355** (2017) 1 [1501.01310].

[114] F. Benini and A. Zaffaroni, *A topologically twisted index for three-dimensional supersymmetric theories*, *JHEP* **07** (2015) 127 [1504.03698].

[115] F. Benini and A. Zaffaroni, *Supersymmetric partition functions on Riemann surfaces*, *Proc. Symp. Pure Math.* **96** (2017) 13 [1605.06120].

[116] S. Gukov, P.-S. Hsin, H. Nakajima, S. Park, D. Pei and N. Sopenko, *Rozansky-Witten geometry of Coulomb branches and logarithmic knot invariants*, *J. Geom. Phys.* **168** (2021) 104311 [2005.05347].

[117] S. Benvenuti and S. Pasquetti, *3D-partition functions on the sphere: exact evaluation and mirror symmetry*, *JHEP* **05** (2012) 099 [1105.2551].

[118] P. Goddard, J. Nuyts and D.I. Olive, *Gauge Theories and Magnetic Charge*, *Nucl. Phys. B* **125** (1977) 1.

[119] A. Hanany and M. Sperling, *Coulomb branches for rank 2 gauge groups in 3d $\mathcal{N} = 4$ gauge theories*, *JHEP* **08** (2016) 016 [1605.00010].

[120] A. Dey, *Three dimensional mirror symmetry beyond ADE quivers and Argyres-Douglas theories*, *JHEP* **07** (2021) 199 [2004.09738].

[121] B. Assel and S. Cremonesi, *The Infrared Fixed Points of 3d $\mathcal{N} = 4$ $USp(2N)$ SQCD Theories*, *SciPost Phys.* **5** (2018) 015 [1802.04285].

[122] E. Witten, *Baryons and branes in anti-de Sitter space*, *JHEP* **07** (1998) 006 [hep-th/9805112].

[123] J. Polchinski, *String theory. Vol. 1: An introduction to the bosonic string*, Cambridge Monographs on Mathematical Physics, Cambridge University Press (12, 2007), 10.1017/CBO9780511816079.

[124] A. Hanany and B. Kol, *On orientifolds, discrete torsion, branes and M theory*, *JHEP* **06** (2000) 013 [hep-th/0003025].

[125] N.J. Evans, C.V. Johnson and A.D. Shapere, *Orientifolds, branes, and duality of 4-D gauge theories*, *Nucl. Phys. B* **505** (1997) 251 [hep-th/9703210].

[126] A. Hanany and R. Kalveks, *Quiver Theories for Moduli Spaces of Classical Group Nilpotent Orbits*, *JHEP* **06** (2016) 130 [1601.04020].

[127] S. Cabrera, A. Hanany and Z. Zhong, *Nilpotent orbits and the Coulomb branch of $T^\sigma(G)$ theories: special orthogonal vs orthogonal gauge group factors*, *JHEP* **11** (2017) 079 [1707.06941].

[128] S. Cabrera, A. Hanany and R. Kalveks, *Quiver Theories and Formulae for Slodowy Slices of Classical Algebras*, *Nucl. Phys. B* **939** (2019) 308 [1807.02521].

[129] C.G. Callan and J.M. Maldacena, *Brane death and dynamics from the Born-Infeld action*, *Nucl. Phys. B* **513** (1998) 198 [hep-th/9708147].

[130] N. Hama, K. Hosomichi and S. Lee, *Notes on SUSY Gauge Theories on Three-Sphere*, *JHEP* **03** (2011) 127 [1012.3512].

[131] N. Hama, K. Hosomichi and S. Lee, *SUSY Gauge Theories on Squashed Three-Spheres*, *JHEP* **05** (2011) 014 [1102.4716].

[132] K.A. Intriligator, D.R. Morrison and N. Seiberg, *Five-dimensional supersymmetric gauge theories and degenerations of Calabi-Yau spaces*, *Nucl. Phys. B* **497** (1997) 56 [hep-th/9702198].

[133] I. Brunner and A. Karch, *Branes and six-dimensional fixed points*, *Phys. Lett. B* **409** (1997) 109 [hep-th/9705022].

[134] O. Bergman and G. Zafrir, *5d fixed points from brane webs and O7-planes*, *JHEP* **12** (2015) 163 [1507.03860].

[135] O. Chacaltana, J. Distler and Y. Tachikawa, *Gaiotto duality for the twisted $A_{2N-1}$ series*, *JHEP* **05** (2015) 075 [1212.3952].

[136] O. Chacaltana and J. Distler, *Tinkertoys for the $D_N$ series*, *JHEP* **02** (2013) 110 [1106.5410].

[137] J. Rasmussen, *Khovanov Homology and the Slice Genus*, *Invent. Math.* **182** (2010) 419 [math/0402131].

[138] Y. Kononov and A. Morozov, *Rectangular superpolynomials for the figure-eight knot $4_1$*, *Theor. Math. Phys.* **193** (2017) 1630 [1609.00143].

[139] M. Kameyama, S. Nawata, R. Tao and H.D. Zhang, *Cyclotomic expansions of HOMFLY-PT colored by rectangular Young diagrams*, *Lett. Math Phys.* **110** (2020) 2573 [1902.02275].

[140] P. Wedrich, *Exponential growth of colored HOMFLY-PT homology*, *Adv. Math.* **353** (2019) 471 [1602.02769].

[141] P. Kucharski, M. Reineke, M. Stosic and P. Sułkowski, *Knots-quivers correspondence*, *Adv. Theor. Math. Phys.* **23** (2019) 1849 [1707.04017].

[142] L.D. Landau and E.M. Lifshitz, *Quantum mechanics: Non-relativistic theory*, vol. 3, Pergamon Press (1958), 10.1007/BF02859578.

[143] L.C. Biedenharn and J.D. Louck, *Angular momentum in quantum physics: theory and application*, Addison-Wesley (1981), 10.1017/CBO9780511759888.

[144] P.H. Butler, *Point group symmetry applications: methods and tables*, Springer Science & Business Media (1981), 10.1007/978-1-4613-3141-4.

[145] D.A. Varshalovich, A.N. Moskalev and V.K. Khersonskii, *Quantum theory of angular momentum*, World Scientific (1988), 10.1142/0270.

[146] A. Mironov, A. Morozov, A. Morozov and A. Sleptsov, *Quantum Racah matrices and 3-strand braids in irreps $R$ with $|R| = 4$*, *JETP Lett.* **104** (2016) 56 [1605.03098].

[147] A. Dey, *Higgs Branches of Argyres-Douglas theories as Quiver Varieties*, 2109.07493.

# 复旦大学
# 学位论文独创性声明

本人郑重声明：所呈交的学位论文，是本人在导师的指导下，独立进行研究工作所取得的成果。论文中除特别标注的内容外，不包含任何其他个人或机构已经发表或撰写过的研究成果。对本研究做出重要贡献的个人和集体，均已在论文中作了明确的声明并表示了谢意。本声明的法律结果由本人承担。

作者签名：_____ 日期：_____

# 复旦大学
# 学位论文使用授权声明

本人完全了解复旦大学有关收藏和利用博士、硕士学位论文的规定，即：学校有权收藏、使用并向国家有关部门或机构送交论文的印刷本和电子版本；允许论文被查阅和借阅；学校可以公布论文的全部或部分内容，可以采用影印、缩印或其它复制手段保存论文。涉密学位论文在解密后遵守此规定。

作者签名：_____ 导师签名：_____ 日期：_____